Studies of photon isolation in large-pileup environment and search for axion-like particles decaying into two photons with the ATLAS detector at the LHC

Thesis defence

29th January 2021

Luis Pascual Domínguez

Supervisor: José Ocariz

Université de Paris

Outline

Theoretical and experimental context

- The Standard Model and its limitations
- Effective Field Theory approach
- The LHC and the ATLAS detector
- Electromagnetic calorimeter

Photon isolation studies

- Photon isolation: an introduction
- Isolation efficiency measurement
- Cluster-based isolation studies

Analysis: resonance search below 65 GeV in the diphoton channel

- Motivation
- Analysis strategy
- Signal and background modelling
- Expected results

Theoretical and experimental context

The Standard Model

The Standard Model (SM) is the quantum field theory that describes the fundamental interactions and fields that constitute matter and radiation.

$$SU(3)_c \times SU(2)_L \times U(1)_Y$$

- Interactions are mediated by gauge bosons
- Field content of the SM:
  - 12 fermions, classified in quarks and leptons
  - Fundamental spin 0 boson, the Higgs field.

Excellent agreement between SM predictions and experimental results…

- Structural problems: naturalness, strong CP problem,…
- Unexplained experimental observations: matter/ antimatter asymmetry, dark matter, …

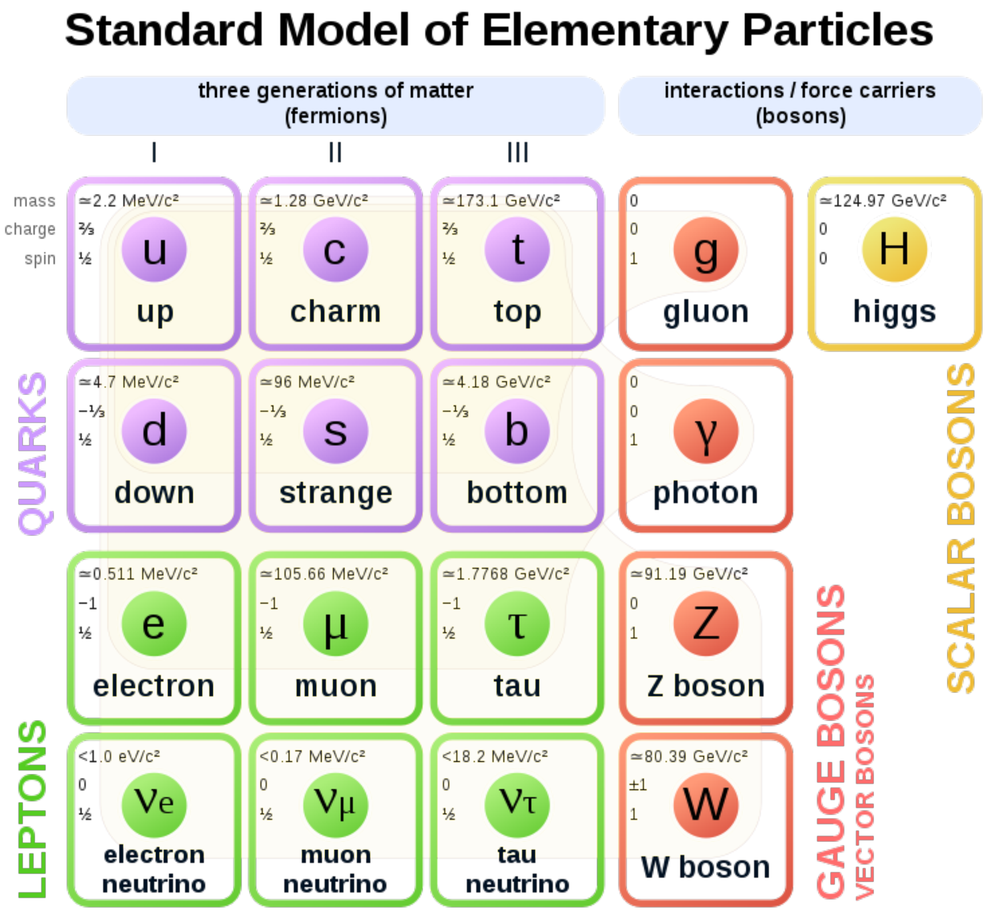

A wide variety of attempts to describe these!

Effective Field Theories

Effective Field Theories (EFT) are a powerful tool to describe low energy phenomena (below high energy scales Λ_{NP})

- Non-understood high energy behaviour is decoupled from low energy interactions.
- Largely model independent

In this framework, New Physics (NP) processes are described by small contributions to a low energy theory (SM in this case)

- Common tool to explore NP scenarios

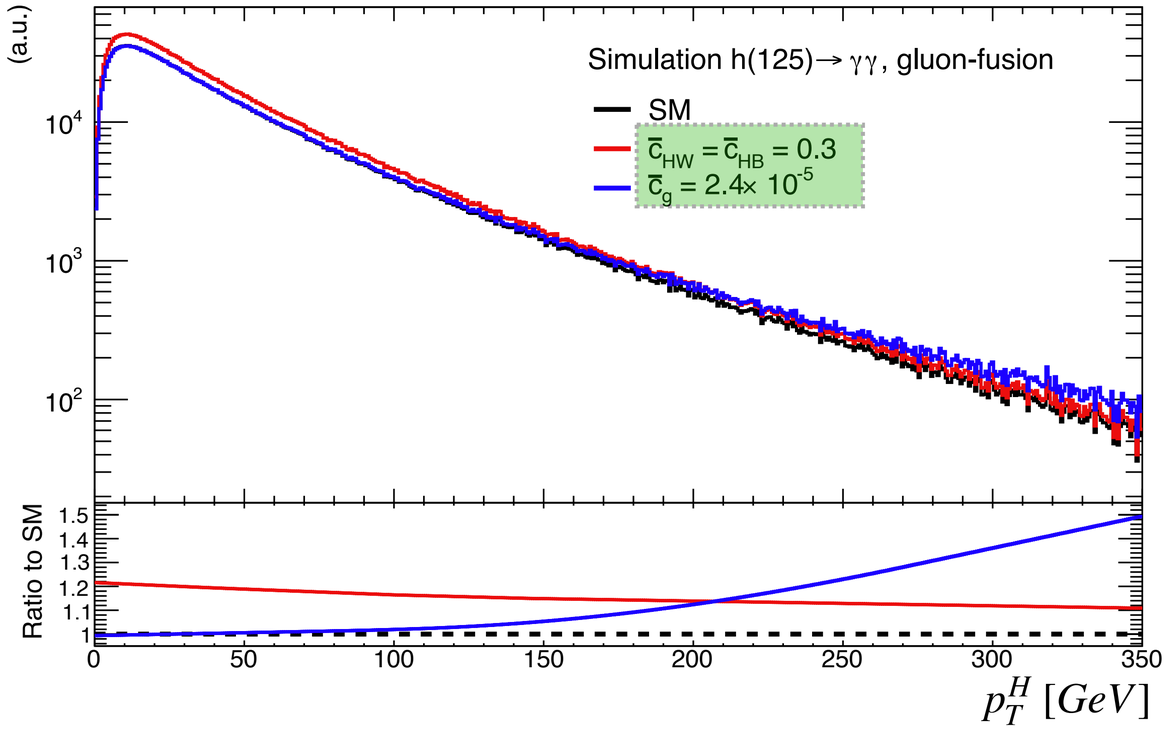

$$\mathscr{L}_{EFT} = \mathscr{L}_{SM} + \sum_i \frac{c_i^D}{\Lambda_{NP}^{D-4}} \mathcal{O}_i^D$$

SM Lagrangian

Wilson coefficient

NP operators

NP energy scale

D≡dimension

The Large Hadron Collider

Largest and most powerful accelerator

- 27km circumference
- Collides protons at a centre-of-mass energy of $\sqrt{s}$ = 13 TeV.

Successful operation for 2015-2018 (Run 2) data-taking period.

- L = 156 fb^{-1} of integrated luminosity

Increased instantaneous luminosity across years

Pileup: additional inelastic pp collisions besides the main hard-scatter process.

- Manageable impact on reconstruction performances

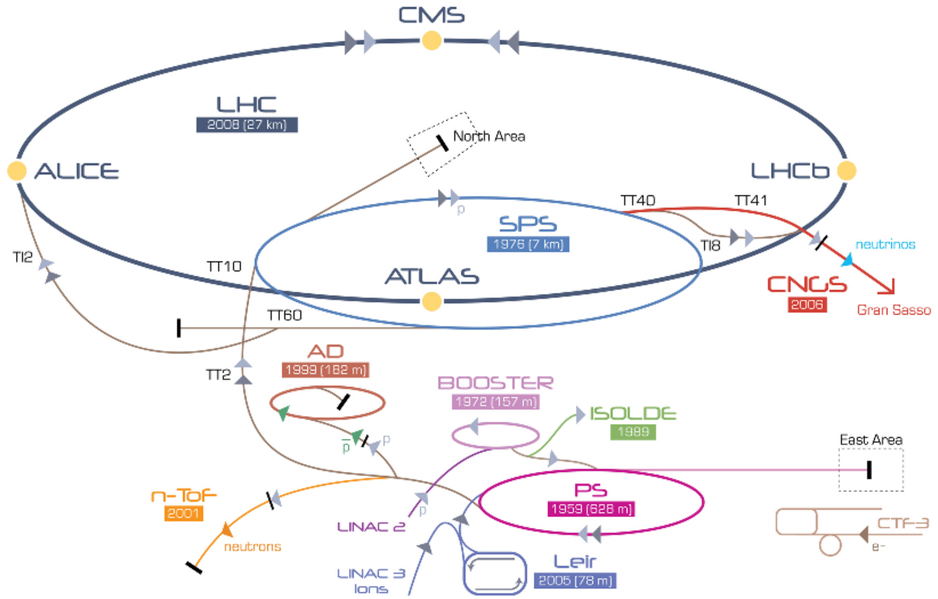

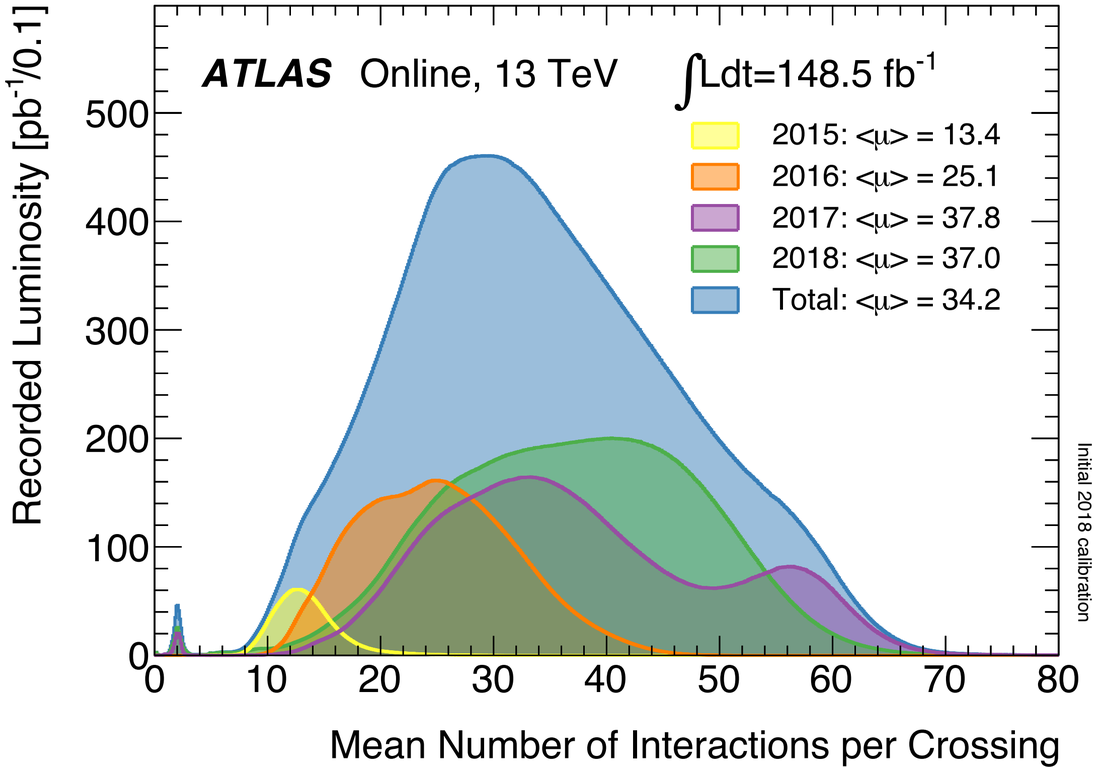

The ATLAS detector

Multipurpose particle physics detector

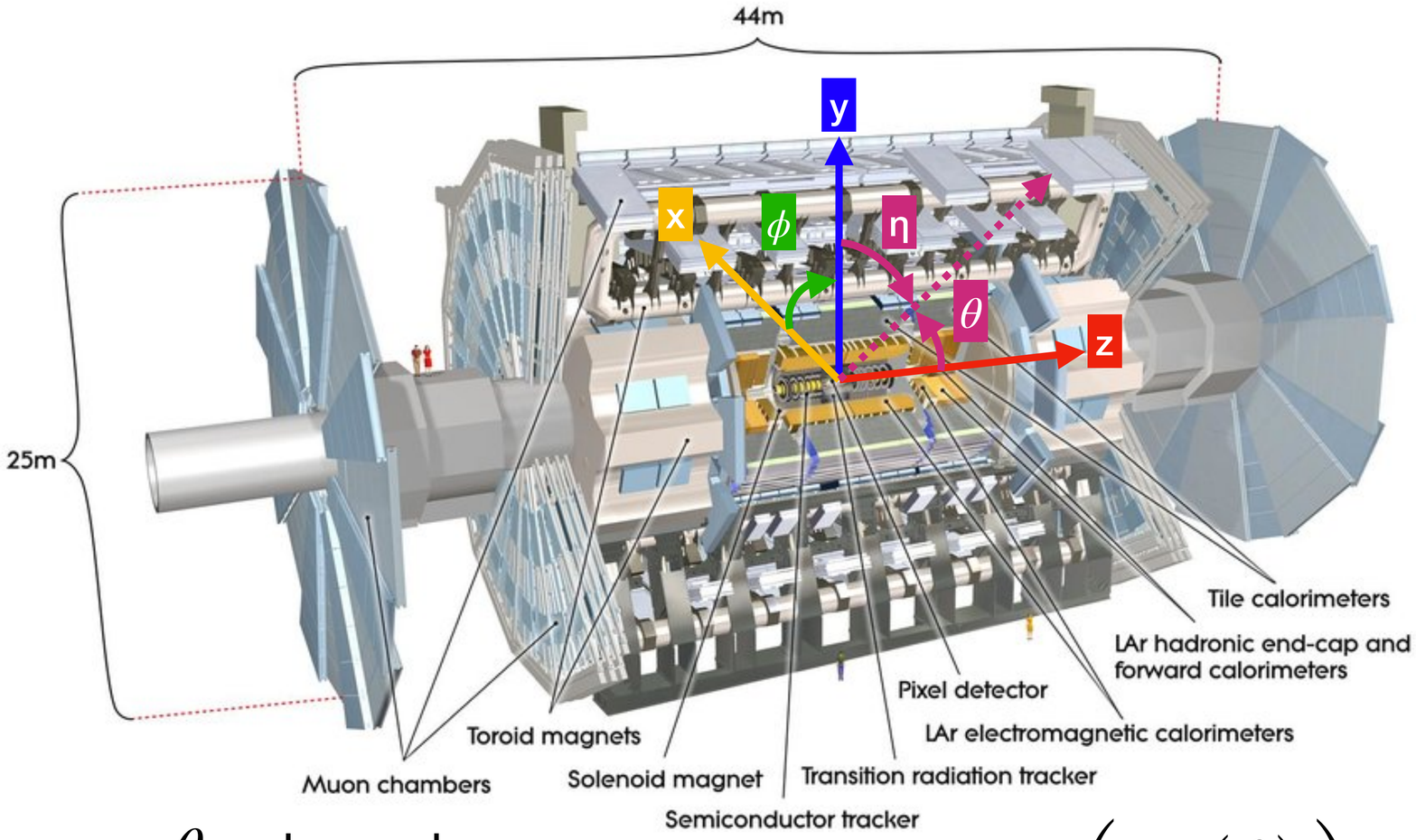

θ: polar angle
ϕ: azimutal angle
η: pseudorapidity

$$\eta = -\log\left(\tan\left(\frac{\theta}{2}\right)\right)$$

Inner detector: charged particle trajectory reconstruction

Electromagnetic (EM) and Hadonic calorimeters: energy measurement of charged and neutral particles: photons, electrons, jets and taus

Muon spectrometer: muon reconstruction

E_T ≡ transverse energy. Commonly used in hadron colliders.

Electromagnetic calorimeter

Sampling EM calorimeter measures the energy of electrons and photons as they interact with matter.

- Interleaves layers of lead and liquid-Argon (LAr,active)

Longitudinally segmented into three layers

Provides an excellent photon energy resolution

$$\frac{\sigma(E)}{E} = \frac{10\,\%\sqrt{GeV}}{\sqrt{E}} \oplus 0.7\,\%$$

- H→ $\gamma\gamma$ crucial for Higgs boson discovery

Energy in the calorimeter cells clustered together into topoclusters.

- Dynamical objects that span over **all layers**

Tracks and clusters matching to identify photons from other objects in the calorimeters.

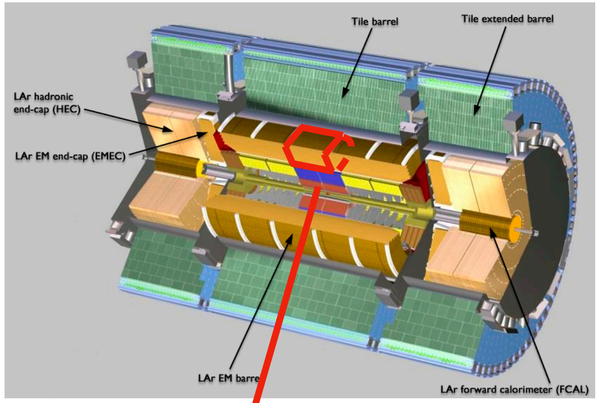

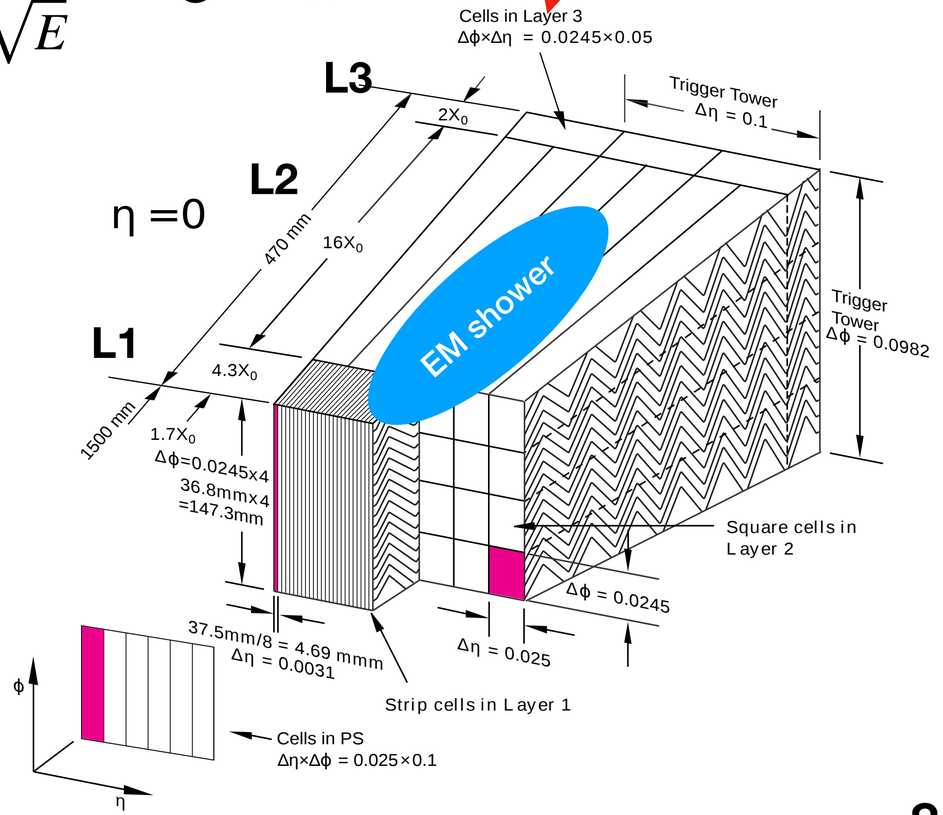

Photon identification

Electromagnetic shower development **almost identical** for any photon/electron.

Photon identification uses shower shape variables to identify photons

Variables that characterize a photon shower longitudinal and lateral profile.

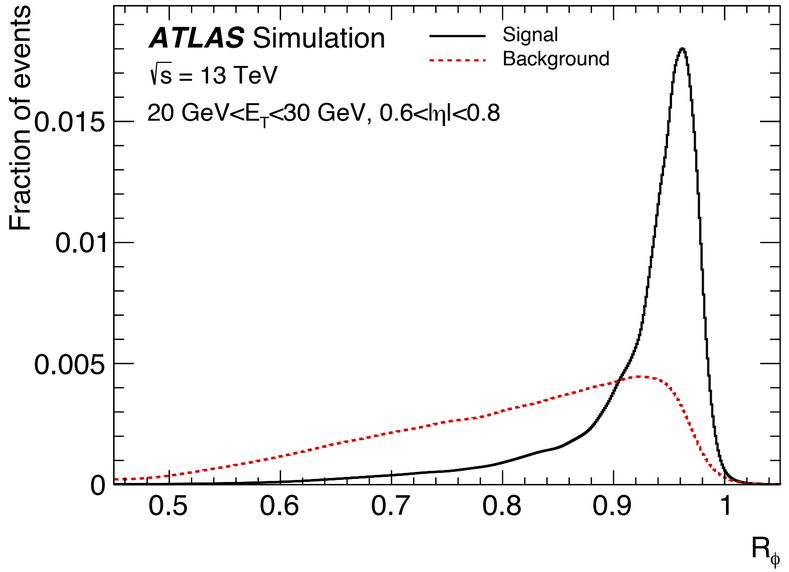

$$R_\eta = \frac{E^{S2}_{3\times7}}{E^{S2}_{7\times7}} \qquad R_\phi = \frac{E^{S2}_{3\times3}}{E^{S2}_{3\times7}}$$

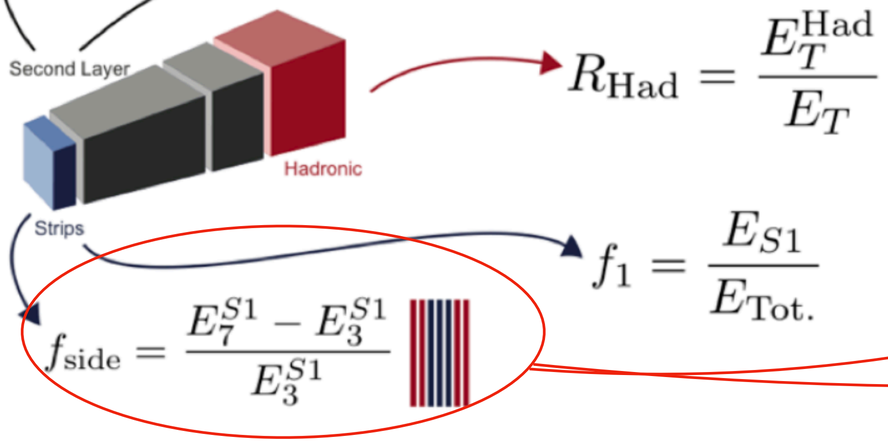

$$R_{\mathrm{Had}} = \frac{E_T^{\mathrm{Had}}}{E_T}$$

$$f_1 = \frac{E_{S1}}{E_{\mathrm{Tot.}}}$$

$$f_{\mathrm{side}} = \frac{E_7^{S1} - E_3^{S1}}{E_3^{S1}}$$

Example of γ/fake discrimination

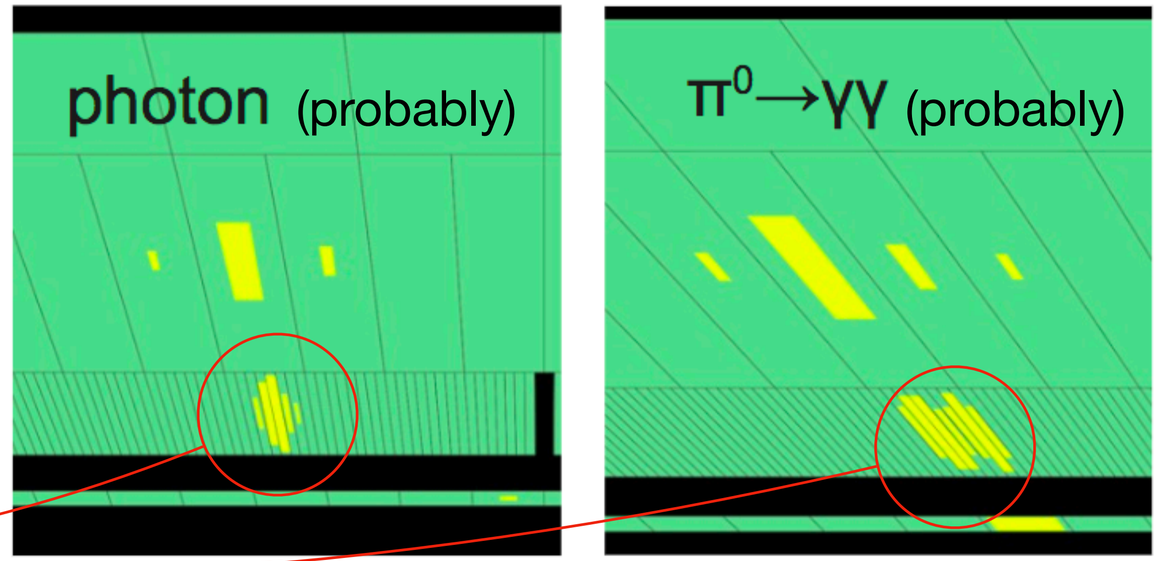

High granularity of the detector plays a crucial role in photon ID.

Photon isolation studies

Photon isolation: an introduction

Photon isolation efficiency measurement

Prospective studies on photon isolation using cluster-level information

Why do we need photon isolation?

Photon isolation rejects further backgrounds on top of photon ID

Prompt photons are typically isolated from hadrons.

- While fakes are usually surrounded by additional particles.

Target background: collimated diphotons from light meson decays identified as single photons.

Prompt photons are those not produced in hadron decays

Non-prompt (or fake) photons arise from hadron decays

Prompt photon **Fake (non-prompt) photon**

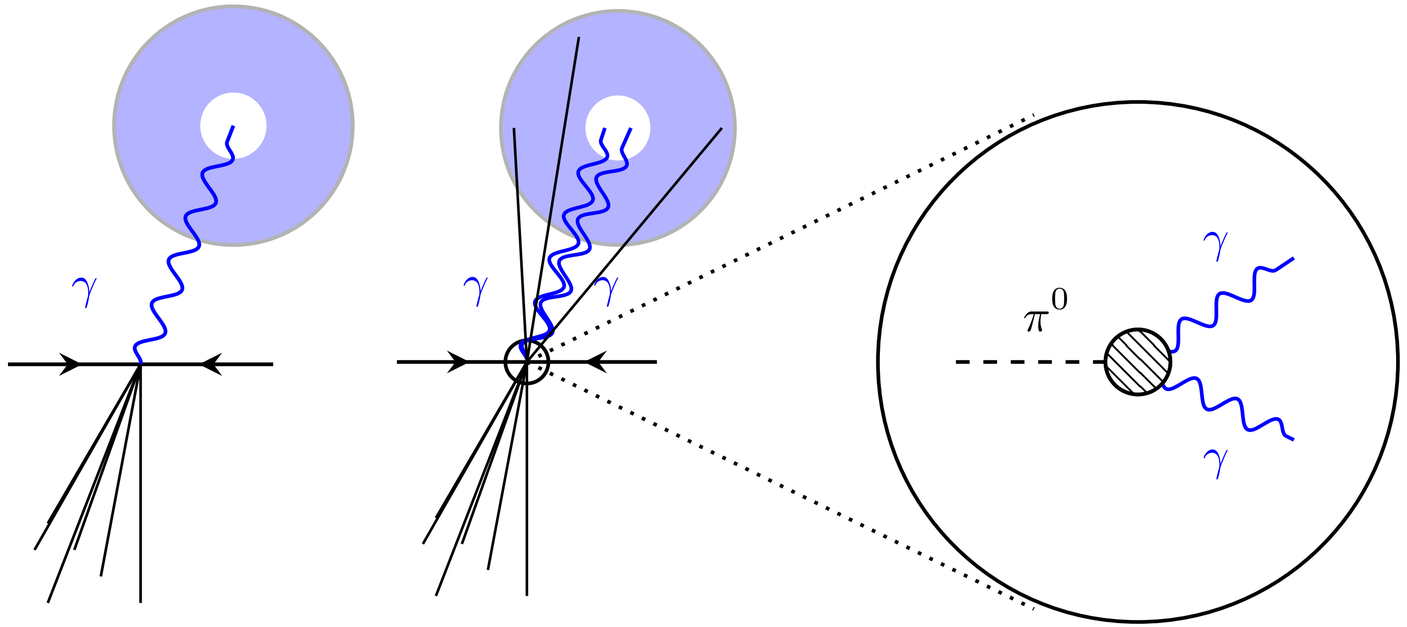

First layer granularity is sometimes not enough!

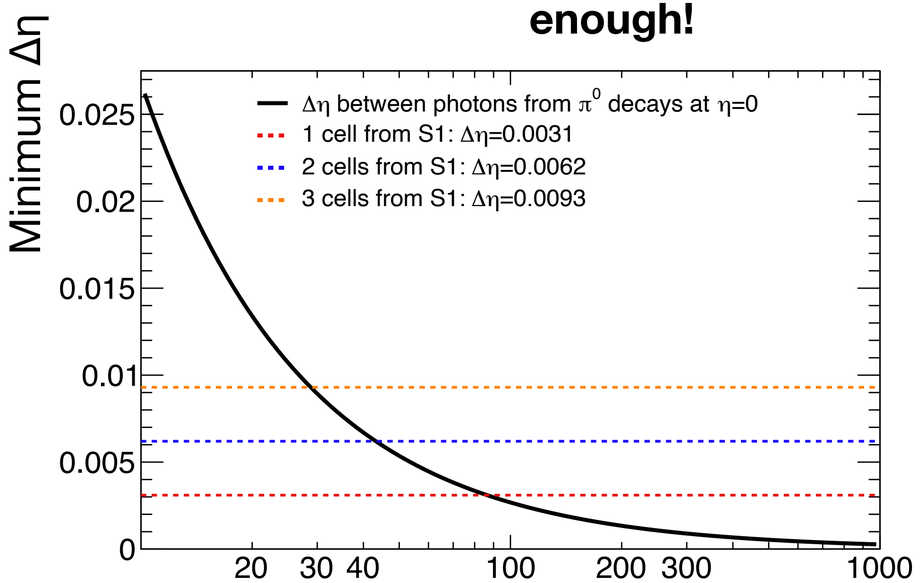

Calorimetric isolation energy

Estimate of the hadronic activity around photon candidates based on information from the tracker and calorimeters. ⟶ **This work!**

$$E_T^{iso}(R) = \sum_{r_i<R}^{clusters} E_T^i - E_T^{core} - E_T^{leakage}(E_T^\gamma, |\eta^\gamma|) - E_T^{pileup}(|\eta^\gamma|)$$

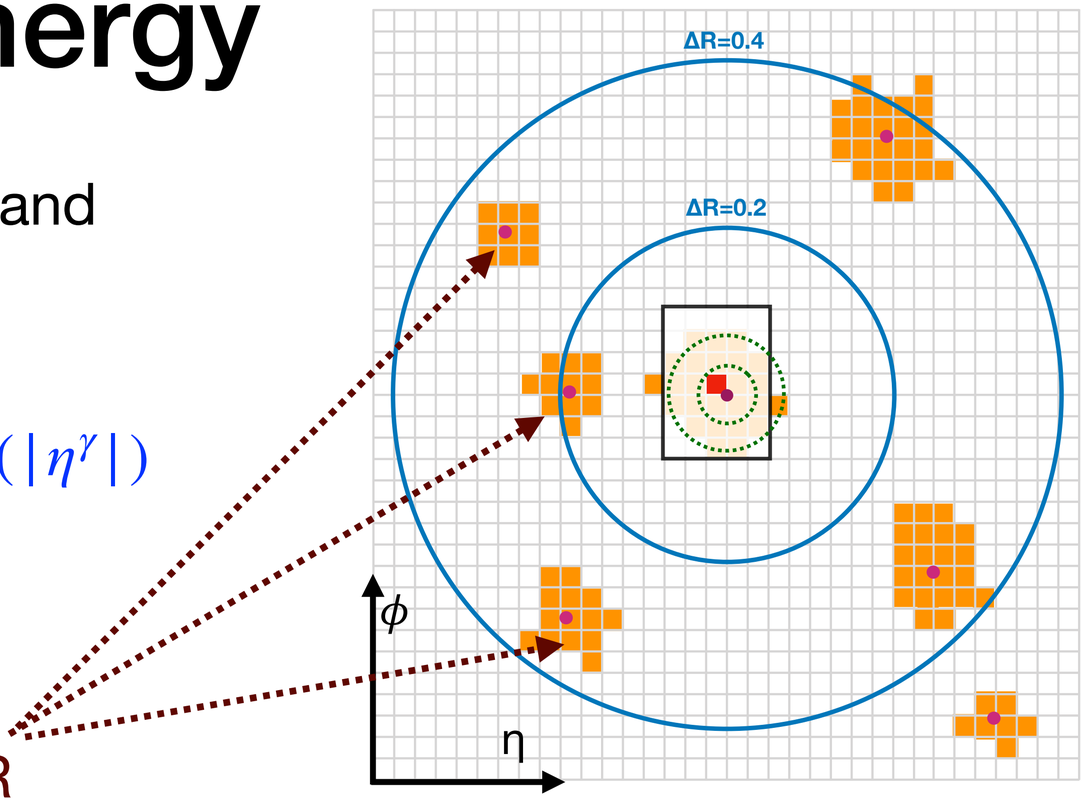

- Sum of all topoclusters within a cone of size ΔR centered in the photon candidate.
- Photon energy subtraction
- Pileup correction, computed in a per-event basis using the ambient energy density (FastJet).

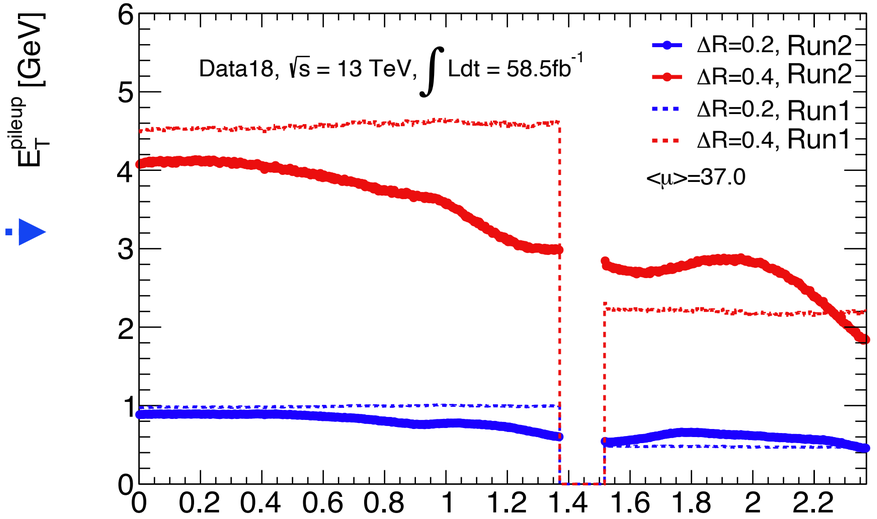

Selecting isolated photons

The isolation energy can help in prompt/fake discrimination

- Prompt photons → E_{iso} ~ 0 GeV.
- Fakes → E_{iso} > 0 GeV.

The efficiencies are defined as:

$$\varepsilon = \frac{N_{Signal,pass}}{N_{Signal,pass} + N_{Signal,fail}}$$

- Efficiency measurements require a precise subtraction of the background

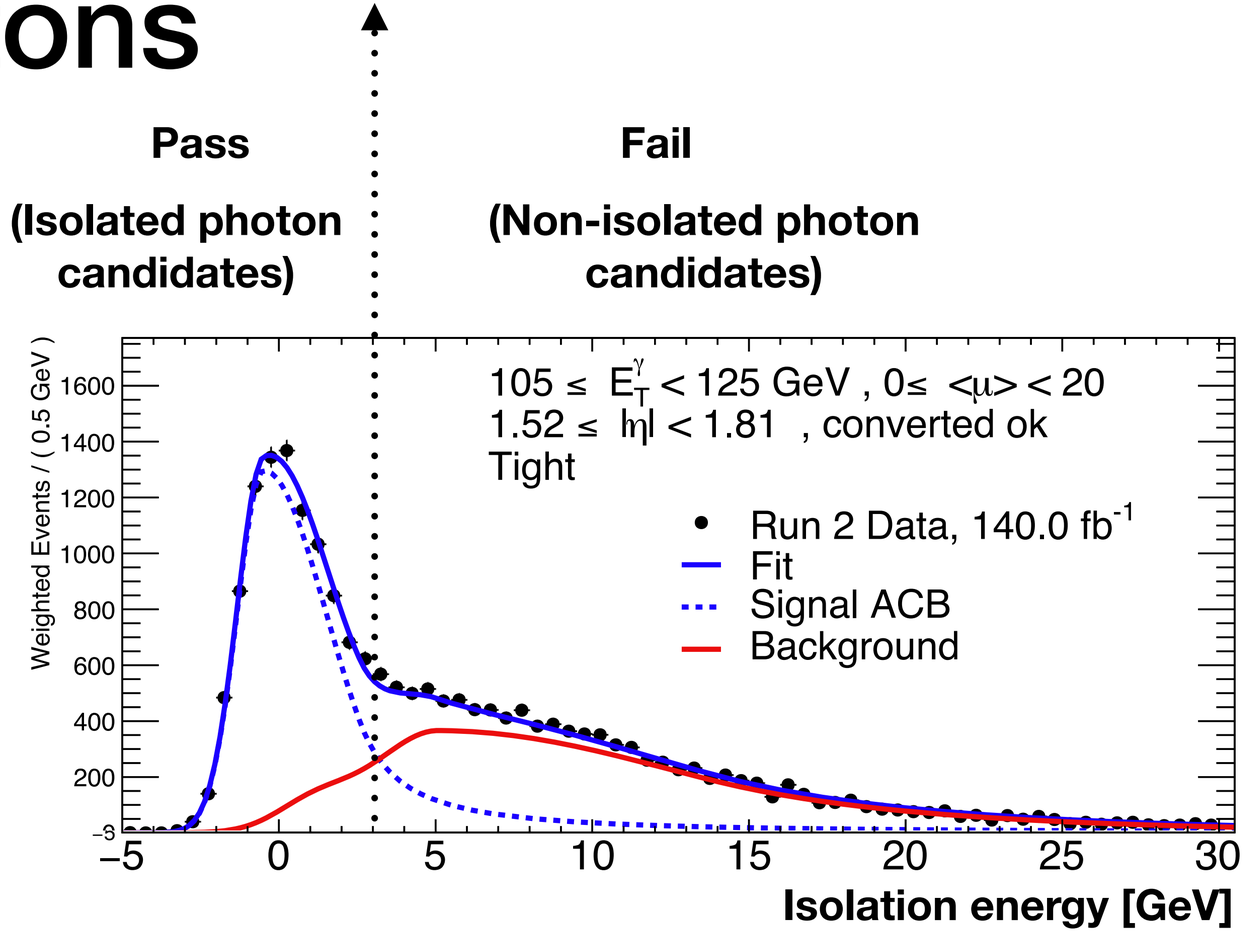

Non-trivial data-driven background shape

Measuring efficiencies

Efficiency measurements are an important ingredient in many physics analyses.

- Efficiencies often obtained in simulated samples.

$$N = \sigma\varepsilon \int \mathscr{L}\, dt$$

Mismodellings in the simulation would translate into differences in the efficiencies.

Two corrections:

- Data-driven shifts: $DD_{shift} = peak_{data} - peak_{simu}$
  - Observed discrepancy between the peak position in data and simulation.
- Scale factors: $\text{scale factor} = \dfrac{\varepsilon_{Data}}{\varepsilon_{Simu}}$
  - Correction factor defined as the ratio of efficiencies that encapsulates the remaining discrepancies.

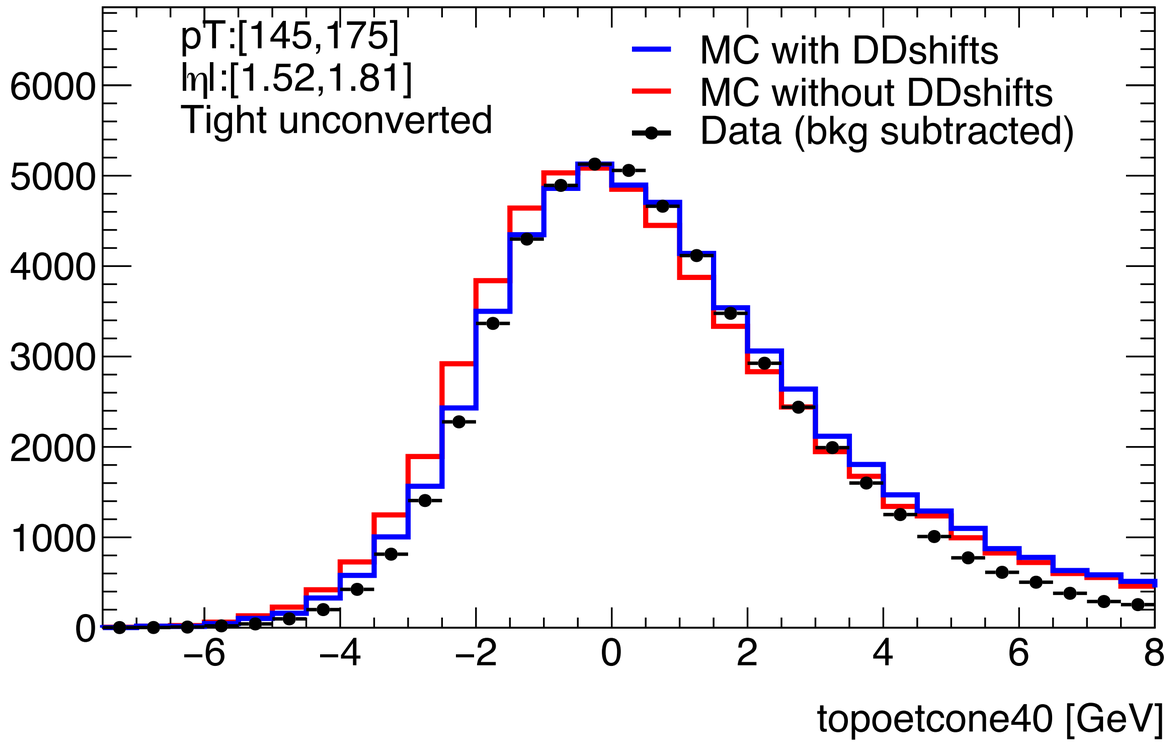

Different widths

Different efficiencies!

Conclusions on isolation measurements

Important pileup dependency

Photon isolation efficiencies measured for the full Run 2 data.

- Scale factors to be used by the ATLAS collaboration: within 2%.
- Systematic uncertainties: 2%-0.1%

Differences with respect to previous results:

- Improved background description.
- Updated estimation of leakage corrections leads up to a 7% efficiency increase for low E_T photons.

Strong dependency with increasing pileup motivates additional studies.

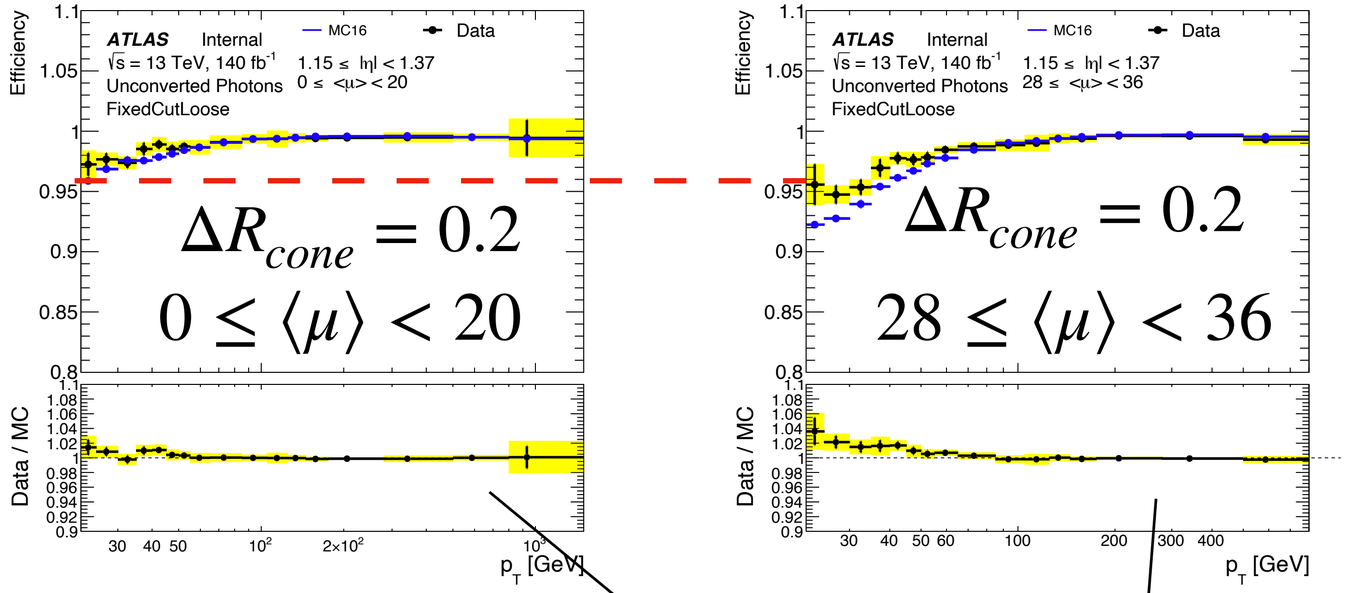

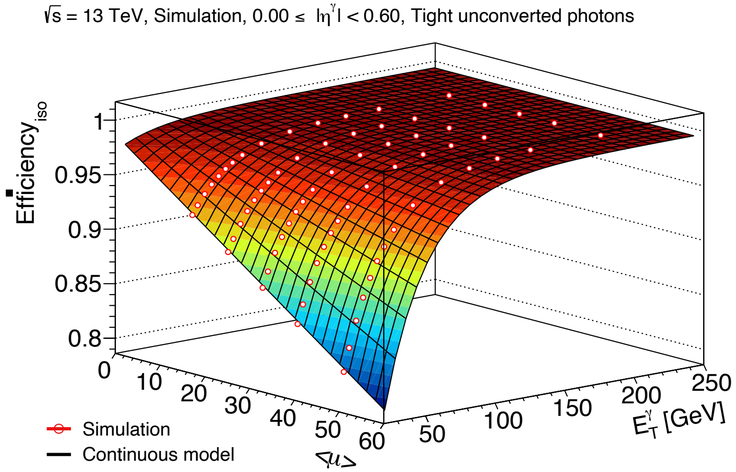

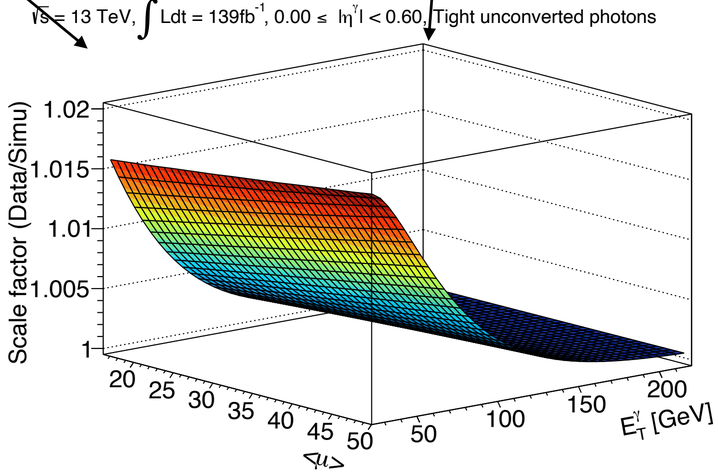

Bidimensional continuous corrections as a function of E_T^γ and $\langle\mu\rangle$.

Robust!

Photon isolation studies

Prospective studies on photon isolation using cluster-level information

Previous slides:

- Prompt photon → signal
- Fakes → background

Next slides:

- Clusters from **fakes** → signal
- Clusters from pileup→ background

Calo isolation vs PILEUP

Photon isolation performances are affected by increasing pileup $\langle\mu\rangle$.

- Additional topoclusters inside the isolation cone worsen the signal resolution, decreasing isolation efficiencies.

In general, topoclusters are reconstructed from two sources inside the isolation cone:

- **Pileup**: uniform distribution of topoclusters around the photon candidate, linear correlation with $\langle\mu\rangle$.
- **Fakes**: closer to the photon candidate, independent of pileup.

Goal: discriminate clusters from pileup and clusters from fakes

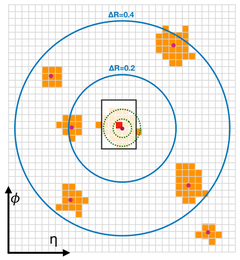

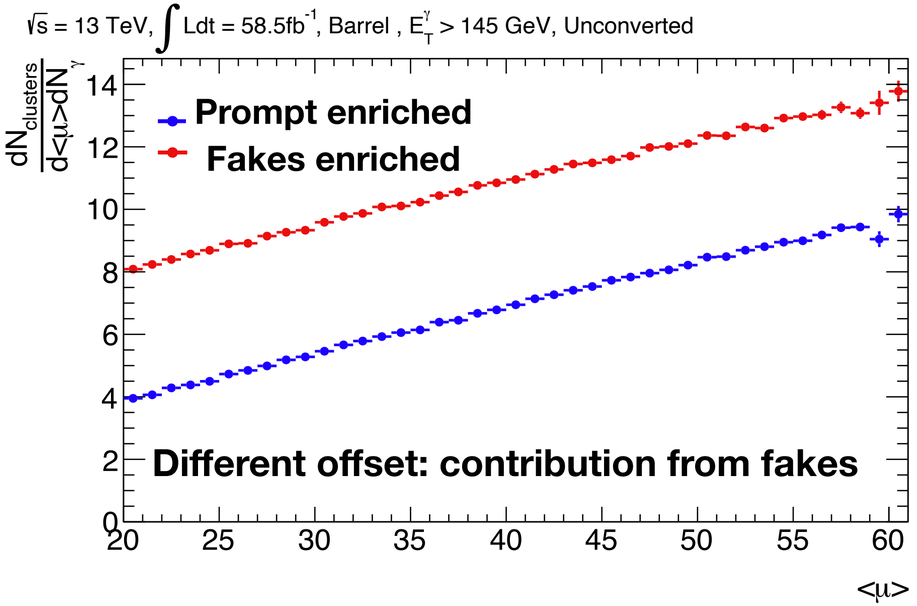

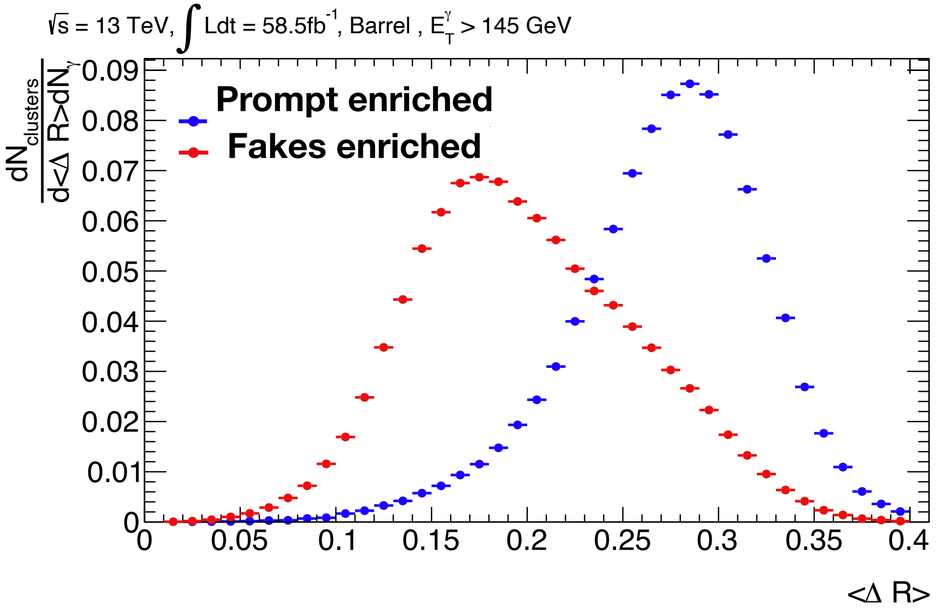

Cluster-level observables

These studies are purely **data-driven**!

Observables extracted from reconstructed clusters

- Calorimetric isolation uses the transverse energy $E_T^{cluster}$ and the angular distance between the cluster and the photon $\Delta R_{cl\gamma}$

Additional variables can provide information to discriminate clusters from fakes from clusters from pileup.

- **Time**: difference in time between the photon and each cluster. $\Delta t = t_{cluster} - t_{\gamma}$
- **EM fraction**: energy fraction of the cluster measured in the EM calorimeter. Four categories.

Pure EM: f_{EM} = 1 **Pure Had: f_{EM} = 0**

Mainly EM: 0.5 <f_{EM} <1 **Mainly Had: 0<f_{EM} <0.5**

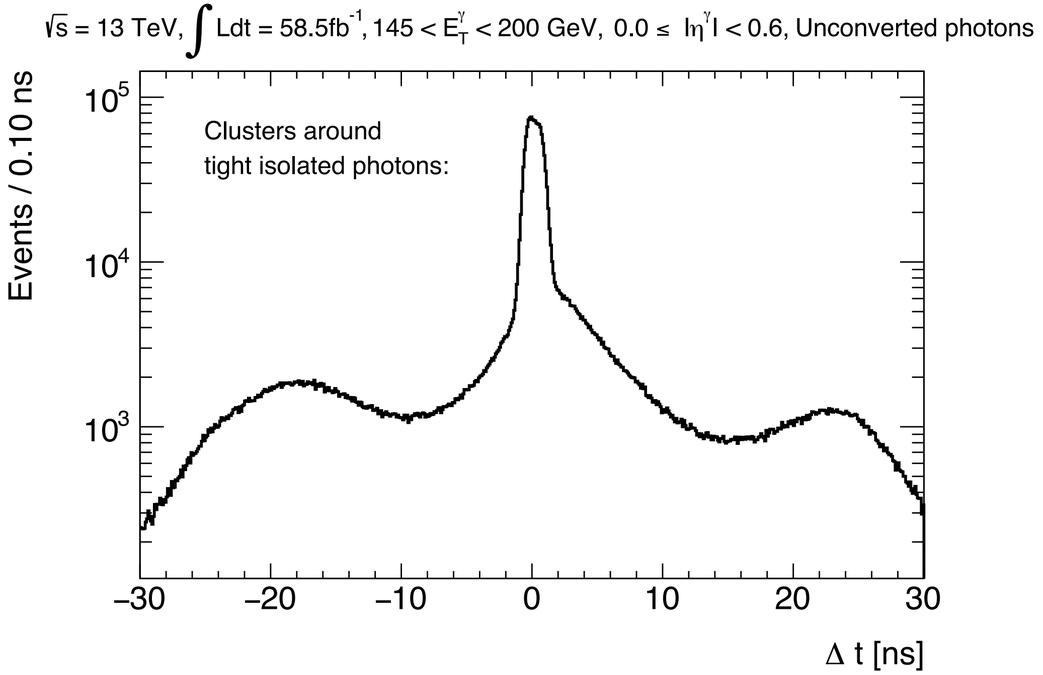

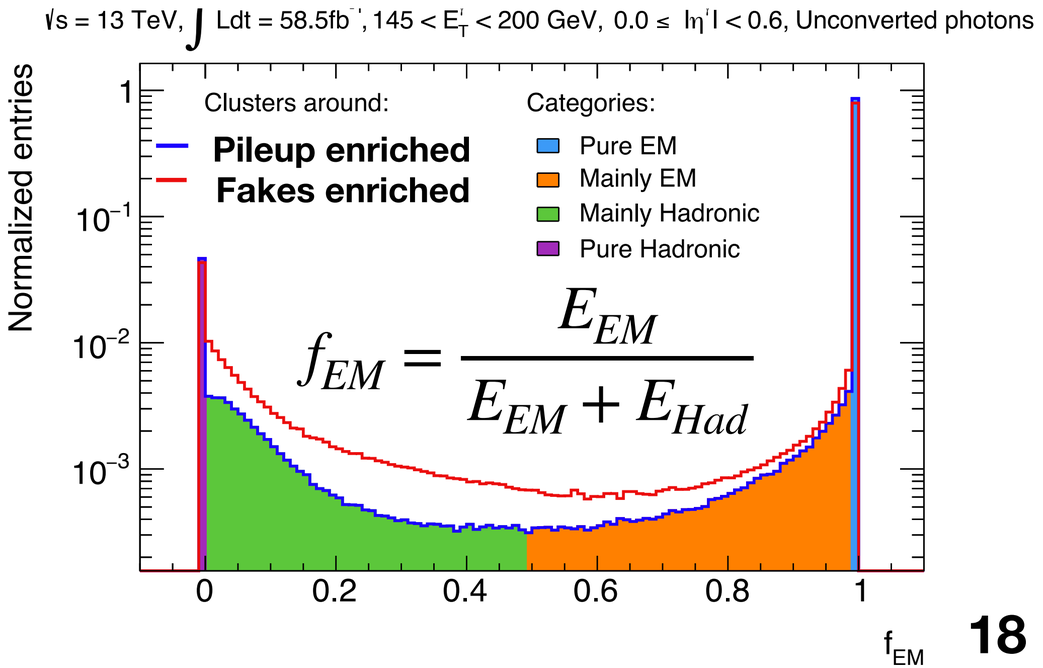

Topocluster characterization

These studies are purely **data-driven**!

Differences between the different categories are exploited to evaluate the likelihood for a topocluster to come from pileup or from a fake.

Model built with three different species:

$$P(\Delta t, E_T^{cluster}) = f_{in}P_{in} + f_{out}P_{out} + f_{fake}P_{fake}$$

P_{fake}: contribution from fakes

P_{in} and P_{out}: in and out of time pileup

Each P_i is the product of two 1-dimensional bifurcated Gaussians: $G(\Delta t) \otimes G(E_T^{cluster})$

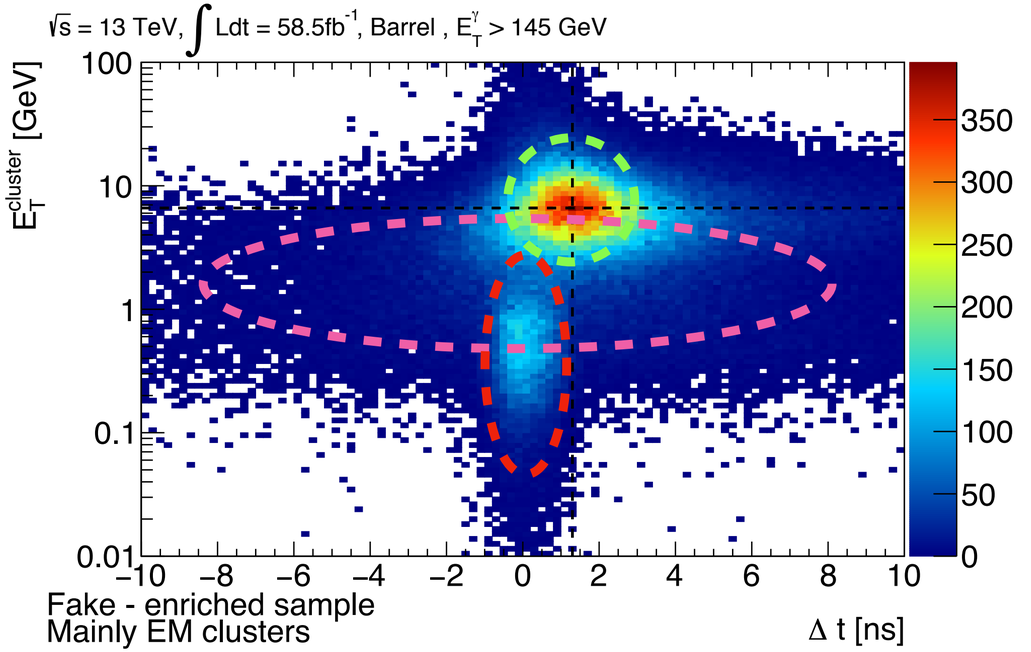

Simultaneous fit: 2 samples **for each** 4 categories

- Pileup enriched
- Fakes enriched

- Pure EM
- Mainly EM
- Mainly Had
- Pure Had

Common model, different fractions f_i

Fake-likelihood weights

These studies are purely **data-driven**!

$$w = \frac{P_{fake}}{P_{fake} + P_{pileup}}$$

with $P_{pileup} = fP_{in} + (1-f)P_{out}$

f ≡ in-time pileup fraction

Weight *w* built from the fitted PDFs.

- A topocluster with weight *w* close to 1 is very likely to originate from a fake.
- A topocluster with weight *w* close to 0 is very likely to originate from pileup.

This weight can be used to classify topoclusters.

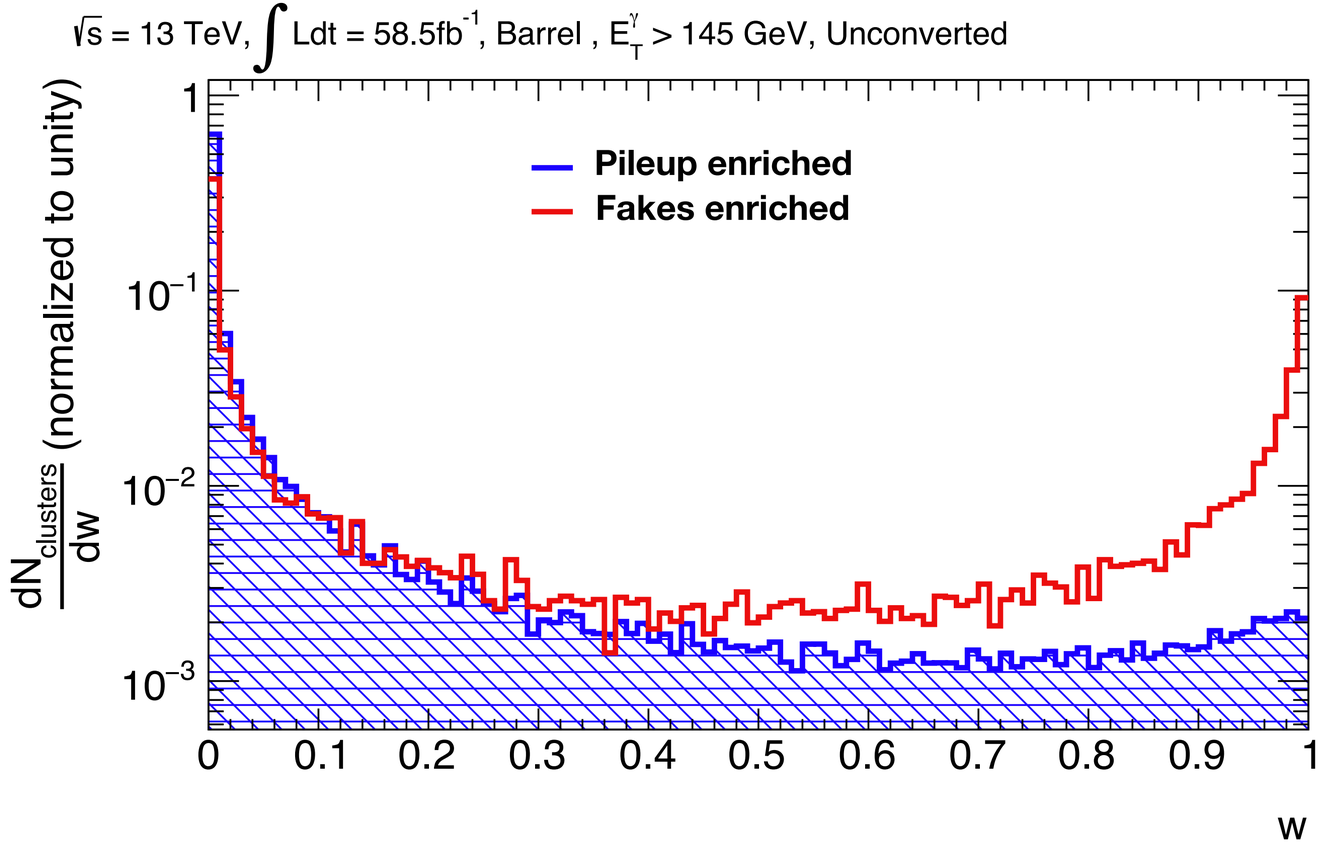

Crosschecks and validation

Validation of the weights *w* is performed under these two assumptions:

- Topoclusters from fakes are **independent from** $\langle\mu\rangle$.
- Topoclusters from pileup increase linearly with $\langle\mu\rangle$.

For each slice of *w*, the contribution of clusters from fakes is constant with $\langle\mu\rangle$.

Only 7% of the energy of the clusters from fakes is misidentified with *w*=0

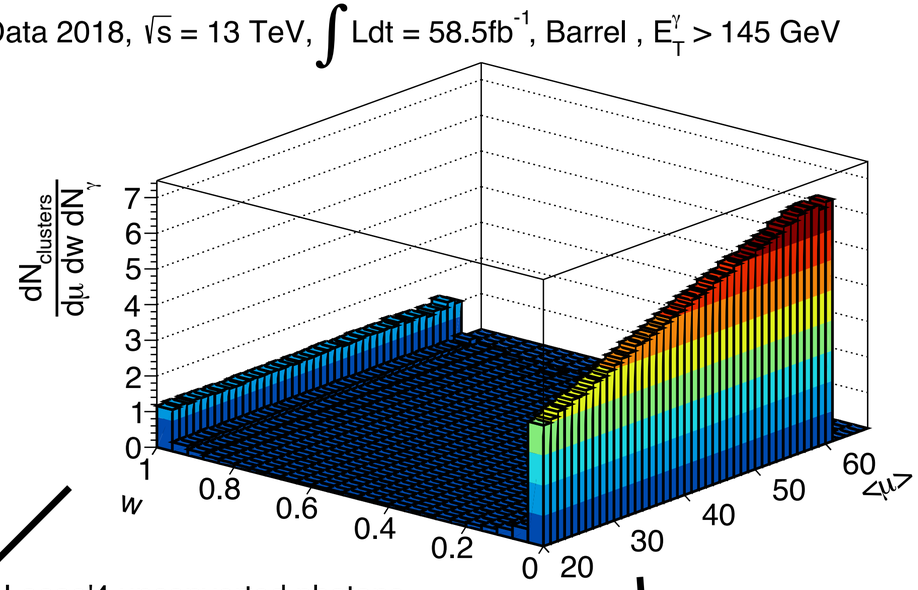

w=1

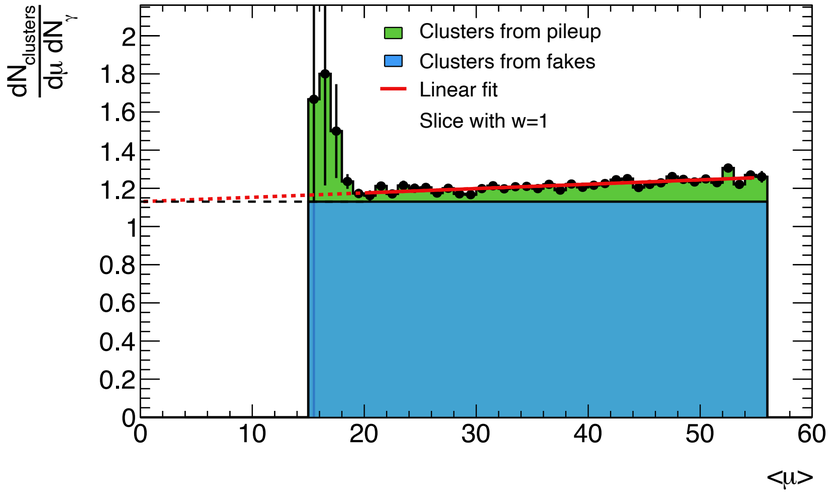

w=0

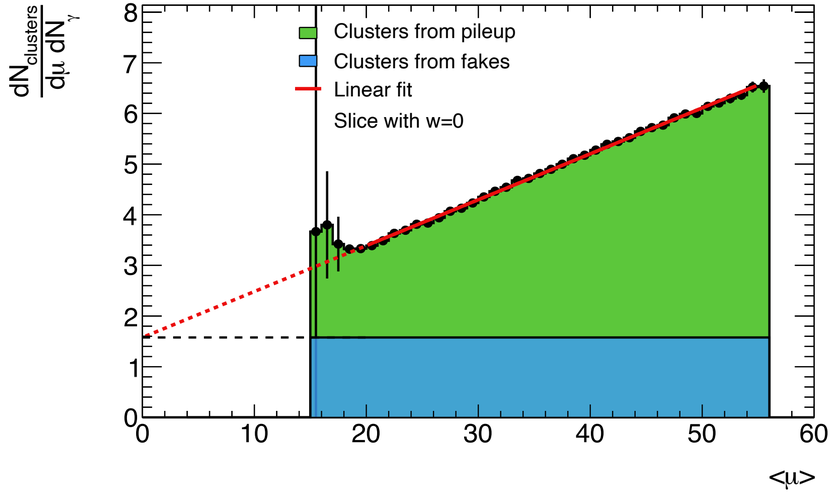

Impact on the isolation energy

Reminder: ideal isolation energy estimation ⟶ **Energy from clusters of the fake**

Proposal: use weights to compute a per-photon correction

$$E_{iso}^{nominal} = \sum_{r_i<\Delta R}^{clusters} E_T^i \rightarrow E_{iso}^{weighted} = \sum_{r_i<\Delta R}^{clusters} w^i(|\eta|, f_{EM}, E_T^i) E_T^i$$

Clusters with w=0 are directly removed!

- Current pileup correction from energy density of the event, which worsens the resolution.

Improves signal resolution by a factor x2

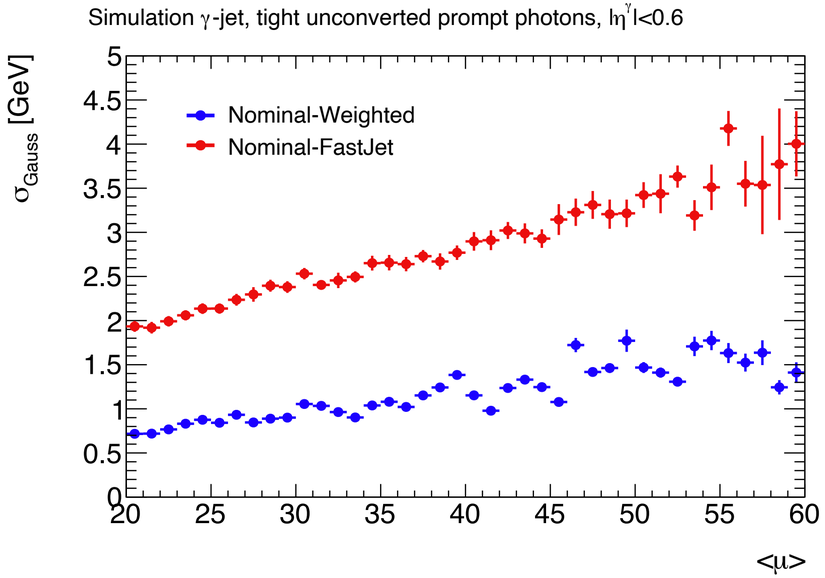

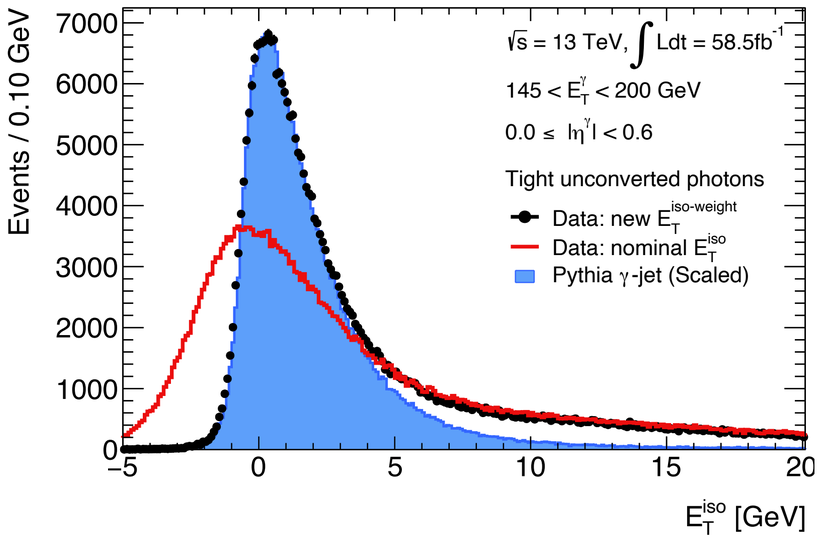

Contribution from fakes remains almost identical

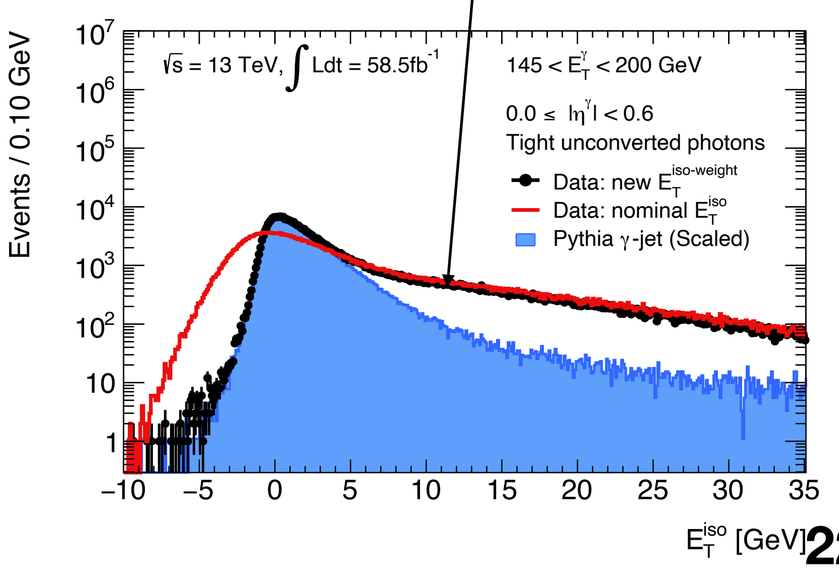

Conclusions on cluster-level studies

Topoclusters provide a larger discrimination between clusters from fakes and from pileup compared to what is currently in use.

- Timing and longitudinal information provide insight on the origin of the energy deposits.

Characterization of clusters from fakes has resulted in the definition of fake-likelihood weights that discriminate pileup energy deposits.

The presented studies are of importance in light of the increasing $\langle\mu\rangle$ environment

- Information can be used to improve prompt-fake discrimination.
- These results are expected to be used in Run 3, where $\langle\mu\rangle$ will increase from 34 to 60

Search for resonances in the diphoton channel below 65 GeV

Axion-like particles at hadron colliders

Hypothesis: New Physics scale, Λ_{NP}, lies beyond the reach of current accelerators.

- Signals at lower energies can appear as pseudo-Nambu-Goldstone bosons (pNGBs) of spontaneously broken approximate U(1) symmetries.

These are often referred to as axion-like particles (ALP)

- Naturally light → Arise from approximate symmetries
- Small couplings with SM fields → Controlled by Λ_{NP}

Given that no new physics has been observed and $m_a \ll \Lambda_{NP}$, the relevant range for the LHC is $f_a \sim 0.1 - 10\ TeV$

- In this range, only couplings to gluons and photons are relevant.

$$\mathscr{L}_{EFT} \ni \frac{a}{4\pi f_a}\left(\alpha_3 c_3 G\tilde{G} + \alpha_2 c_2 W\tilde{W} + \alpha_1 c_1 B\tilde{B}\right)$$

Dominates the production of ALP

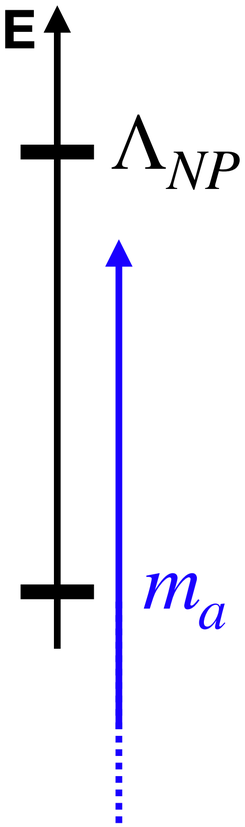

No restriction for the ALP mass below Λ_{NP}

$g_* \equiv 4\pi$

$f_a \equiv$ decay constant (scale of the U(1) breaking)

$$\Gamma_{gg} \propto \alpha_s^2 \frac{m_a^3}{f_a^2} \qquad \Gamma_{\gamma\gamma} \propto \alpha_{QED}^2 \frac{m_a^3}{f_a^2}$$

Narrow resonances for our mass range

Theoretical motivations

Such a light particle appears in a plethora of theoretical models:

- Strong CP problem: no CP violation in the strong sector
  - "Heavy axion": inspired on the QCD axion from Peccei & Quinn.

$$\mathscr{L}_{QCD} \ni \frac{\theta g^2}{32\pi} G\tilde{G} + \frac{a}{f_a} G\tilde{G}$$

Neutron EDM $\frac{d_{n,exp}}{d_{n,theo}} \sim 10^{-9}$

- Dark Matter (DM) mediators
  - Many theories include pseudoscalar particles, mediators between a dark sector and the SM

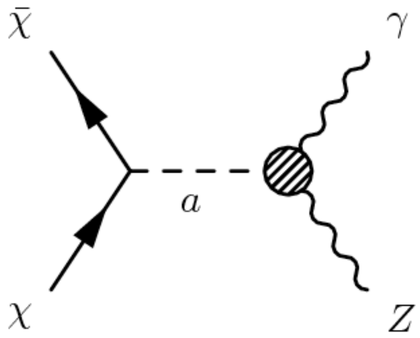

- Naturalness of the EW scale
  - Such ALP appears in frameworks that provide an explanation to this, like SUSY (R-axion)

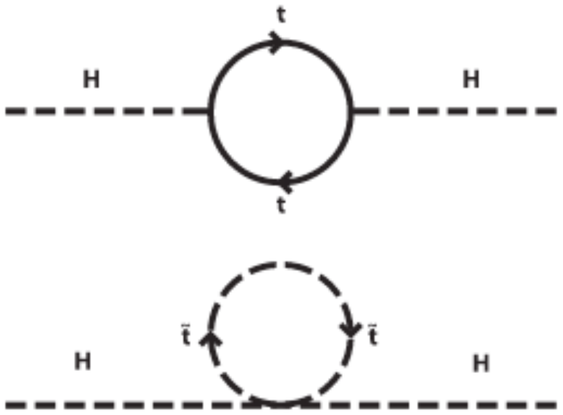

Experimental constraints

Existing search **gap** in resonance searches.

Both ATLAS and CMS experiments have set limits down to to 65 GeV up to 2 TeV masses.

Goal: push the 65 GeV limit towards lower masses.

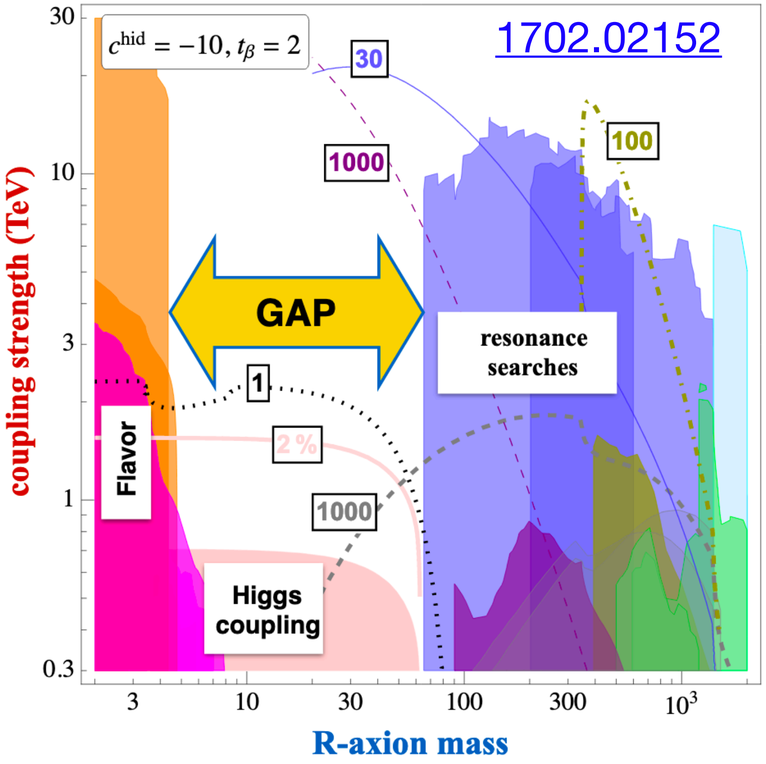

Poorly explored region!

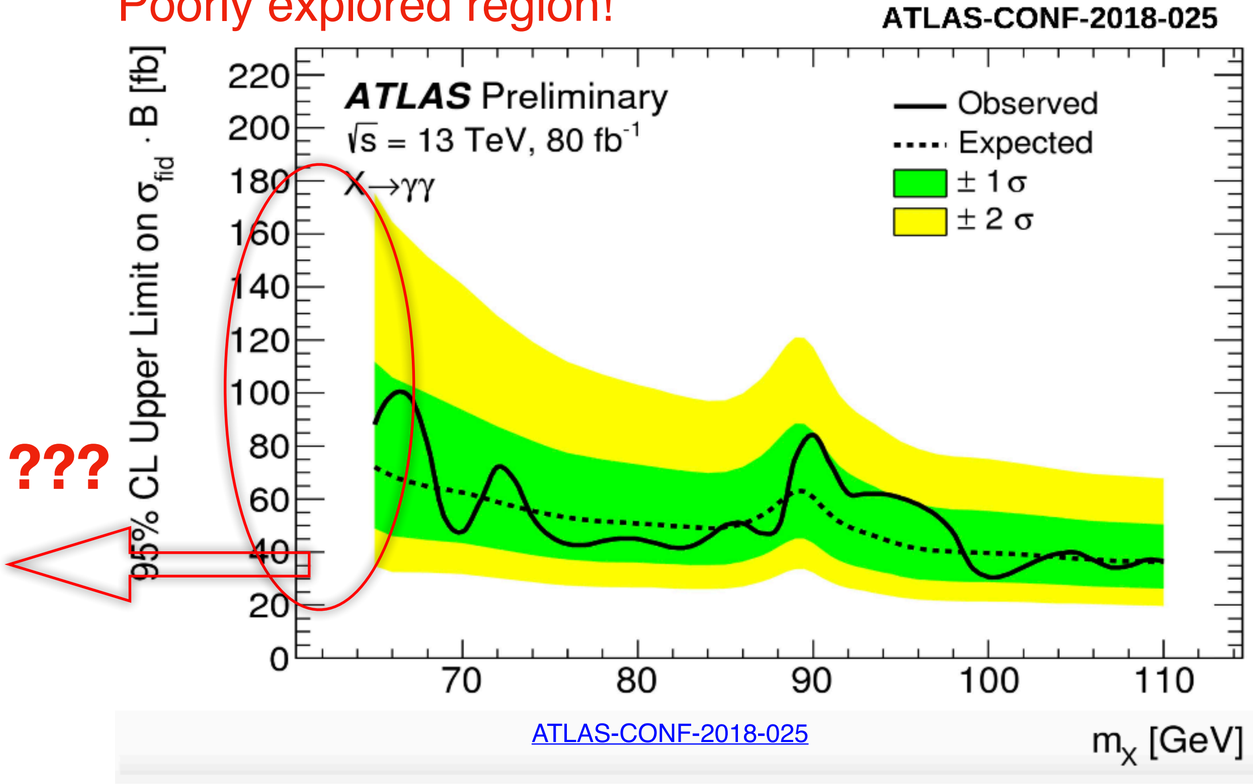

ATLAS-CONF-2018-025

Experimental limitations

Three main aspects set a lower bound in the mass that can be reached.

- Trigger
- Performance efficiencies
- Isolation

QCD rate of two low energy photons is too large.

- Only photons with energies over certain energy threshold are recorded

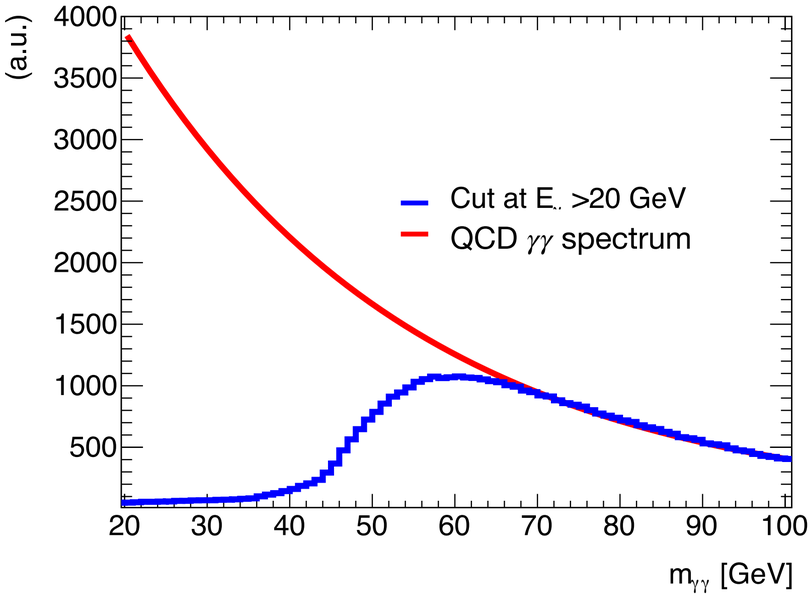

Trigger thresholds shape the $m_{\gamma\gamma}$ distribution, making difficult its description

Photon ID and isolation efficiencies decrease at lower photon energies

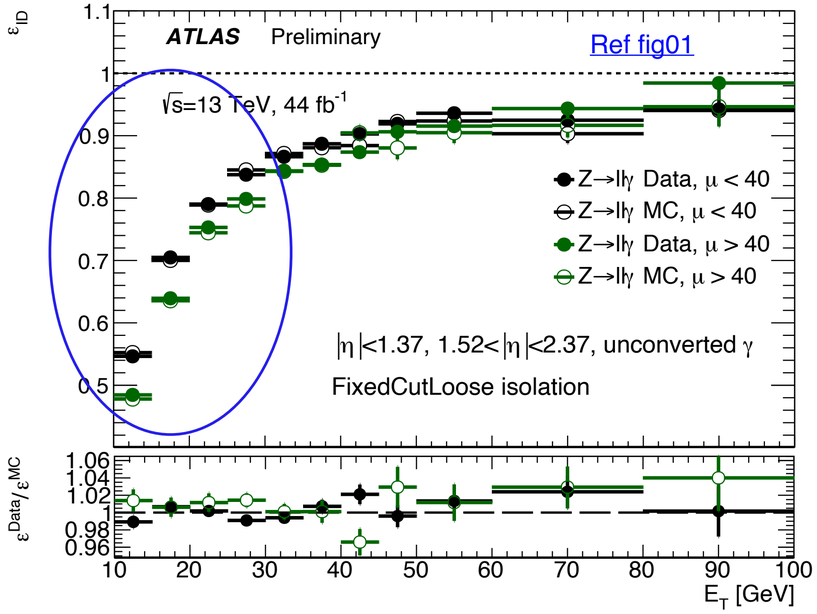

Two close-by photons may “kill” each other if they are within the isolation cone of the other photon.

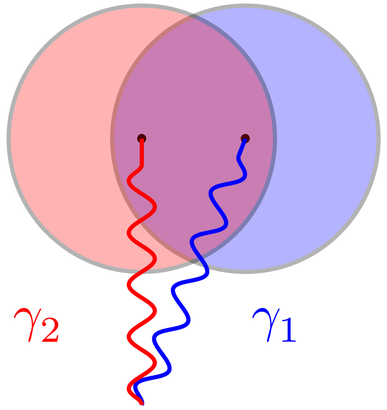

Given:

$\Delta R_{\gamma_1\gamma_2} > 0.2$

$P_{T,\gamma_1}, P_{T,\gamma_2} > 22GeV$

$m_{\gamma\gamma} \sim 10\ GeV$

Analysis strategy

Bump search strategy: benefit from the excellent performance of the EM calorimeter to look for an event excess over a known background.

Selection: 2 triggered photons, tightID, isolation, and ET>22 GeV

Boosted diphoton selection: flattens out diphoton background shape.

- Diphoton system is required to have large transverse momentum.
- Trade-off between sensitivity and low mass reach: $p_T^{\gamma\gamma} > 50\ GeV$

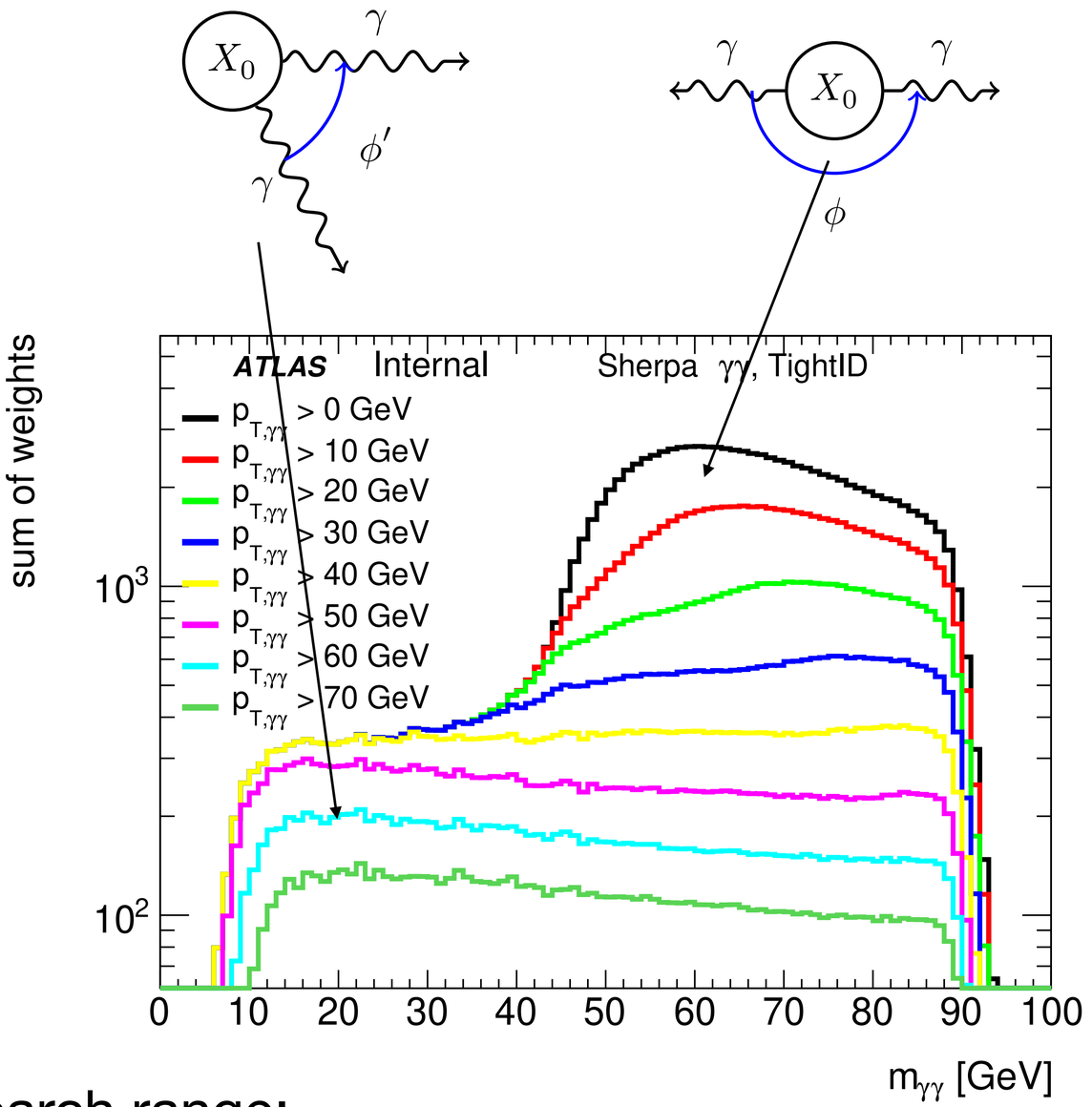

Search range:

- Low mass turn-on description
- Z boson resonance and trigger turn-on

Statistical framework

Maximum likelihood fit to data.

Model with two species: signal and background

Test-statistic: $q_{\mu_{test}} = -2\dfrac{\mathscr{L}\left(\mu_{test}, \hat{\hat{\theta}}\right)}{\mathscr{L}\left(\hat{\mu}, \hat{\theta}\right)}$

Signal and background PDFs

Nuisance parameters constraints

$$\mathscr{L}\left(data \,|\, \sigma_{fid}, \boldsymbol{\theta} : \{\boldsymbol{\theta_s}, \boldsymbol{\theta_X}, \boldsymbol{\theta_b}\}\right) = e^{-(N_X+N_b)} \left[\prod_{i=0}^{n} N_X(\sigma_{fid}) \cdot S(m_{\gamma\gamma,i}) + N_b \cdot B(m_{\gamma\gamma,i})\right] \left[\prod_{i=0}^{dim\boldsymbol{\theta}} Gauss(\theta_i)\right]$$

Signal and background Yields

Ingredients:

- Analytical description of the PDFs
- Signal efficiencies as a function of m$\gamma\gamma$
- Systematics

Statistical framework

Maximum likelihood fit to data.

Model with two species: signal and background

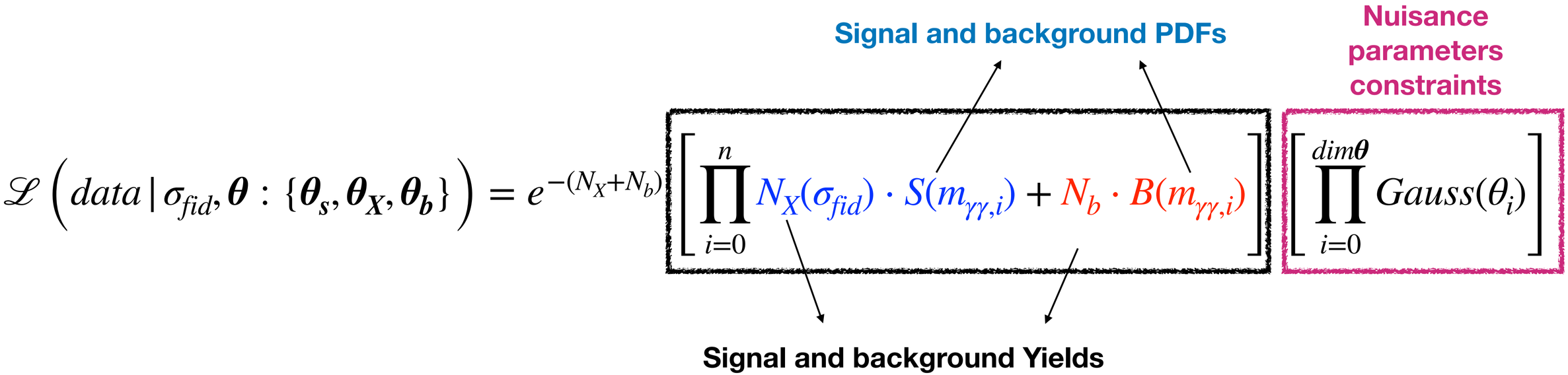

Ingredients:

- Analytical description of the PDFs
- Signal efficiencies as a function of m$\gamma\gamma$
- Systematics

Signal modelling

Signal shape obtained from simulated samples

- Signal parametrization obtained using a Gaussian core + 2 power law tails
- The width arises from the resolution of the detector.

Signal width increases with $m_{\gamma\gamma}$ (0.2-1.0 GeV)

Excellent mass resolution

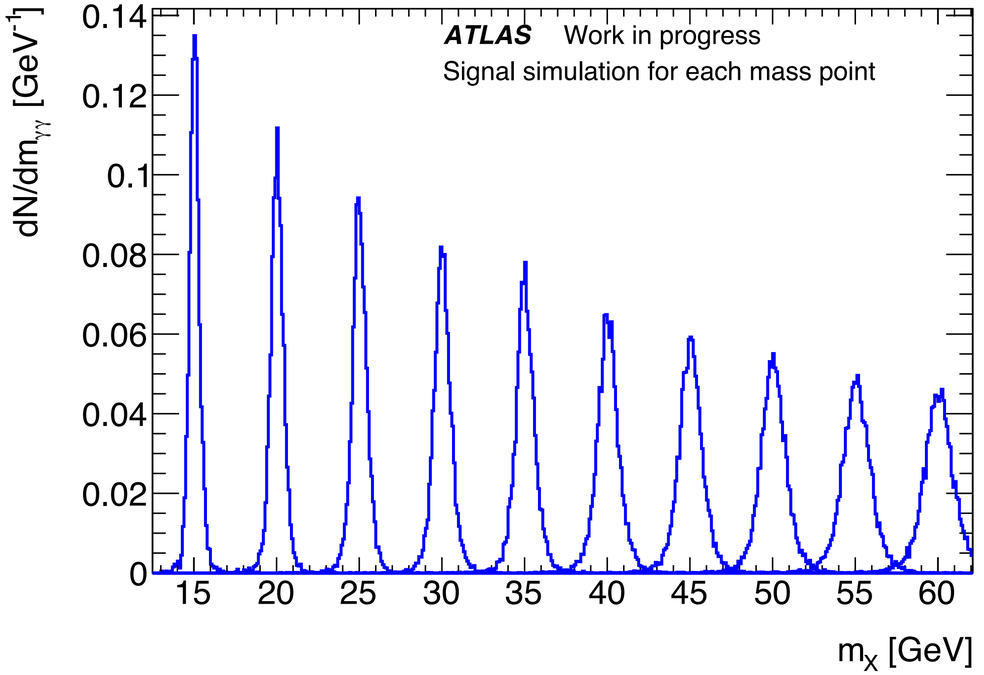

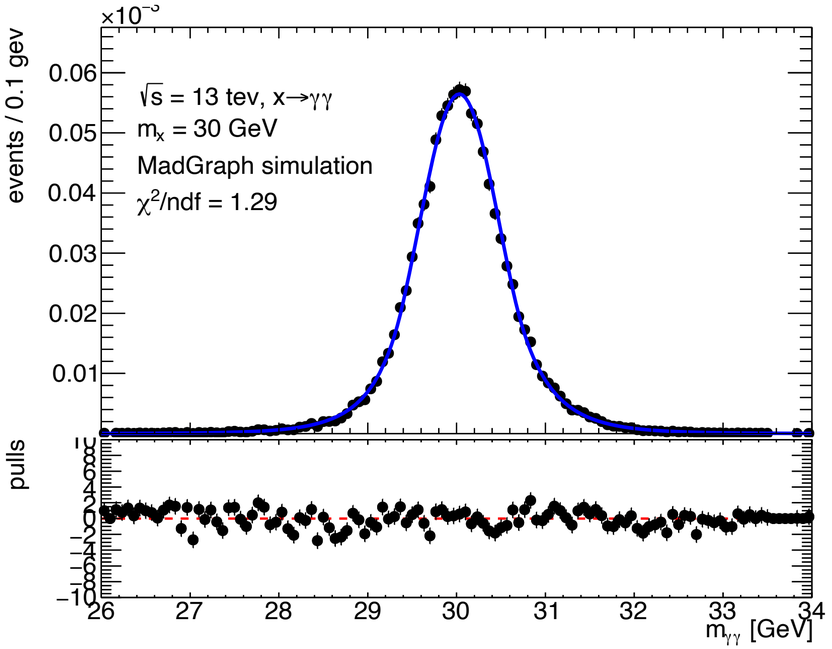

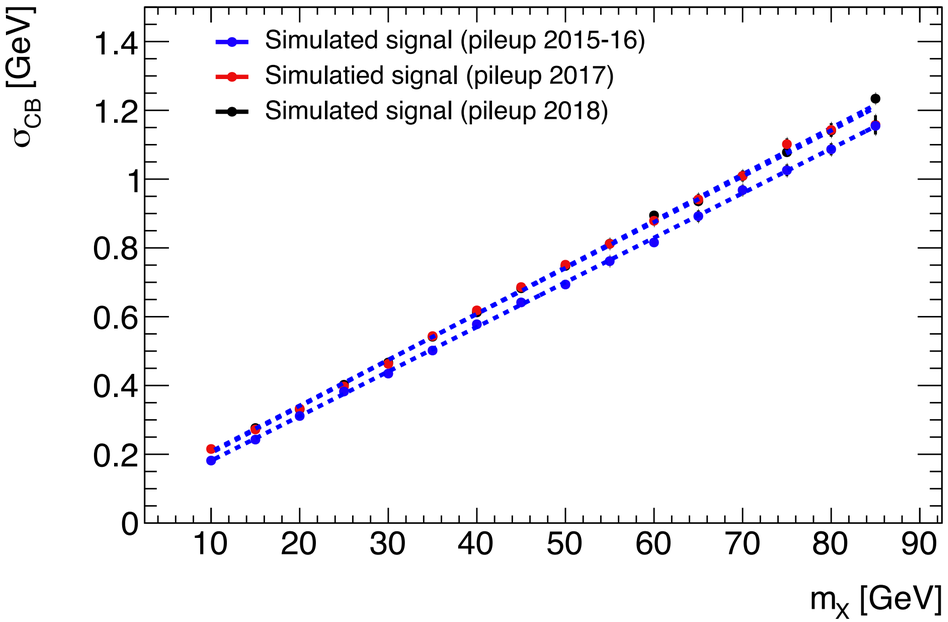

$$\frac{\sigma}{m_{\gamma\gamma} = 80\ GeV} = 1.3\,\%$$

$$\frac{\sigma}{m_{\gamma\gamma} = 10\ GeV} = 2.0\,\%$$

Background modelling introduction

Diphoton analysis is affected by non-resonant background from:

- Irreducible **($\gamma\gamma$)** from QCD diphotons.
- Reducible background **(γjet)** QCD γjet or dijet events in which one or both jets are misidentified as photons (γj, jγ or jj)

Strategy: build a full background template which is then described by an analytical function.

- Obtain irreducible and reducible templates (shapes) independently.
- Estimate the $\gamma\gamma$ purity and combine the two components accordingly.

Irreducible $\gamma\gamma$

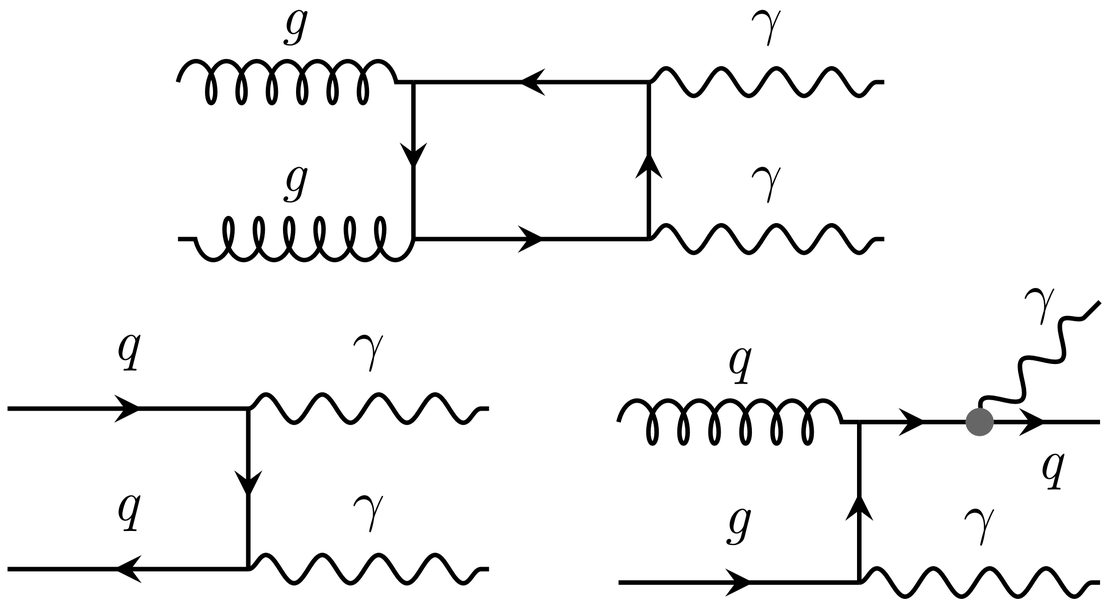

Reducible γ-jet and dijet

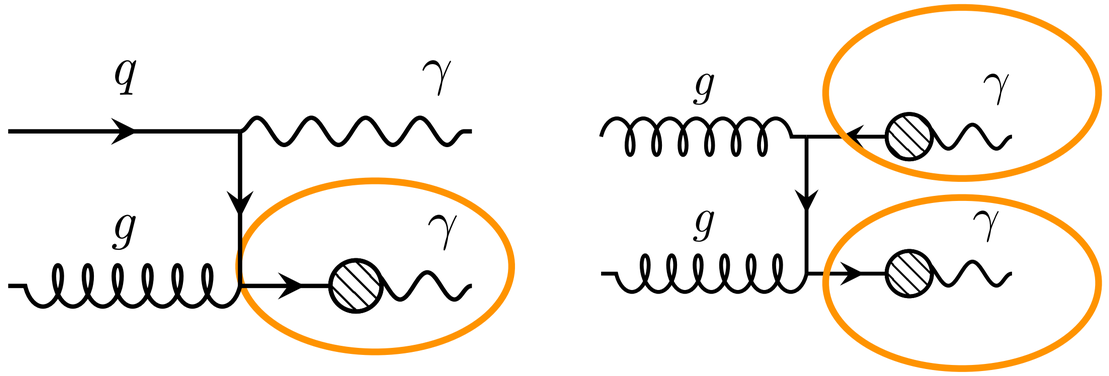

Identified as a prompt photons!

Background modelling

The $\gamma\gamma$ component is extracted directly from simulated QCD diphoton events.

The γjet component is obtained from **data control regions**.

- Limited in statistics

Diphoton purity: $f_{\gamma\gamma} = 0.64 \pm 0.03$

Complete background template is obtained by reweighing the $\gamma\gamma$ template.

Background shape is described with analytical functions

- $\gamma\gamma$ component: turn-on + decreasing exponential
- γjet component: decreasing exponential

New MC samples 15x larger was produced during Christmas break.

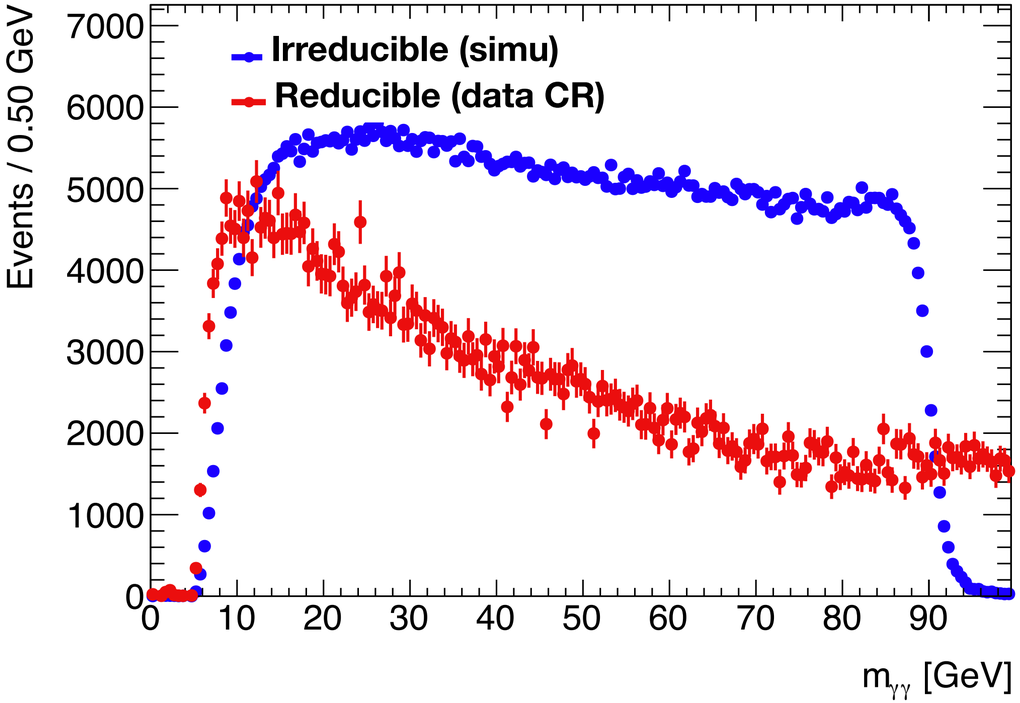

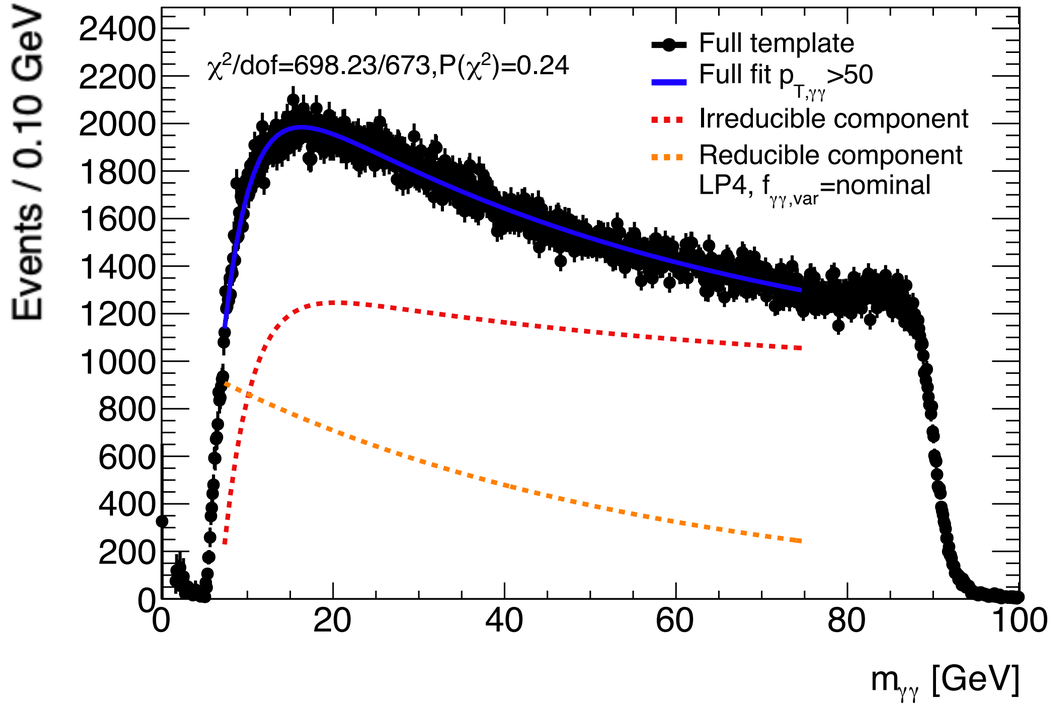

Statistical framework

Significance of an event excess extracted from likelihood fit to data

Model with two species: signal and background

Nuisance parameters constraints

$$\mathscr{L}\left(data\,|\,\sigma_{fid},\boldsymbol{\theta}:\{\boldsymbol{\theta_s},\boldsymbol{\theta_X},\boldsymbol{\theta_b}\}\right) = e^{-(N_X+N_b)}\left[\prod_{i=0}^{n} N_X(\sigma_{fid})\cdot S(m_{\gamma\gamma,i}) + N_b\cdot B(m_{\gamma\gamma,i})\right]\left[\prod_{i=0}^{dim\boldsymbol{\theta}} Gauss(\theta_i)\right]$$

Signal and background **Yields**

Ingredients:

- Analytical description of the PDFs
- Signal efficiencies as a function of m$\gamma\gamma$
- Systematics

$$N_X(m_X,\sigma_{fid},\boldsymbol{\theta}_X) = \sigma_{fid}\cdot\mathscr{L}_{int}\cdot C_X(m_X)$$

Cross-section **Luminosity** **Signal Efficiency**

Signal efficiencies

Sensitivity usually provided in terms of **cross-sections**

- Induces model-dependencies

Approach: provide limits in a **fiducial phase-space**

- Detector effects → correction factor C_X
- From fiducial to full phase space → acceptance Ax

Fiducial volume is defined by applying truth-level cuts that match closely the reconstruction selection.

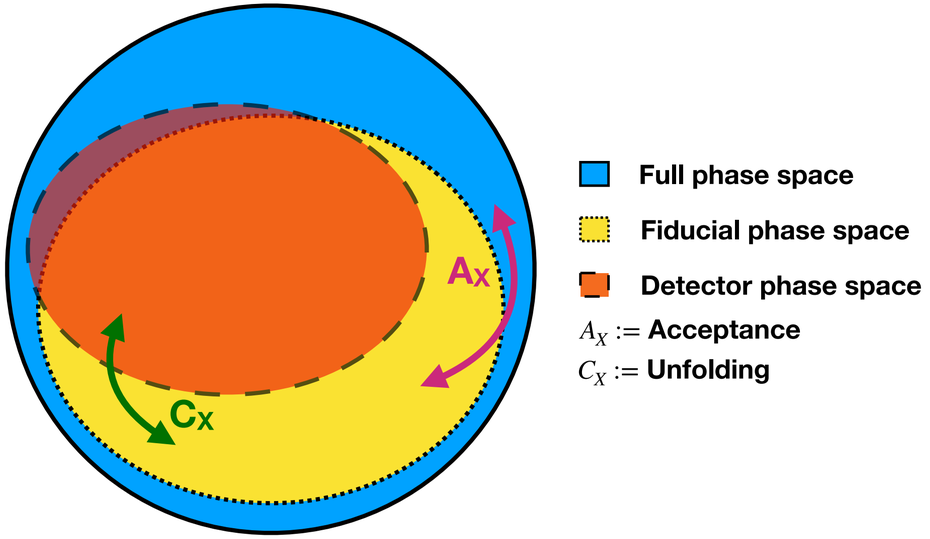

$$\sigma_X \cdot \mathcal{B}(X \to \gamma\gamma) = \frac{\sigma_{X,fid} \cdot \mathcal{B}(X \to \gamma\gamma)}{A_X} = \frac{N^{reco}_{selection}}{A_X C_X \mathcal{L}}$$

$$C_X = \frac{N^{reco}_{selection}}{N^{truth}_{fiducial}} \qquad A_X = \frac{N^{truth}_{fiducial}}{N^{truth}_{all}}$$

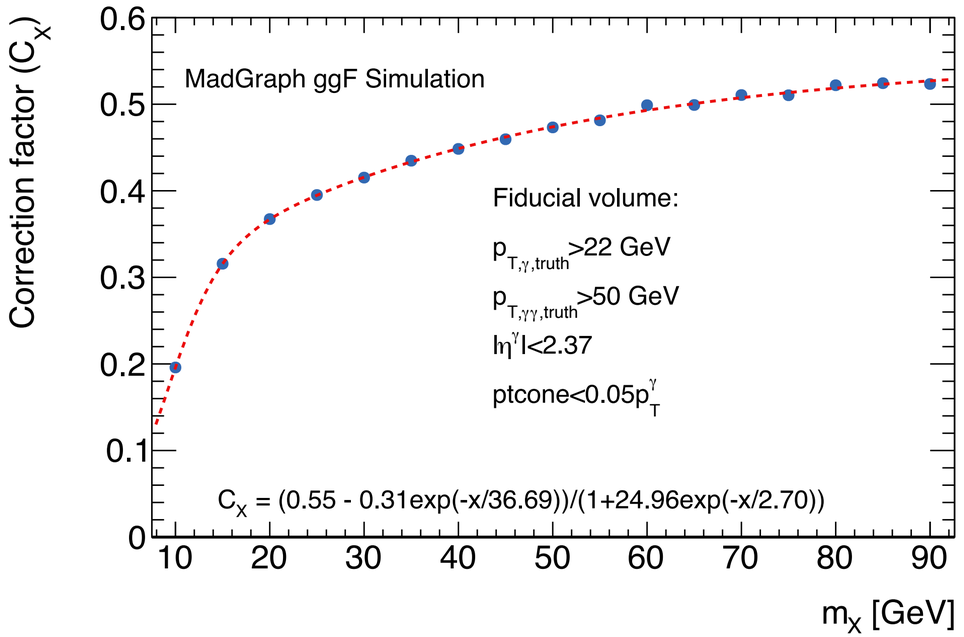

Statistical framework

Significance of an event excess extracted from likelihood fit to data

Model with two species: signal and background

Nuisance parameters constraints

$$\mathscr{L}\left(data\,|\,\sigma_{fid},\boldsymbol{\theta}:\{\boldsymbol{\theta_s},\boldsymbol{\theta_X},\boldsymbol{\theta_b}\}\right) = e^{-(N_X+N_b)}\left[\prod_{i=0}^{n} N_X(\sigma_{fid})\cdot S(m_{\gamma\gamma,i}) + N_b\cdot B(m_{\gamma\gamma,i})\right]\left[\prod_{i=0}^{dim\boldsymbol{\theta}} Gauss(\theta_i)\right]$$

Signal and background Yields

Ingredients:

- Analytical description of the PDFs
- Signal efficiencies as a function of m$\gamma\gamma$
- Systematic uncertainties

$$N_X(m_X,\sigma_{fid},\boldsymbol{\theta}_X) = \sigma_{fid}\cdot\mathscr{L}_{int}\cdot C_X(m_X)\cdot\prod_{k=0}^{dim\boldsymbol{\theta}_X} K_k(\theta_k) + \sigma_{SS}\theta_{SS}$$

Fit bias

Nuisance parameters

Systematic uncertainties: Fit bias

Definition: difference between fitted and expected signal yield

Estimated from S+B fits to background-only templates

Significant source of systematic uncertainty in various ATLAS analyses.

- Smoothing techniques mitigate the impact of statistical fluctuations in the template

With the current available MC, SS is below 50% of the statistical uncertainty in the whole mass range.

- Will be reevaluated with extended MC.

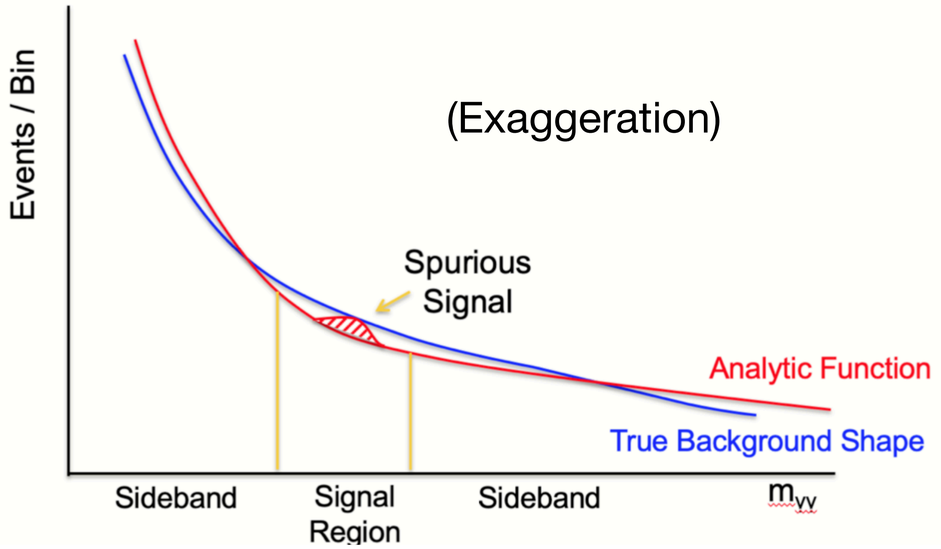

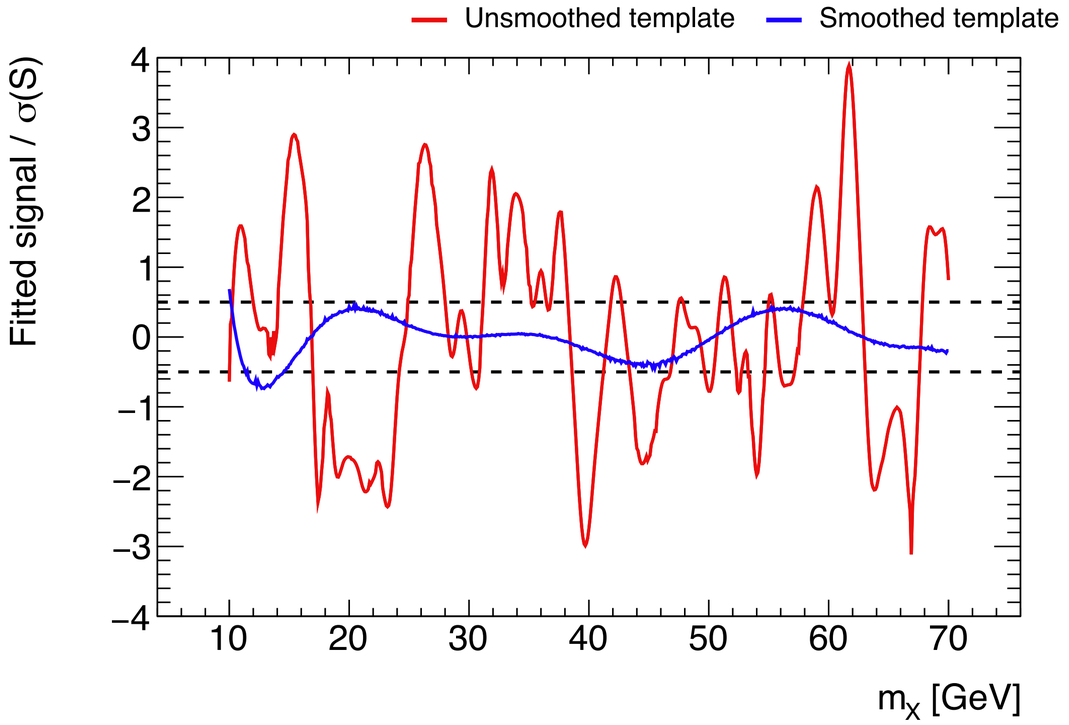

Summary of systematics

Source	Uncertainty
Signal yield	
Theoretical uncertainty	$^{+9}_{-5}$% (at 10 GeV) – 2.0% (beyond 85 GeV)
Pile-up reweighting	± 3.5% (at 10 GeV) – 2 % (beyond 15 GeV), mass dependent
Photon identification	±2.0%
Isolation efficiency	±2.0%
Trigger	±1.0%
Luminosity (2015–2018)	±1.7%
Photon energy scale/resolution	negligible
Signal modeling	
Photon energy resolution	$^{+6\%}_{-5\%}$
Photon energy scale	negligible
Pile-up reweighting	negligible
Background	
Spurious signal	$0.5\sigma_{\text{stat}}$ 160-110 events, NWA

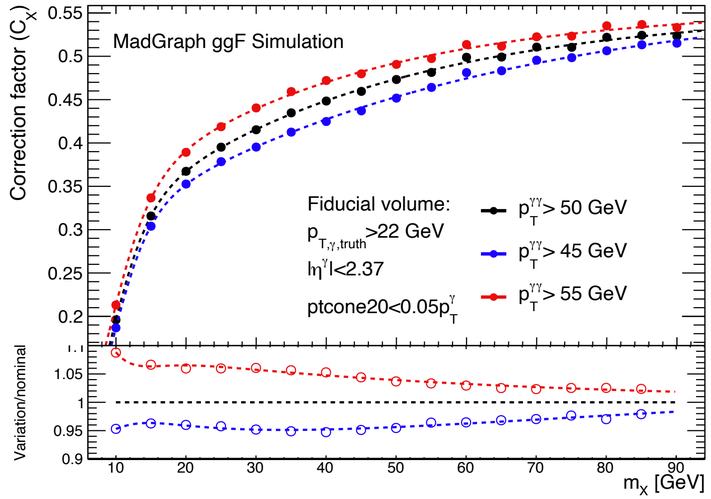

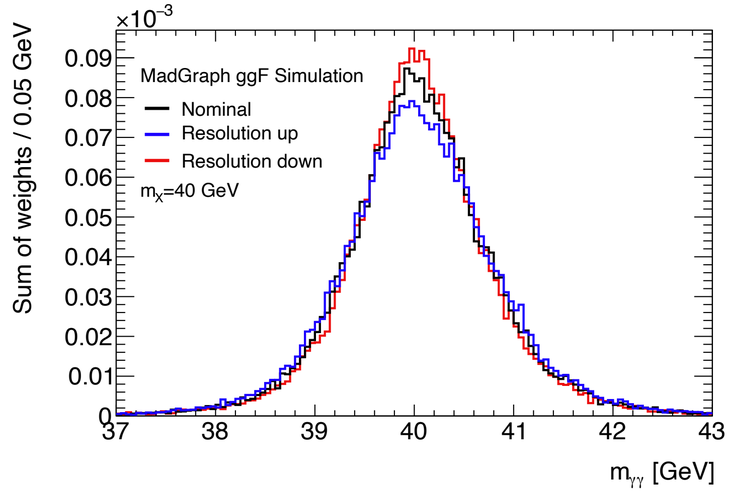

- In general, small systematics compared to the statistical uncertainty.
- Largest expected systematic from spurious signal.

Definitive value for the spurious signal systematic to be evaluated with the new sample extension

Expected limits

Expected sensitivity obtained through a maximum likelihood fit to an Asimov dataset of the background model.

Compensation of competing effects leads to a relatively flat limit

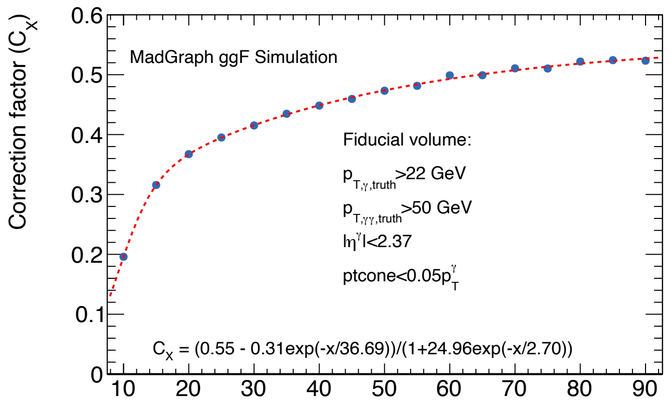

Signal efficiencies

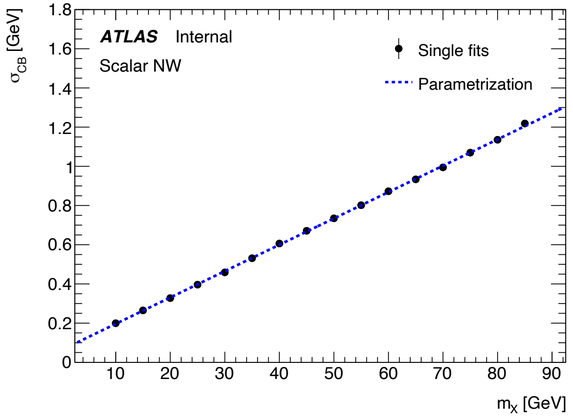

Signal width

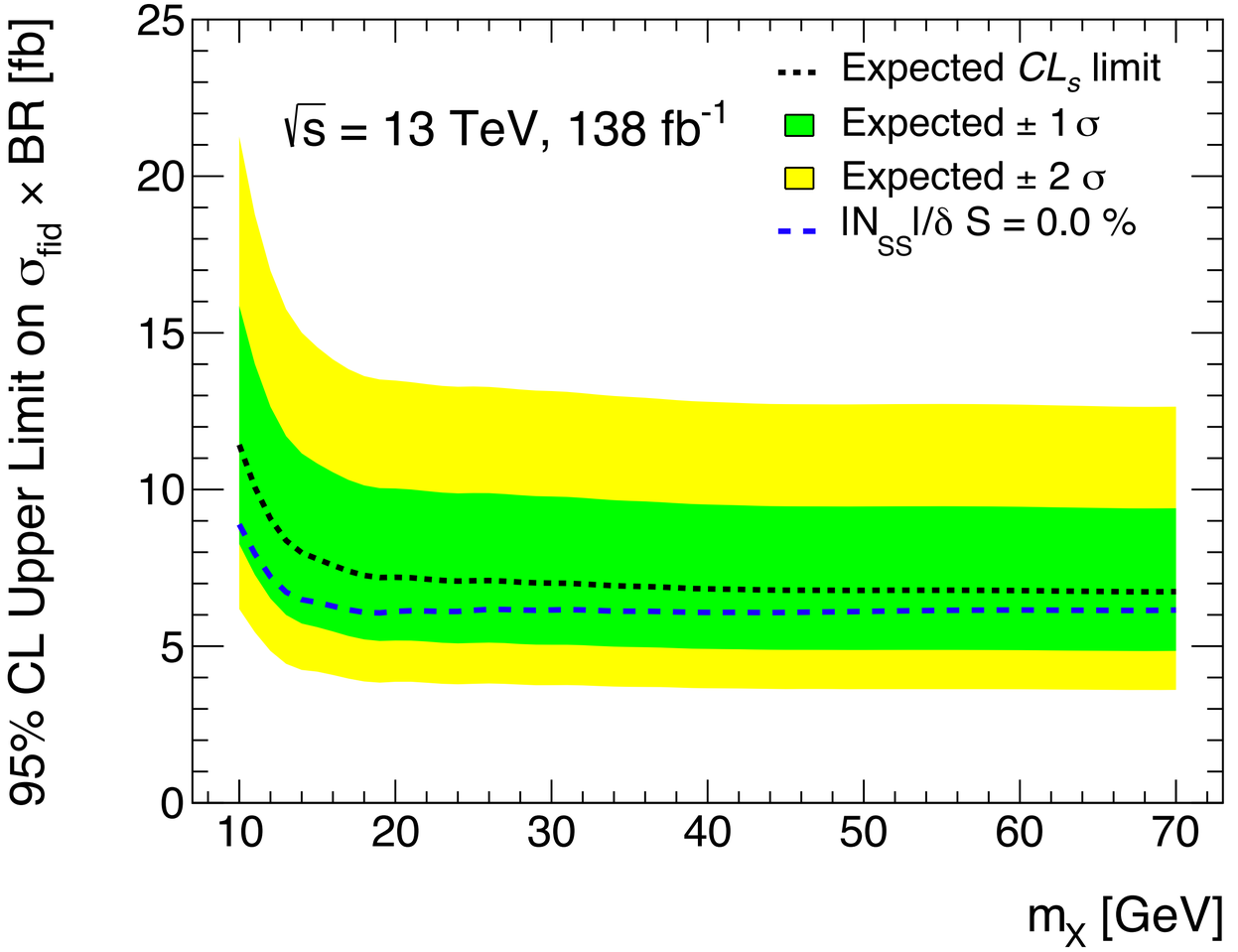

Current search range [10,70], to be validated with the extended MC

Where are our limits placed in the ALP landscape?

Limits set on the EFT decay constant f_a (theory section!)

- Model dependent limit (ggF, $p_T^{\gamma\gamma}$ cut,…)
- Similar sensitivity to more inclusive searches in the common region.

This analysis provides the strongest limits on a hypothetical resonance produced in gluon fusion that decays to two photons.

- Other searches limited by the production mechanism (for instance, light-light scattering in heavy ion collisions)

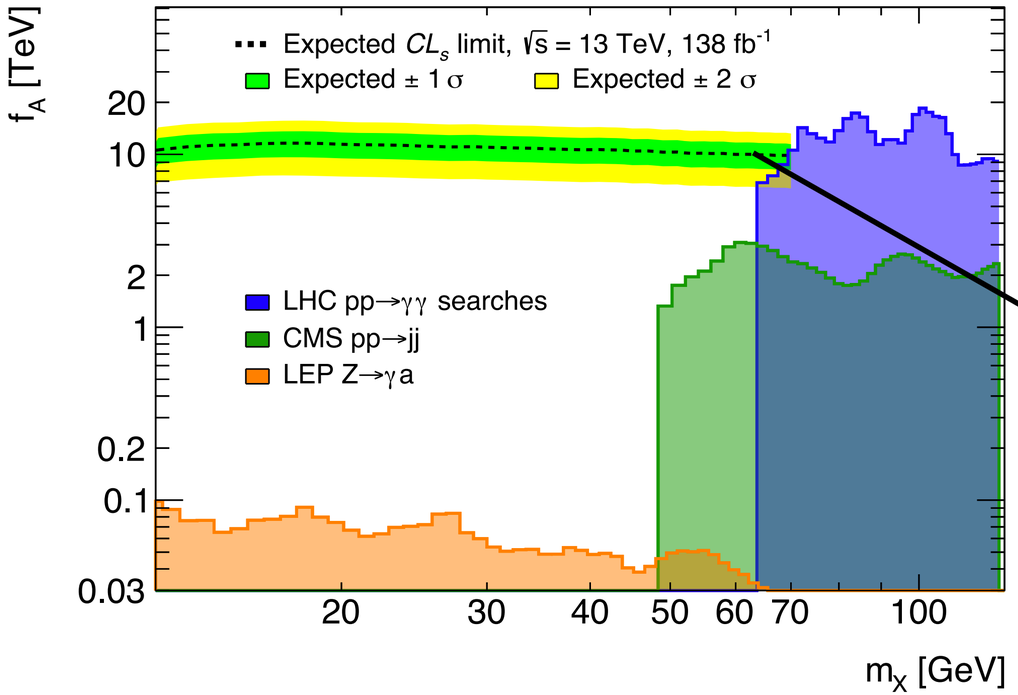

$$\Lambda_a \sim 32\pi^2 \frac{f_a^2}{\alpha_{em}^2} \sim 6 \cdot 10^6 f_a^2$$

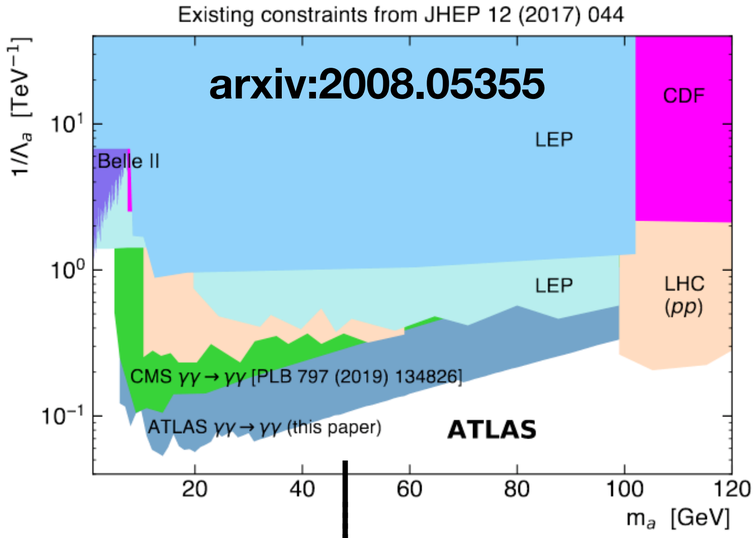

$$\frac{1}{\Lambda_a} \sim 10^{-6} \frac{1}{6 f_a^2} \sim 10^{-8}$$

Much stronger!

Conclusions on the diphoton search

Analysis strategy for diphoton resonance searches for masses below 65 GeV

- Edge of performances and efficiencies

Boosted selection eases the description of the background

- Allows to attain lower diphoton masses

Strongest limit on a hypothetical resonance produced in gluon fusion that decays to two photons below 65 GeV

- Statistically dominated except for the fit bias uncertainty
- Analysis currently under internal review. Moriond as target conference.

Summary

Works performed during my thesis cover photon performances and a search in the diphoton channel.

Photon isolation performances

- Extraction of scale factors to be used by the ATLAS collaboration
- Prospective studies to make calorimetric isolation more resilient against pileup
- Cluster-level pileup subtraction more robust than per-event subtraction

Search for resonances below 65 GeV in the diphoton channel

- Analysis covers a poorly explored region with an original approach
- Contributions to almost every step of the analysis
- Diphoton ALP searches at the LHC during Run 3 will be able to explore orthogonal regions of the phase space.

Thanks for your attention

Backup

Backup list

- Topocluster reconstruction
- Photon calibration
- Topocluster sample definition
- Track iso (and also against pileup)
- XTalk
- Timing topocluster
- Cb things
- Myy y ptyy, how low
- Isolation details
- Pileup mismodelling
- Primakoff effect
- ILC

Expected questions

Expected question #1

- **Why is there a time delay of 1-2ns for the clusters from fakes?**

- Time of each cluster computed as the energy squared-weighted average of the cells time.
- The time of each cell is calibrated in such a way that a neutrino traveling from the IP would give a signal measured at t=0 s.
- The t=0 s in the cell is placed in the expected barycentre for an EM shower.
- Our understanding of the time delay is that clusters from fakes are essentially leaving energy in the final part of the cell of the EM calorimeter, and thus shifted in time with respect to the t=0.

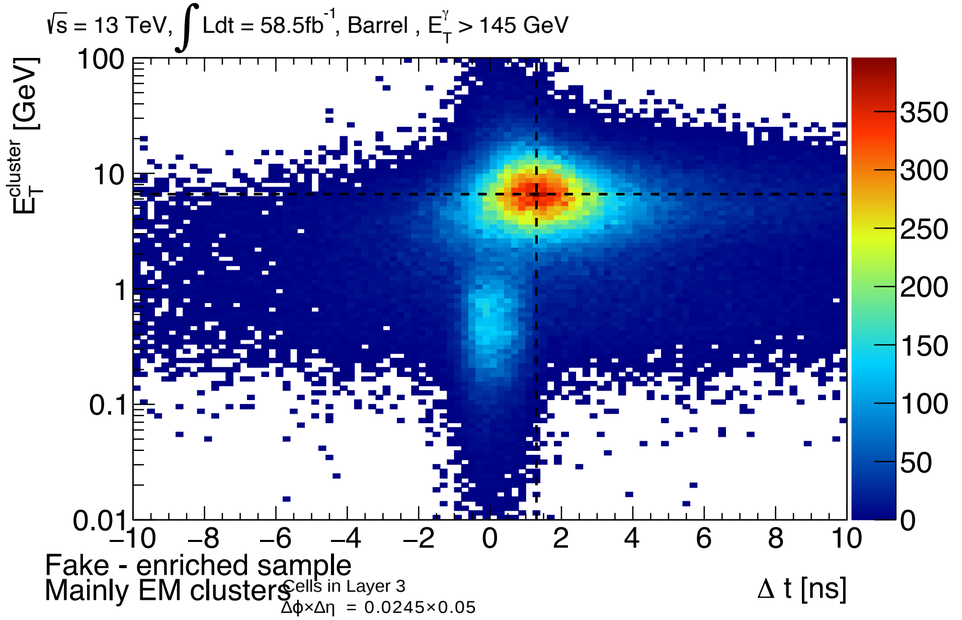

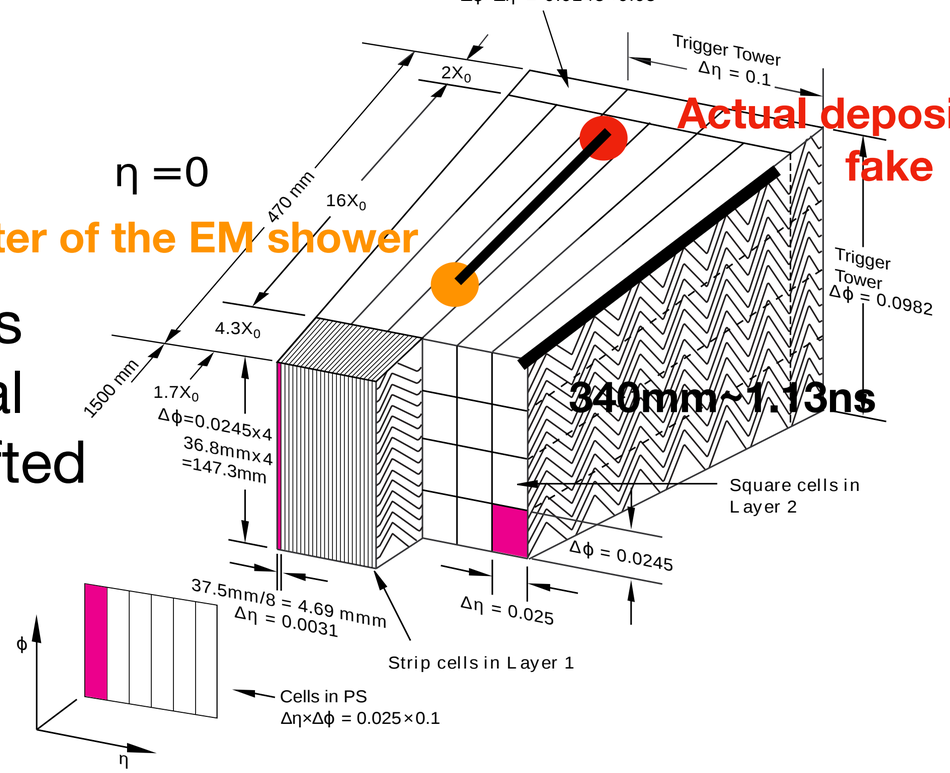

Expected question #2

- **ATLAS vs CMS**

ATLAS LAr calorimeter

- **Sampling: liquid Argon (active) lead (passive)**
- **Longitudinal segmentation**
- **Solenoid in front of the calorimeters.**

$$\frac{\sigma(E)}{E} = \frac{10\,\%\sqrt{GeV}}{\sqrt{E}} \oplus 0.7\,\%$$

CMS ECAL

- **Homogeneous: PbWO4 (lead tungstate)**
- **Online energy response calibrations.**
- **Calorimeters inside the 4 T solenoid**

$$\frac{\sigma(E)}{E} = \frac{3\,\%\sqrt{GeV}}{\sqrt{E}} \oplus 0.3\,\%$$

Introduction

Photon production in pp collisions

Several sources exist for photon production in pp collisions

- Prompt photons are those not produced in hadron decays and they are mainly those of interest to us.
  - QCD photon production, fragmentation photons, …
- Non-prompt (or fake) photons arise from hadron decays and they are the main background in analyses with photons in the final state.

Good photon reconstruction techniques are necessary to provide good physics results.

Prompt photons

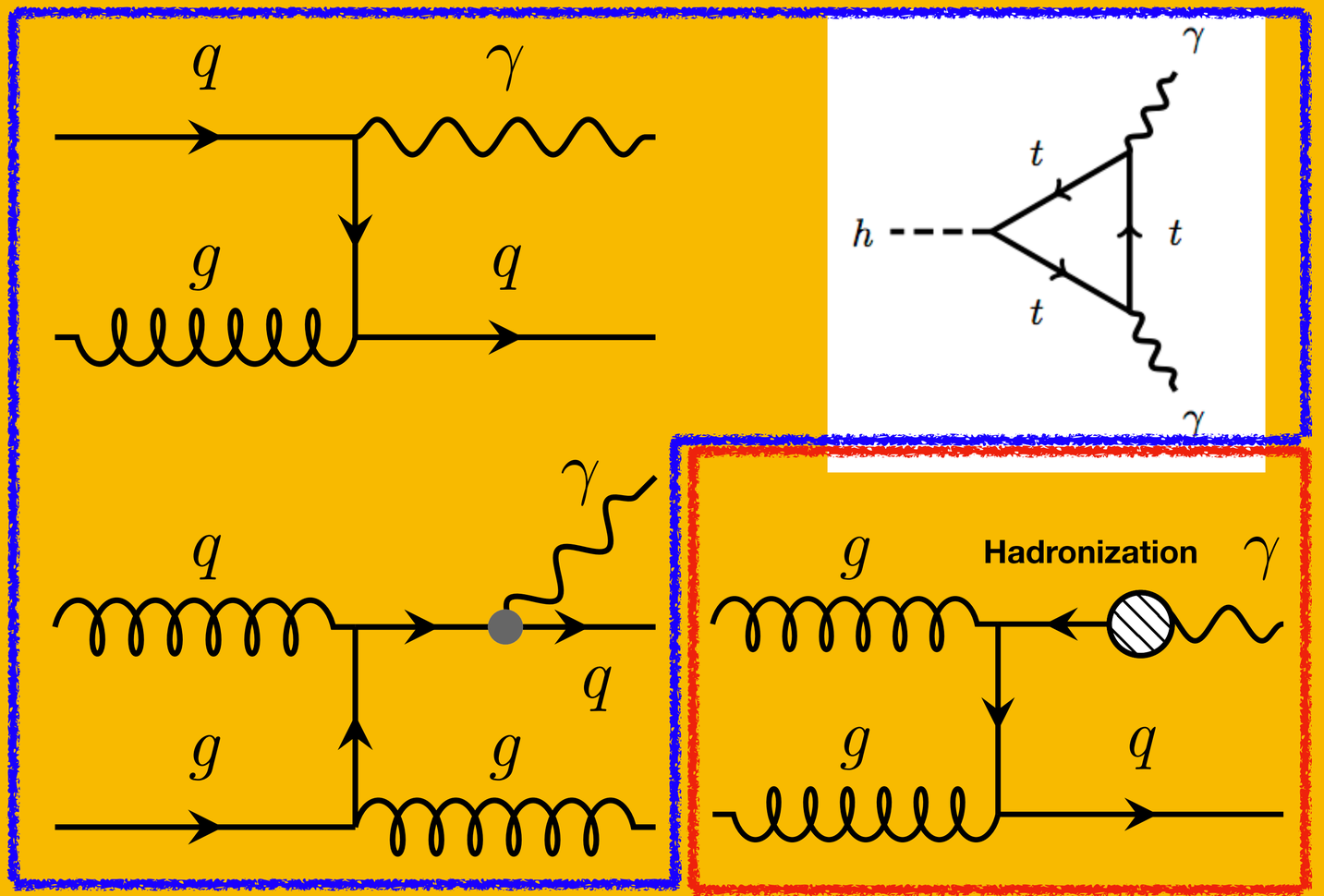

Non-prompt (fake photon)

Photon reconstruction

Particles traversing the LAr calorimeter develop EM showers, depositing energy in the calorimeter cells.

- Collections of cells are clustered together into topoclusters.

Match clusters to tracks

- Distinguish electrons from unconverted photons.

Match track to secondary vertex

- Distinguish electrons from converted photons

Energy obtained by summing the energy of the cells in the topocluster

- Calibration procedure to obtain the best estimate of the energy of the initial electromagnetic particle.

Topoclusters: dynamically sized objects that span over **all layers** of the calorimeters.

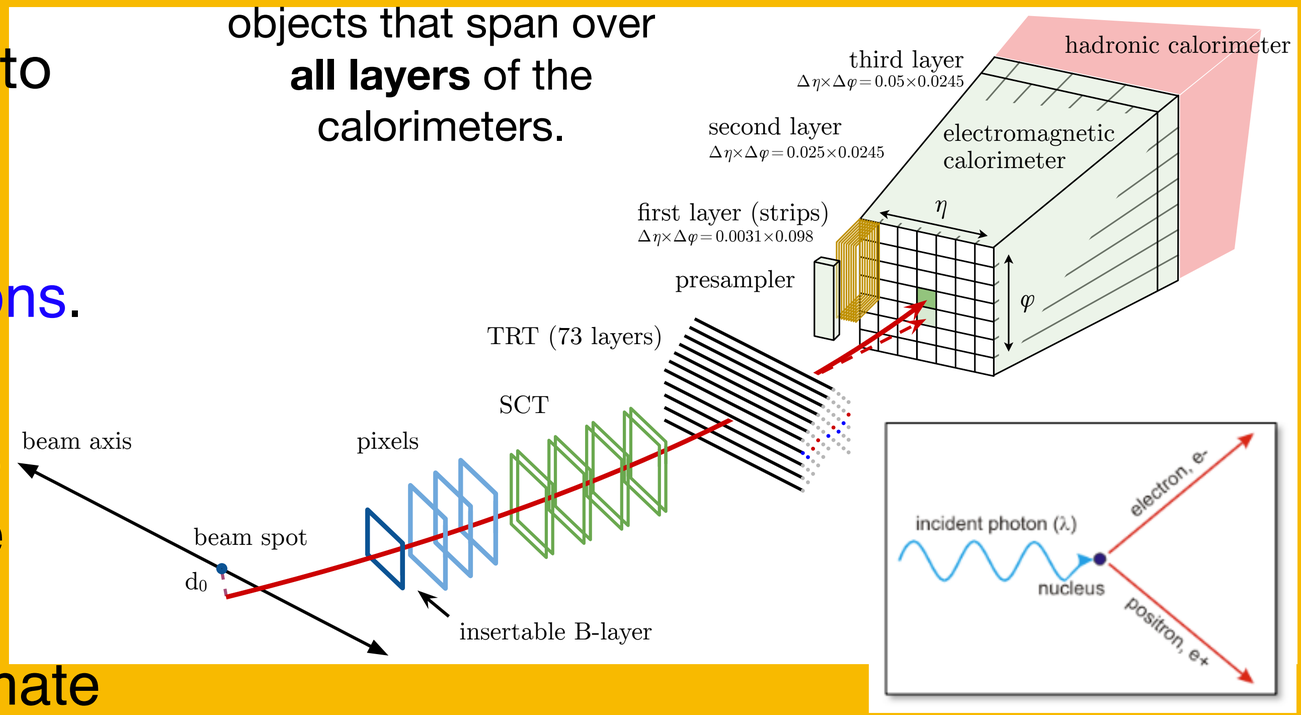

Photon energy calibration

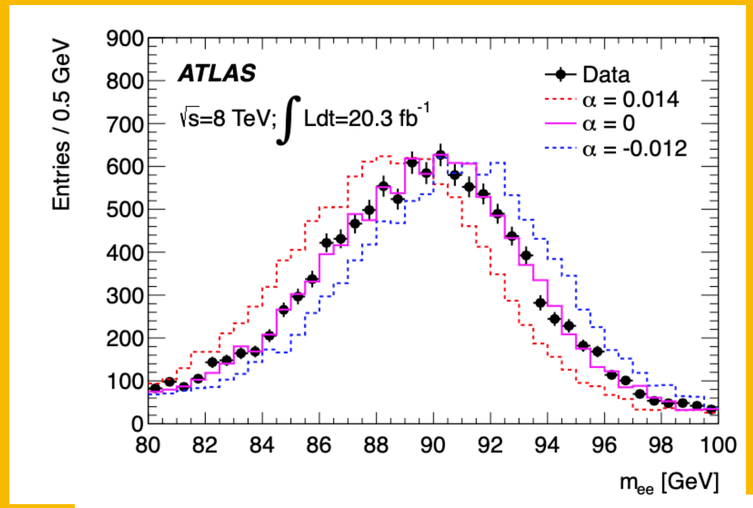

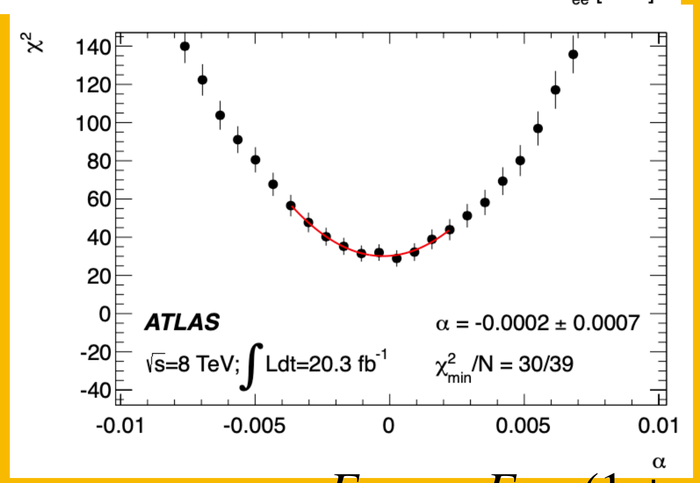

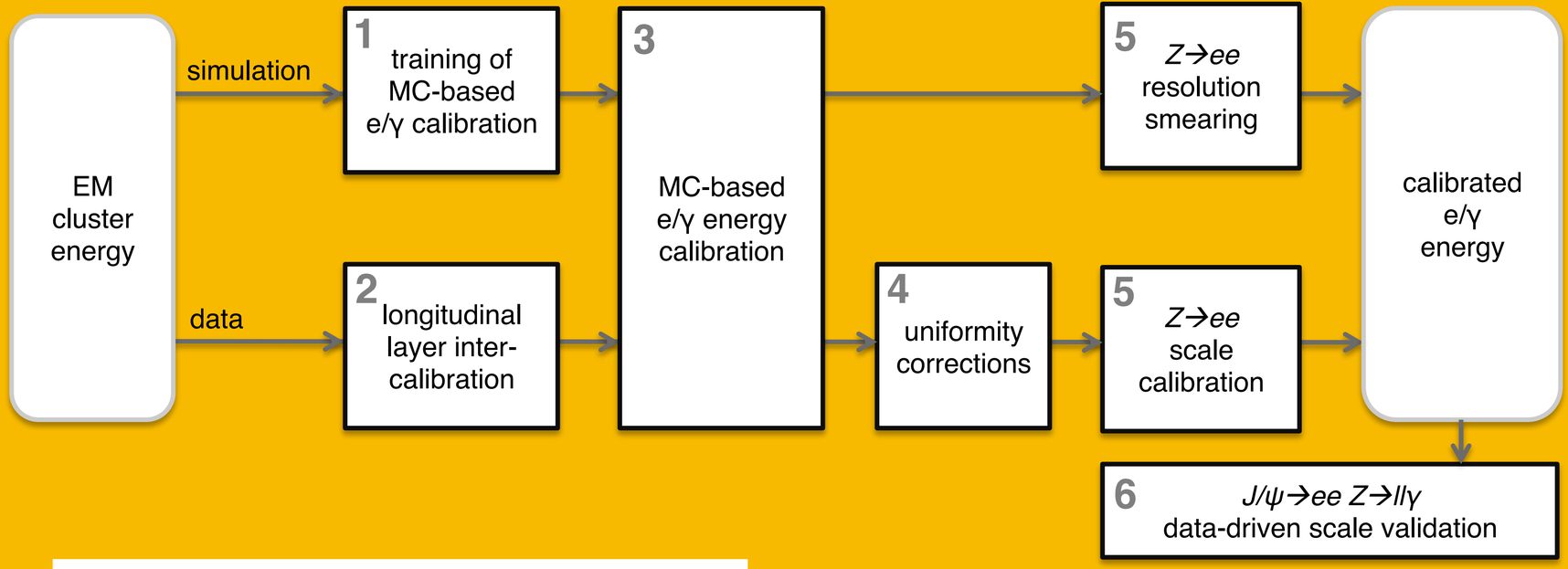

$$E_{data} = E_{simu}(1 + \alpha_i)$$

$$\left(\frac{\sigma_E}{E}\right)^{data} = \left(\frac{\sigma_E}{E}\right)^{simu} \oplus c_i$$

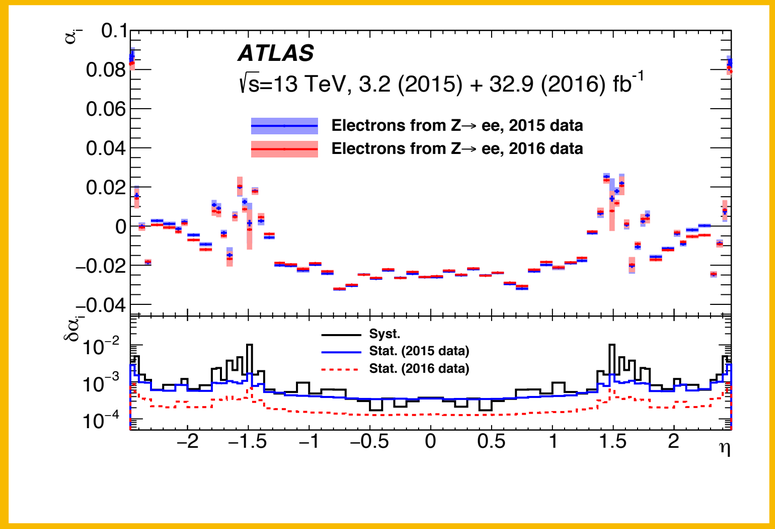

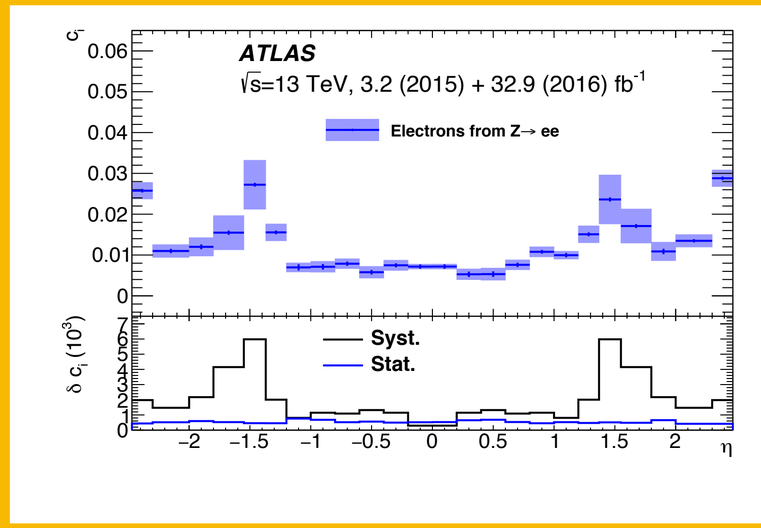

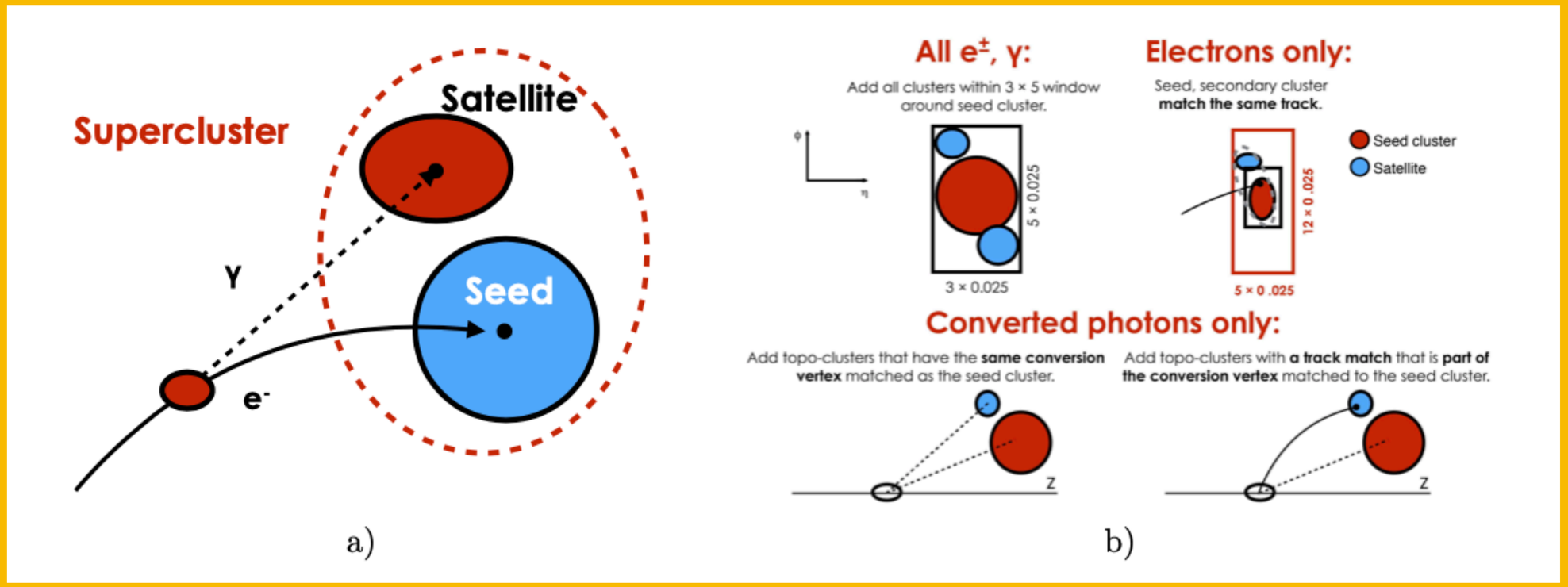
Supercluster
Satellite
Seed
γ
e-
a)
All e±, γ:
Add all clusters within 3 × 5 window around seed cluster.
3 × 0.025
5 × 0.025
Electrons only:
Seed, secondary cluster match the same track.
Seed cluster
Satellite
12 × 0 .025
5 × 0 .025
Converted photons only:
Add topo-clusters that have the same conversion vertex matched as the seed cluster.
Add topo-clusters with a track match that is part of the conversion vertex matched to the seed cluster.
Z
Z
b)

$$\zeta = \left| \frac{E_{cell}^{EM}}{\sigma_{noise,cell}^{EM}} \right|$$

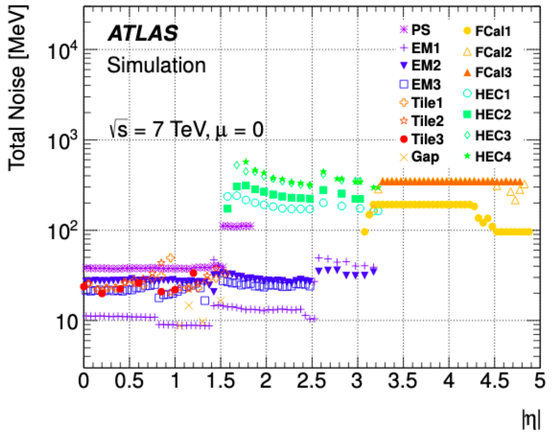

(a) $\sigma_{\text{noise}}(|\eta|)$ in 2010 ($\mu = 0$)

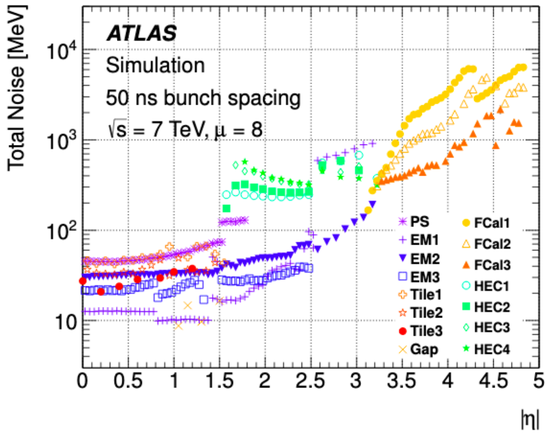

(b) $\sigma_{\text{noise}}(|\eta|)$ in 2011 ($\mu = 8$)

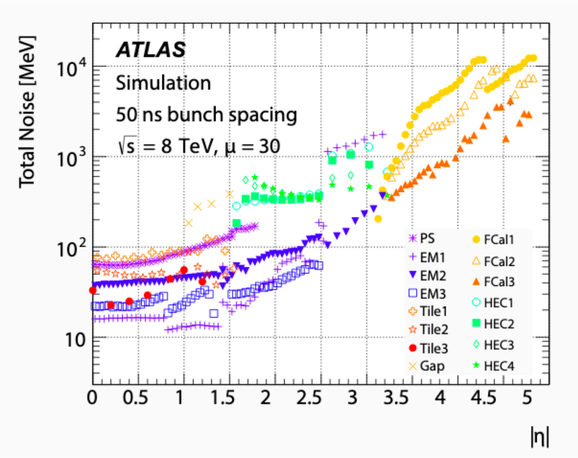

(c) $\sigma_{\text{noise}}(|\eta|)$ in 2012 ($\mu = 30$)

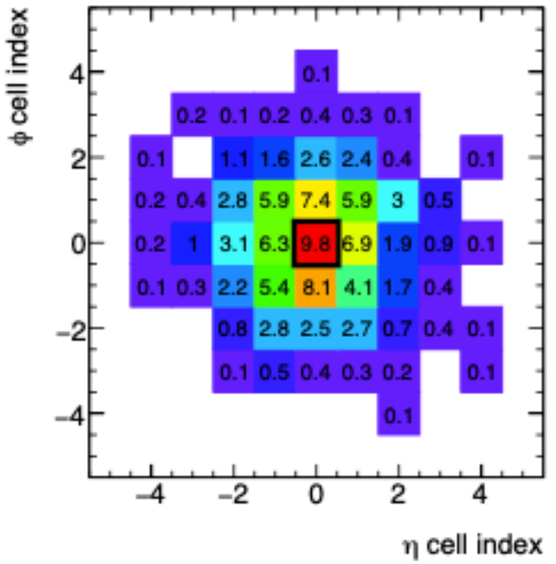

First step: most significant cell marked as proto-ster seed with $\zeta_{cell}^{EM} > 4$

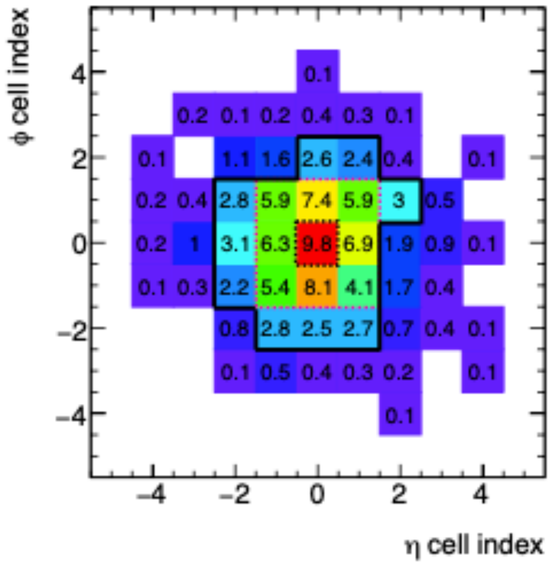

b) *Second step: adding neighbours with* $\zeta_{cell}^{EM} \geq 2$

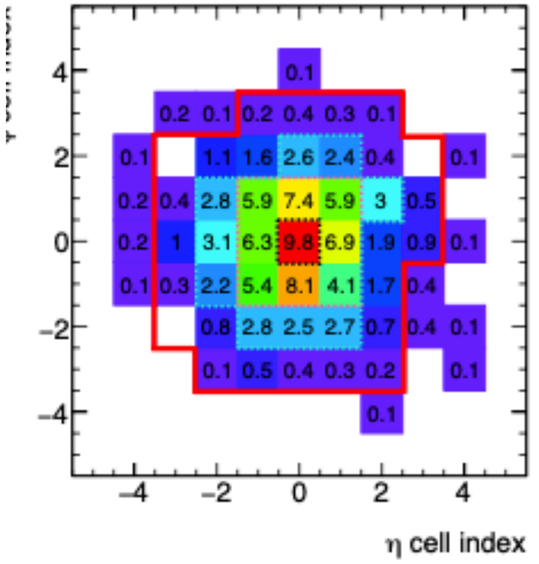

) *Final step: adding neighbours with* $\zeta_{cell}^{EM} \geq 0$

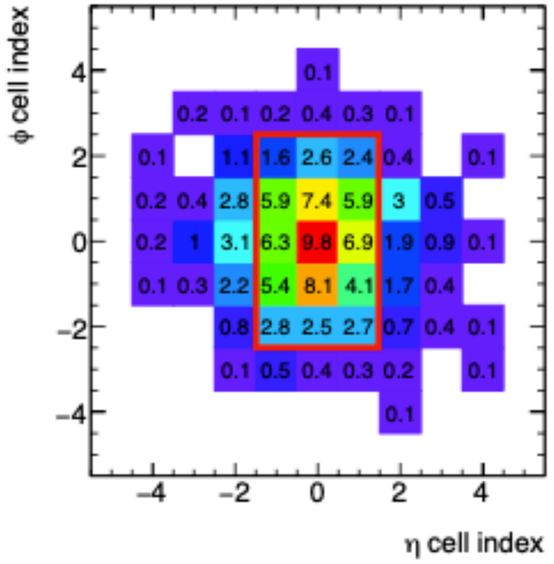

d) *Sliding-window cluster*

Photon isolation

On Crystal Balls

Large correlations between α and n parameters (even in the single sided CB)

Moreover, n values above 10 do not modify significantly the shape (loss of information, degeneracy)

Double Sided Crystal Ball

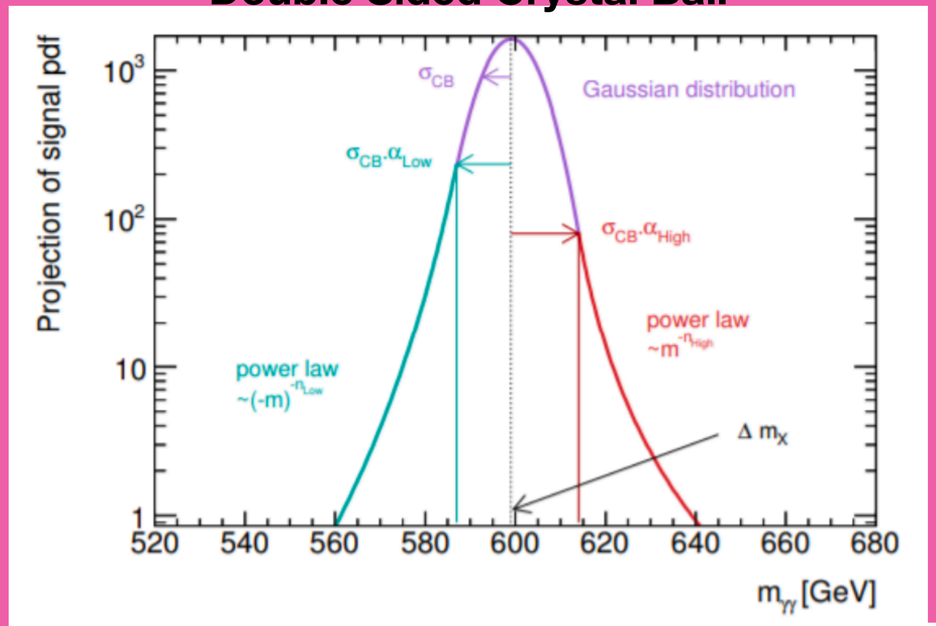

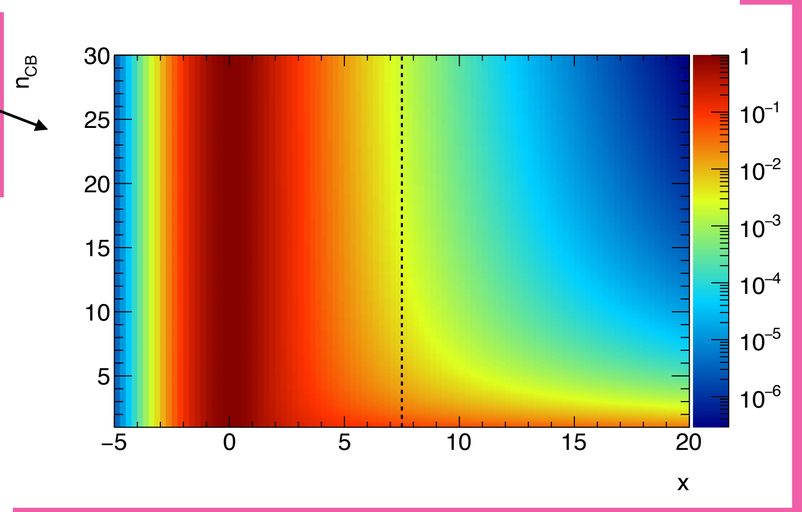

Single Sided Crystal Ball

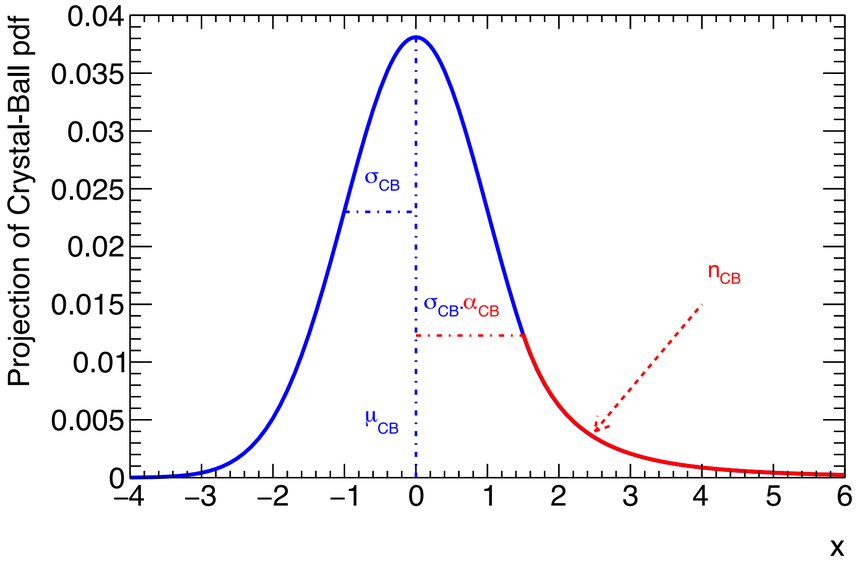

Single Sided Crystal Ball Correlation Matrix

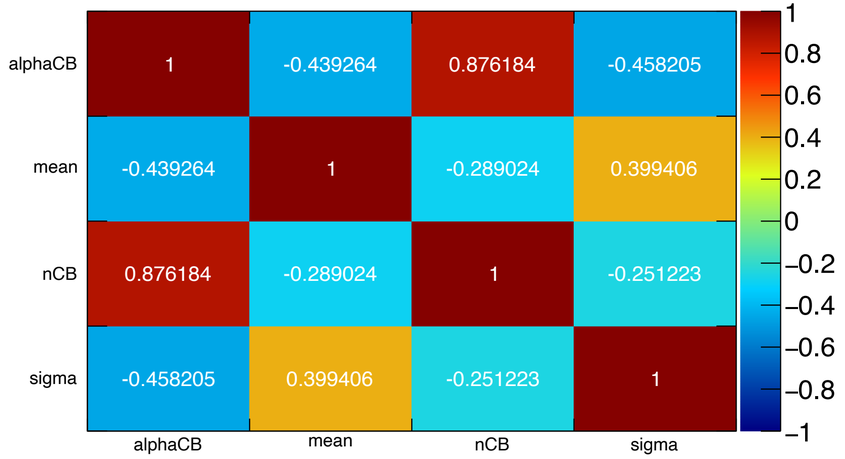

Samples

Two different samples with different characteristics are used to study photon performances:

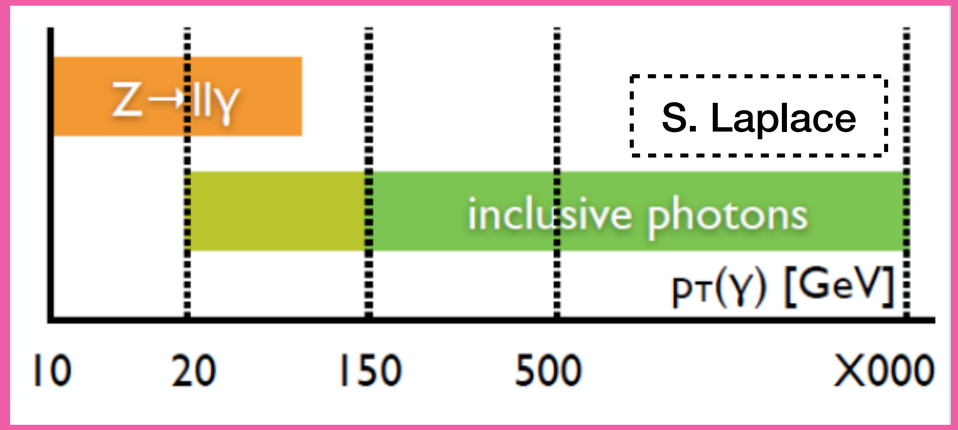

Photons from Radiative Z samples

- Events with Z→ llγ candidates are selected
- Extremely clean final state, with purities larger than 95%
- Covers only up to ~100 GeV in E_T
- Statistically limited

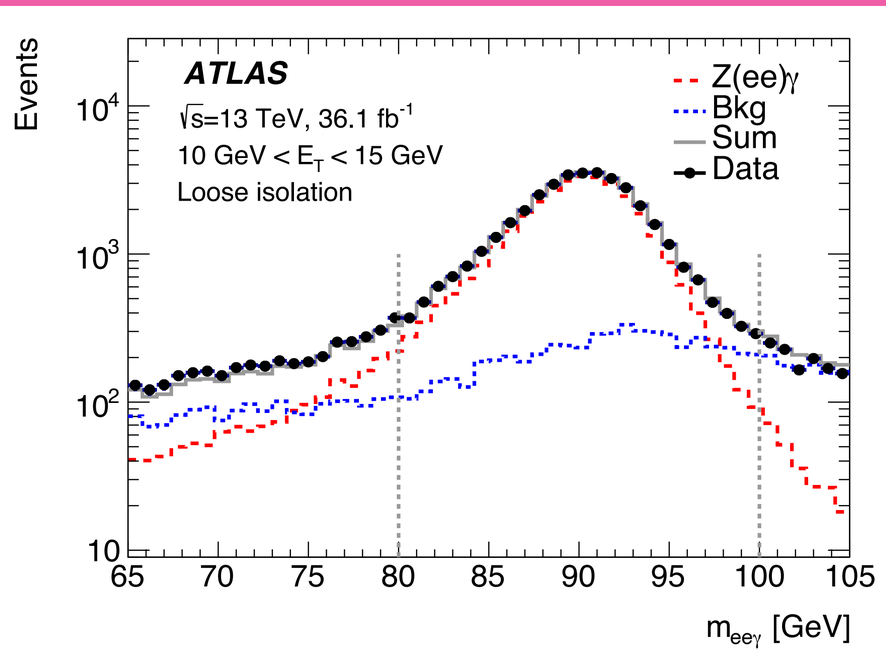

Inclusive photons

- Very large statistics, specially above 150 GeV.
- Large E_T coverage, up to the ~TeV level.
- Sample purity varies with E_T, conversion category and η.
- Suffers from large backgrounds difficult to subtract, specially at low E_T.

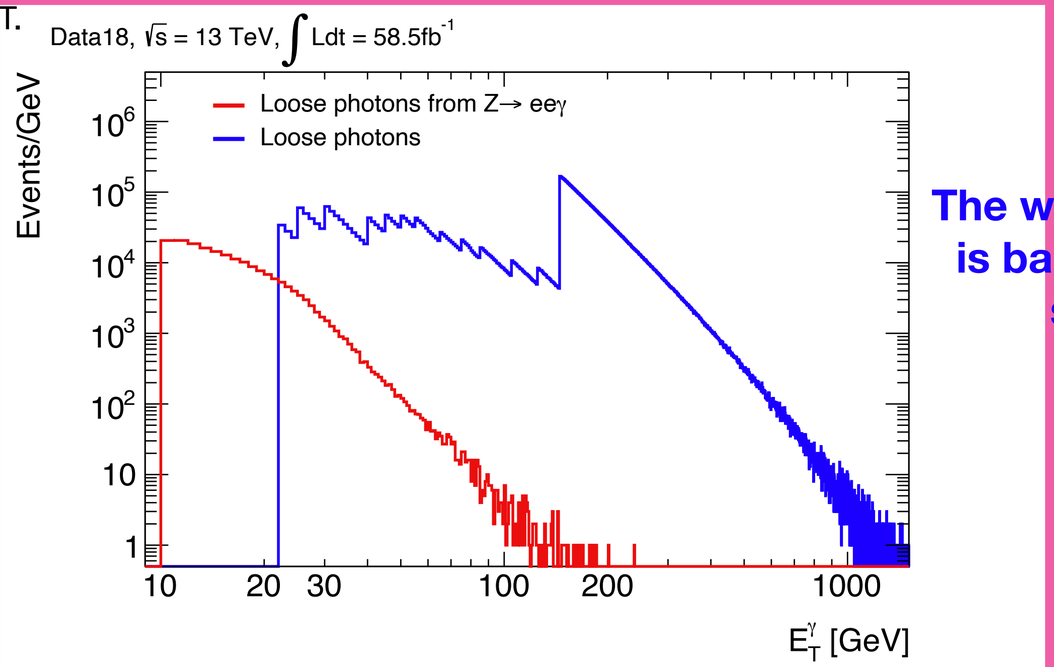

The work presented is based on these samples

Background subtraction

Signal yields obtained from template fit:

- Signal and background shapes modelled with an Asymmetric Crystal Ball (ACB).
- Signal yield is extracted from the integral of the fitted shape above a cut

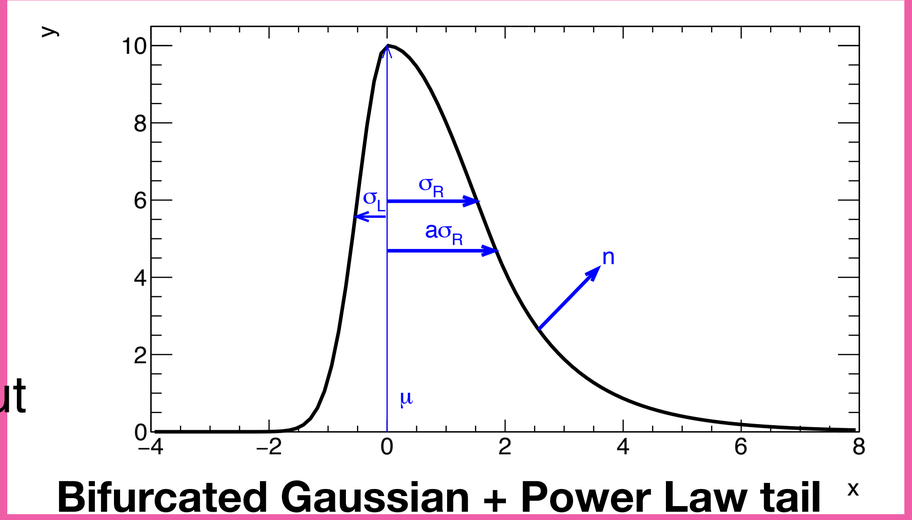

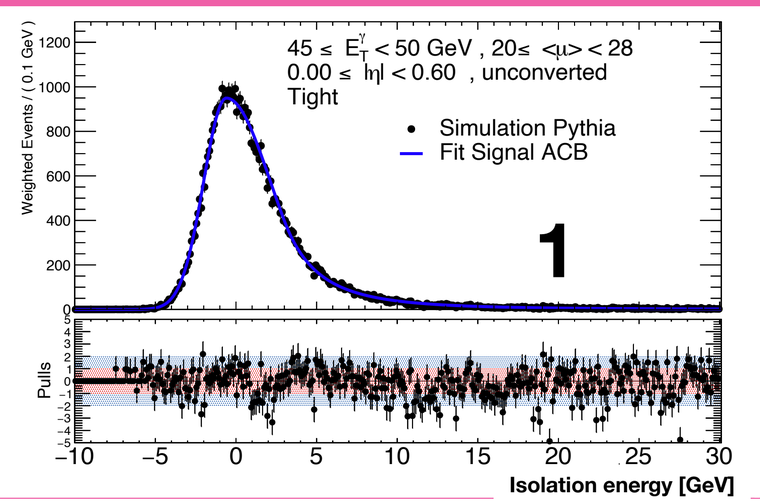

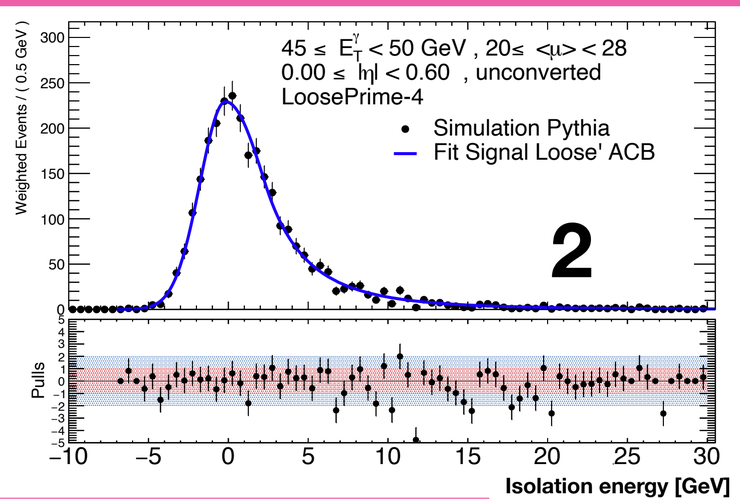

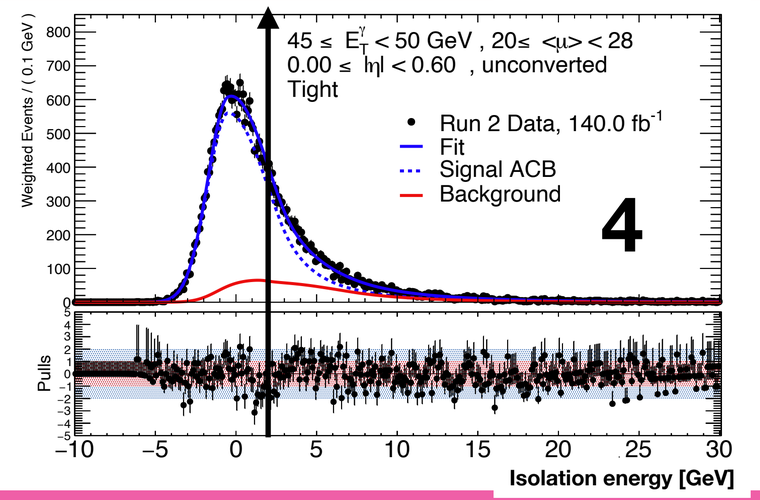

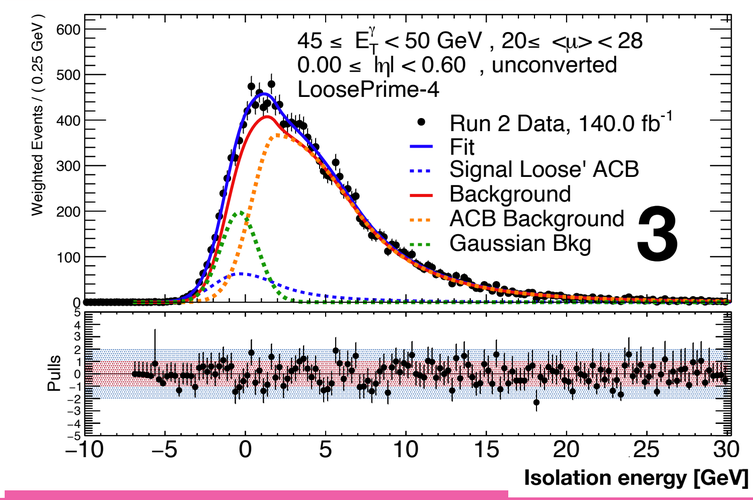

1. Signal shape is obtained from MC signal region.
2. Signal shape of photons leaking in the control region is obtained from MC control region.
3. Signal photons in the control region are subtracted to obtain the background shape.
4. Signal + background fit in the data signal region.

Results

Efficiencies obtained for different selection criteria, isolation cone sizes, conversion status and |η| bins.

Signal resolution worsens with increasing pileup

- Direct impact in efficiencies

Dominant systematic uncertainty from signal yield estimation:

- Integral of the signal model differs from signal measured after statistical subtraction of the background.
- Ranges from 2% at low E_T to less than 0.1% at high E_T

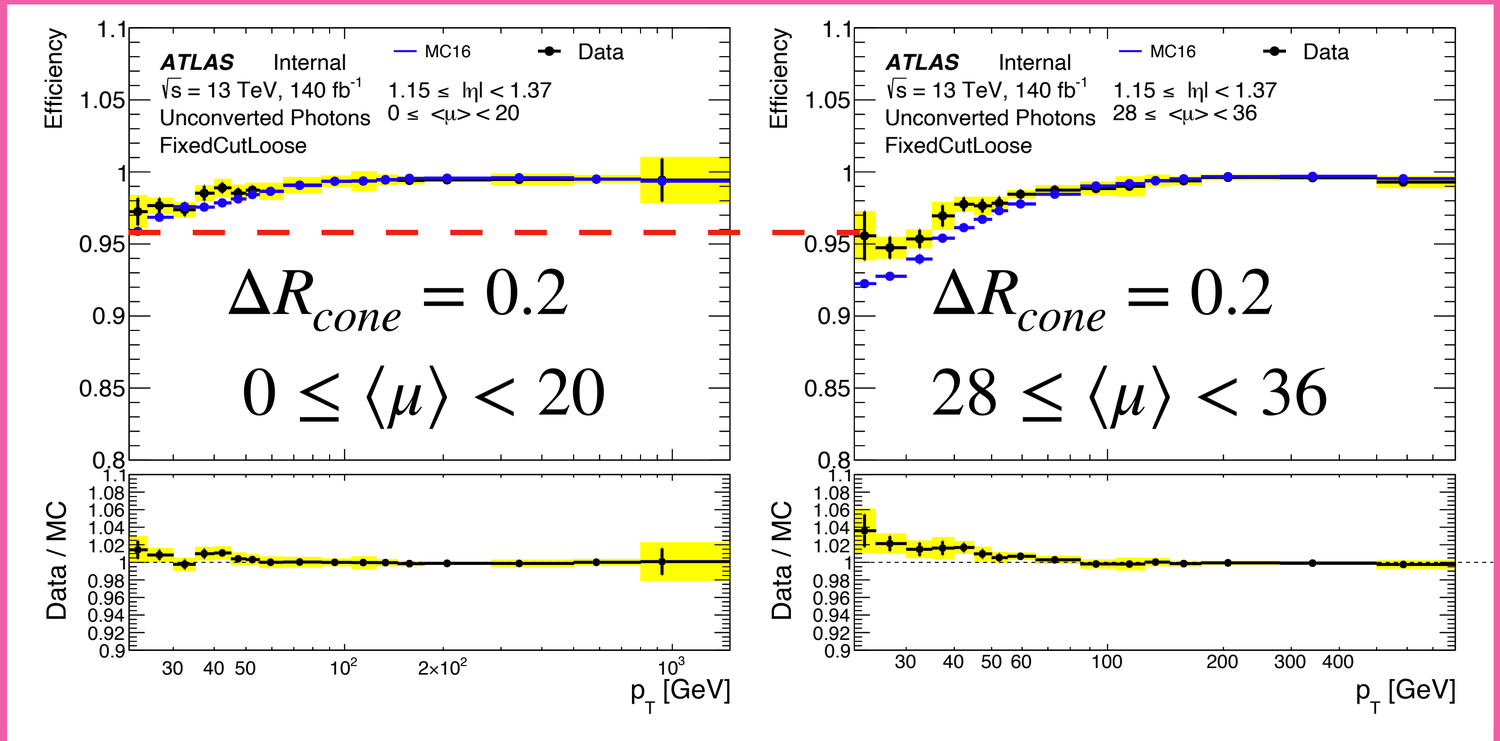

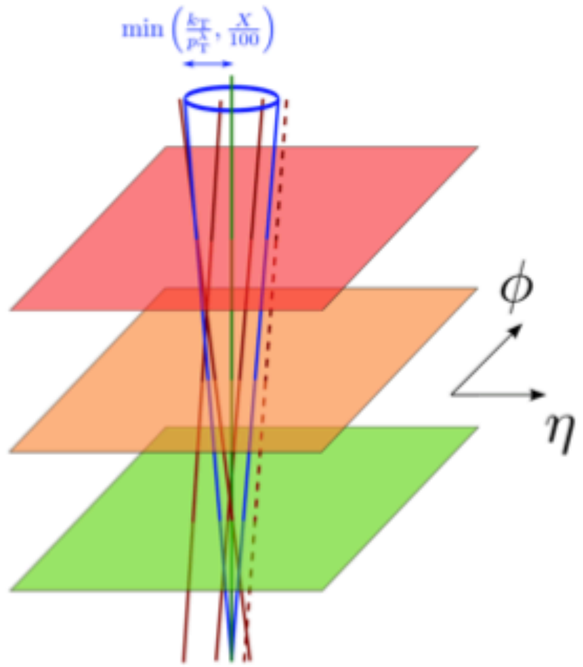
$\min\left(\frac{k_T}{p_T^{\gamma}}, \frac{X}{100}\right)$
ϕ
η

a)

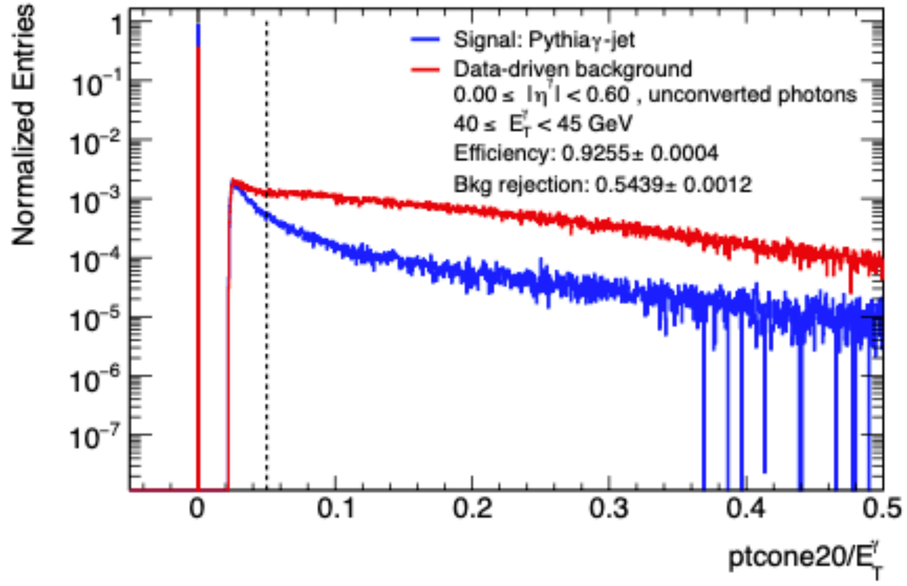
Normalized Entries
Signal: Pythiaγ-jet
Data-driven background
0.00 ≤ |η^γ| < 0.60 , unconverted photons
40 ≤ E_T^γ < 45 GeV
Efficiency: 0.9255± 0.0004
Bkg rejection: 0.5439± 0.0012
ptcone20/E_T^γ

b)

On the core subtraction

Energy leakage subtracted on average widens the distribution

Supercluster core subtraction is in principle more robust, but…

- Supercluster reconstruction also captures topoclusters from fakes, leading to worse prompt-fake discrimination. [Photons, Electrons, Electrons]
- Additional clusters far from the photon (>5 cells) at high energies (>100 GeV) in the endcaps create structures in the isolation energy, decreasing efficiencies. [here]

☐ Can the supercluster reconstruction be improved to catch these clusters and discriminate between “fake/prompt-like” clusters?

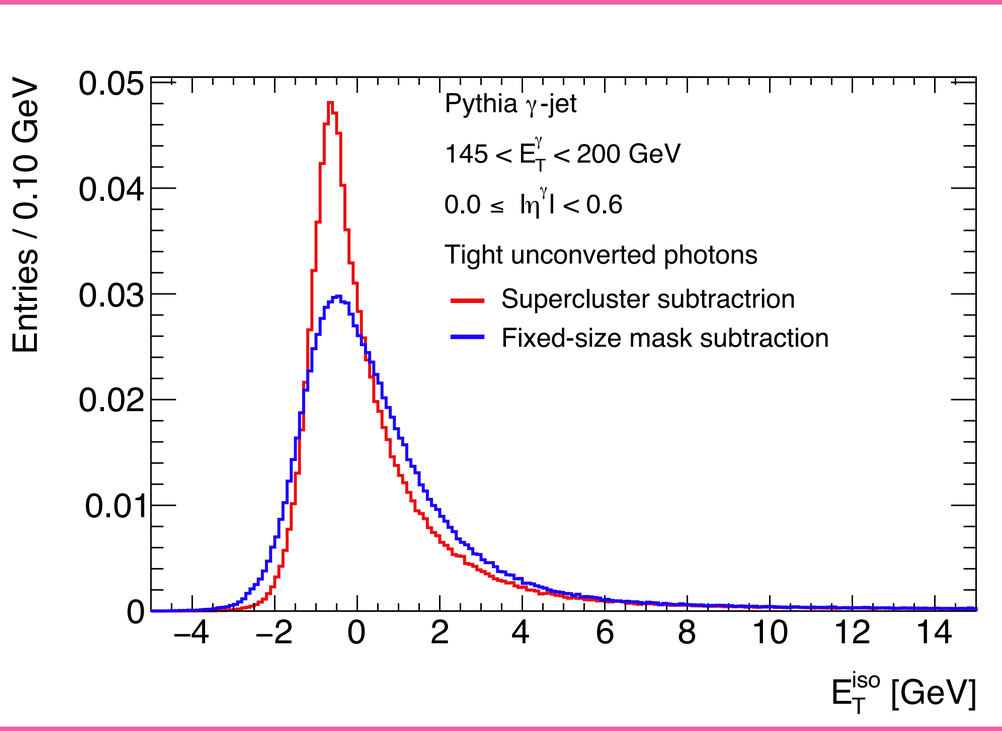

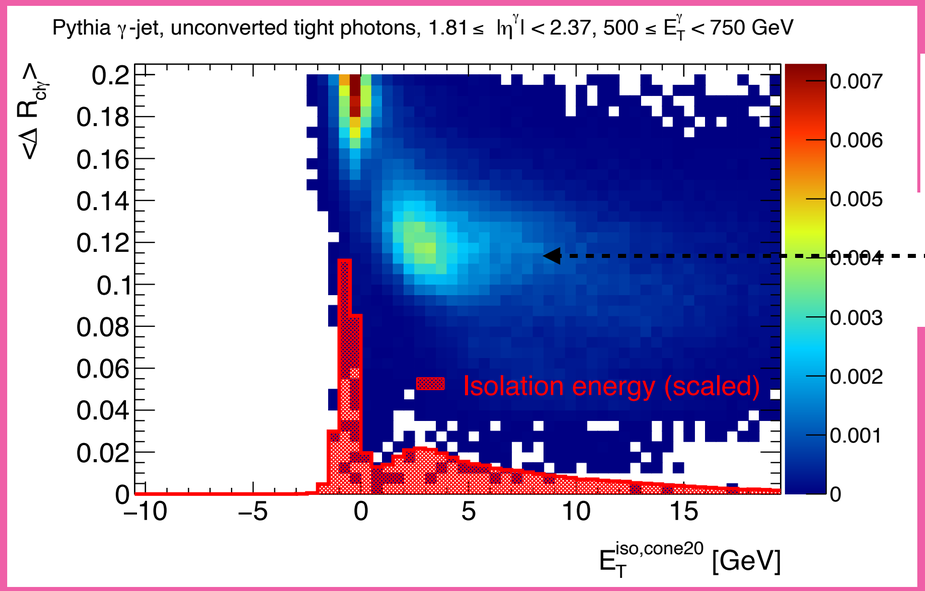

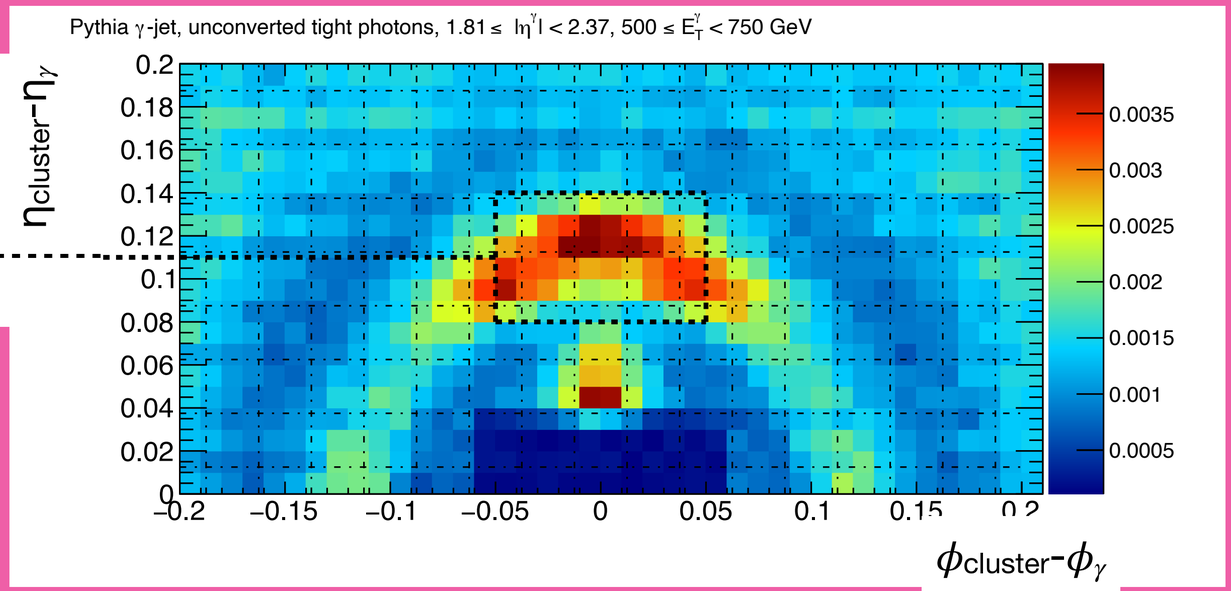

Improved isolation leakage correction

Problem: negative corrections down to -600 MeV are applied below ~ 60 GeV.

- This increases artificially the isolation energy, hence decreasing efficiencies.
- Linear fit in long range takes negative values at low E_T.

Solution: perform a log-log fit

- Restricts corrections to only positive values.

- Shifted distribution towards negative isolation values with new correction at low E_T.
- ~7% difference in efficiency at low E_T with respect to the old correction.
  - Improvement varies with |η|

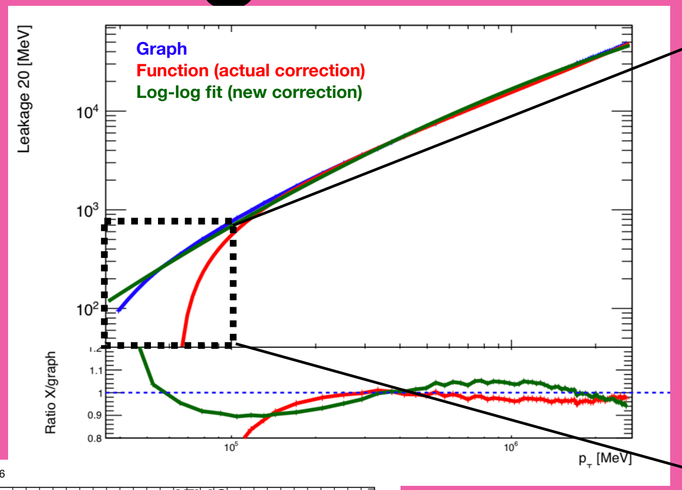

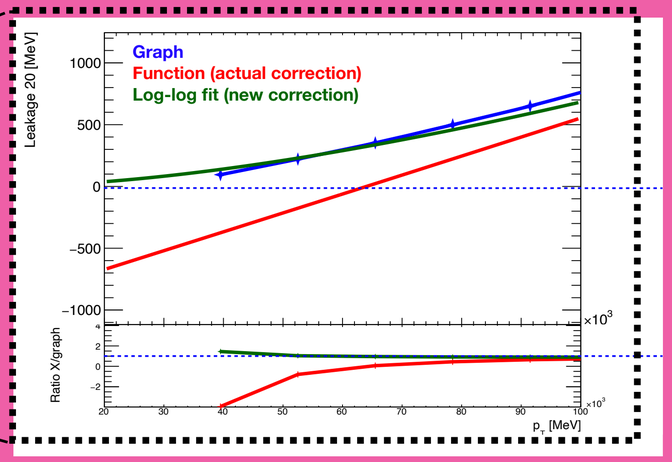

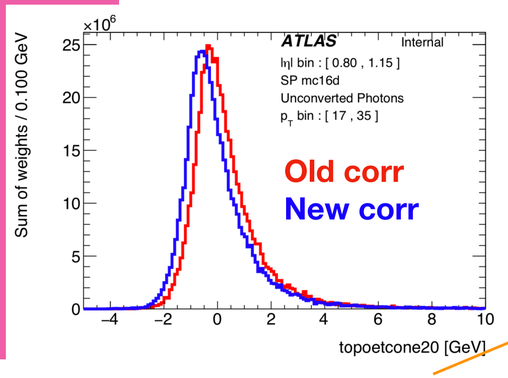

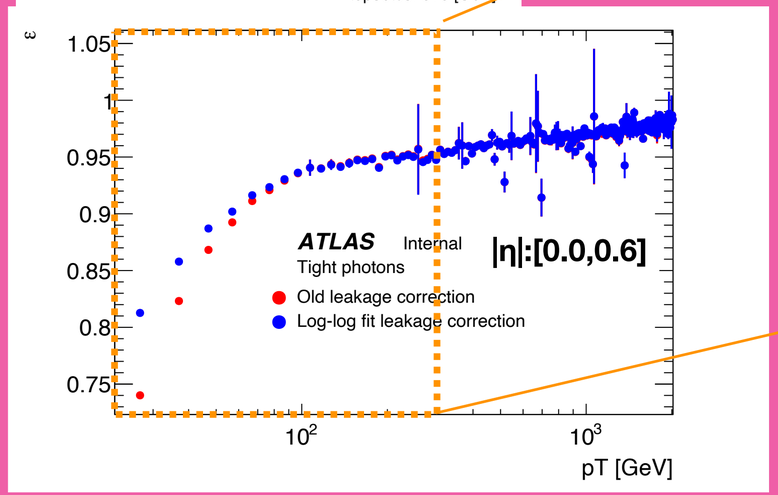

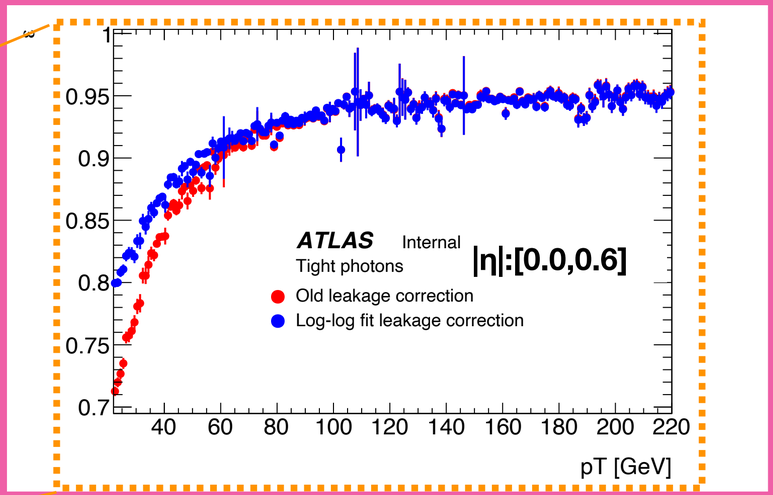

FixedCutLoose (calo only!): y_topoetcone20 < 0.065E_T

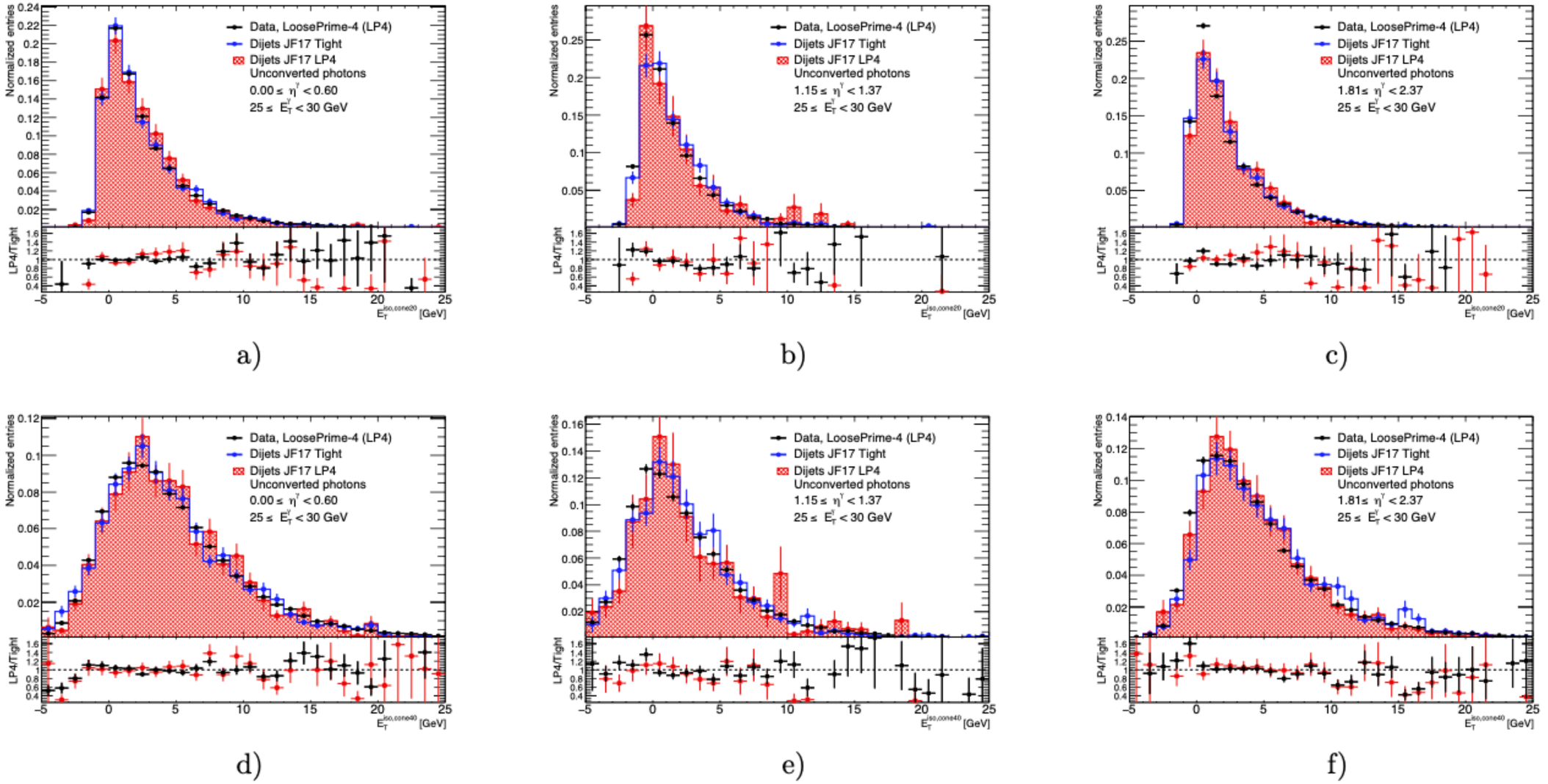

Figure 4.8: *Isolation energy distributions for background simulated events passing tight identification (blue solid line) and Loose'4 identification (red filled dashed) and for data events passing Loose'4 identification (black solid dots).*

Photon isolation II

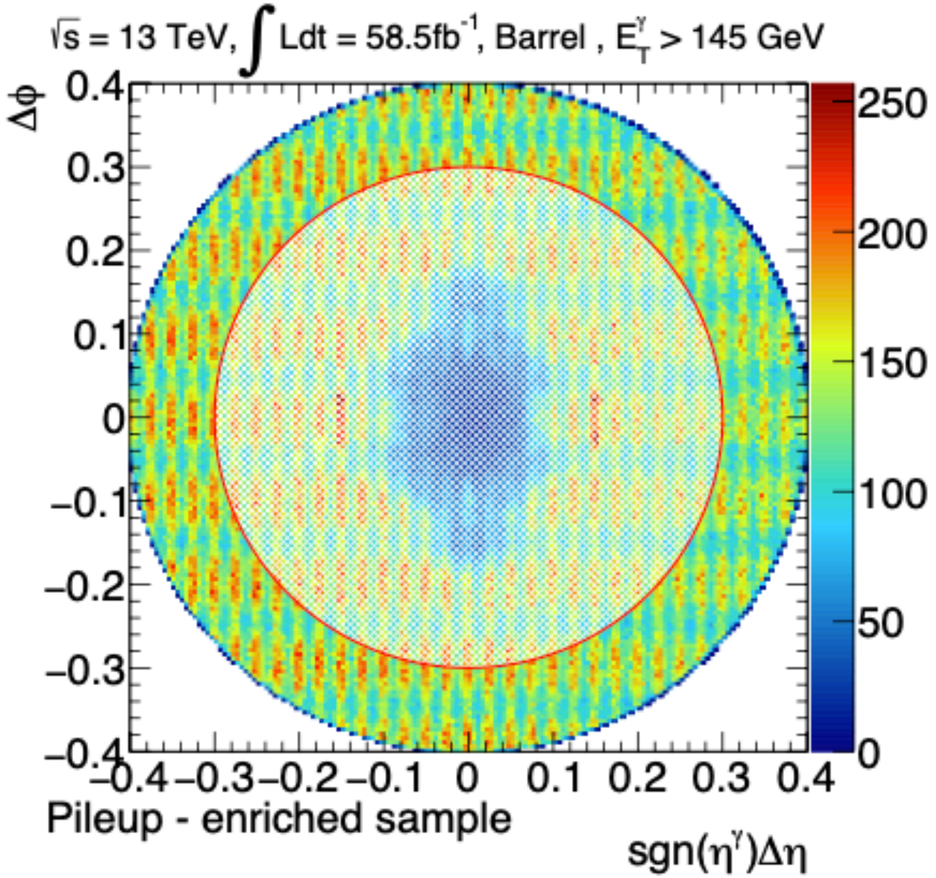

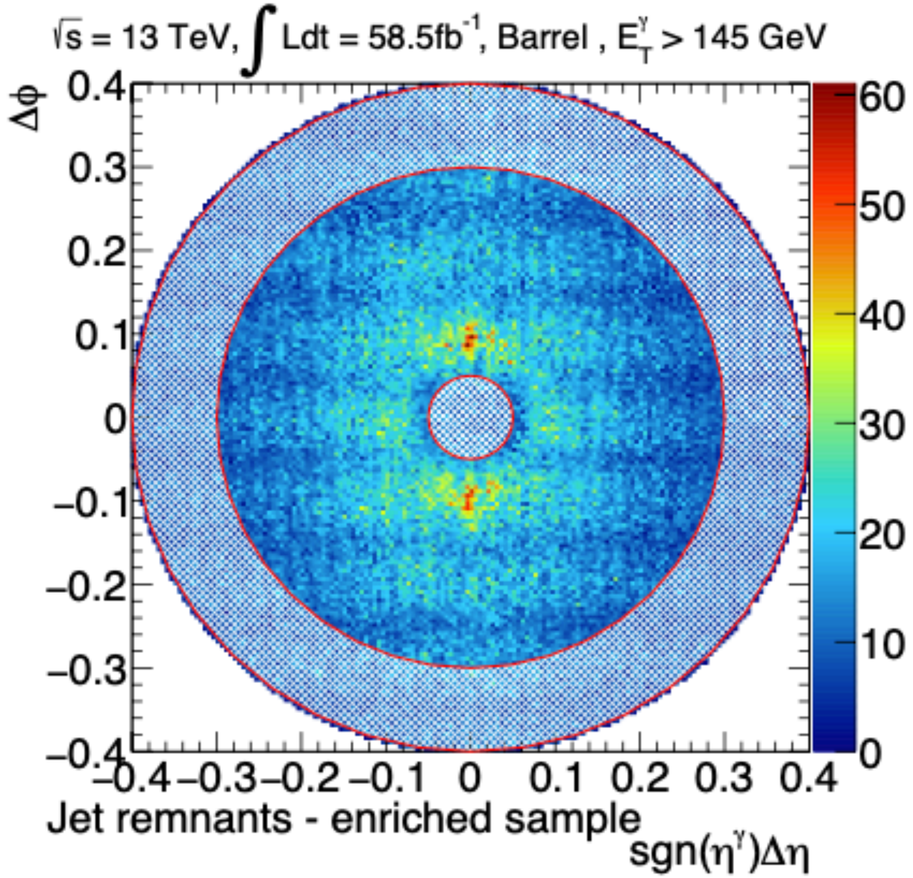

- Tight isolated photon candidates
- High pileup
- Outer ring

- Loose’4 photon candidates
- Low pileup
- Close

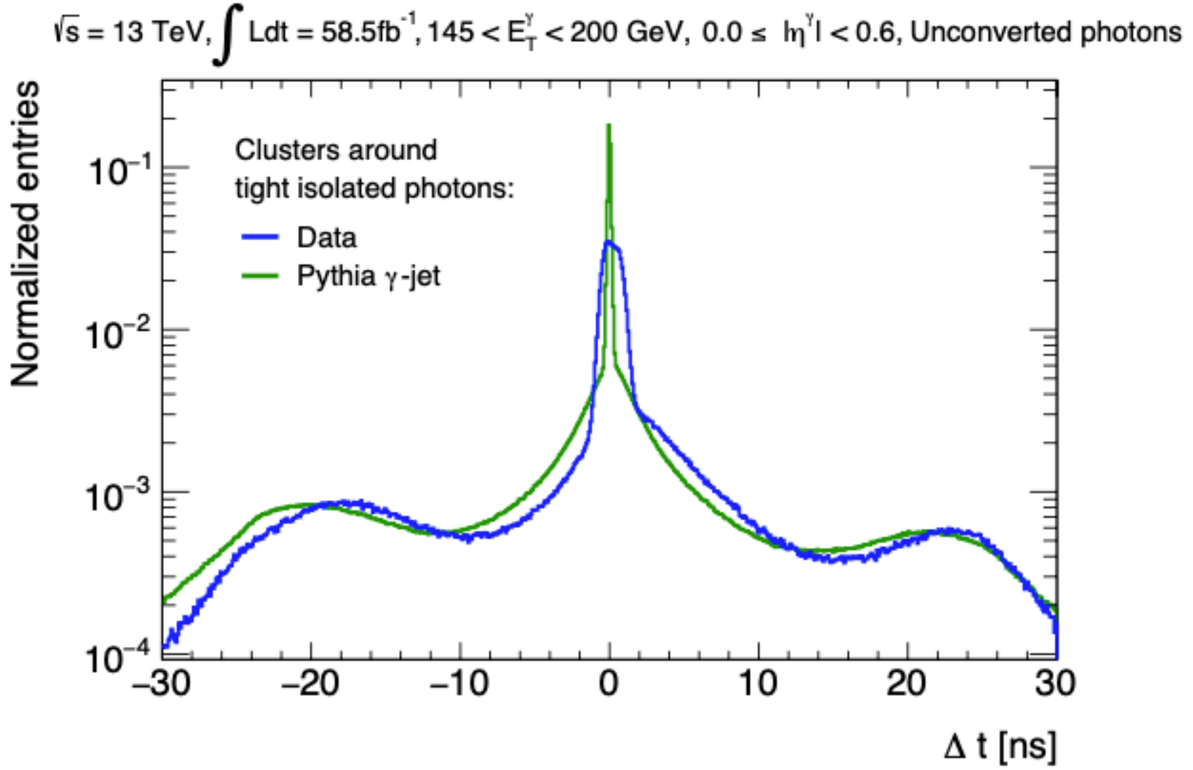

Figure 5.4: *The time difference Δt between topoclusters and photon candidates from tight, isolated photon in data and in simulation.*

Topocluster characterization (I)

These studies are purely **data-driven**!

Previous classification allows to characterize clusters from fakes and from pileup.

- Pure EM category is dominated by

  .

- Mainly EM category shows clear different features for clusters from fakes and from pileup.
  - Clusters from pileup are soft and in-time.
  - Clusters from fakes are harder, up to tens of GeV, with a small delay wrt the photon (1-2 ns)

Pileup-enriched topocluster sample | **Fake-enriched topocluster sample**

Pure EM topoclusters

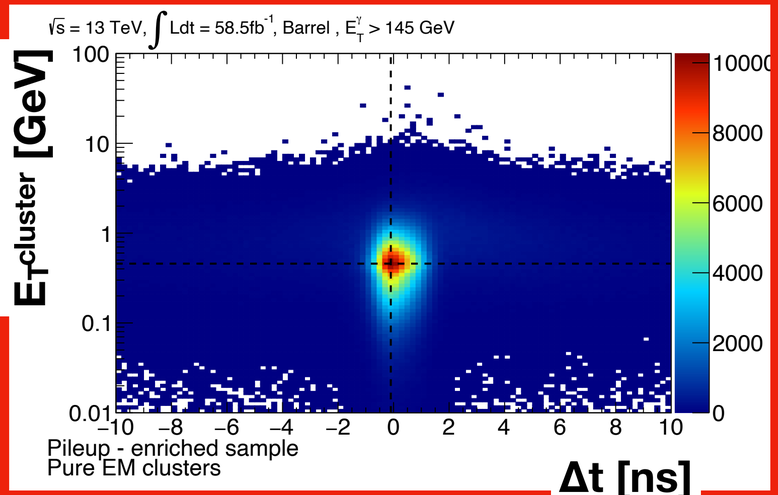

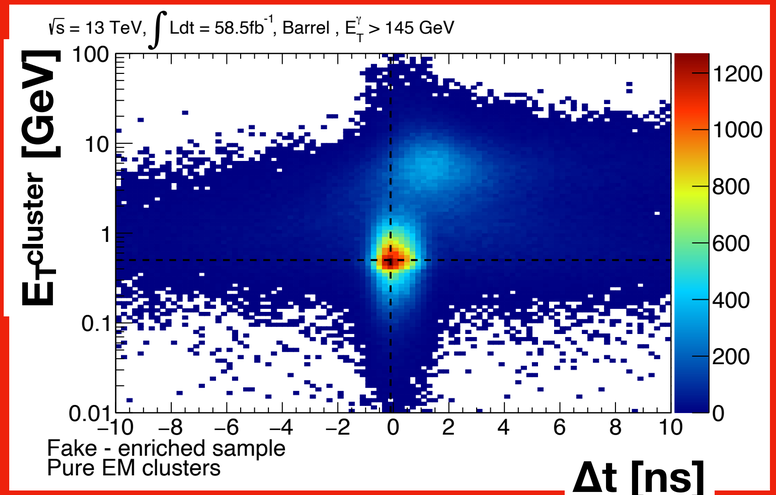

Mainly EM topoclusters

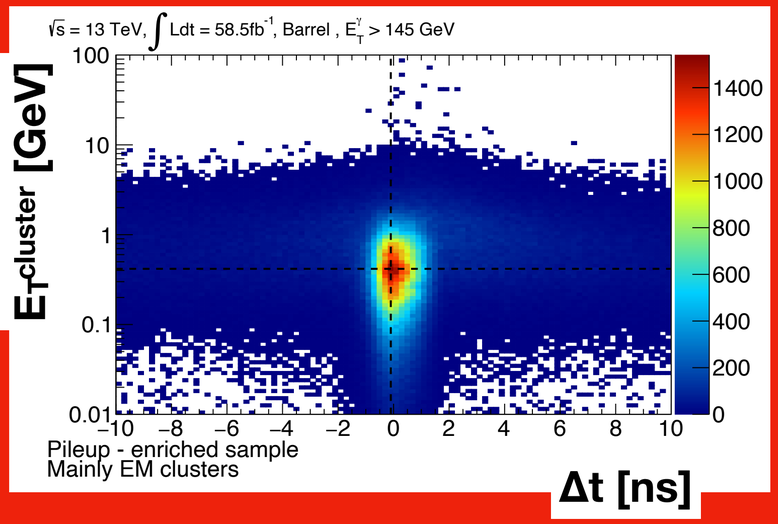

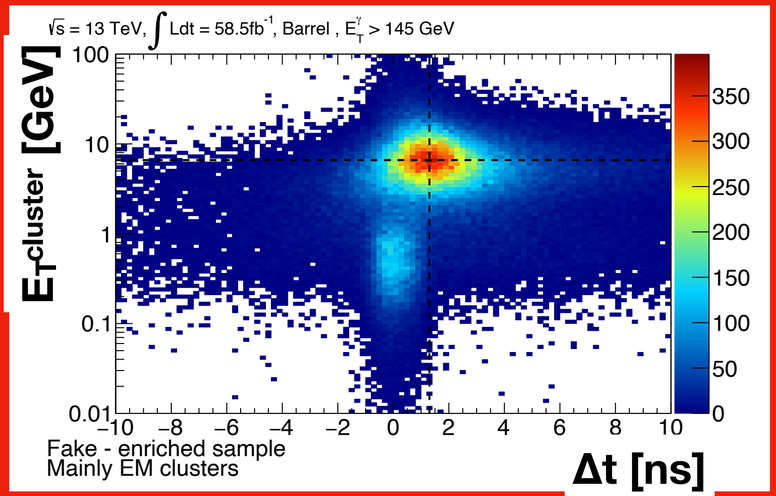

Similar features for the hadronic categories

Details on simultaneous fit

Pileup-enriched topocluster sample

Fake-enriched topocluster sample

Mainly EM topoclusters

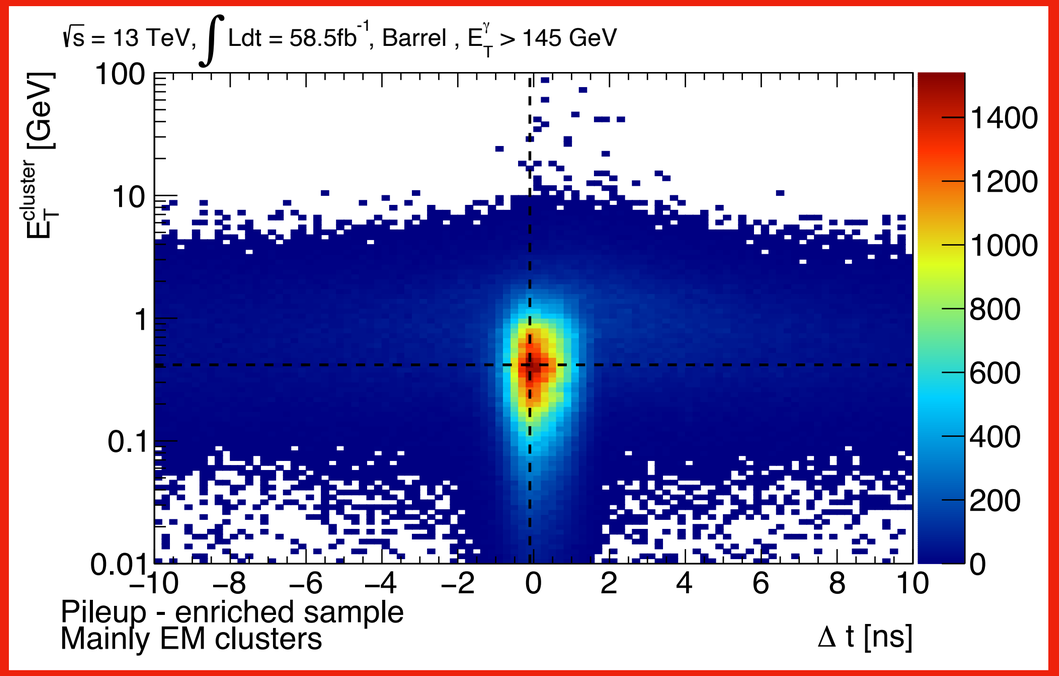

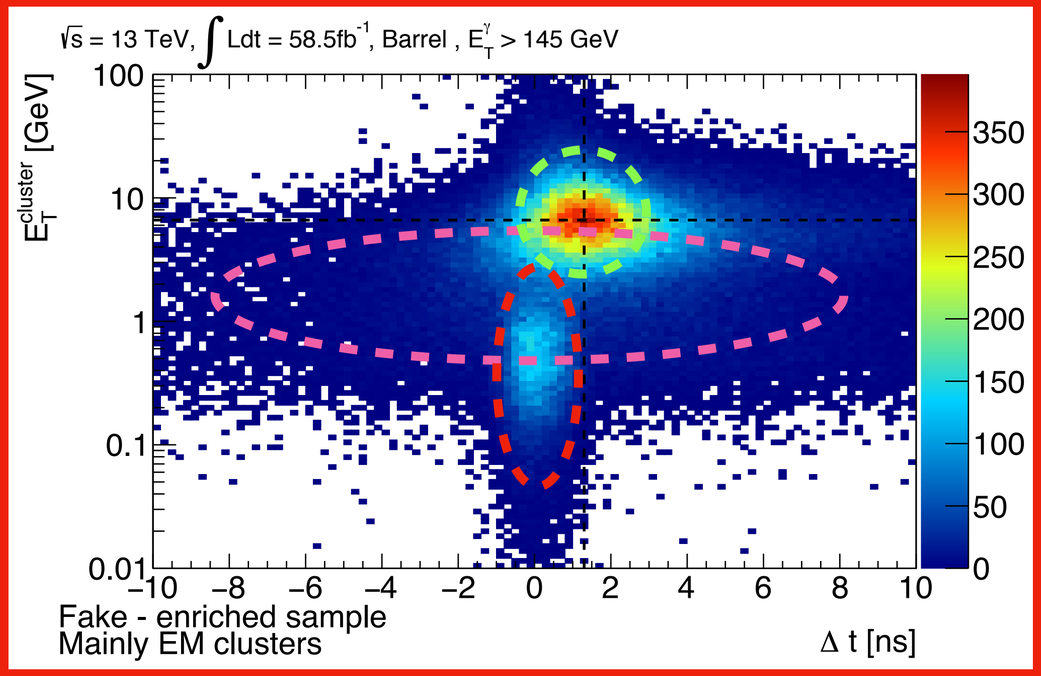

- Same shapes for each species, different relative contributions!

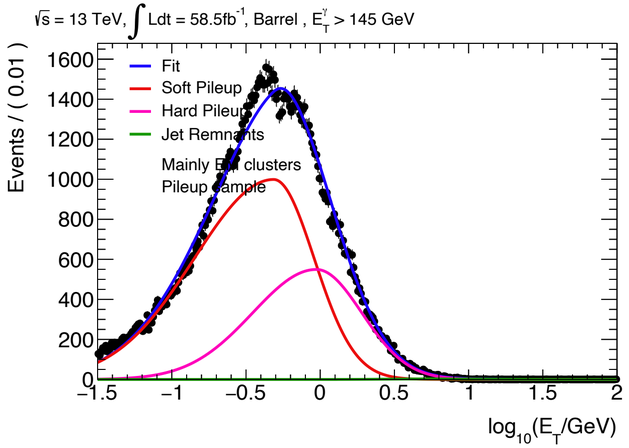

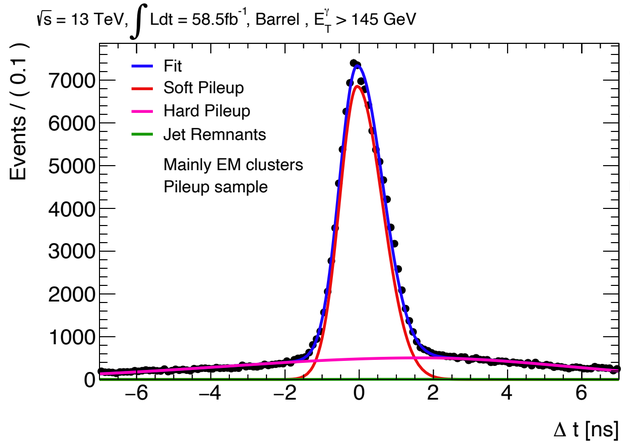

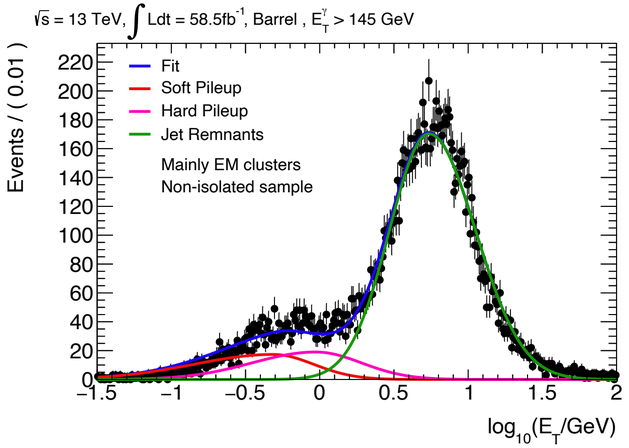

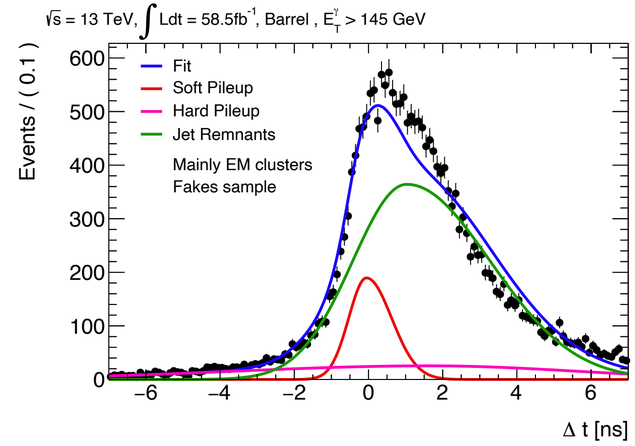

Category	Species	$\mu_{\Delta t}[ns]$	$\sigma^{L}_{\Delta t}[ns]$	$\sigma^{R}_{\Delta t}[ns]$	μ_{pt} [GeV]	σ^{L}_{pt} [GeV]	σ^{R}_{pt} [GeV]
Pure EM	Soft-pileup	-0.063 ± 0.002	0.468 ± 0.002	0.673 ± 0.002	$0.554^{+0.001}_{-0.001}$	$2.730^{+0.005}_{-0.005}$	$0.216^{+0.000}_{-0.000}$
	Hard-pileup	1.504 ± 0.041	4.748 ± 0.039	3.767 ± 0.040	$1.039^{+0.006}_{-0.006}$	$2.835^{+0.012}_{-0.012}$	$0.254^{+0.001}_{-0.001}$
	Fakes	0.878 ± 0.024	1.300 ± 0.018	2.291 ± 0.019	$4.481^{+0.048}_{-0.047}$	$2.310^{+0.029}_{-0.028}$	$0.300^{+0.002}_{-0.002}$
Mainly EM	Soft-pileup	-0.055 ± 0.005	0.477 ± 0.004	0.677 ± 0.004	$0.486^{+0.004}_{-0.004}$	$3.421^{+0.024}_{-0.024}$	$0.272^{+0.002}_{-0.002}$
	Hard-pileup	1.661 ± 0.074	5.276 ± 0.078	3.938 ± 0.079	$0.942^{+0.011}_{-0.010}$	$2.682^{+0.020}_{-0.020}$	$0.306^{+0.002}_{-0.002}$
	Fakes	1.029 ± 0.025	1.455 ± 0.019	2.249 ± 0.019	$5.435^{+0.054}_{-0.054}$	$1.844^{+0.017}_{-0.016}$	$0.315^{+0.002}_{-0.002}$
Mainly Tile	Soft-pileup	0.050 ± 0.065	0.874 ± 0.074	1.222 ± 0.085	$1.981^{+0.116}_{-0.109}$	$5.148^{+0.252}_{-0.240}$	$0.211^{+0.009}_{-0.009}$
	Hard-pileup	2.542 ± 0.138	5.567 ± 0.142	3.439 ± 0.129	$1.454^{+0.017}_{-0.017}$	$2.452^{+0.022}_{-0.022}$	$0.285^{+0.002}_{-0.002}$
	Fakes	0.238 ± 0.023	1.230 ± 0.017	1.471 ± 0.019	$6.481^{+0.091}_{-0.090}$	$2.160^{+0.025}_{-0.024}$	$0.313^{+0.003}_{-0.003}$
Pure Tile	Soft-pileup	-7.489 ± 0.254	2.600 ± 4.339	2.734 ± 0.107	$0.726^{+0.015}_{-0.015}$	$3.340^{+0.115}_{-0.112}$	$0.061^{+0.001}_{-0.001}$
	Hard-pileup	2.352 ± 0.038	4.498 ± 0.036	4.702 ± 0.118	$0.739^{+0.003}_{-0.003}$	$2.594^{+0.012}_{-0.012}$	$0.254^{+0.001}_{-0.001}$
	Fakes	0.140 ± 0.025	1.180 ± 0.023	1.524 ± 0.029	$1.721^{+0.025}_{-0.025}$	$1.982^{+0.032}_{-0.032}$	$0.386^{+0.004}_{-0.004}$

Category	Species	Pileup-enriched [%]	Fakes-enriched [%]	Fakes-enriched (non-isolated photons)[%]
Pure EM	Soft-pileup	74.85 ± 0.05	39.11 ± 0.23	36.90 ± 0.28
	Hard-pileup	24.93 ± 0.05	15.75 ± 0.18	15.30 ± 0.21
	Fakes	0.22 ± 0.01	45.14 ± 0.24	47.80 ± 0.29
Mainly EM	Soft-pileup	66.15 ± 0.12	12.39 ± 0.22	10.85 ± 0.25
	Hard-pileup	33.73 ± 0.12	11.50 ± 0.21	11.03 ± 0.25
	Fakes	0.13 ± 0.01	76.11 ± 0.29	78.11 ± 0.33
Mainly Tile	Soft-pileup	14.93 ± 0.19	$< 0.01 \pm 0.00$	0.10 ± 0.03
	Hard-pileup	84.75 ± 0.19	14.61 ± 0.29	14.69 ± 0.36
	Fakes	0.32 ± 0.03	85.39 ± 0.29	85.20 ± 0.36
Pure Tile	Soft-pileup	5.89 ± 0.13	$< 0.01 \pm 0.00$	0.02 ± 0.03
	Hard-pileup	91.14 ± 0.16	41.82 ± 0.80	41.01 ± 0.96
	Fakes	2.97 ± 0.10	58.18 ± 0.80	58.97 ± 0.97

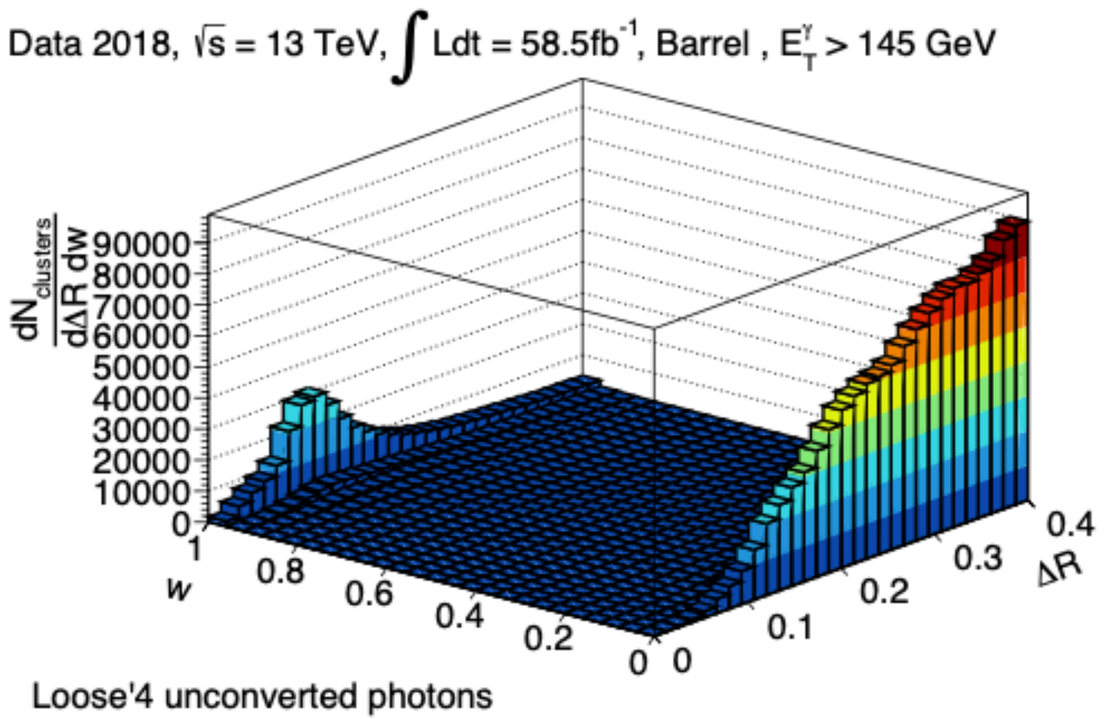

a)

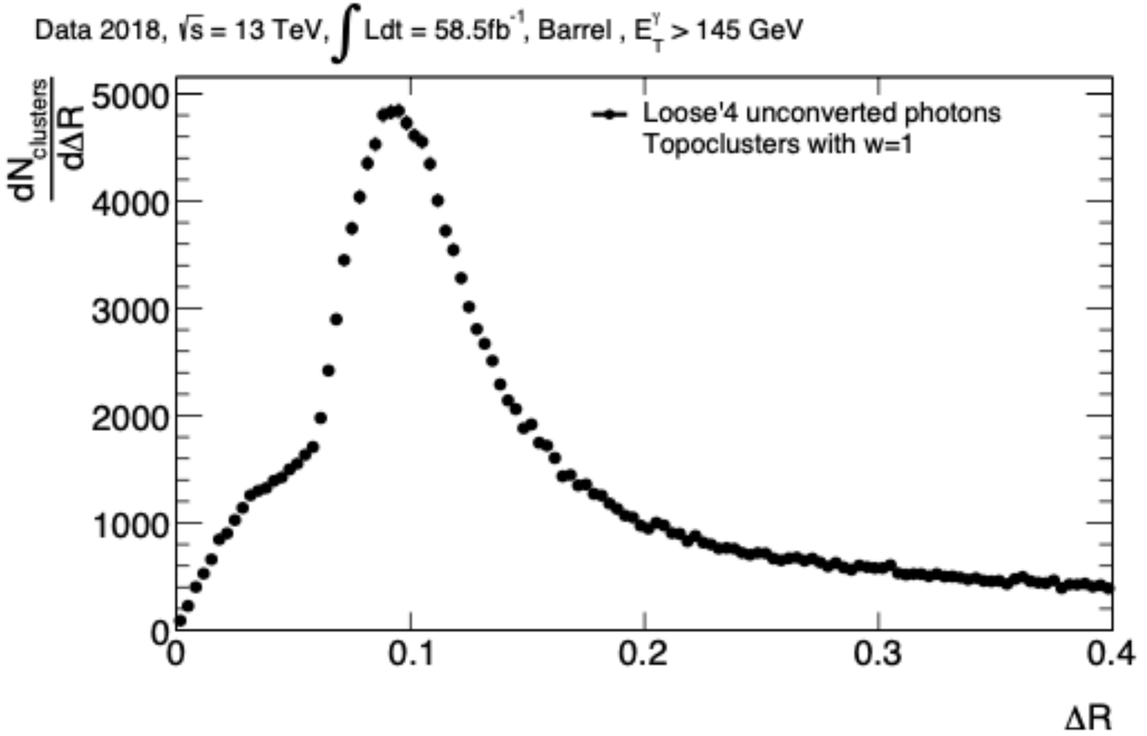

b)

Figure 5.15: *(a) The number of clusters as a function of ΔR and w around tight non isolated unconverted photon candidates in the barrel. (b) Slice of the histogram shown in (a) with $w = 1$, showing the density of topoclusters as a function of $\Delta R_{cl\gamma} \sim 0.1$.*

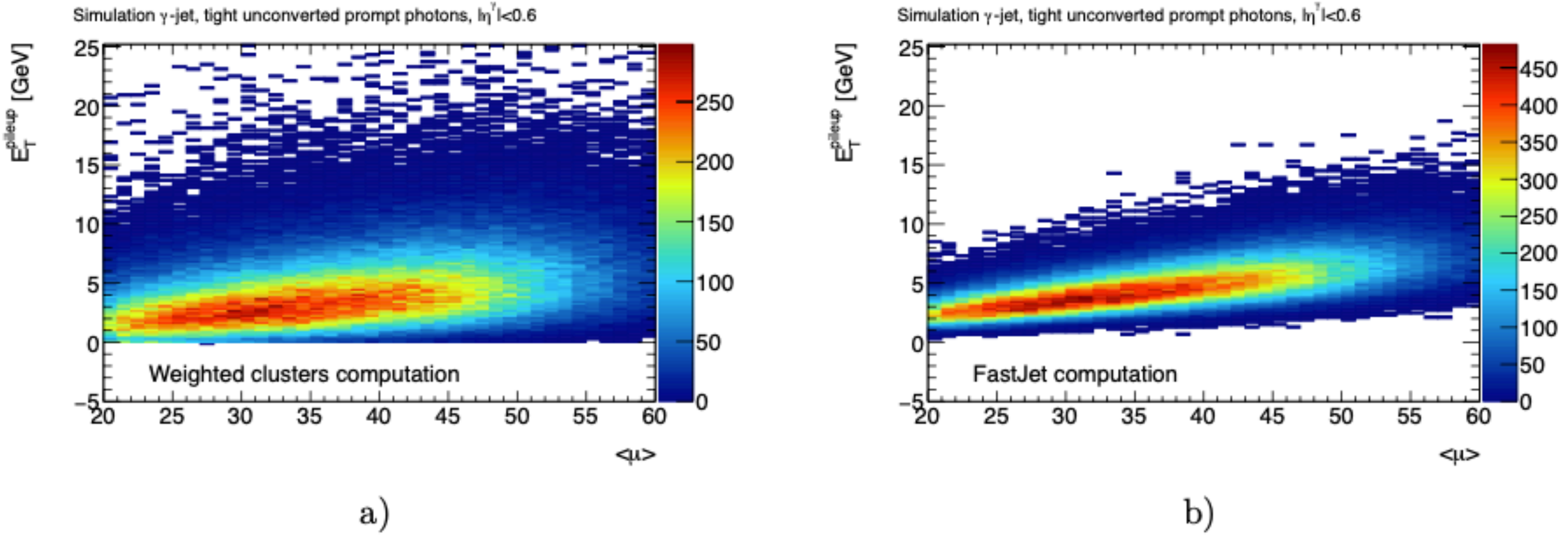

Figure 5.17: *Bidimensional distributions of the pileup energy contribution in the isolation cone for prompt simulated photons. (a) Estimate using the weighted isolation energy computation (b) Estimate computed with FastJet.*

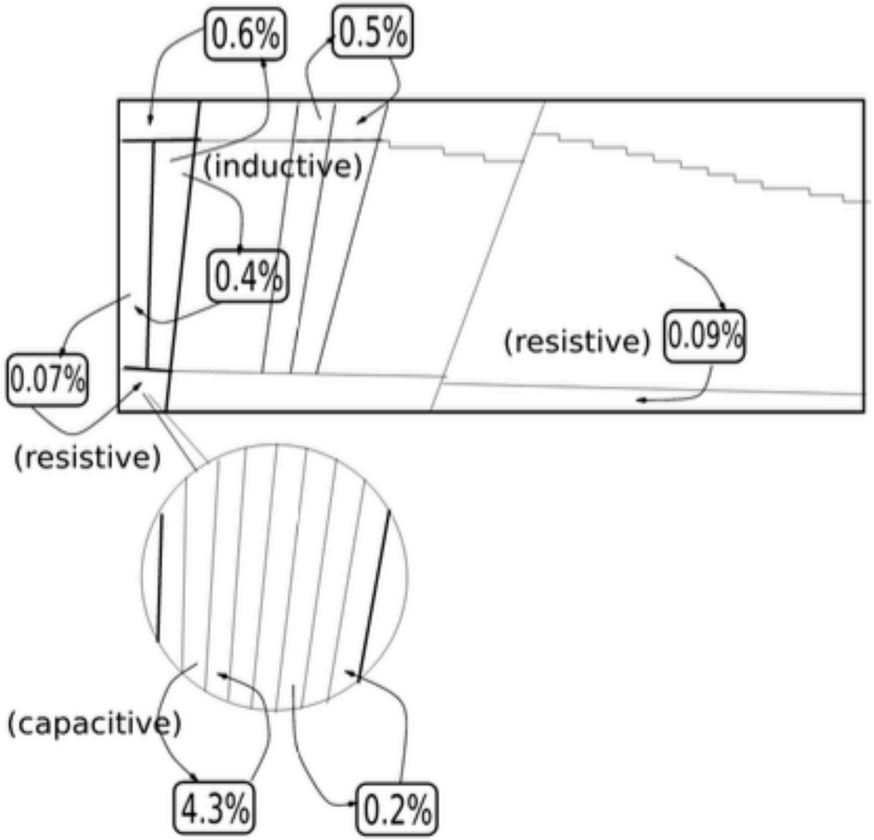

a) *Barrel map*

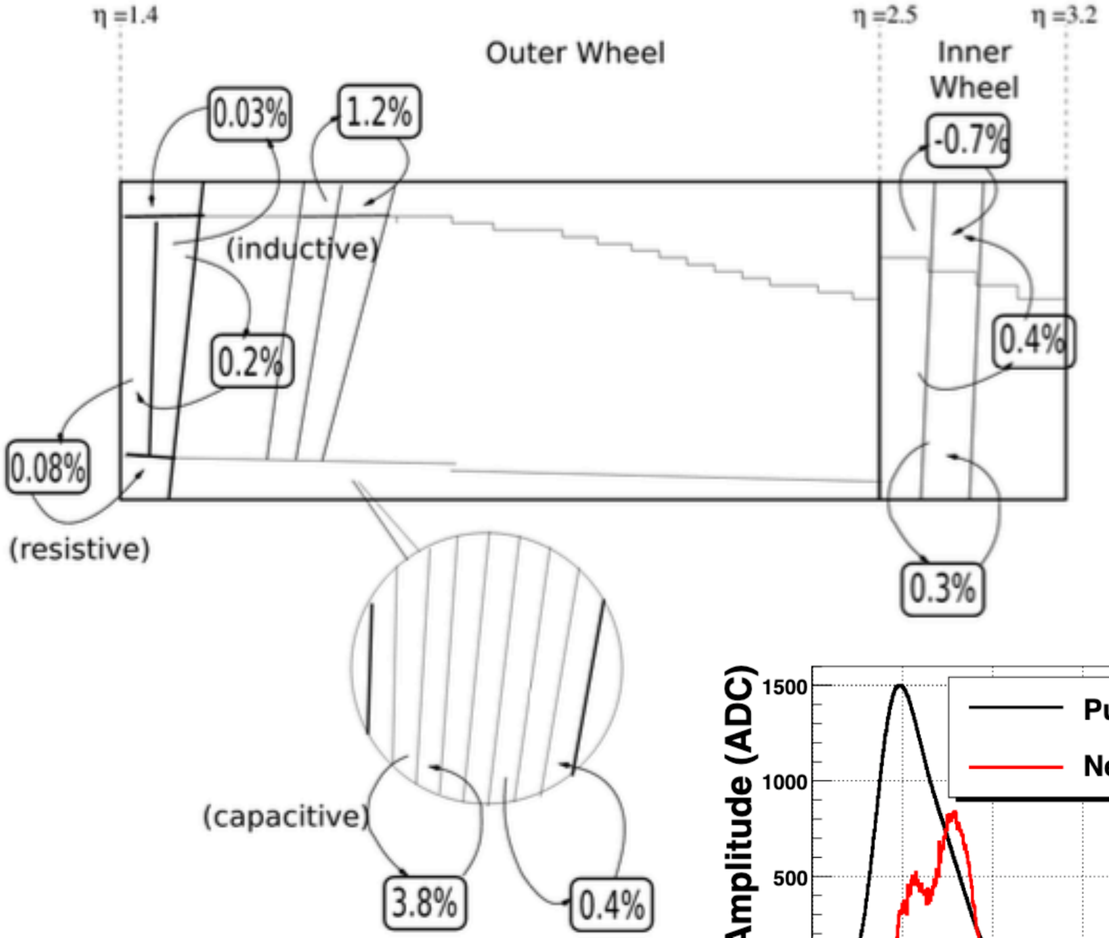

b) *Endcap map*

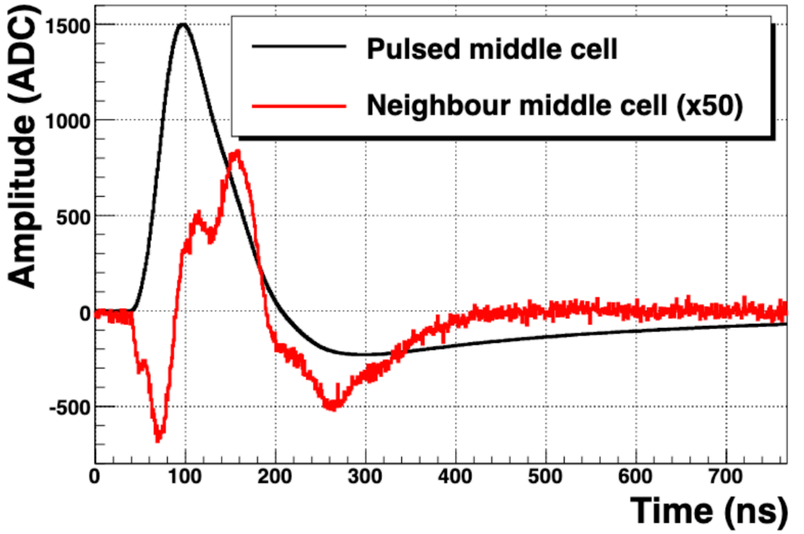

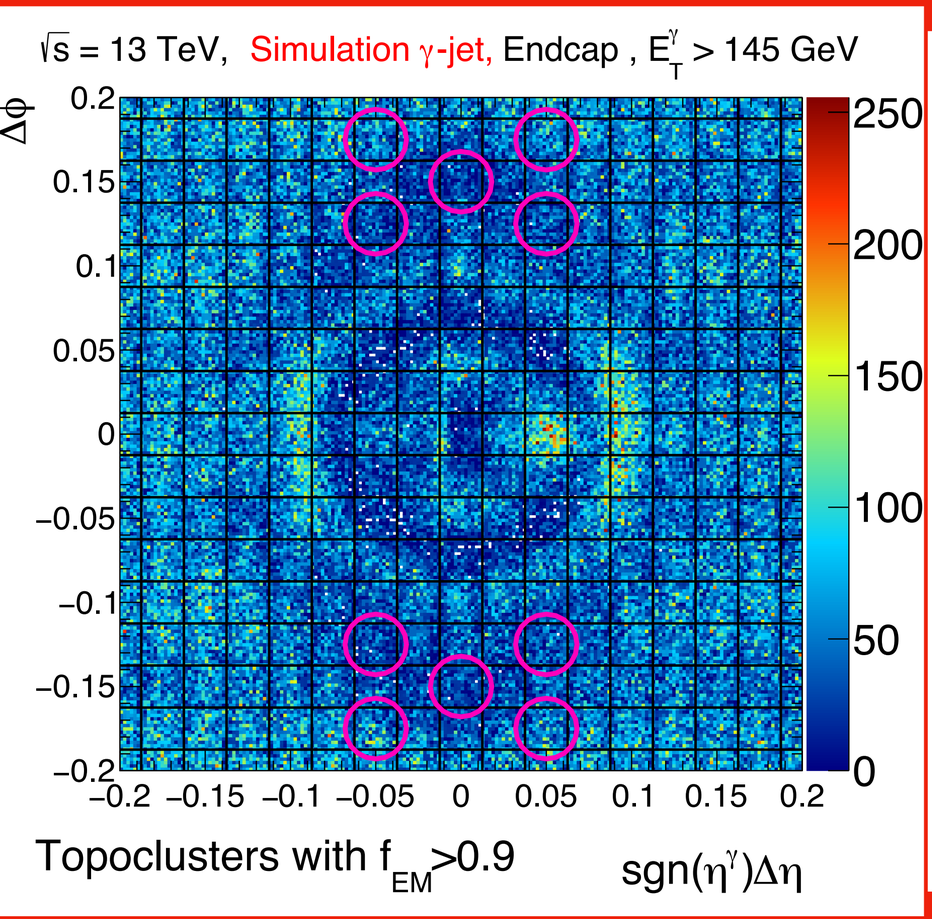
√s = 13 TeV, Simulation γ-jet, Endcap , E_T^γ > 145 GeV
Δφ
sgn(η^γ)Δη
Topoclusters with f_EM>0.9

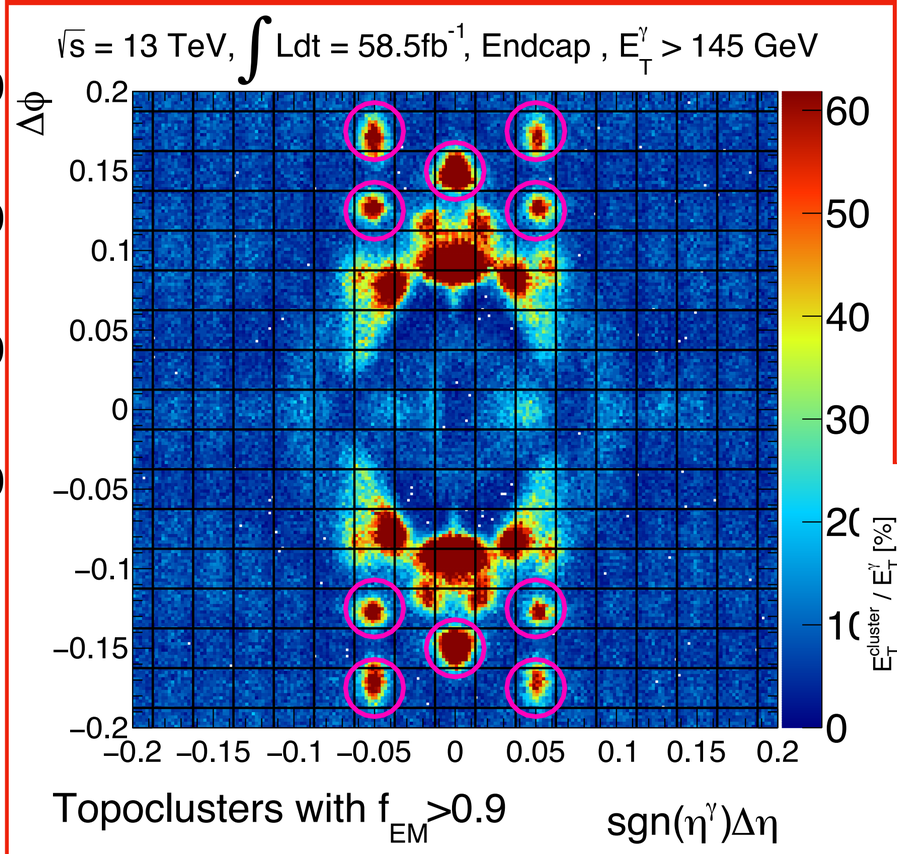
√s = 13 TeV, ∫ Ldt = 58.5fb^-1, Endcap , E_T^γ > 145 GeV
Δφ
sgn(η^γ)Δη
Topoclusters with f_EM>0.9

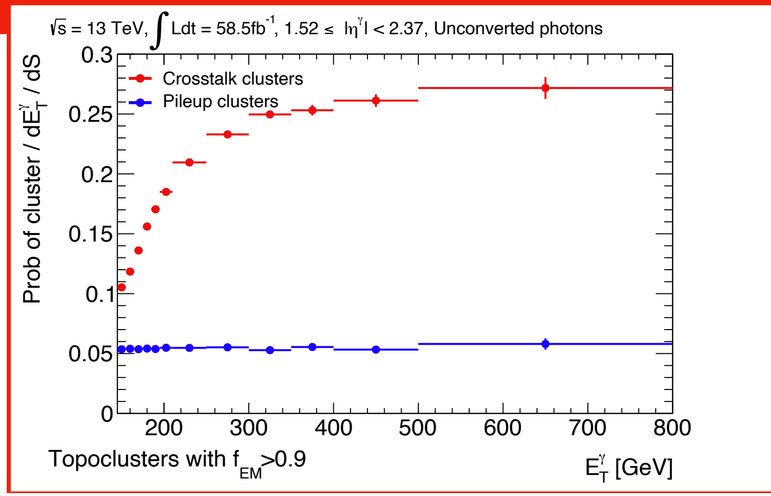
√s = 13 TeV, ∫ Ldt = 58.5fb^-1, 1.52 ≤ |η^γ| < 2.37, Unconverted photons
Crosstalk clusters
Pileup clusters
Prob of cluster / dE_T^γ / dS
E_T^γ [GeV]
Topoclusters with f_EM>0.9

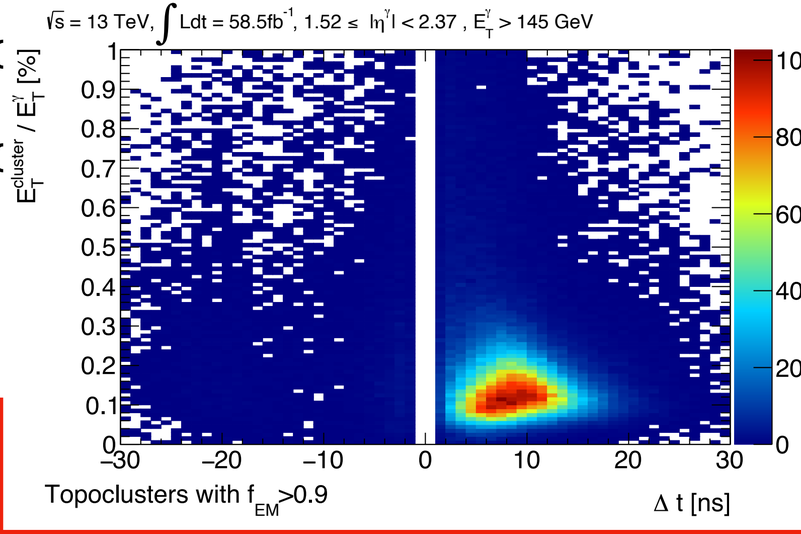
√s = 13 TeV, ∫ Ldt = 58.5fb^-1, 1.52 ≤ |η^γ| < 2.37 , E_T^γ > 145 GeV
E_T^cluster / E_T^γ [%]
Δ t [ns]
Topoclusters with f_EM>0.9

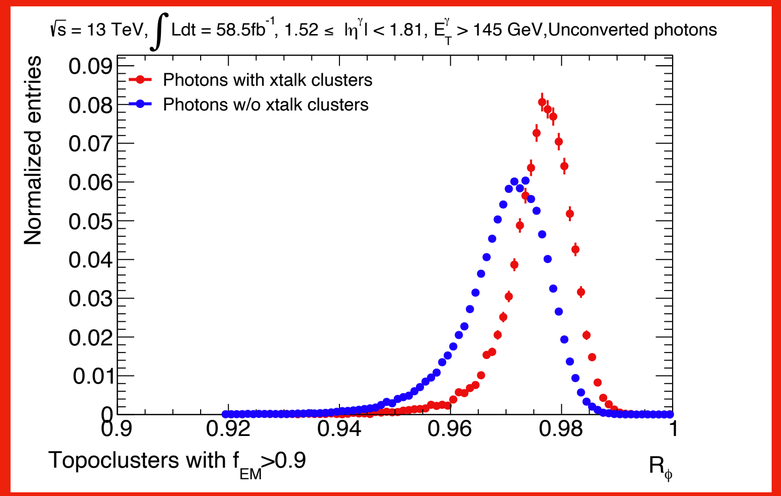
√s = 13 TeV, ∫ Ldt = 58.5fb^-1, 1.52 ≤ |η^γ| < 1.81, E_T^γ > 145 GeV,Unconverted photons
Photons with xtalk clusters
Photons w/o xtalk clusters
Normalized entries
R_φ
Topoclusters with f_EM>0.9

Analysis

$m_{\gamma\gamma} = 20$ GeV

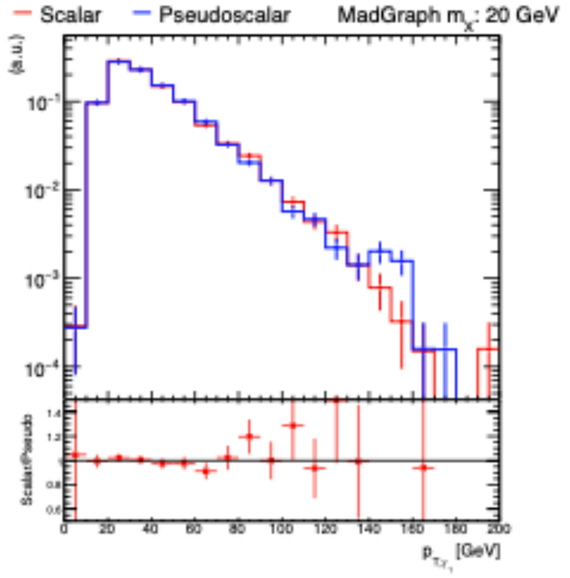

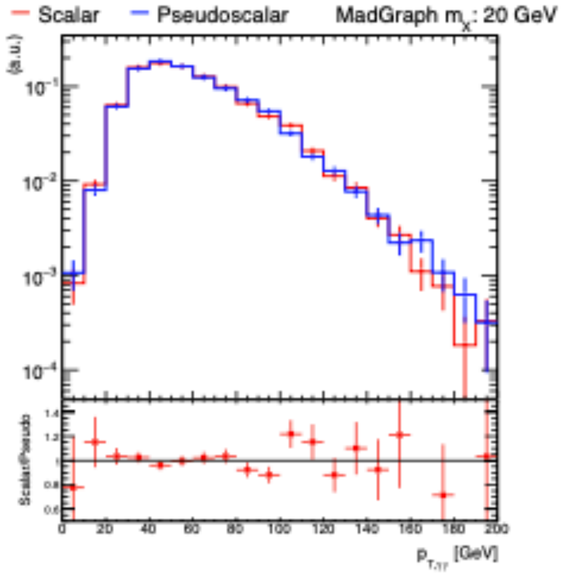

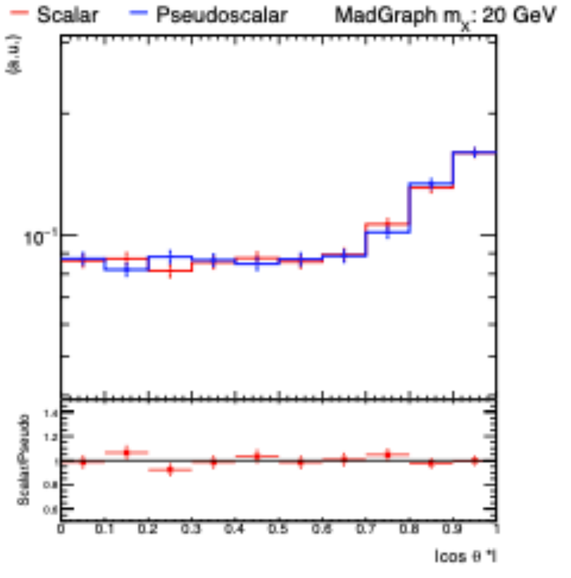

$m_{\gamma\gamma} = 60$ GeV

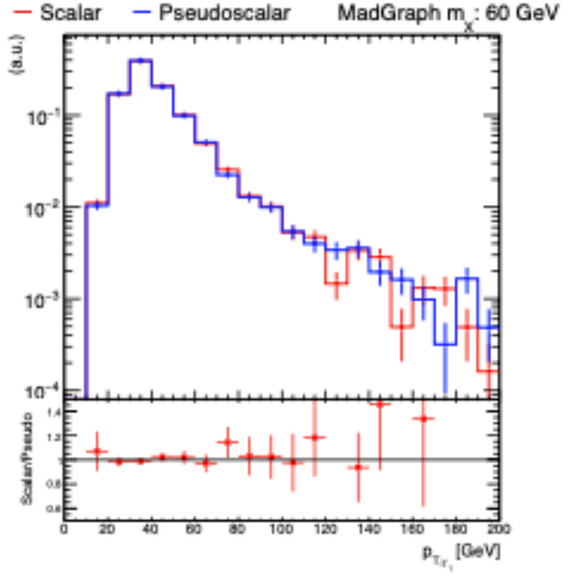

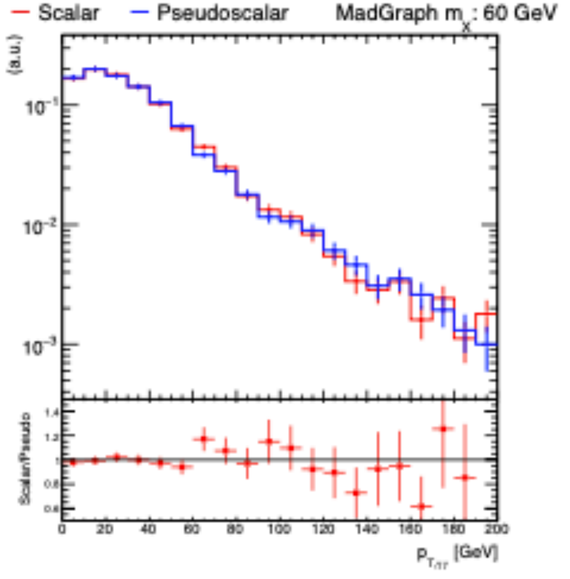

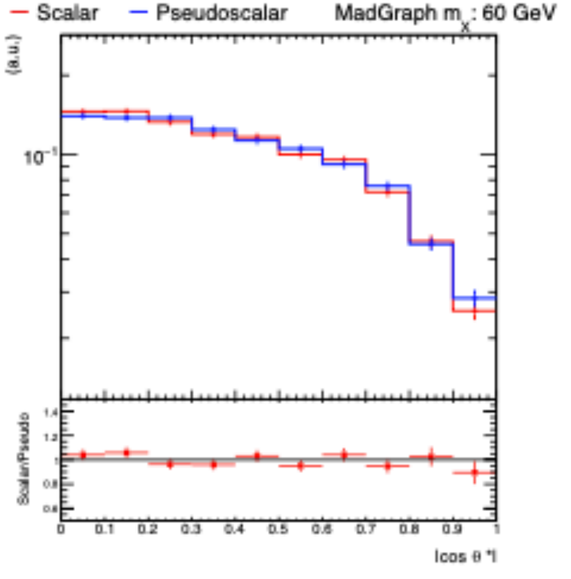

Filter bias estimation

Bias evaluated on inclusive Sherpa $\gamma\gamma$ samples

Two different contributions in the $p_{T,\gamma\gamma,\text{parton}}$ distribution for events with $p_{T,\gamma\gamma,\text{particle}} > 40$ GeV

- A δ at $p_{T,\gamma\gamma,\text{parton}} = 0$: events generated at NLO without any jets that after showering acquire $p_{T,\gamma\gamma,\text{particle}} > 40$ GeV. This represents 5.5% of the distribution
- Expected smoothly falling distribution.

Events in the δ in $m_{\gamma\gamma}$ fall in the region of the observed discrepancy.

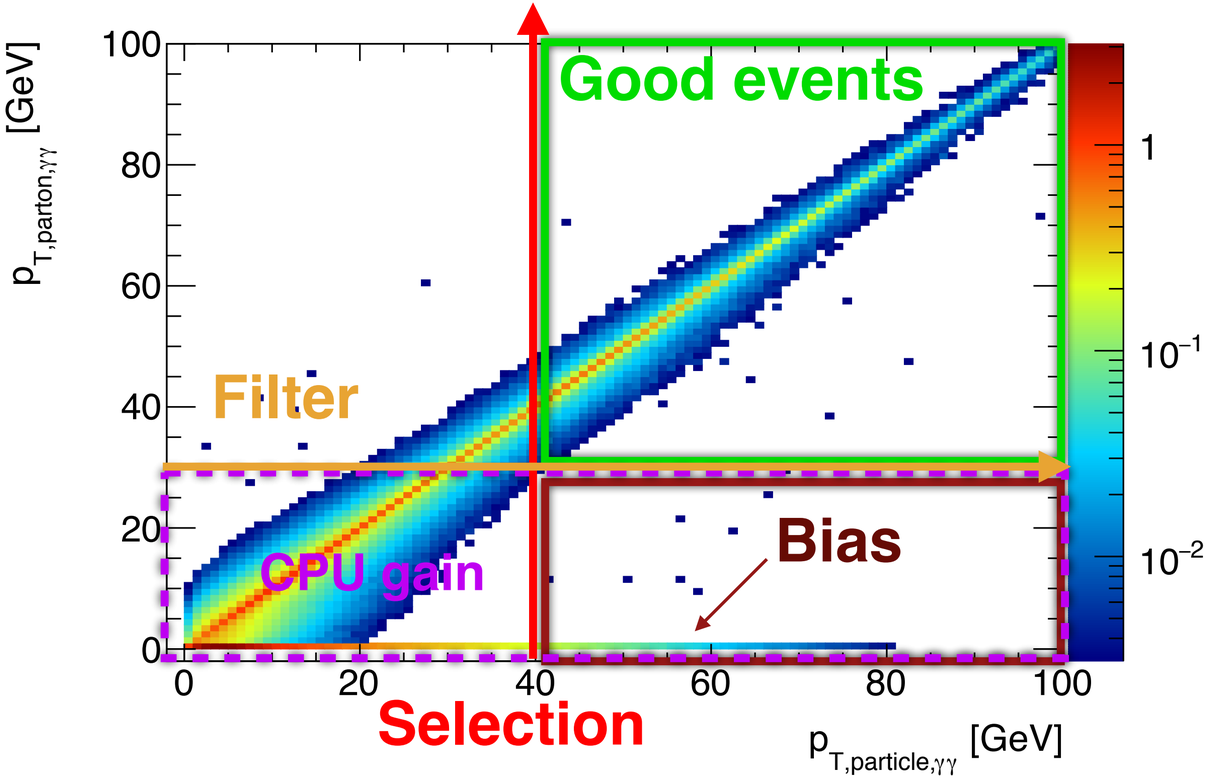

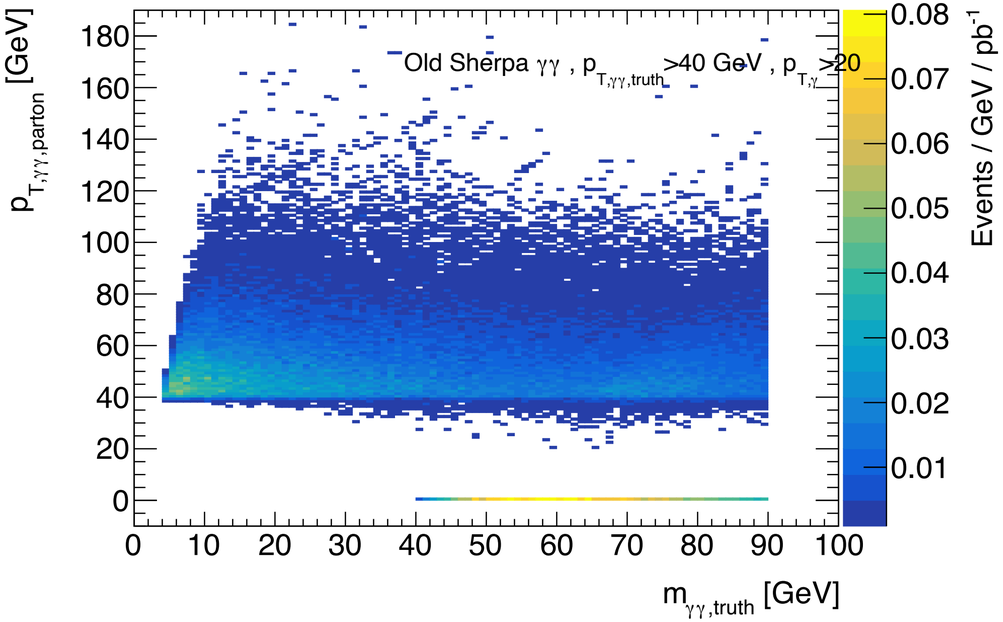

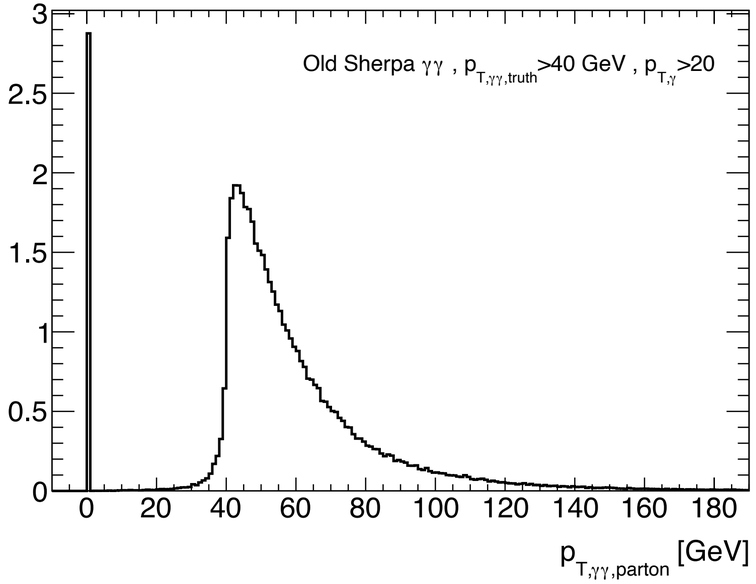

$p_{T,\gamma\gamma,\text{particle/truth}} > 40$ GeV

Some distributions

- Events in the delta not considered when evaluating the bias in JIRA.
- Any filtering in $p_{T,\gamma\gamma,parton}$ would create this bias since the contribution from NLO without jets is systematically removed.
  - The filter is necessary to produce sufficient statistics for the analysis.

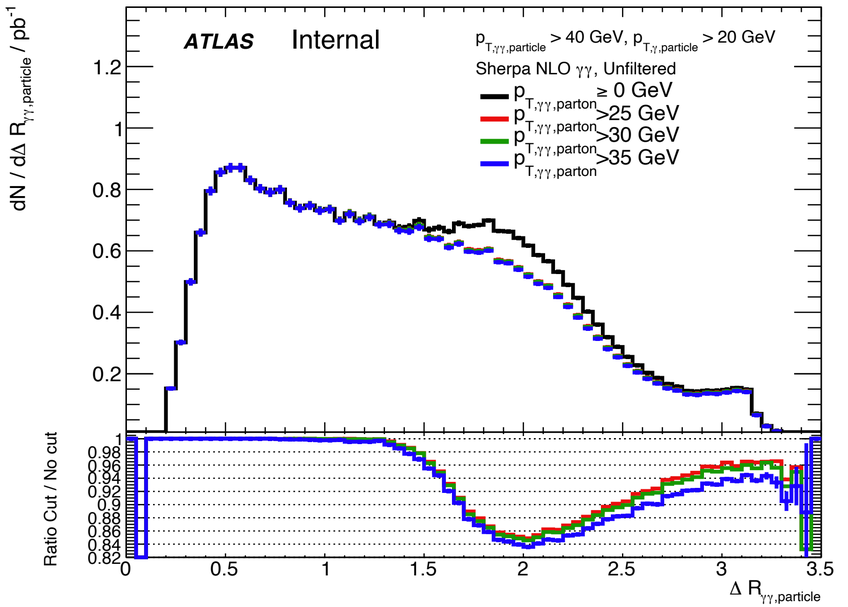

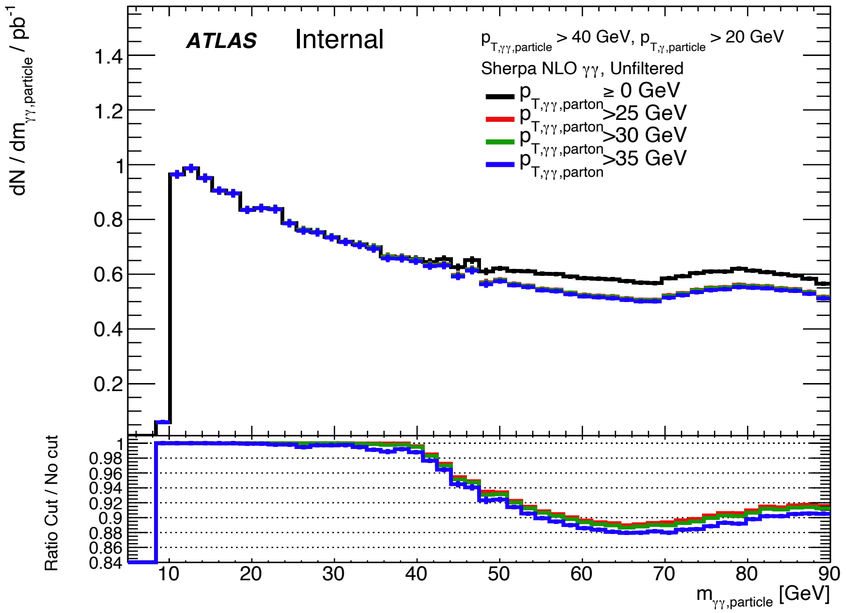

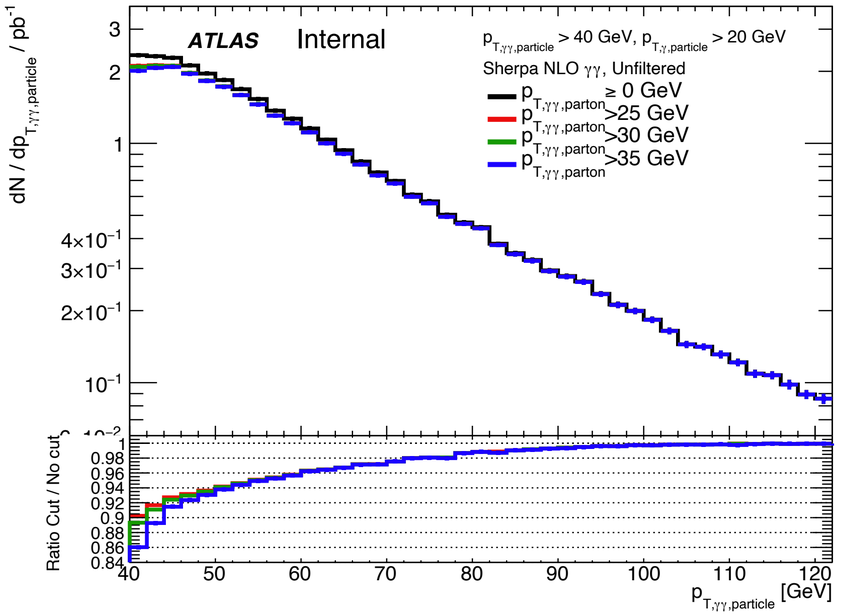

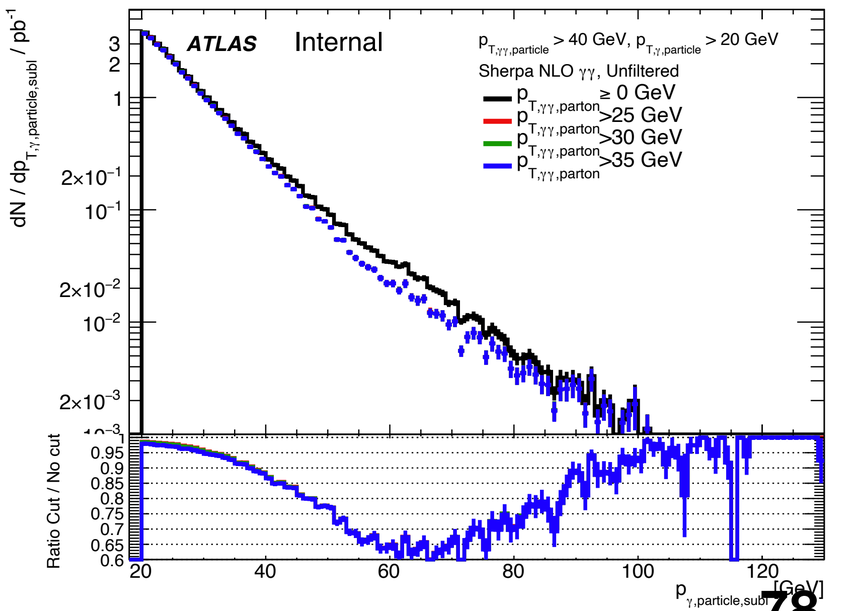

Bias correction: events reweighing

Events are reweighed using a 2D-map of weights computed from truth level Sherpa $\gamma\gamma$ samples.

- Good improvement is observed at truth level.
- Reduced bias after reconstruction down to 5% difference
  - Possibly due to remaining disagreement in $p_{T,\gamma,subl}$ at truth level.

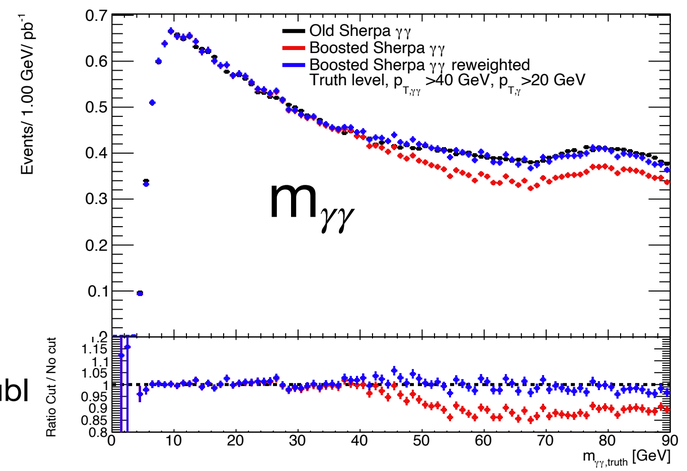

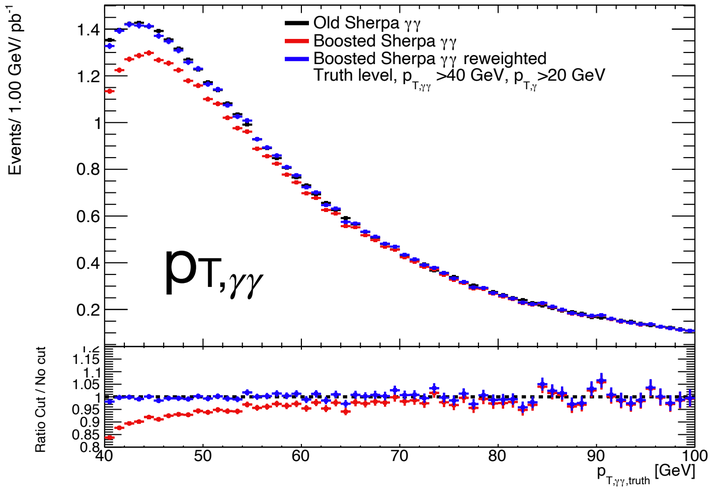

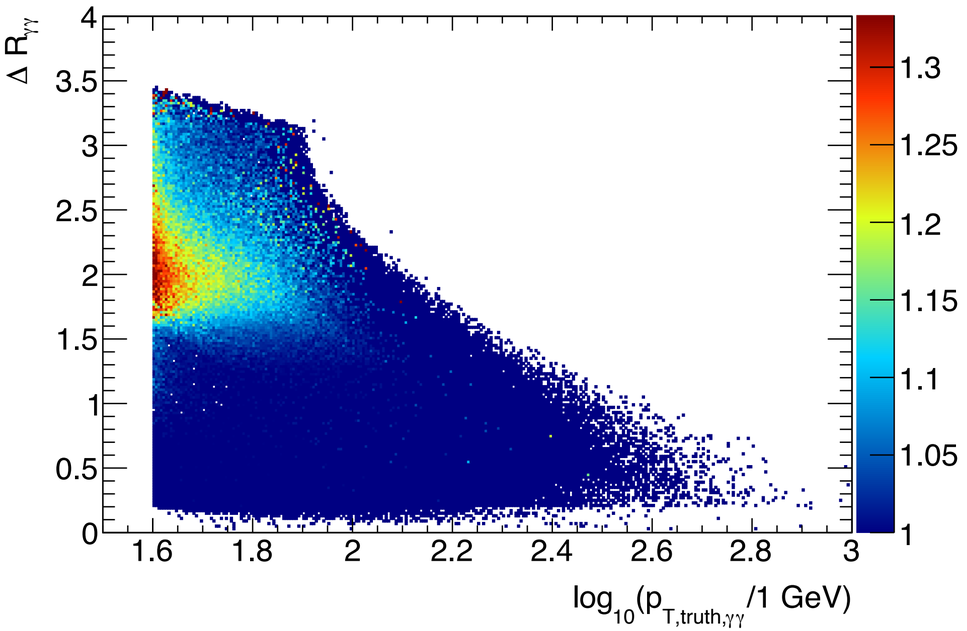

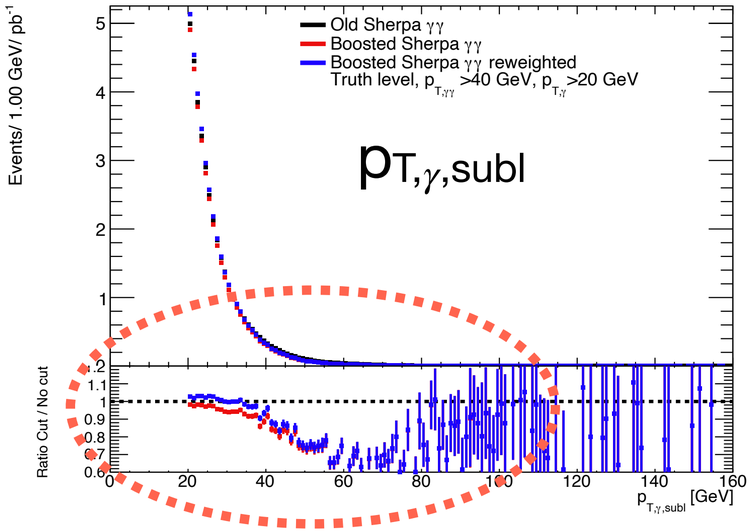

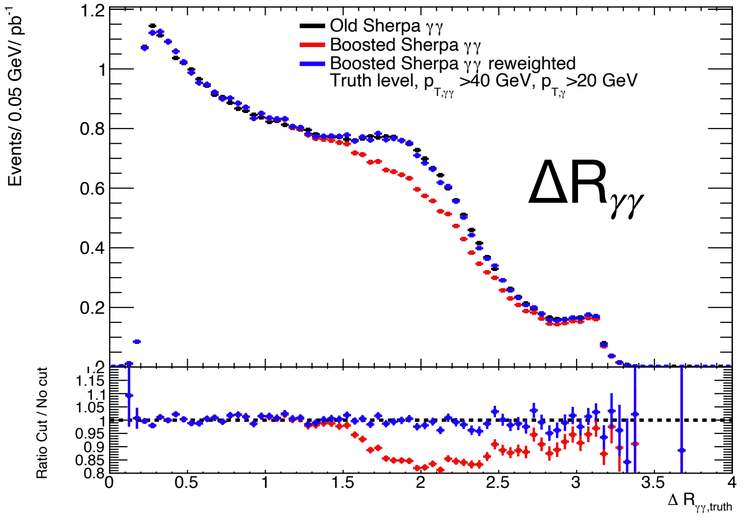

Differences between Sherpa samples

Unfiltered Sherpa $\gamma\gamma$ NLO (old sample) Fullsim:

- Per-photon filters at parton level: $p_{T,\gamma,lead} > 20$ GeV and $p_{T,\gamma,subl} > 18$ GeV
- Diphoton filter: $\Delta R_{\gamma\gamma} > 0.2$
- Two slices with different statistics: $m_{\gamma\gamma}$:[0,50] and [50,100]

New filtered sample: boosted Sherpa $\gamma\gamma$ NLO Fastsim:

- Same cuts on the per-photon filters.
- $\Delta R_{\gamma\gamma} > 0.15$.
- $p_{T,\gamma\gamma,parton} > 35$ GeV

Significant difference observed after reconstruction driven by bias underestimation.

- Fair agreement between fastsim and fullsim simulations with the old samples observed.

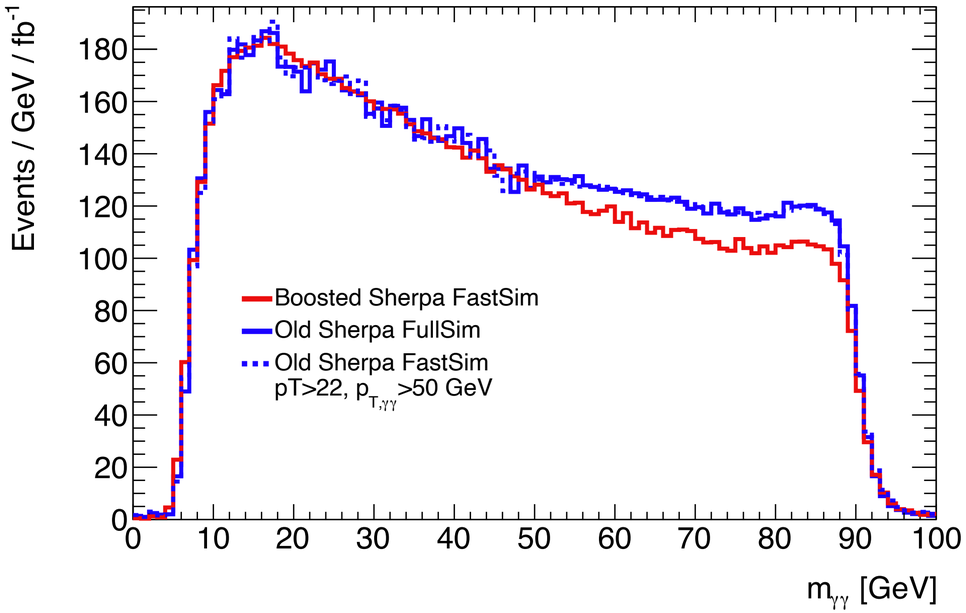

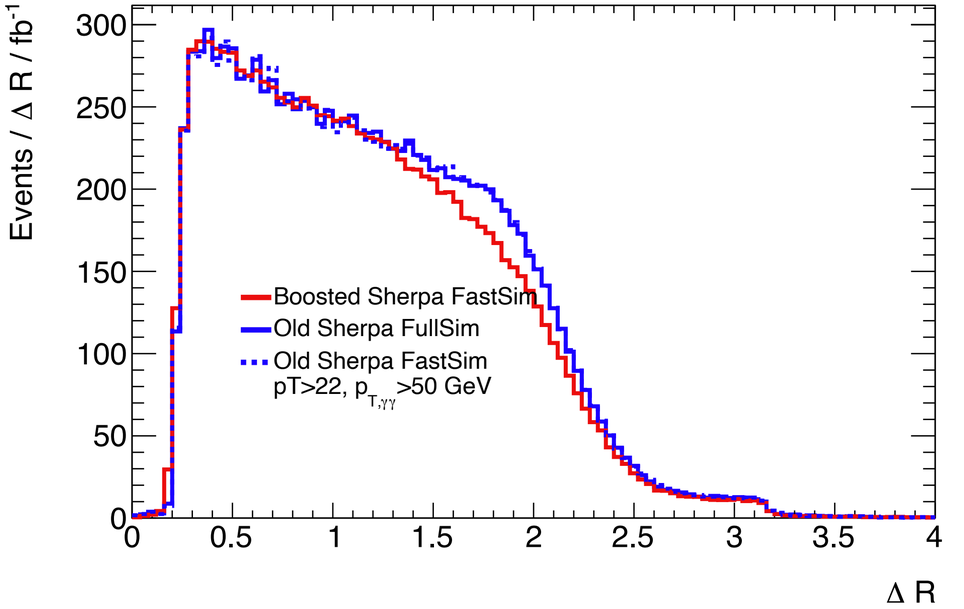

Template comparison

Relative effective statistics between old and boosted Sherpa $\gamma\gamma$.

- Factor ~x6 gain compared to the first slice
- Half the statistical power in the second slice.

Possible templates:

- Statistically limited, small bias (larger ΔR) and sliced Sherpa $\gamma\gamma$
- Biased, unsliced and with larger statistics boosted Sherpa $\gamma\gamma$.

Visible statistical gain in the low mass region

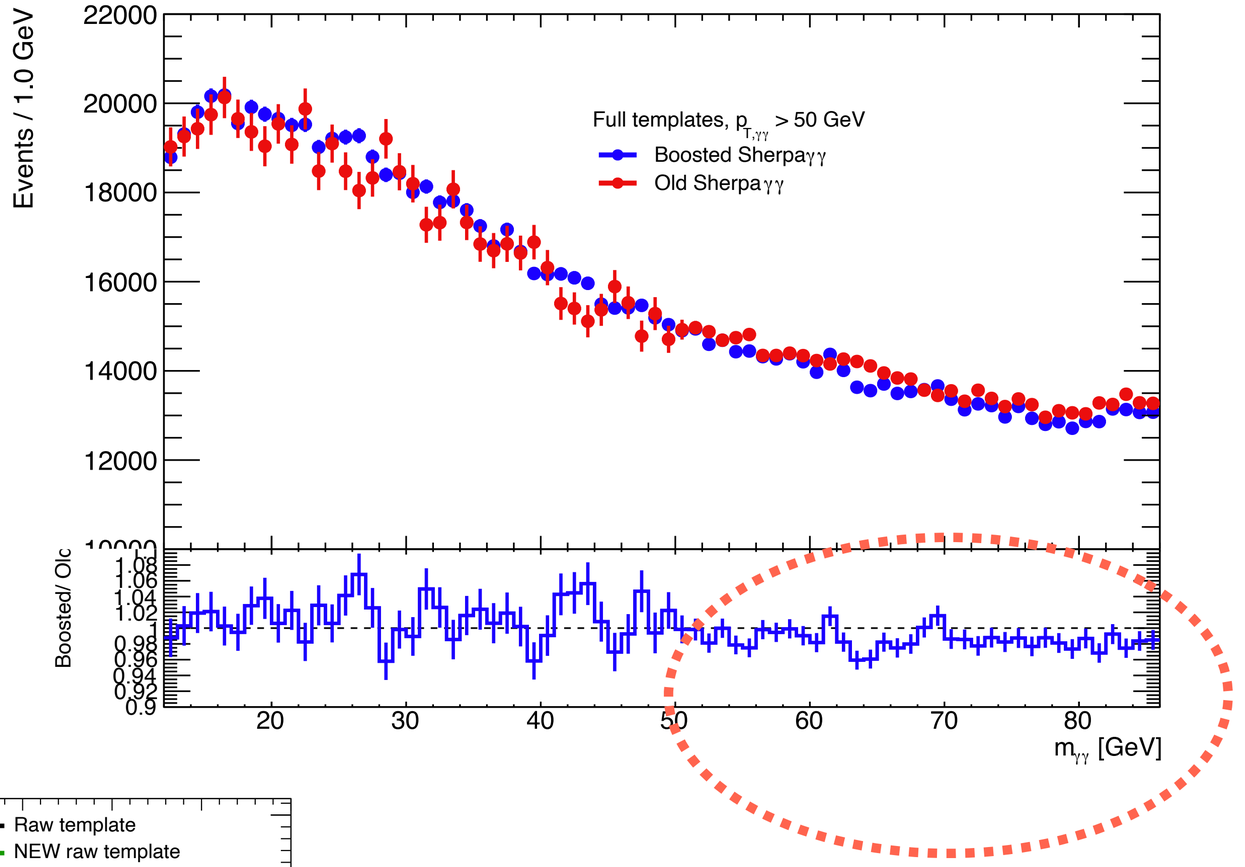

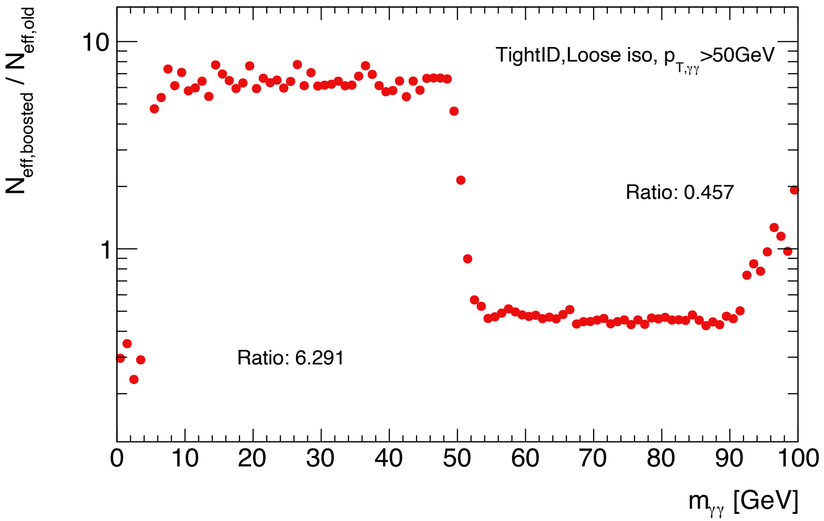

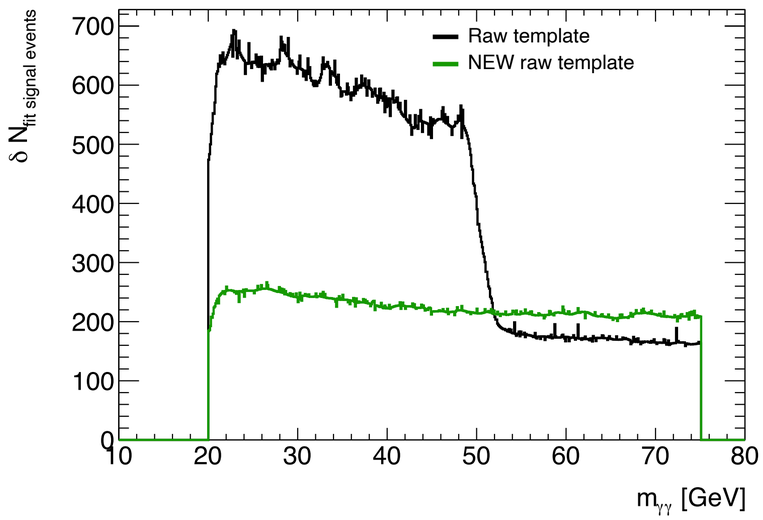

Remaining bias from $\gamma\gamma$ component

Factor ~x√6 gain in the error of fitted signal yield in bkg-only templates

Event selection: triggers

Lowest unprescaled diphoton triggers are chosen to attain the lowest invariant mass possible.

Diphoton triggers have evolved during Run2 to cope with increasing luminosity and rates.

- From 2017, isolation at trigger level is applied on both photon candidates.

Year	2015	2016 up to D3	2016 from D3	2017	2018
L1 item	L1_2EM10VH	L1_2EM15VH	L1_2EM15VH	L1_2EM15VHI	L1_2EM15VHI
HLT item	2g20_tight	2g20_tight	2g22_tight	2g20_tight_icalovloose	2g20_tight_icalovloose
luminosity $[fb^{-1}]$	3.2	11.5	21.5	43.6	58.5

Events recorded with prescaled triggers used for background shape estimation.

- Very limited statistics due to large prescalings on the L1 item (6.3 fb^{-1} of integrated luminosity)
- Only loose identification required.

Year	2015	2016	2017	2018
HLT item	2g20_loose	2g20_loose	2g20_loose	2g20_loose
luminosity $[fb^{-1}]$	0.32	3.3	1.56	1.08

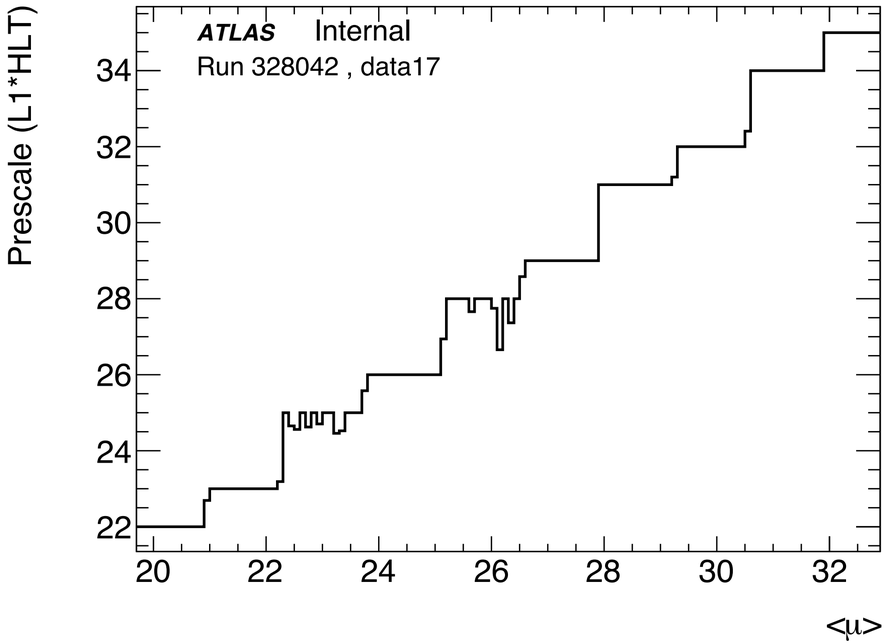

Event and diphoton selection

Events recorded with a diphoton trigger with $E_T^\gamma > 20\ GeV$

Standard diphoton selection common to other $\gamma\gamma$ analyses + boosted selection:

- Two reconstructed photons with $E_T^\gamma > 22\ GeV$
- Tight identification
  - Relaxed photonID used for background estimation purposes
- Loose track and calorimetric isolation

Selection on the diphoton transverse momentum $p_T^{\gamma\gamma}$ cut trade of two criteria:

- Enhance signal significance
- Keep sensible low mass reach

Photon pairs are required to have $p_T^{\gamma\gamma} > 50\ GeV$

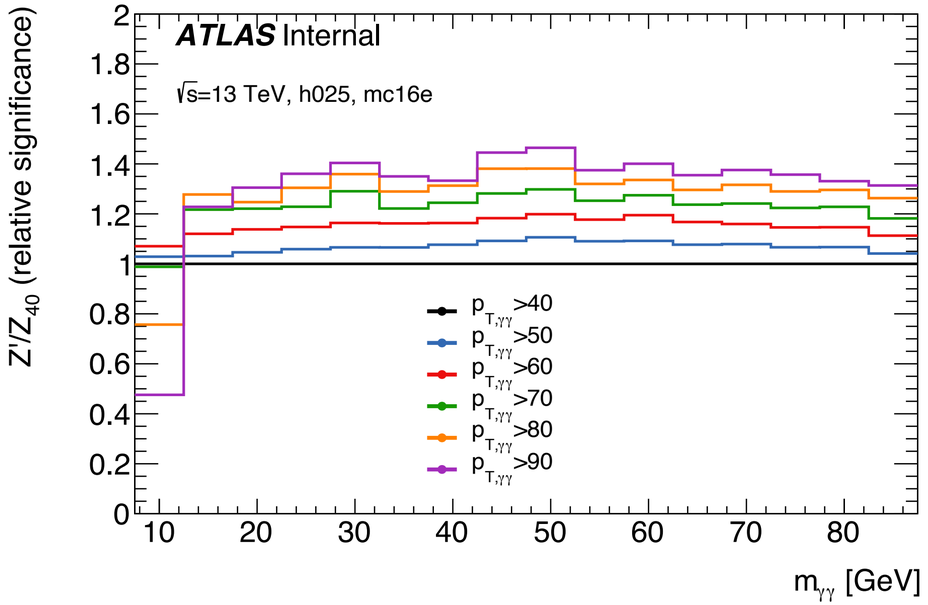

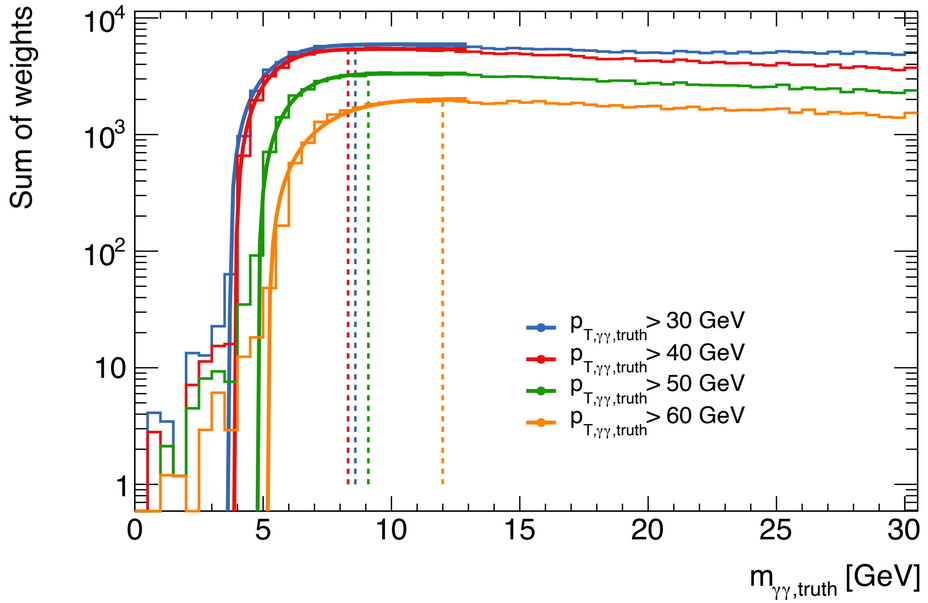

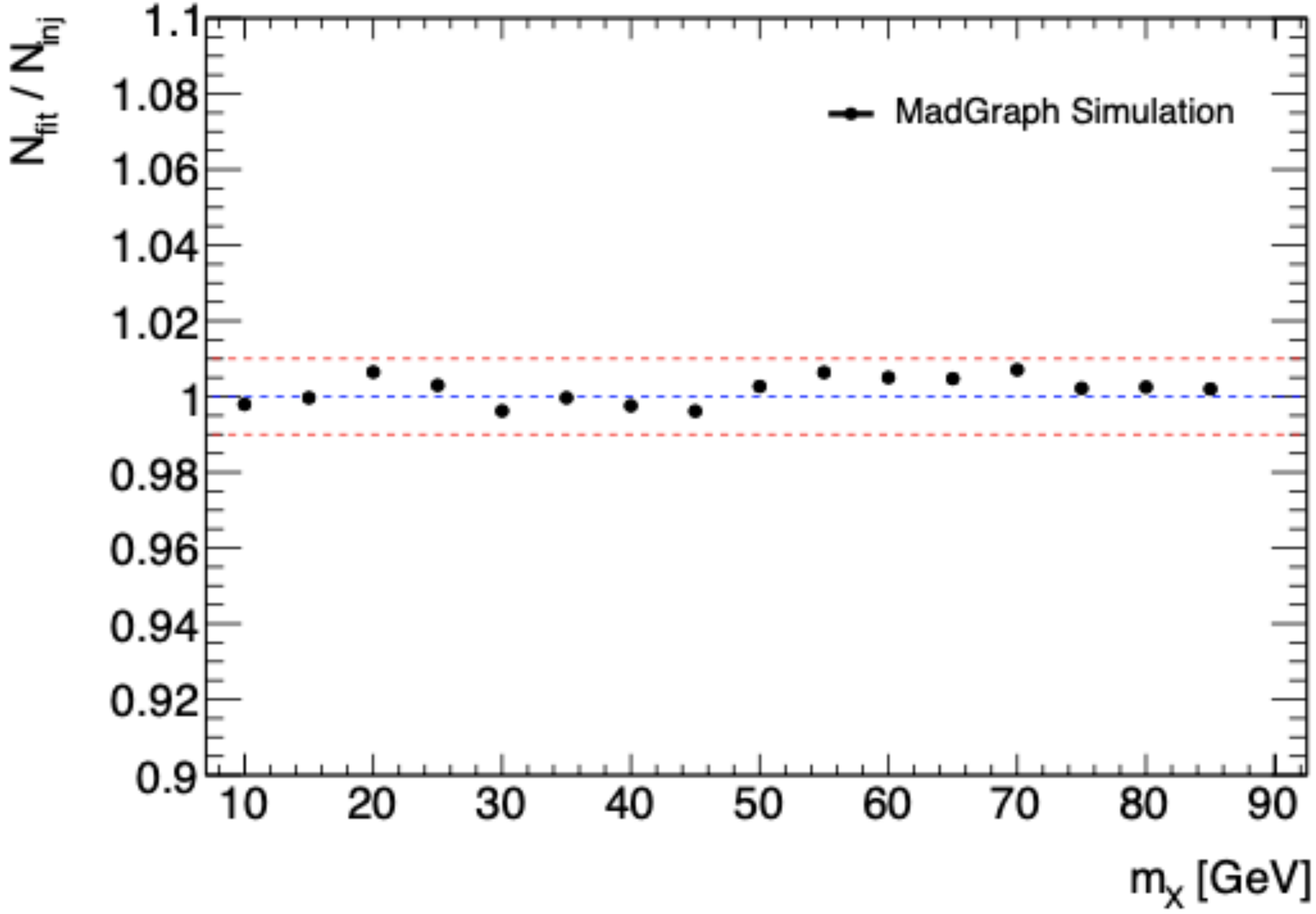
N_{fit} / N_{inj}
1.1
1.08
1.06
1.04
1.02
1
0.98
0.96
0.94
0.92
0.9
MadGraph Simulation
10
20
30
40
50
60
70
80
90
m_X [GeV]

Background decomposition

The respective fraction of each component is obtained from a 2xABCD (two photons) method.

- Extrapolates number of background events in the signal regions from control regions.
- Signal region defined as tightly identified and isolated diphoton pairs.
- Control regions defined by inverting photonID and/or isolation requirements for leading/ subleading or both photon candidates.
  - Limited in statistics.

$$f_{\gamma\gamma} = \frac{N_{\gamma\gamma}}{N_{\gamma\gamma} + N_{\gamma j/j\gamma} + N_{jj}}$$

$$f_{\gamma\gamma} = 0.642 \pm 0.006(stat)^{+0.028}_{-0.032}(syst)$$

Reducible background component increases towards lower masses.

2x

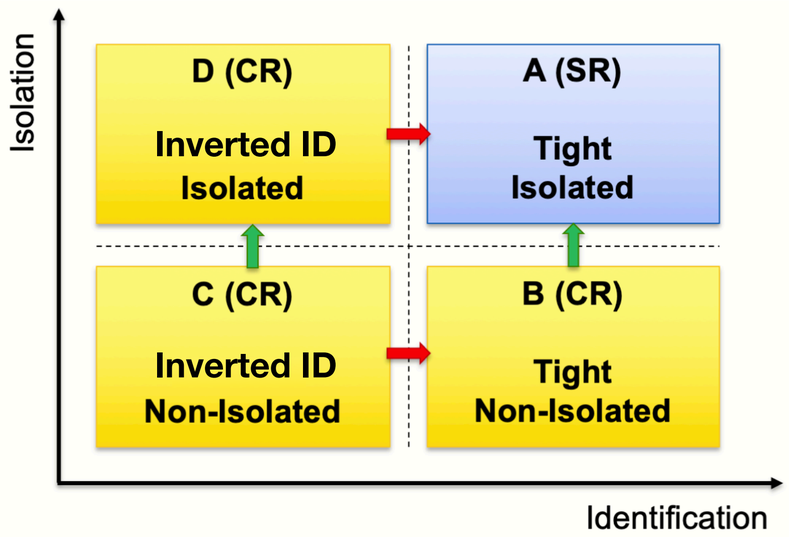

Methodology limited by poor statistics

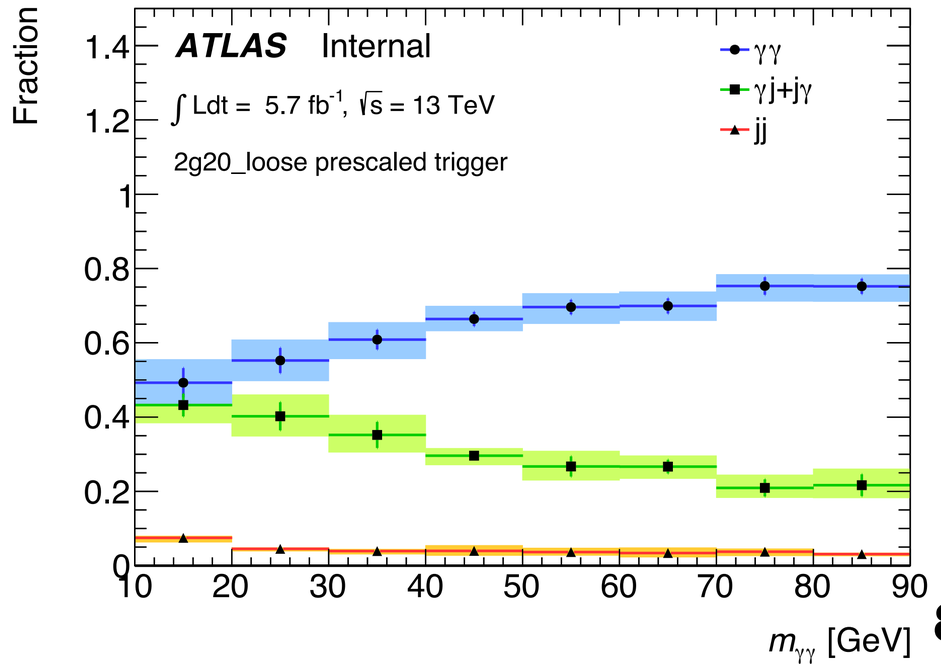

Background decomposition

2x2D method used to estimate the relative fractions of irreducible and reducible backgrounds.

- Extrapolates number of background events in the signal regions from control regions.
- Signal region defined as tight and isolated diphoton pairs.
- Control regions defined by inverting photonID and/or isolation requirements for leading/ subleading or both photon candidates.

  - Other definitions will be accounted for as systematic variations of the template

- Limited in statistics due to usage of prescaled triggers: 5.71 fb^{-1}
- Reducible background component increases towards lower masses.

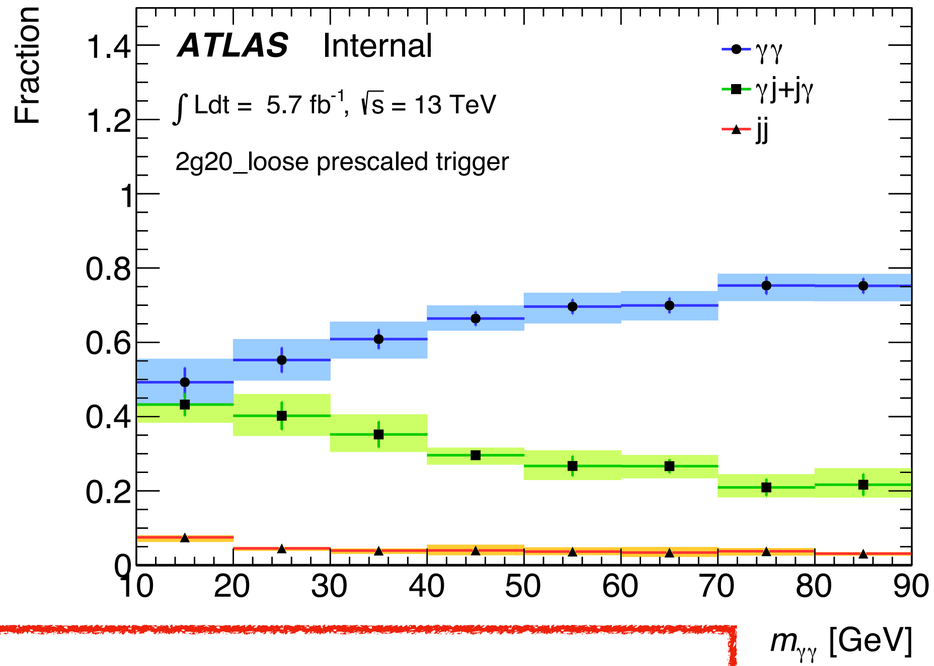

$$f_{\gamma\gamma} = 0.642 \pm 0.006(stat)^{+0.028}_{-0.032}(syst)$$

Reducible template corrections

Shape of control regions is not directly representative of the background in the signal region.

- True diphoton events can fail tight identification and be in the control region samples.
  - Contribution estimated from Sherpa $\gamma\gamma$ and statistically subtracted.
- Different diphoton triggers are used for signal and control regions.
  - Different efficiency due to different L1 seeds modifies background shape in data17-18.
  - Correction estimated from simulation.

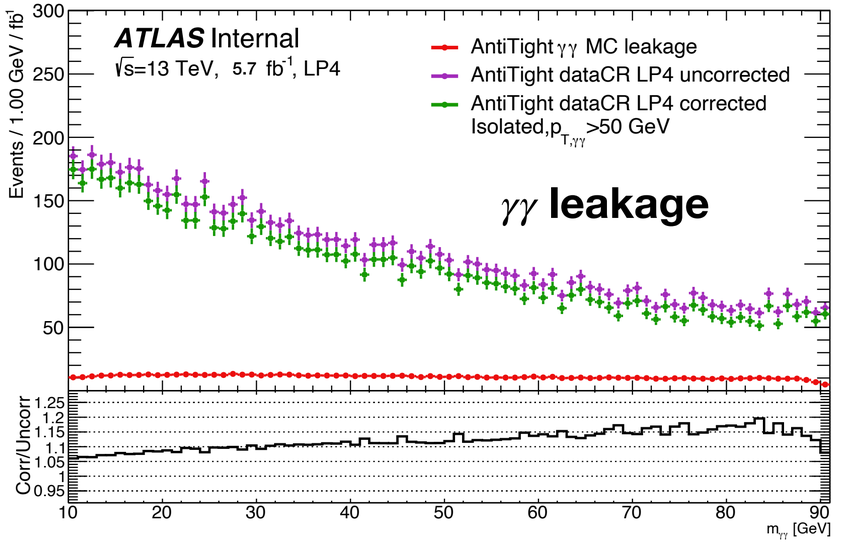

Trigger correction

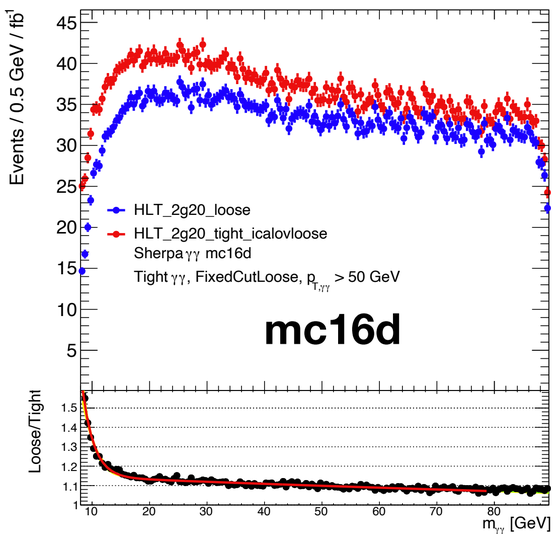

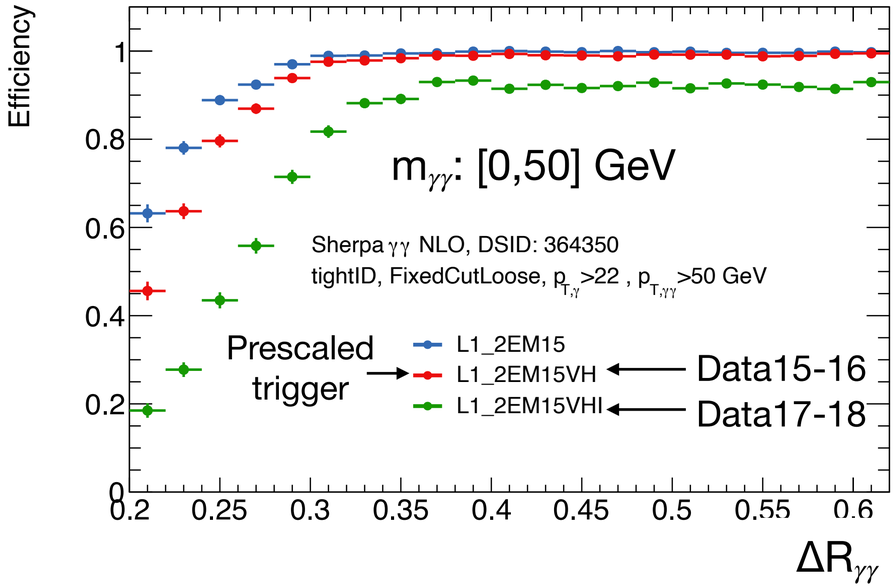

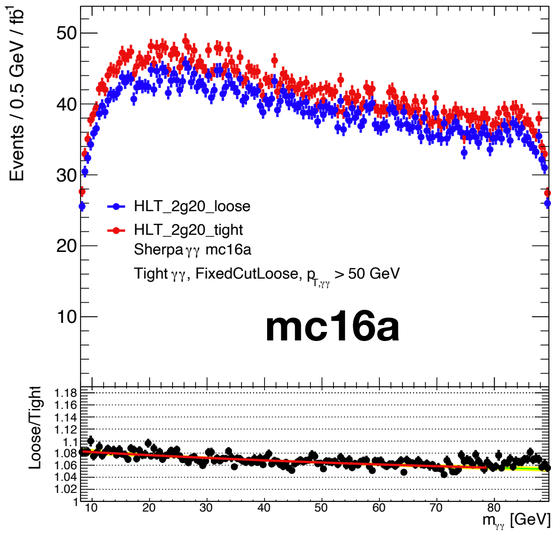

Background components

The irreducible $\gamma\gamma$ component is extracted directly from simulated QCD diphoton events.

The reducible component is more complicated:

- Fake rejection of photon identification is very large (thousands)
- If simply simulating γj/jγ, the sample would be very limited in statistics.

Instead, it is obtained from **data**.

- Control regions (CR) defined by inverting photon identification for leading/ subleading or both photon candidates.
- Needs some corrections:

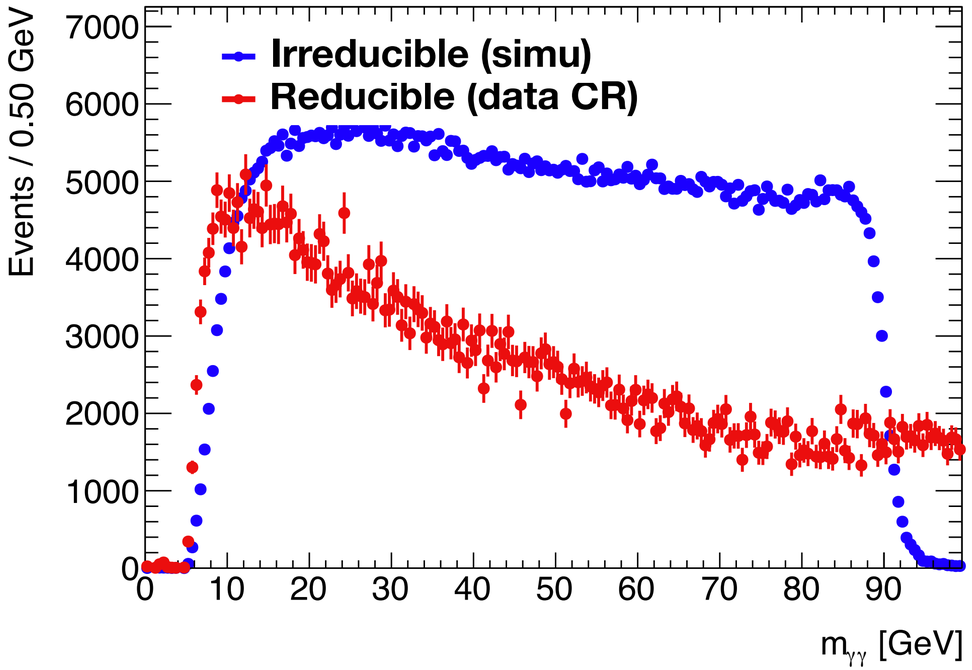

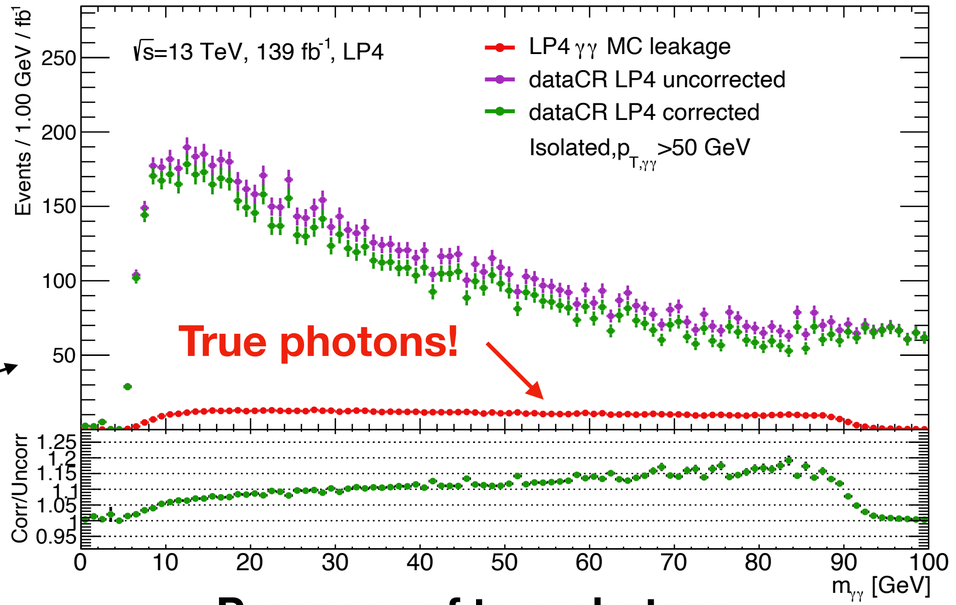

Photon identification is not 100% efficient: some photons end up in the CR and need to be subtracted

Presence of true photons modifies the shape!

Irreducible component

To ensure that we can reach the lowest possible masses, the turn-on needs to be robustly described.

- Two main functional forms evaluated: “FermiDirac-like” function and an “inverted ”exponential (1-exp(-x))

Shape beyond 20 GeV described with a monotonically decreasing function.

- With current statistics, a simple exponential provides a reasonable shape description

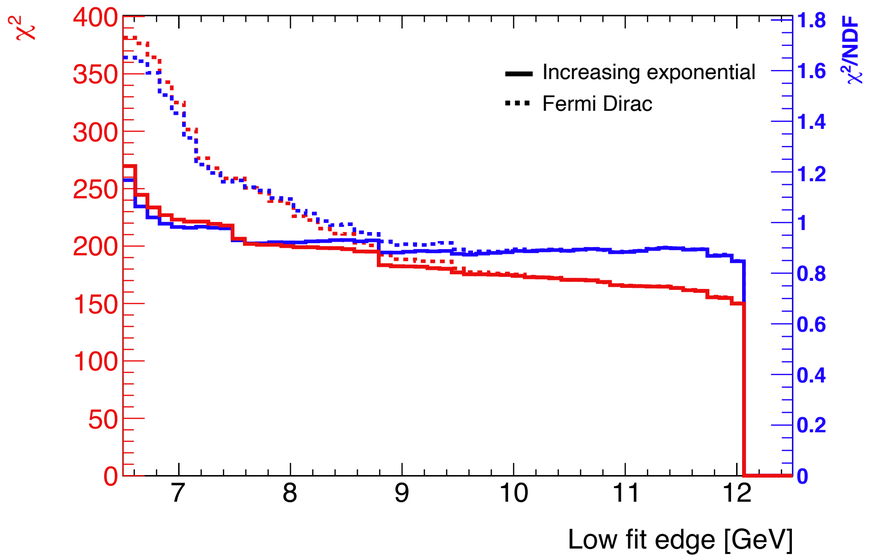

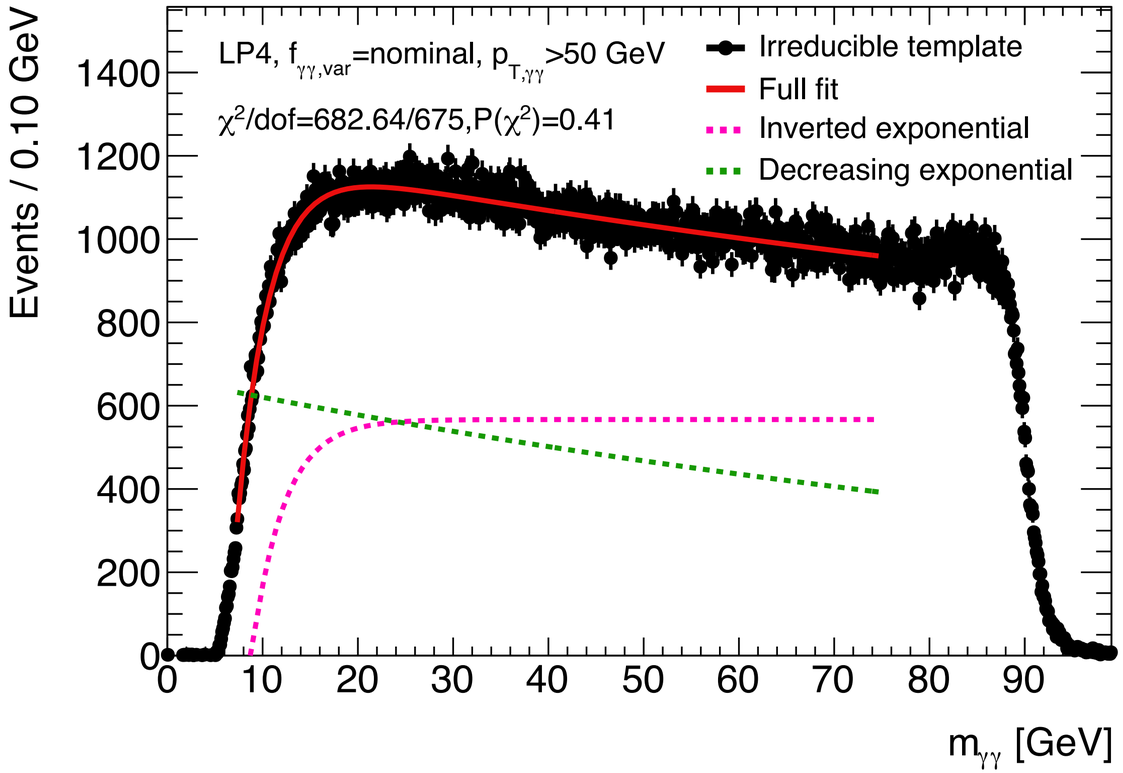

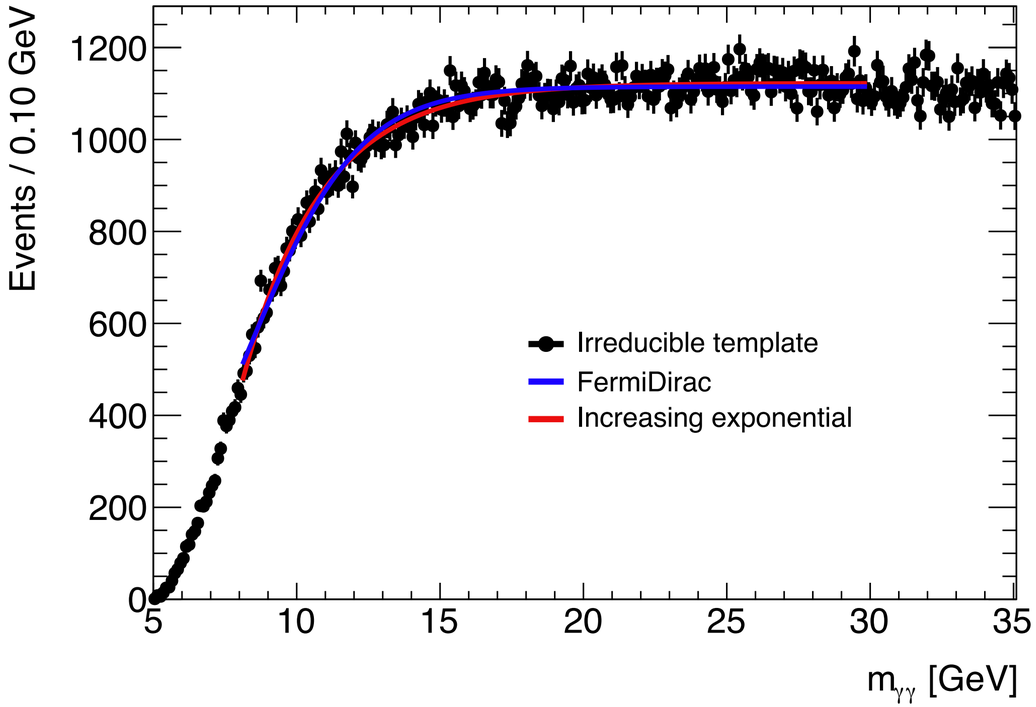

$$irred(x) = f_{turn-on}\, F_{turn-on} + (1 - f_{turn-on}) F_{decreasing}$$

Background shape description

Background shape is described with analytical functions

- Special care is given to the turn-on region

Strategy: describe separately each component; then combine the functions

A robust description will allow the search to reach very low masses!

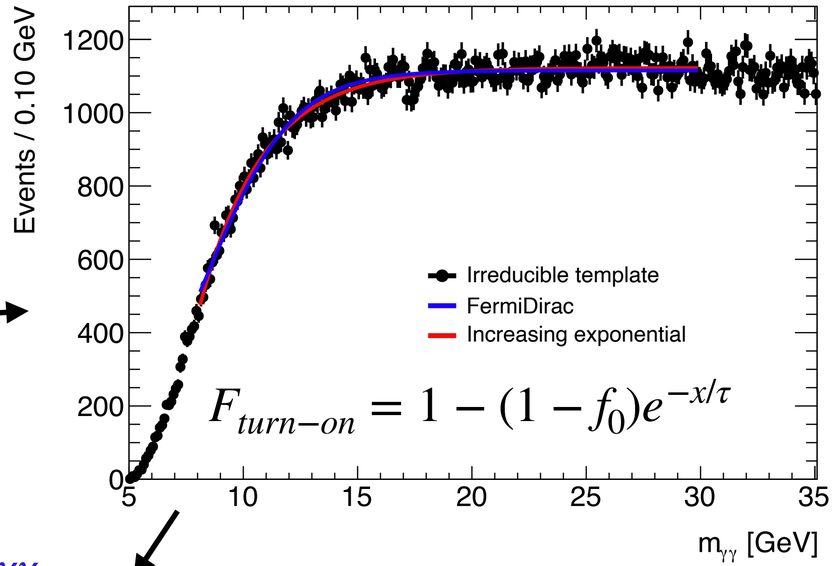

Reducible γ-jet and dijet

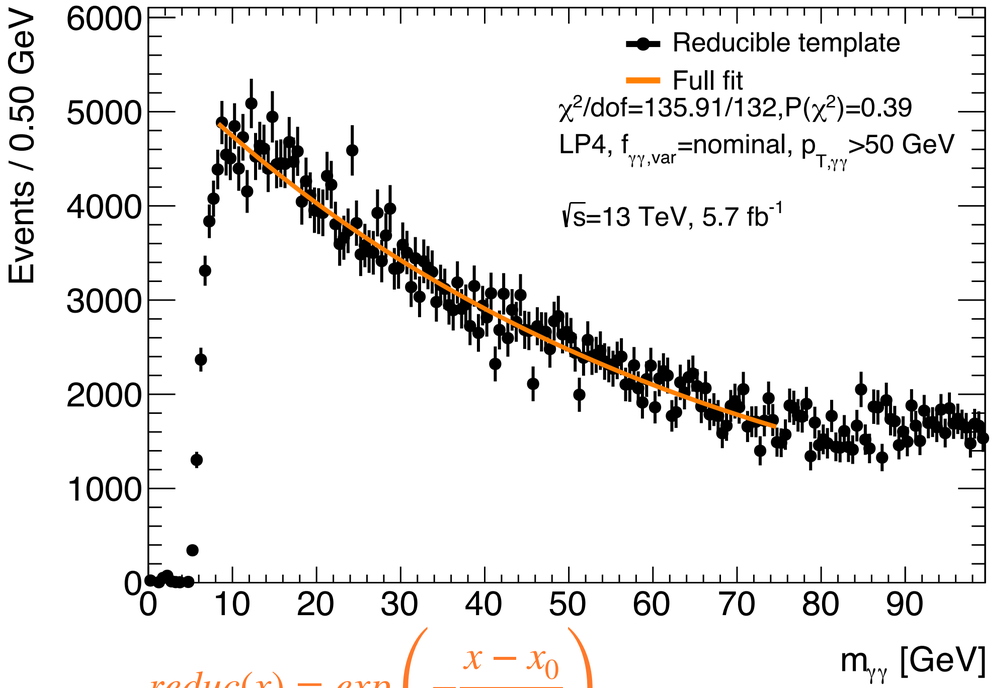

$$reduc(x) = exp\left(-\frac{x - x_0}{\tau_{reduc}}\right)$$

Irreducible $\gamma\gamma$

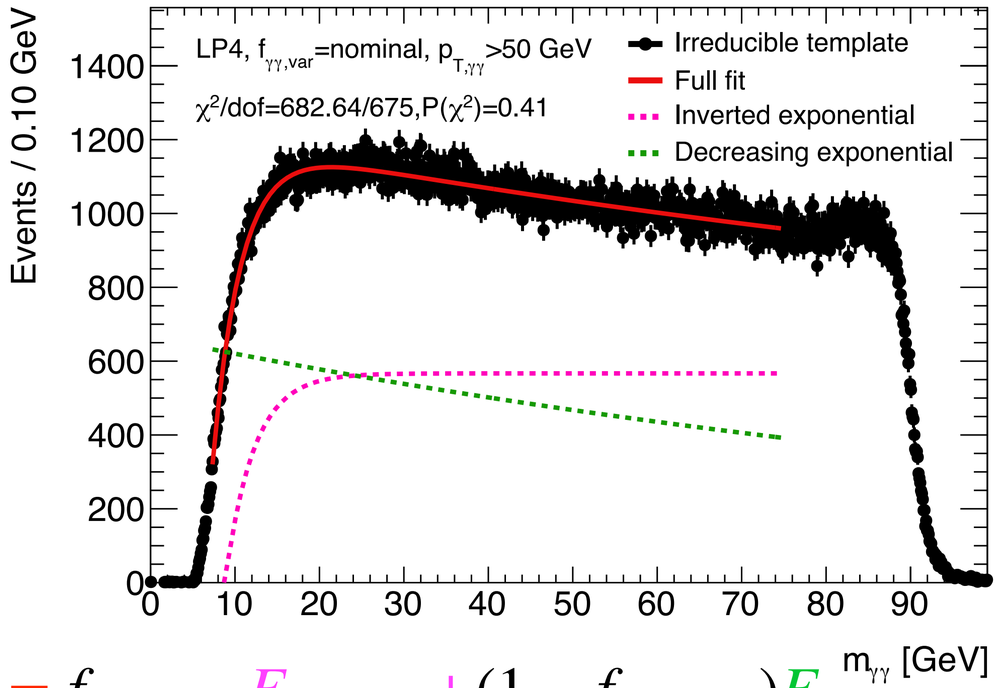

$$irred(x) = f_{turn-on}\, F_{turn-on} + (1 - f_{turn-on}) F_{decreasing}$$

Full template description

Full template described with this strategy by the sum of the irreducible and reducible functions.

- Reasonable and robust description based on the background decomposition

Characteristics of a good function:

- Flexible enough to describe variations of the turn-on.
- Sensible changes in curvature to avoid “absorbing” a signal in the background.

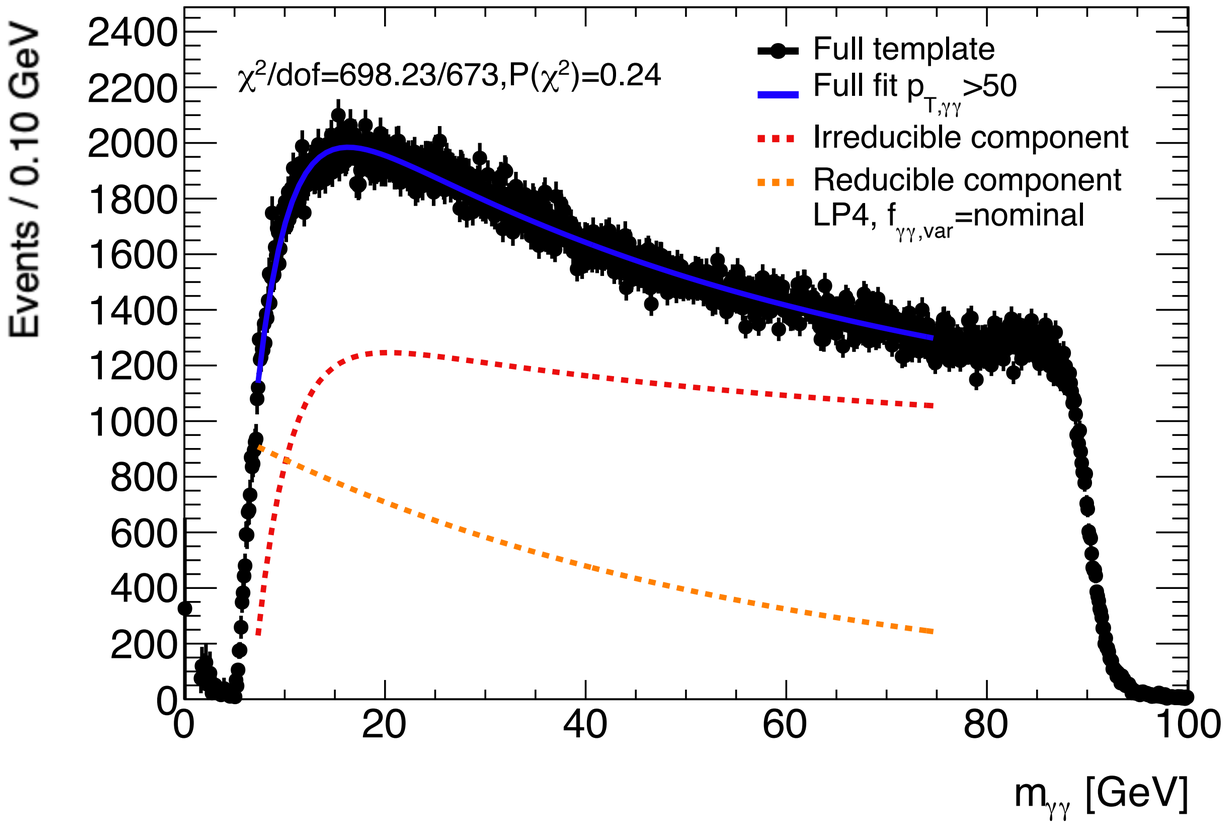

$$f_x = f_{\gamma\gamma}\, irred(x) + (1 - f_{\gamma\gamma})\, reduc(x)$$

$$f_{\gamma\gamma} = 0.66 \pm 0.02$$

Small caveat: limited simulated samples (in statistics) make difficult the decision on the analytical function to be used.

Consistency checks (I)

Same model appears to be flexible enough to describe the systematic template variations:

- LoosePrime control regions induce a slightly different turn-on shape.
  - Worse fit quality for LP2 and LP3.
- Systematic $\gamma\gamma$ purity normalization variations are trivially absorbed in the $f_{\gamma\gamma}$ parameter, leading to the same fit result.

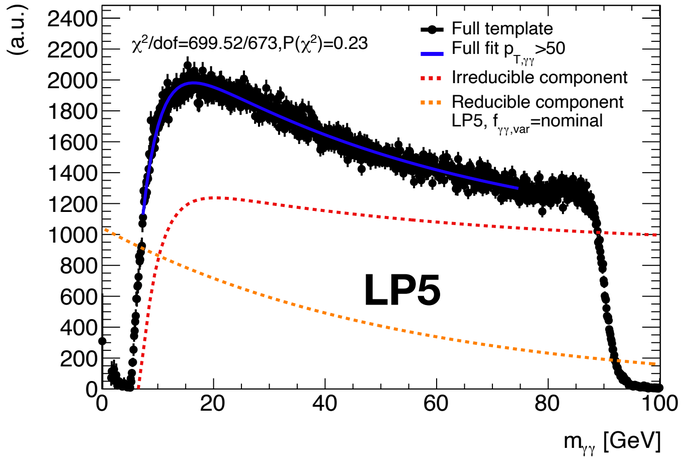

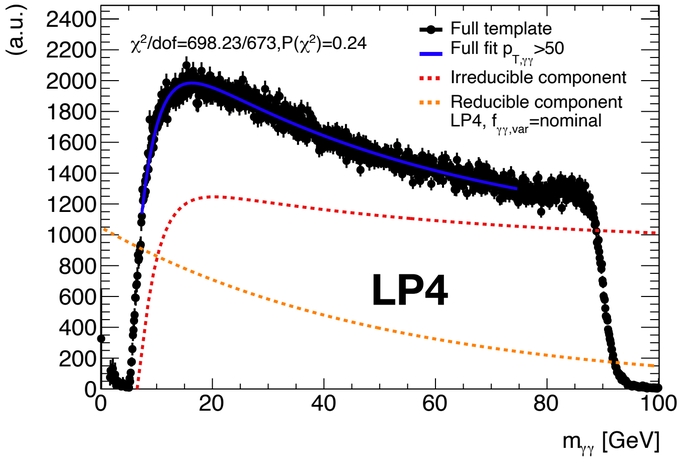

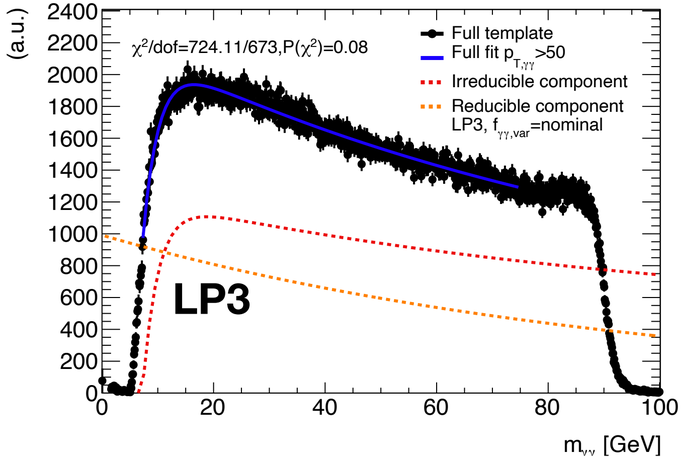

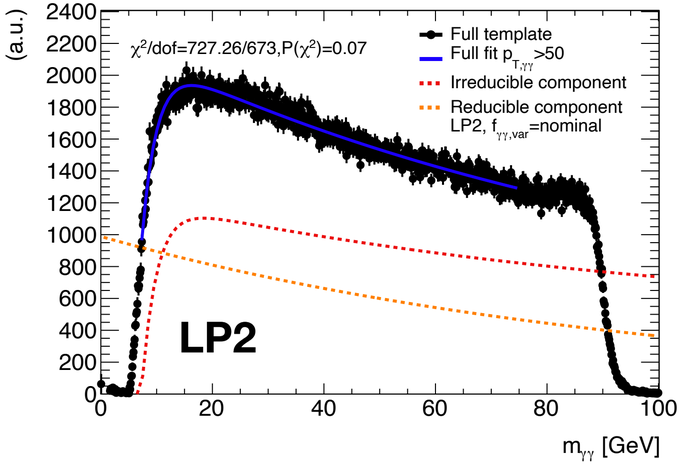

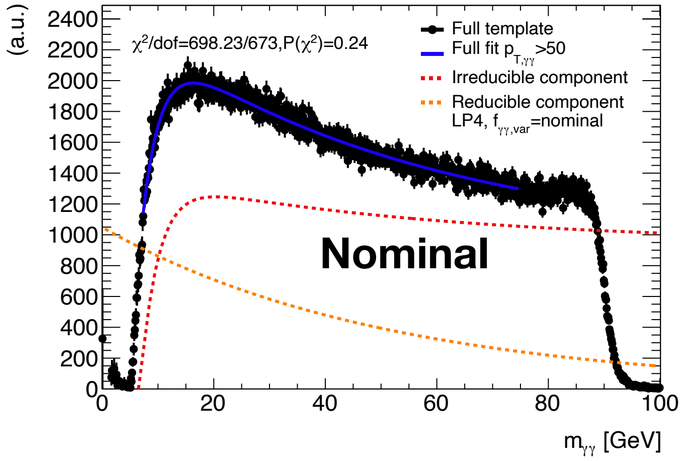

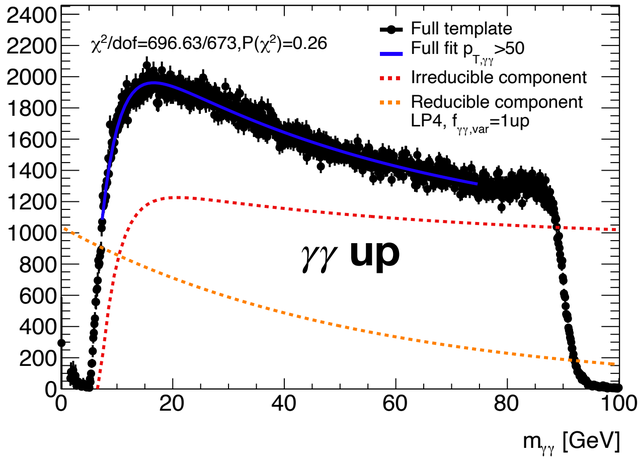

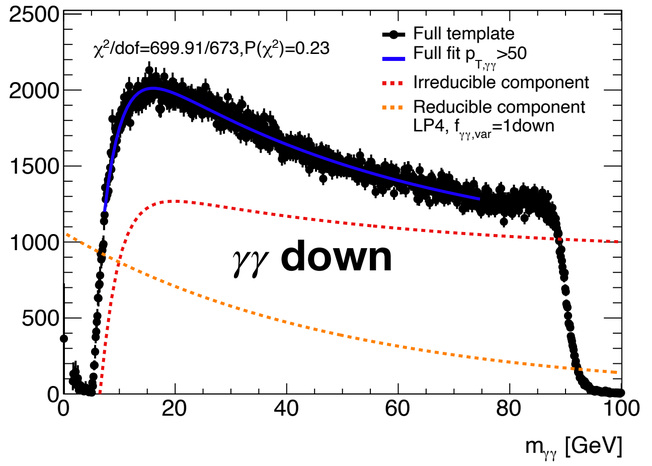

Consistency checks (II)

The turn-on region is a crucial part of the background shape.

Flexibility of its modelling is evaluated modifying the kinematic selection.

- Turn-on shape changes when loosening/tightening the $p_{T,\gamma\gamma}$ cut.

Better description of the turn-on when tightening the selection.

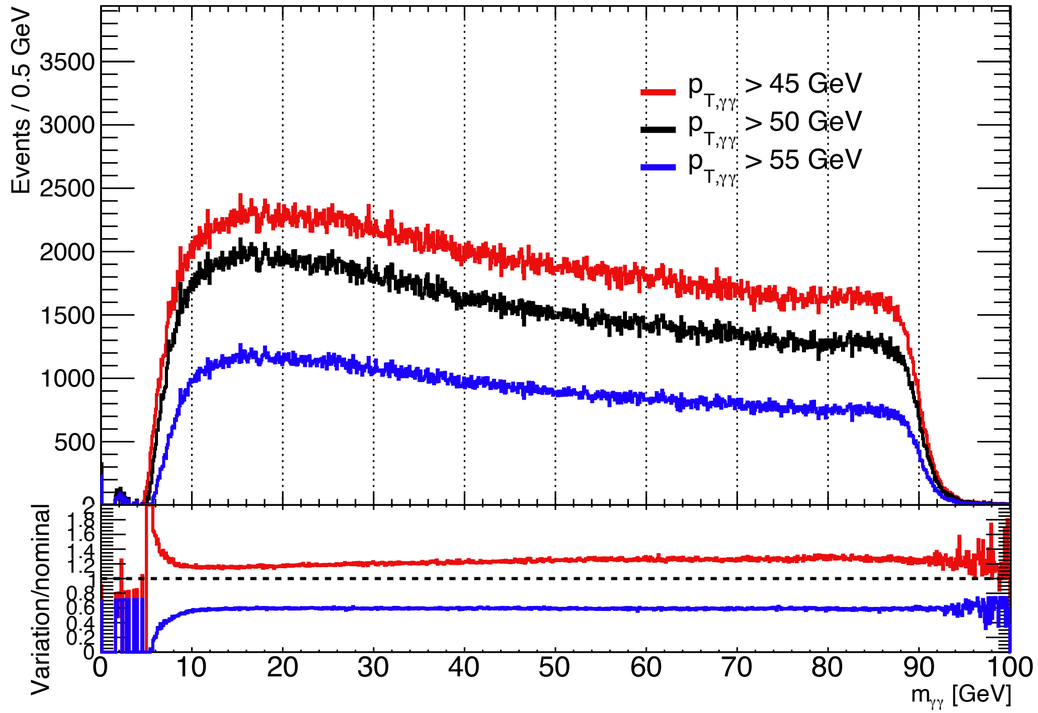

$\tau_{turn-on} = 3.53 \pm 0.11\ GeV$

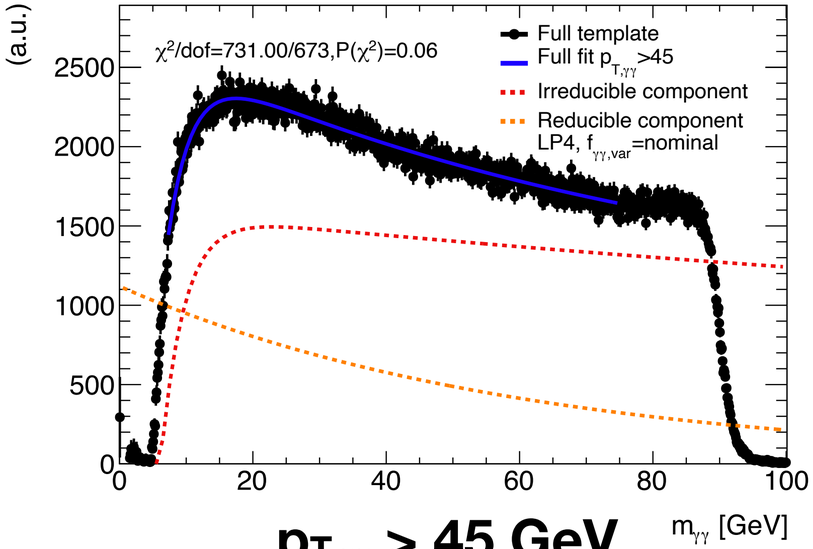

$p_{T,\gamma\gamma}$ > 45 GeV

$\tau_{turn-on} = 3.21 \pm 0.11\ GeV$

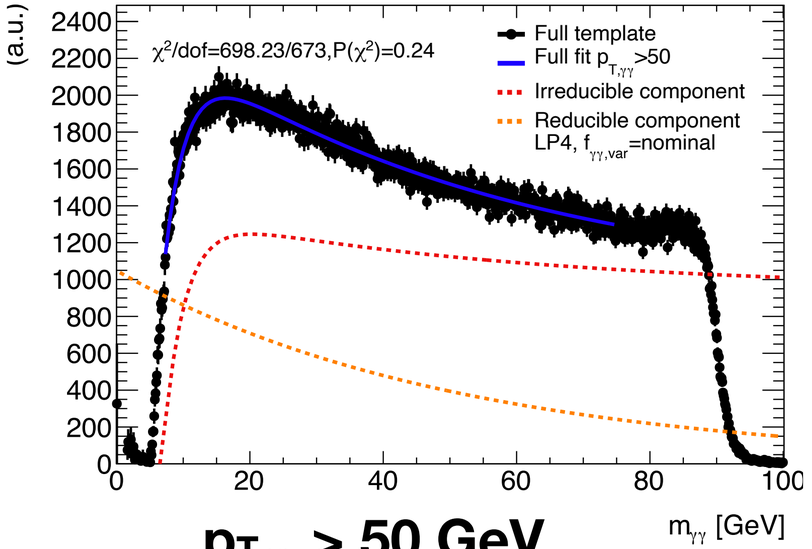

$p_{T,\gamma\gamma}$ > 50 GeV

$\tau_{turn-on} = 3.06 \pm 0.08\ GeV$

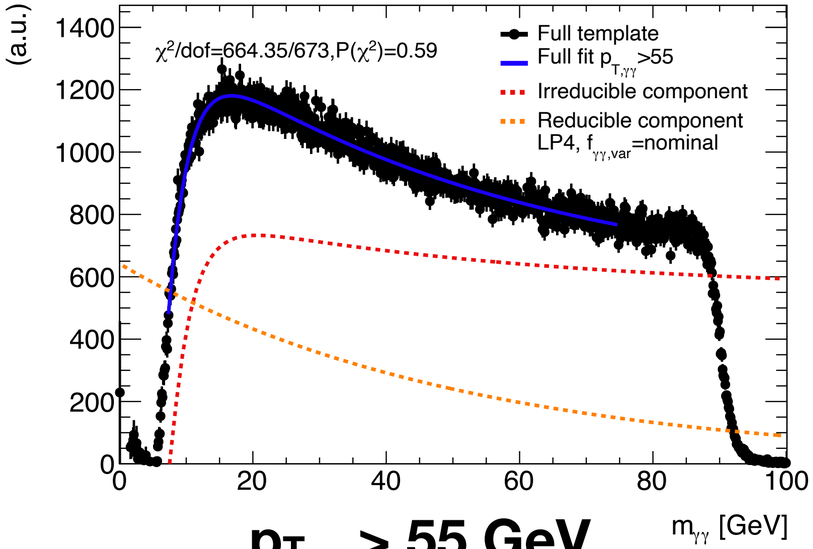

$p_{T,\gamma\gamma}$ > 55 GeV

Fiducial phase space

Limits provided on the fiducial cross-section σ_{fid}

- More model-independent than limits on the total cross-section
- Detector effects are encapsulated in the correction factor C_X

$$\sigma_{X,fid} \cdot \mathcal{B}(X \to \gamma\gamma) = \frac{N_{sig}^{reco}}{C_X \mathcal{L}}$$

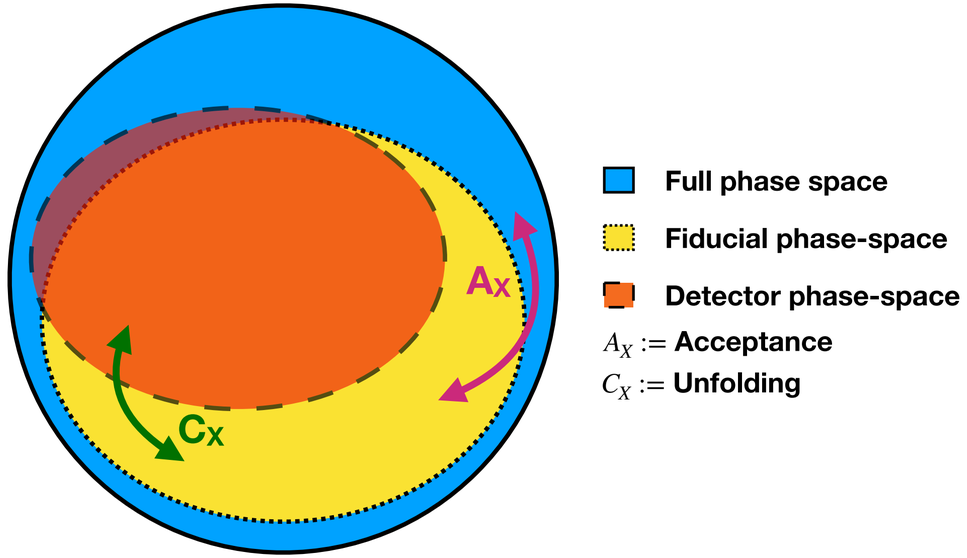

Fiducial volume is defined by applying truth-level cuts that match closely the reconstruction selection:

Fiducial phase space

$p_{T,truth}^{\gamma} > 22\ GeV \quad p_{T,truth}^{\gamma\gamma} > 50\ GeV$

$|\eta| < 2.37$

Truth isolation:

$$\sum_{\Delta R<0.2} E_T < 0.05 p_{T,truth}^{\gamma}$$

Reco phase space

$p_T^{\gamma} > 22\ GeV \quad p_T^{\gamma\gamma} > 50\ GeV$

$|\eta| < 2.37$

FixedCutLoose isolation:

$ptcone20 < 0.05 p_T \quad topoetcone20 < 0.065 p_T$

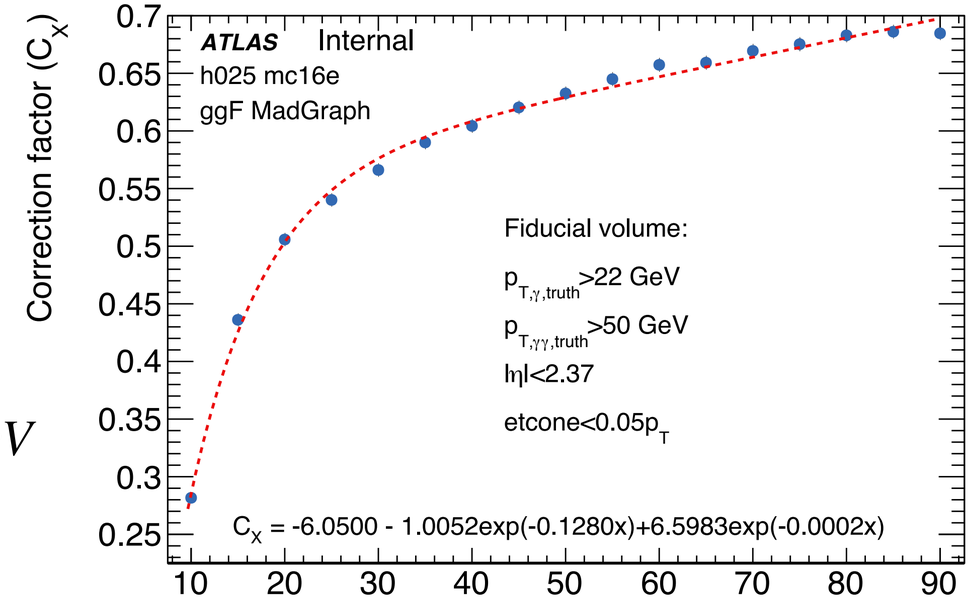

Signal yield systematics

Signal systematics divided in two categories:

- Systematics affecting the signal shape
- Systematics affecting the signal yield

Signal yield systematics implemented as variations on the correction factor C_X

- Between 1-2% variation with respect to the nominal correction factor, relatively constant with the mass.

Trigger

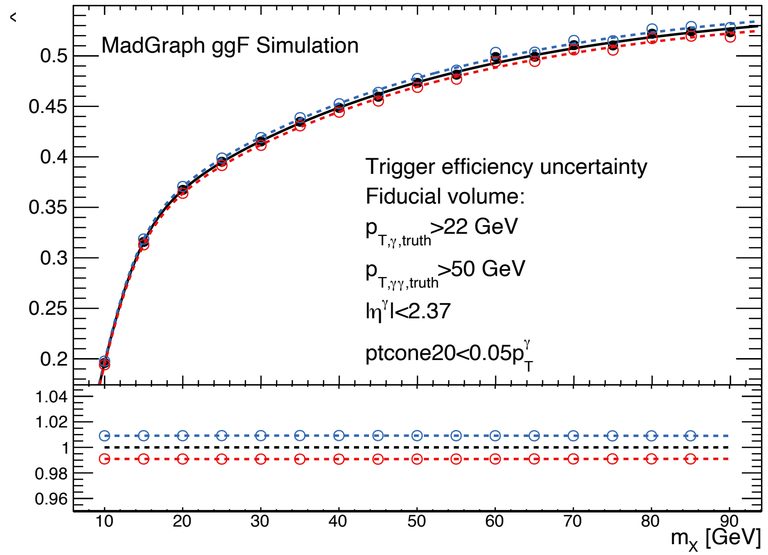

Identification

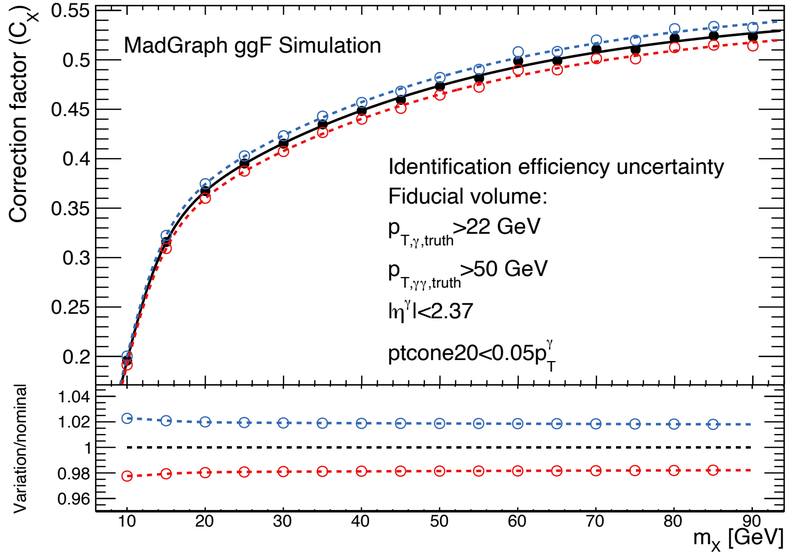

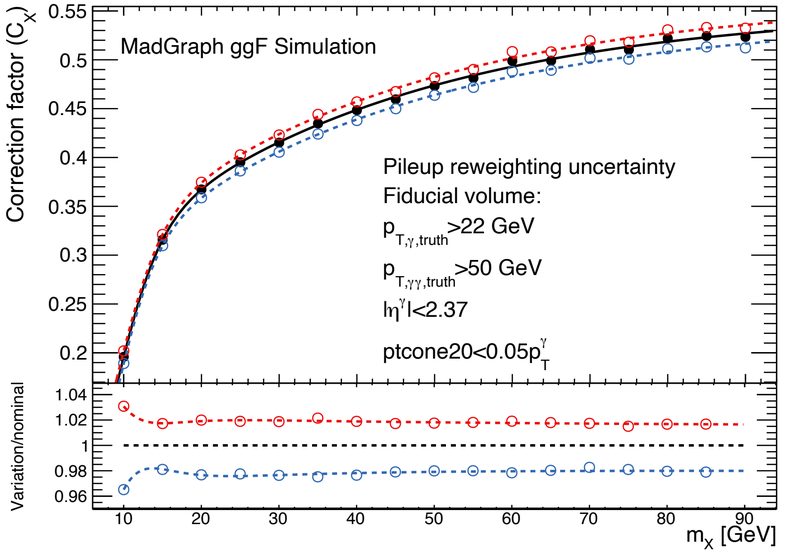

PRW

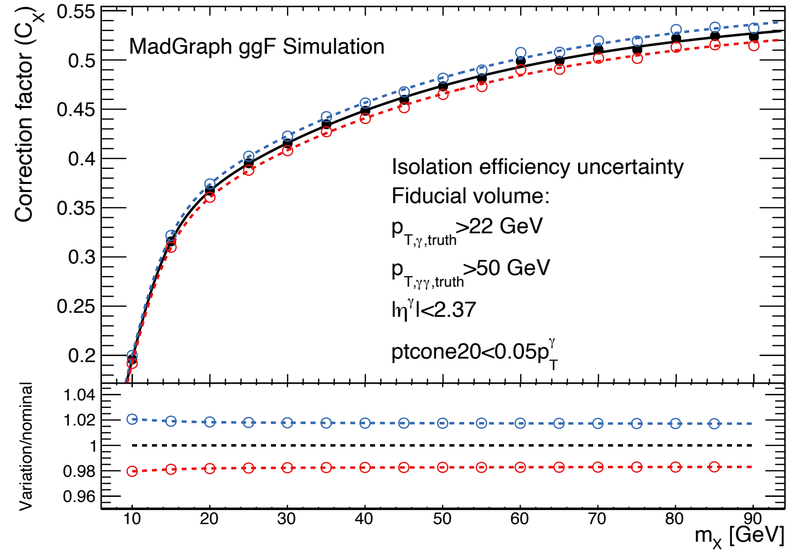

Isolation

Signal shape systematics

Signal shape variations arise from calibration uncertainties from the official Egamma measurements:

- Photon energy scale variations induce shifts in the $m_{\gamma\gamma}$ peak position of the order of 0.5%.
- Photon energy resolution variations widens/narrows the signal resolution of the order of 5-6%, slightly increasing towards higher masses.

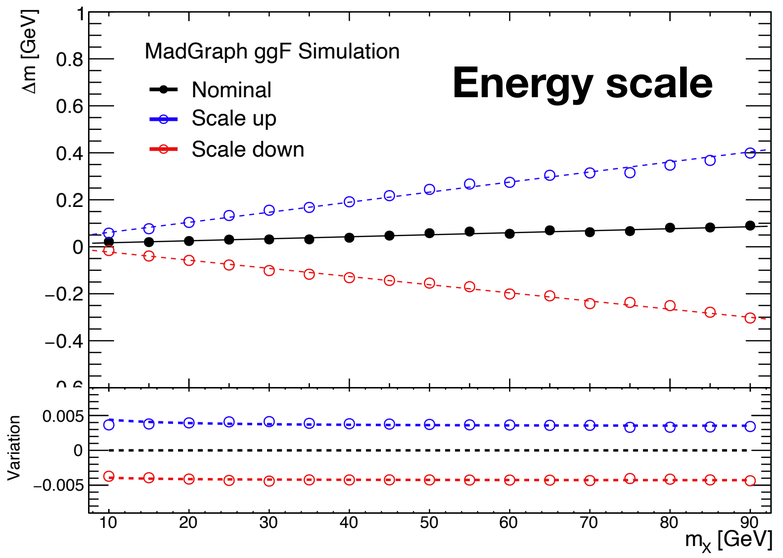

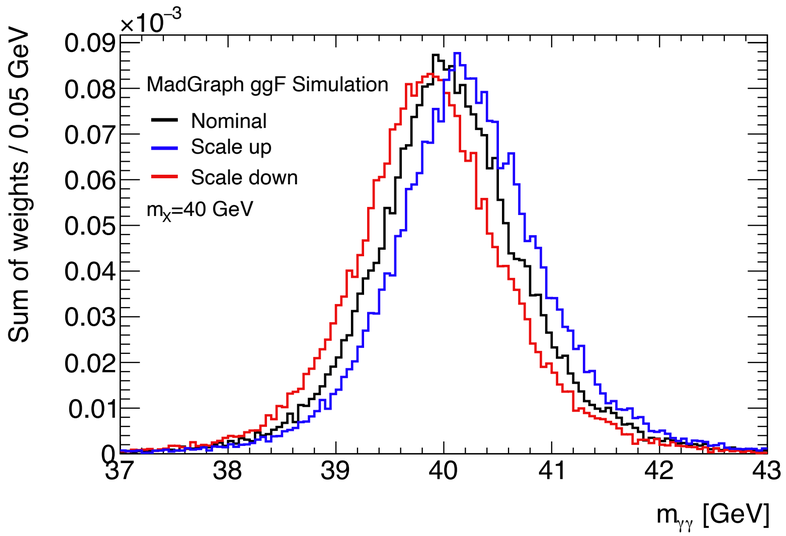

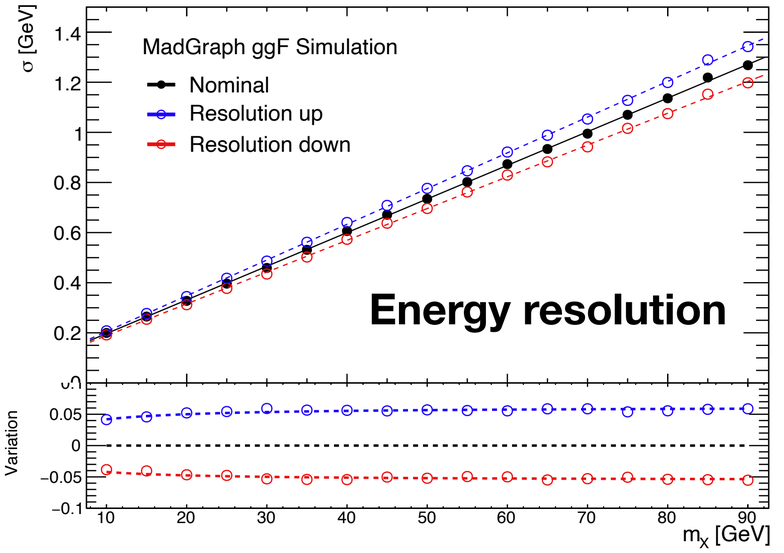

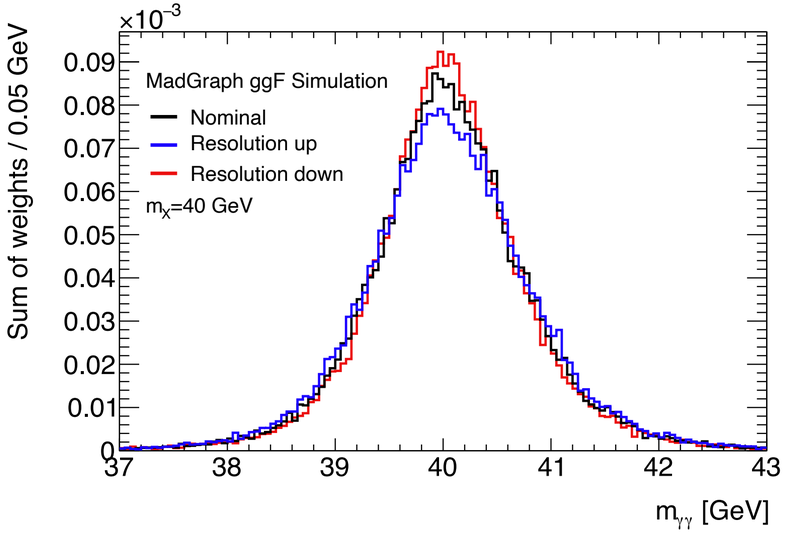

Spurious signal: smothing

Sherpa $\gamma\gamma$ heavily affected from low statistics

- For a correct evaluation of spurious signal systematics a smoothing is required.

Gaussian Process Regression (GPR) method provides an estimation of the true background shape.

- Two main inputs are needed:
  - A *kernel function* used to correlate information between bins spaced up to the length scale.
  - Length scale: measure of possible the size of structures in our mass range.

Turn-on region can be affected from biases due to the smoothing procedure: evaluated in the following slides.

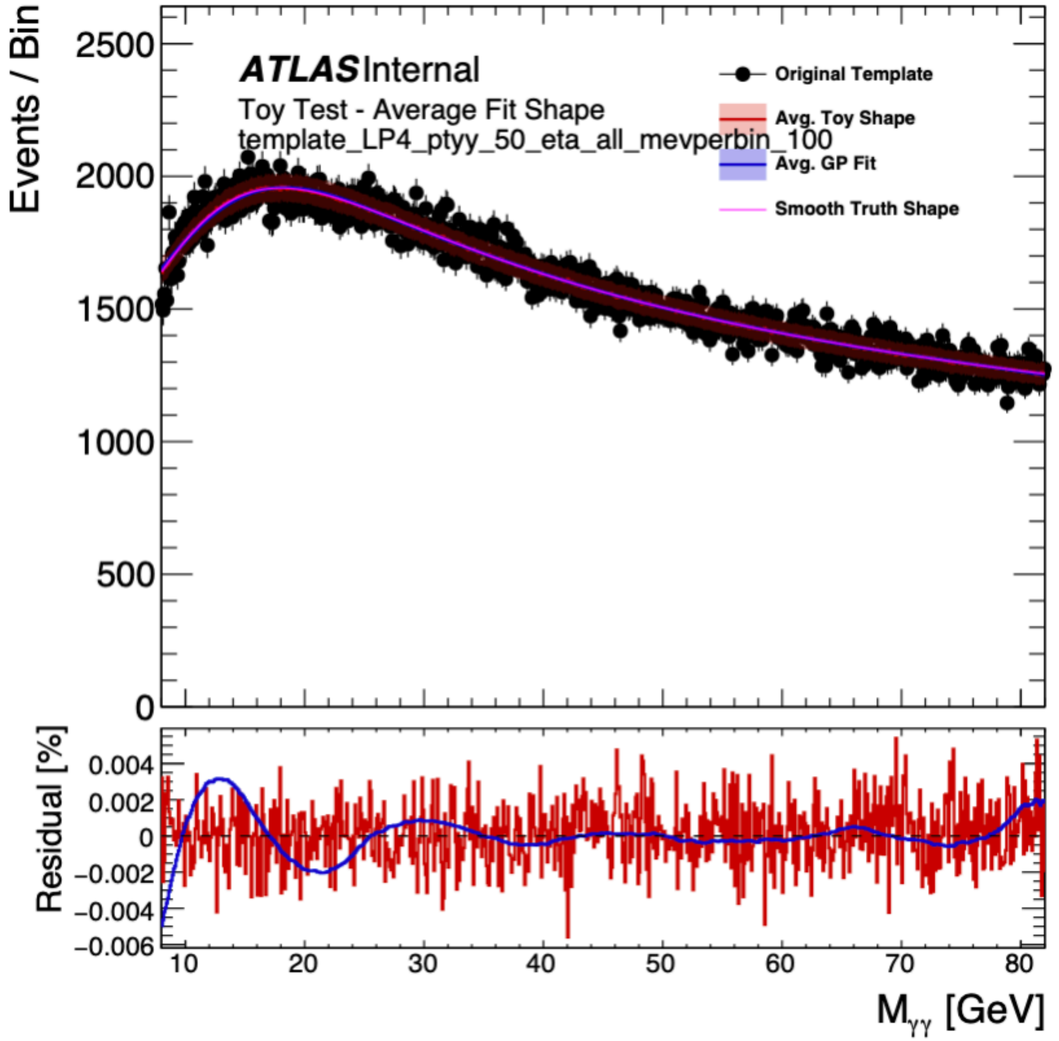

GPR toy testing for bias estimation

Idea:

- Generate toys from an analytic function with a turn-on feature
  - Function(s) obtained from a fit to the template.
- Perform the GPR smoothing on each of the toys
  - Each toy has an unsmoothed and smoothed version.
- Evaluate the spurious signal systematic on each toy before and after the smoothing.
  - The bias caused by the smoothing will show as differences between the spurious signal observed in the template before and after the smoothing.

FDPowLog0 (true function)

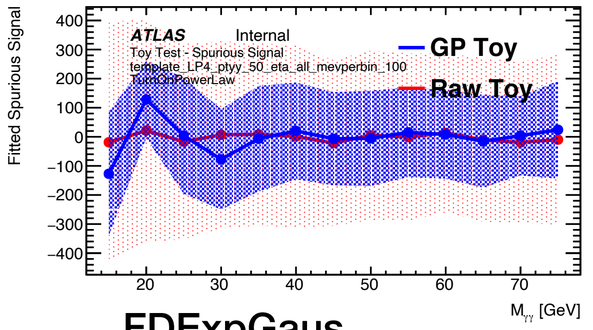

FDGaus

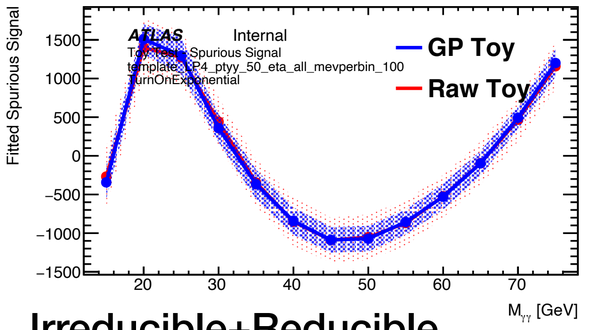

FDExpGaus

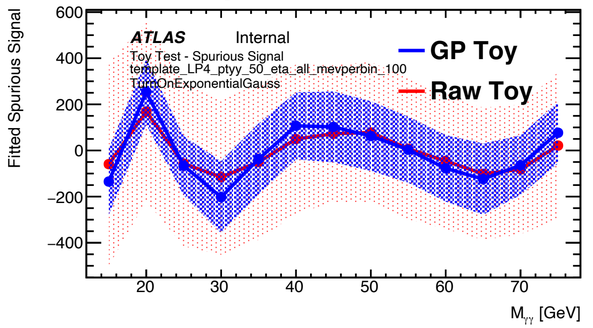

Irreducible+Reducible

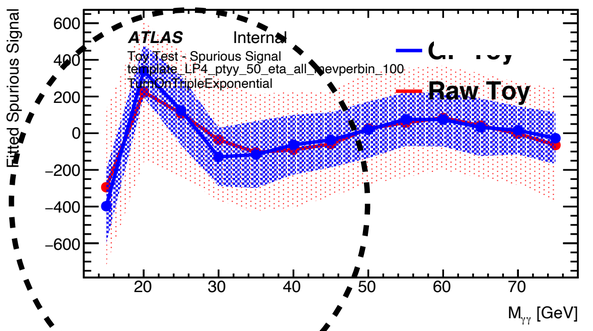

In general:

- SS computed before and after the smoothing procedure consistent within errors everywhere
- Small uncertainty could be assigned, but negligible compared to the expected spurious signal.

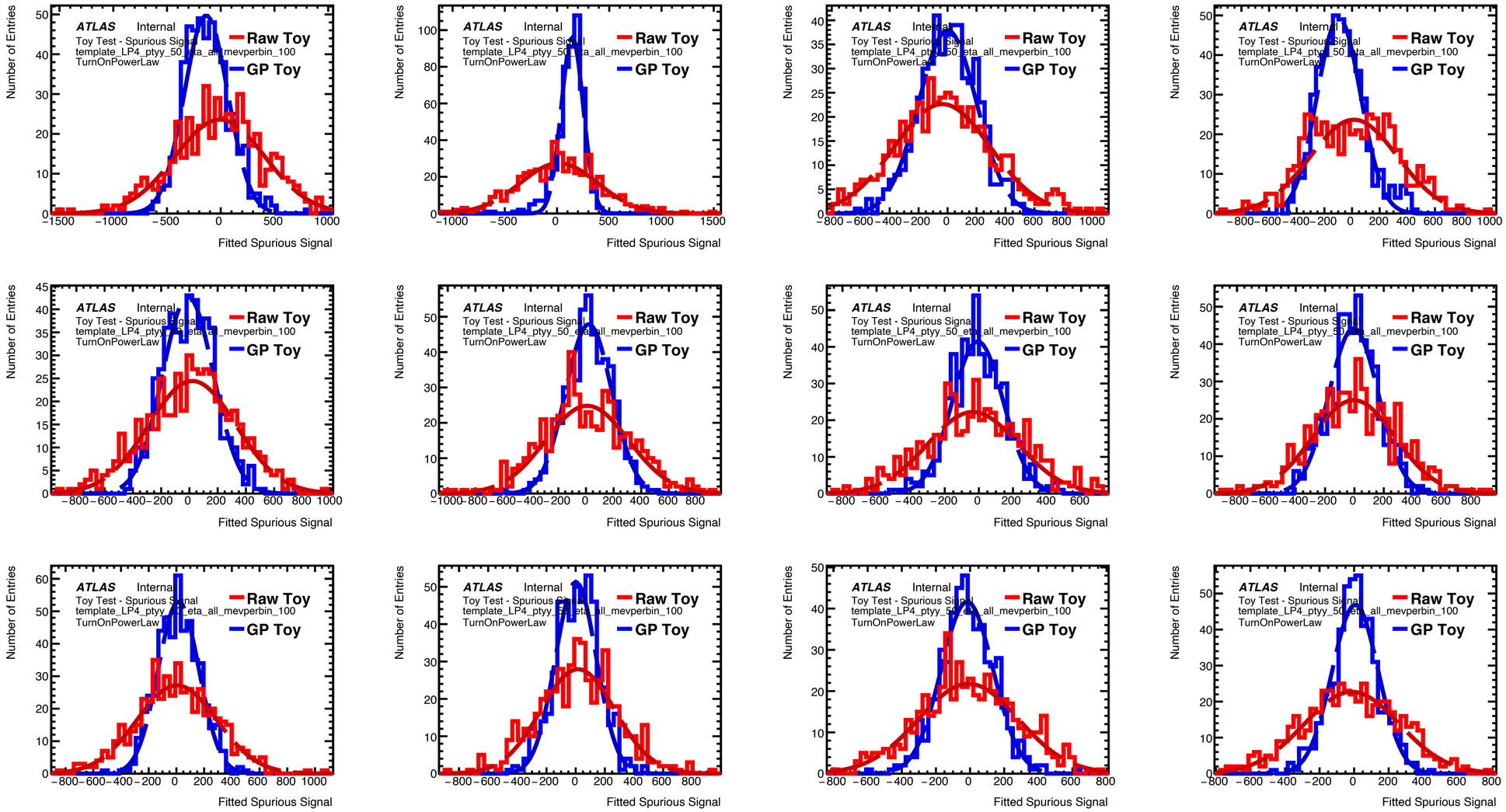

Plots showing the spurious signal computed in the toys before and after the smoothing for various mass points.

- Difference of the peak position between them indicate the bias of the smoothing procedure.

Fit bias (spurious signal)

A bad description of the background shape can potentially absorb/induce signals.

Estimated from S+B fits to background-only templates

- Very sensitive to statistical fluctuations!
- Estimated from a smoothed template version

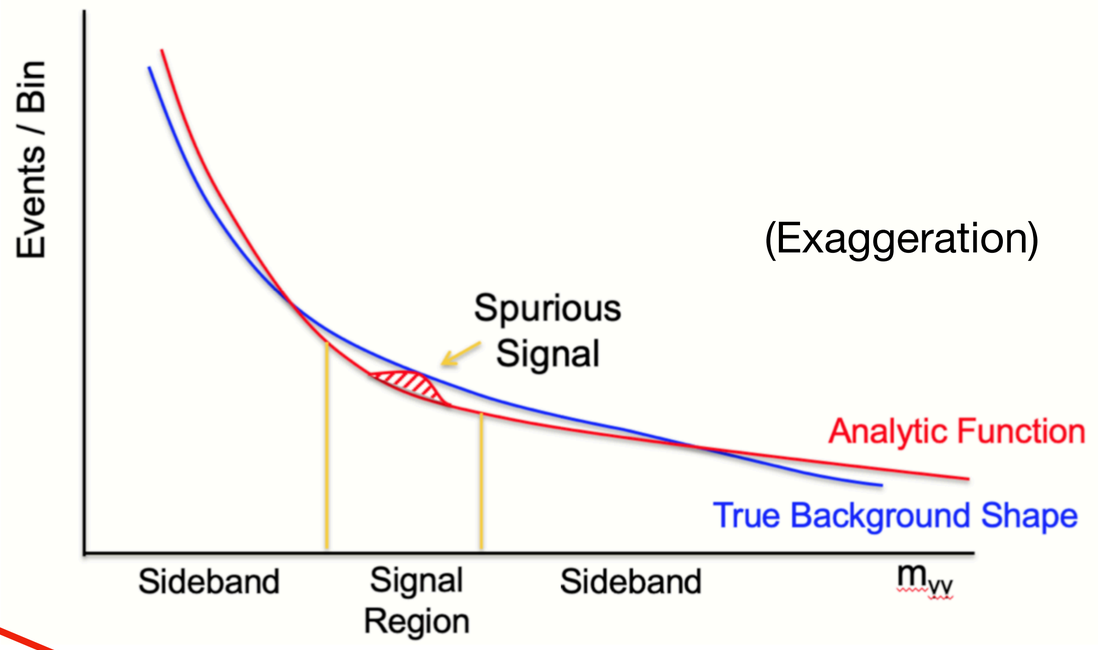

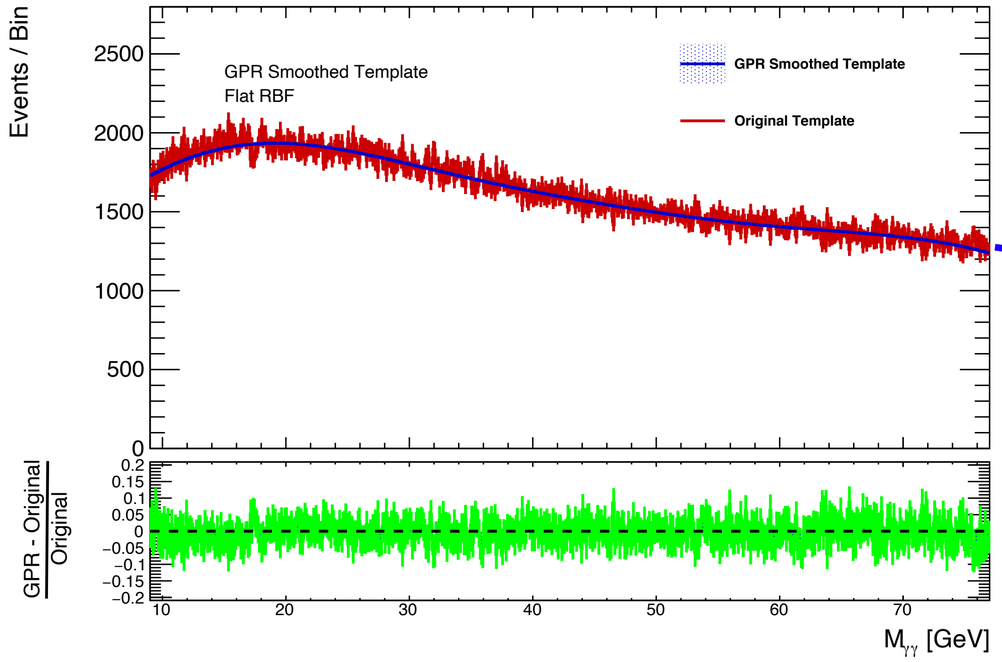

Systematic required to be less than $0.5\sigma_{stat}$

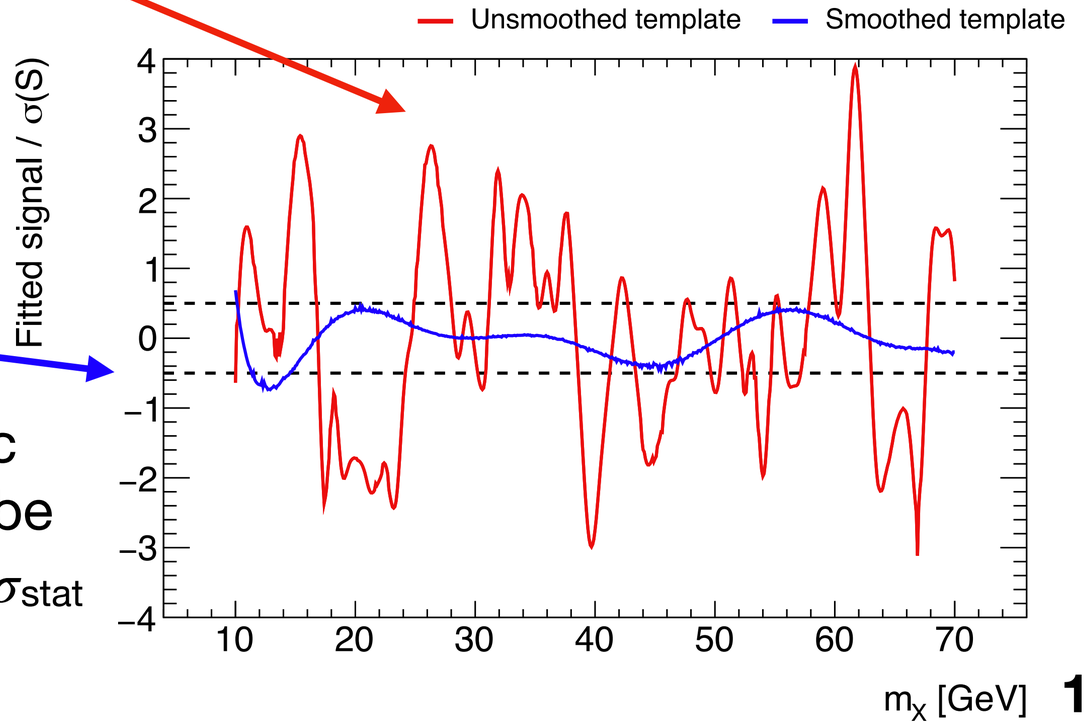

From σ_{fid} to ALP parameter space

arxiv:1710.01743

- Total cross section for a resonance produced with a certain center-of-mass energy and with f_a equal to a given value (1 TeV in this case)

$$\sigma_{theo} \sim \frac{g(m_a)}{f^2_{a,theo}} \longrightarrow \frac{\sigma_{theo}}{\sigma_{exp}} = \frac{f^2_{a,exp}}{f^2_{a,theo}}$$

where $g(m_a)$ is a function of the mass.

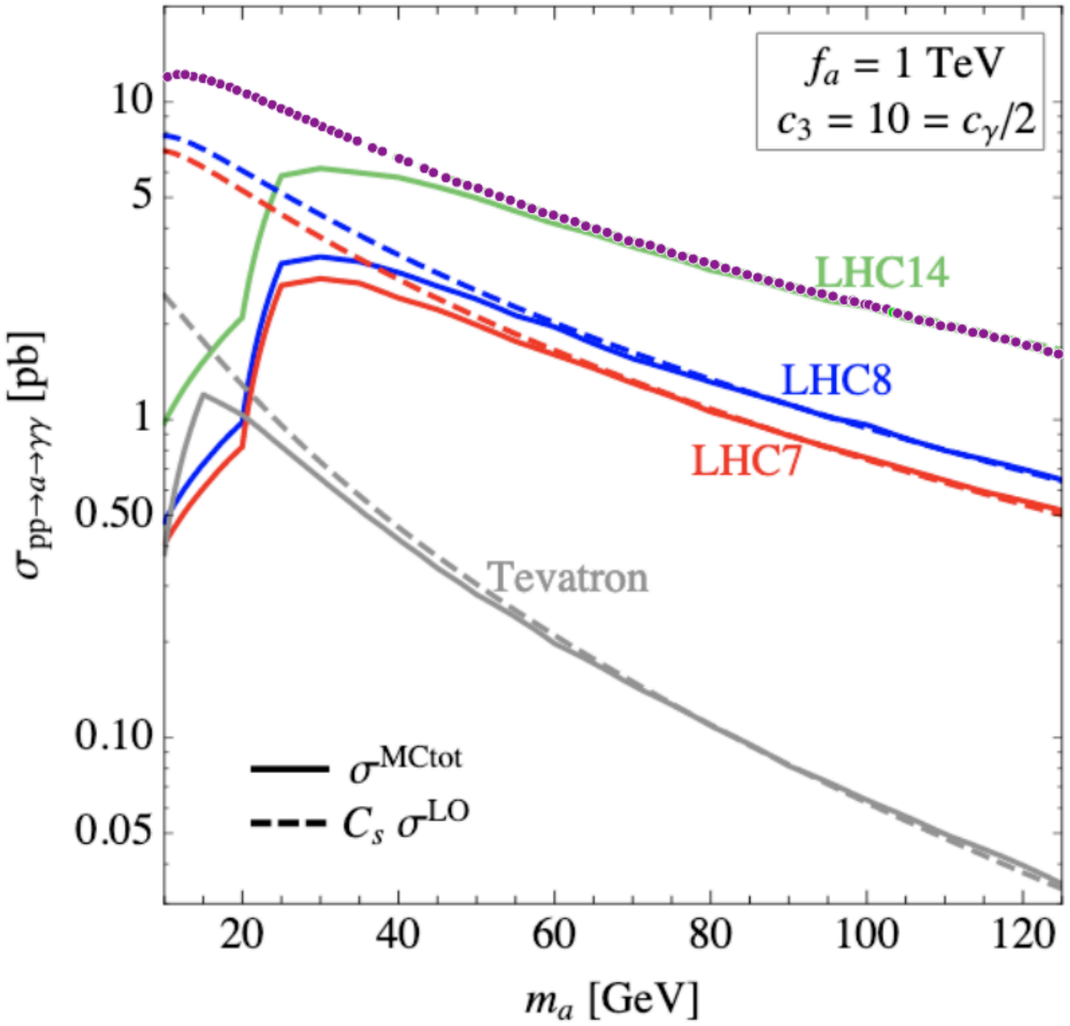

Additional backgrounds

Around 2-1 events as a function of the mass between 20 and 80.

- This represents around 1-2% of the events per bin.
- Annoying slope below 20

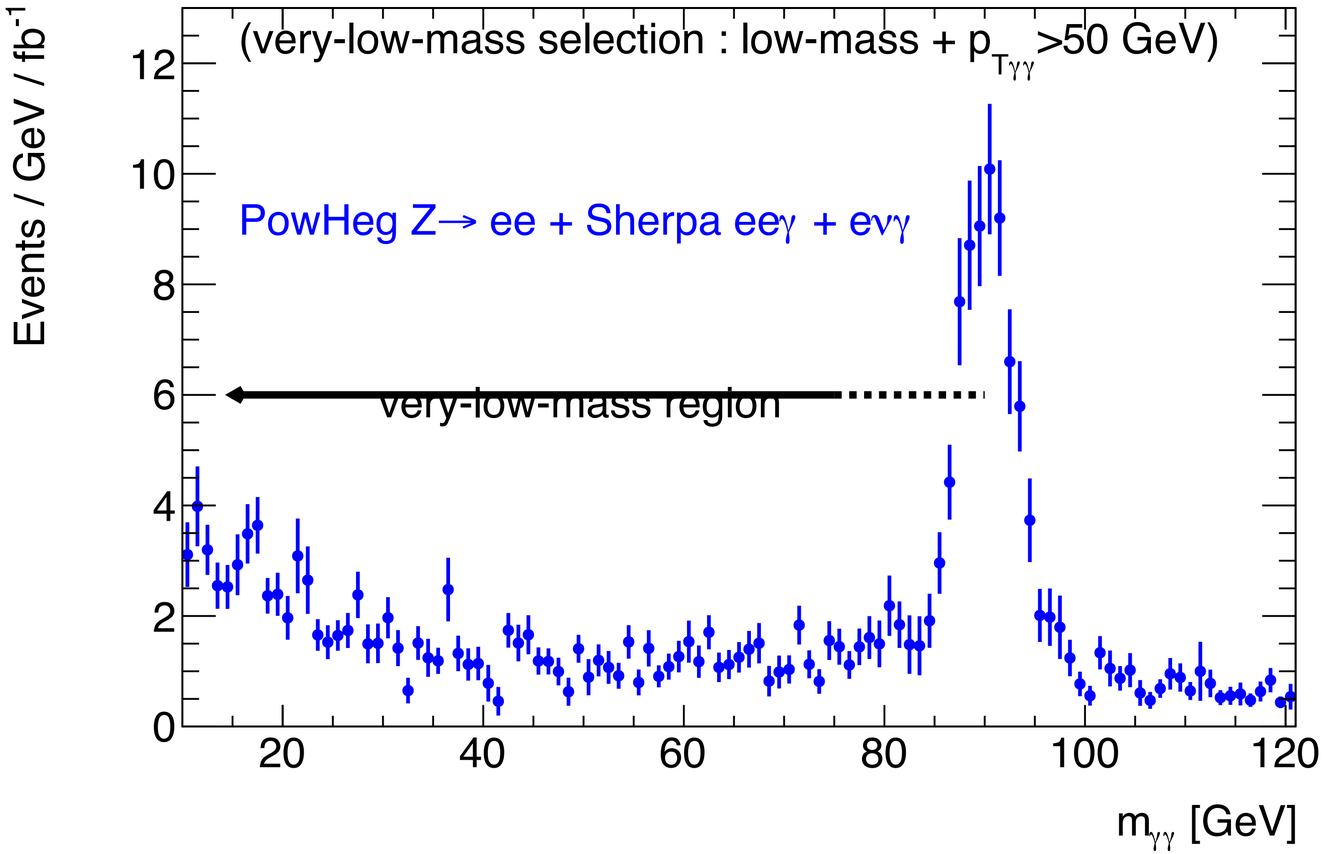

Triggers in detail

Triggers have evolved across Run2 in order to cope with the increasing diphoton rate while keeping energy thresholds as low as possible.

- Different L1 seeds (increasing ET thresholds and isolation in 2017-2018)
- HLT isolation items contribute to this (present only in 2017-2018)
- How diphoton triggers behave for collimated photon topologies?

L1_2EM15VHI (as example)

- 2 EM seeds requiring transverse energy thresholds of 15 GeV
- η dependent threshold due to EMscale variations (from -2 to +3 GeV)
- Hadronic veto in the towers behind the central region:
  - If $E_{T,had} > 1$ GeV, $E_{T,\gamma}$ /23-0.2 > $E_{T,had}$
- Isolation (for $E_{T,\gamma}$ <50 GeV)
  - If $E_{T,iso} > 2$ GeV, $E_{T,\gamma}$ *0.125-1.8 > $E_{T,iso}$

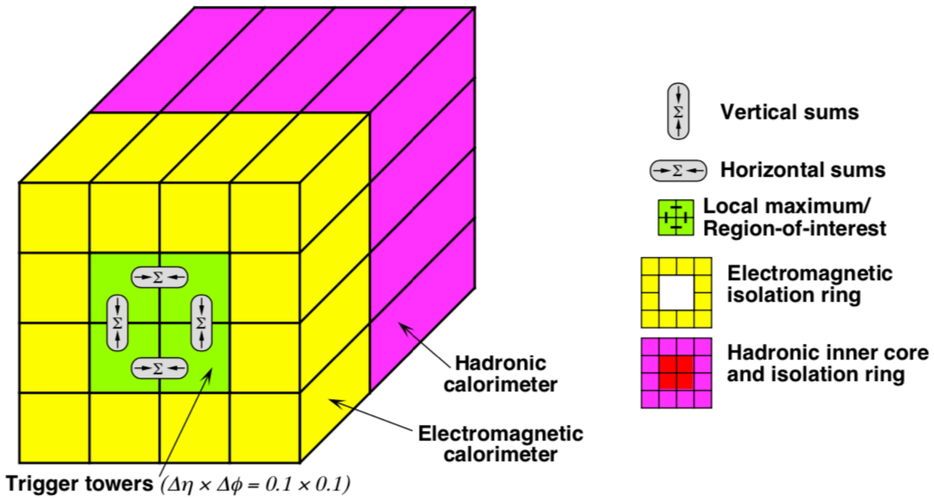

Year	2015	2016 up to D3	2016 from D3	2017	2018
L1 item	L1_2EM10VH	L1_2EM15VH	L1_2EM15VH	L1_2EM15VHI	L1_2EM15VHI
HLT item	2g20_tight	2g20_tight	2g22_tight	2g20_tight_icalovloose	2g20_tight_icalovloose
luminosity $[fb^{-1}]$	3.2	11.5	21.5	43.6	58.5

Efficiency vs ΔR in signal samples

MadGraph signal samples for resonances at different masses are used.

Efficiency is defined as the ratio of reconstructed events over events in the truth **fiducial** region.

Visible drop at small ΔR below 0.3.

- No scale factors exist for this region.
- Systematics could be large.

Fraction of true events falling in this region increases towards lower masses (overlap between drop in efficiency and grey distribution)

- This could potentially limit lowest attainable mass.

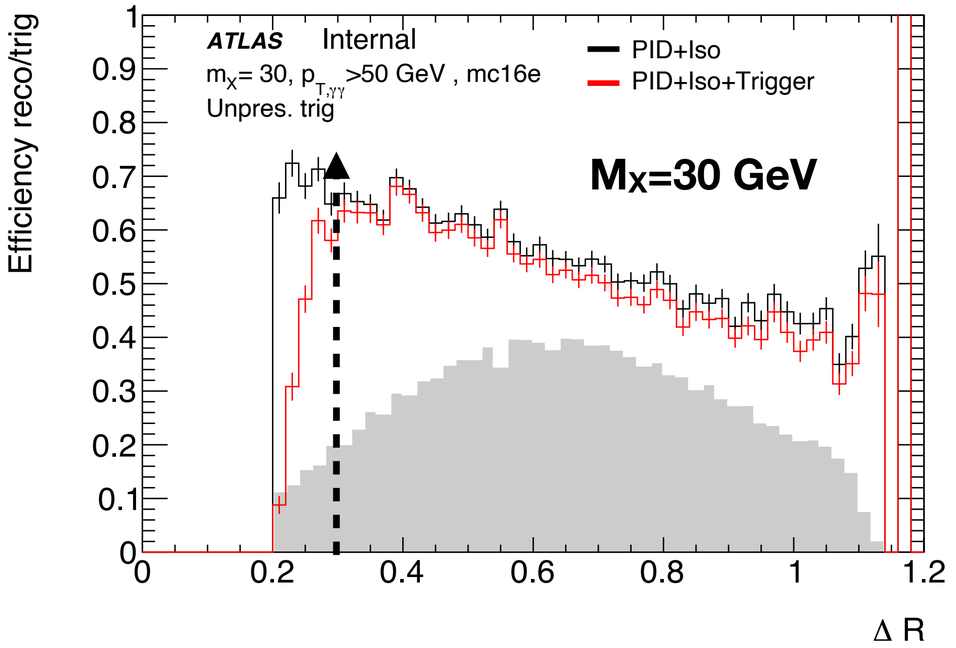

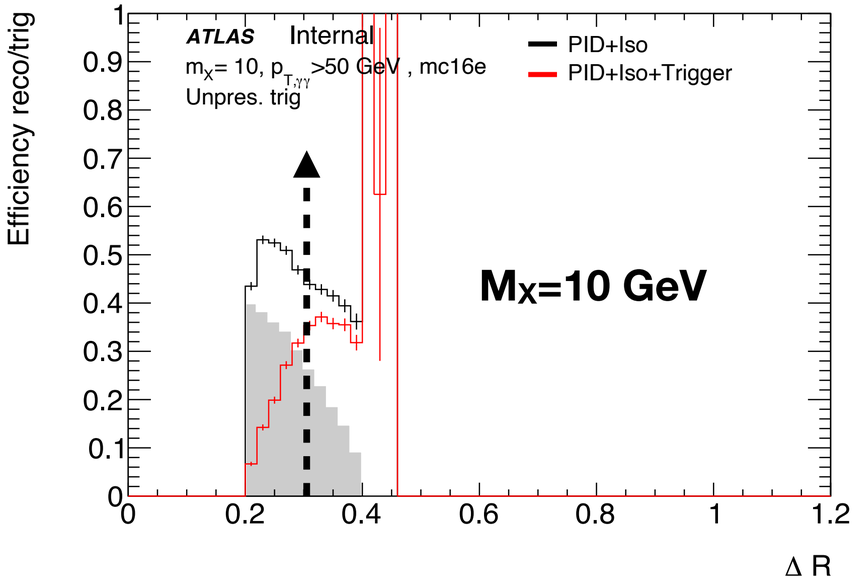

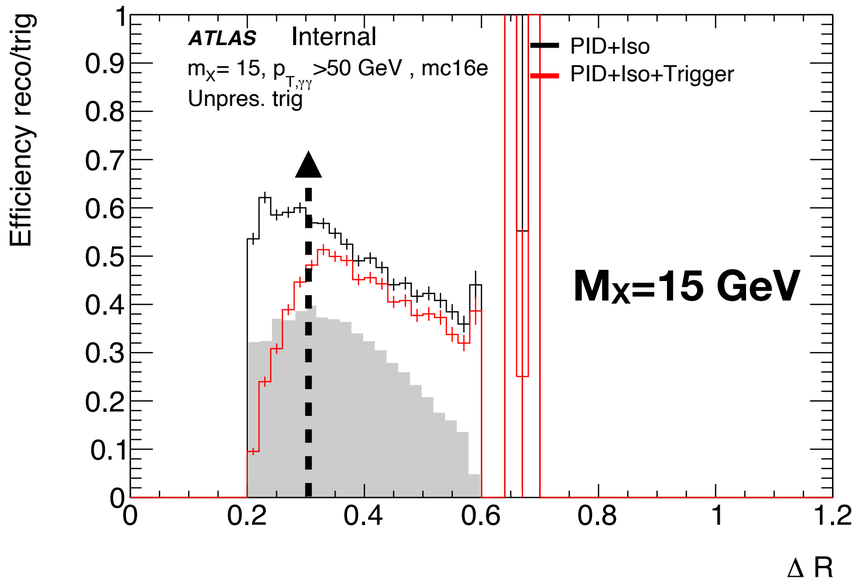

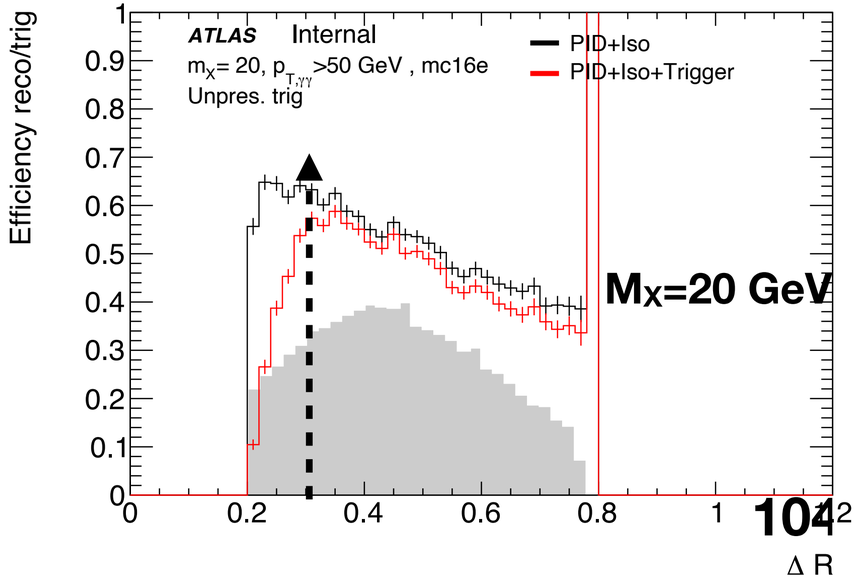

Alternative measurement

Difficult measurement of diphoton trigger efficiency in data

- Current measurement provided by product of single photon triggers.
- No clean source of diphotons in data

Alternative: use radiative Zee events to study if single photon triggers are affected by nearby EM objects.

Event selection: (EGAM3 derivation, dielectron tag , photon probe)

- Dielectron mass: [40,83] GeV
- Dielectron-γ mass: [80,100] GeV
- $p_{T,l} > 10$ GeV , $p_{T,\gamma} > 22$ GeV
- TightID, loosely isolated (FixedCutLoose) photons

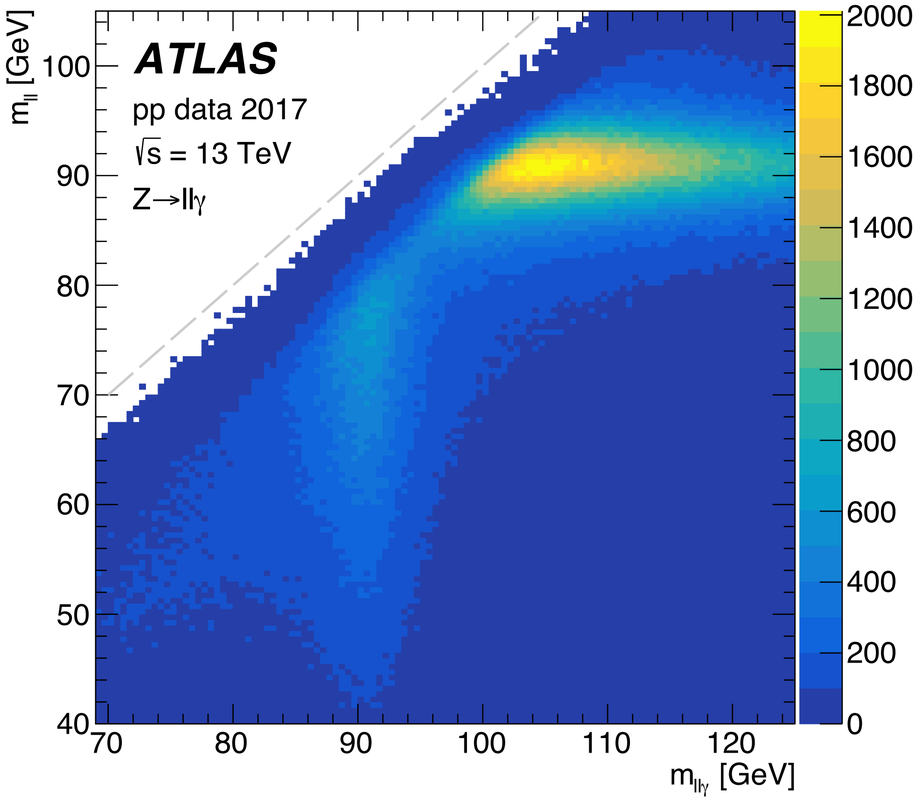

Conclusion on triggers study

Efficiency drop is observed for radiated photons at low ΔR with respect to the closest electron.

- Fair agreement between data and MC.
- Same behaviour observed at L1 triggers.

Proposal for the analysis:

- Use difference in efficiency between data and MC (plot on the right) as systematic uncertainty for small ΔR
- Discussed in Trigger E/γ signature group meeting: green light with this procedure

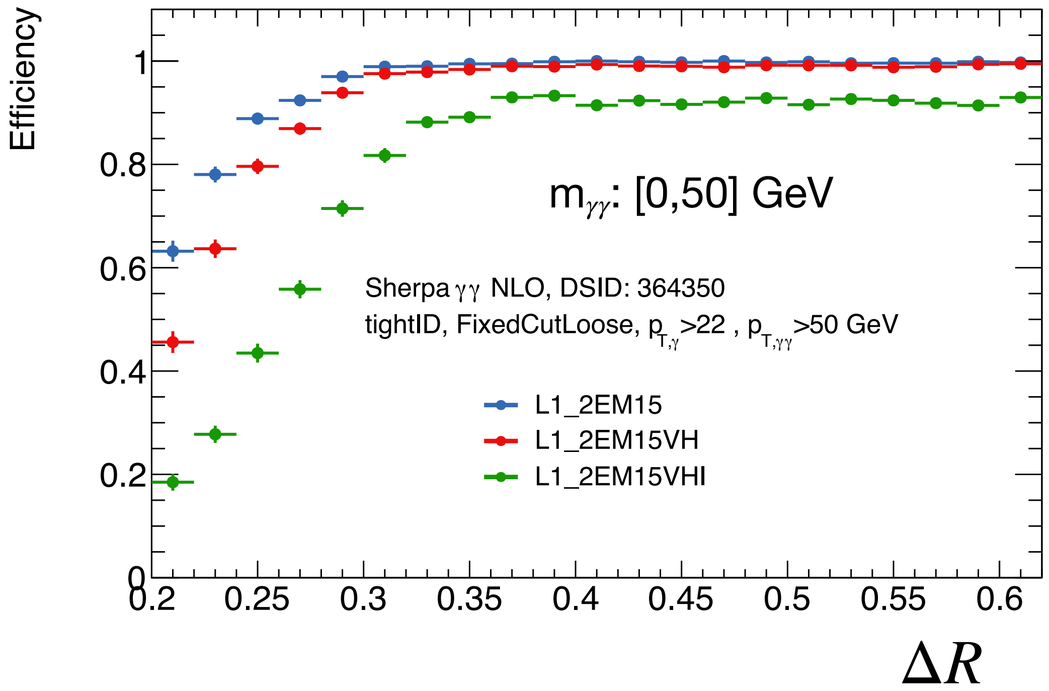

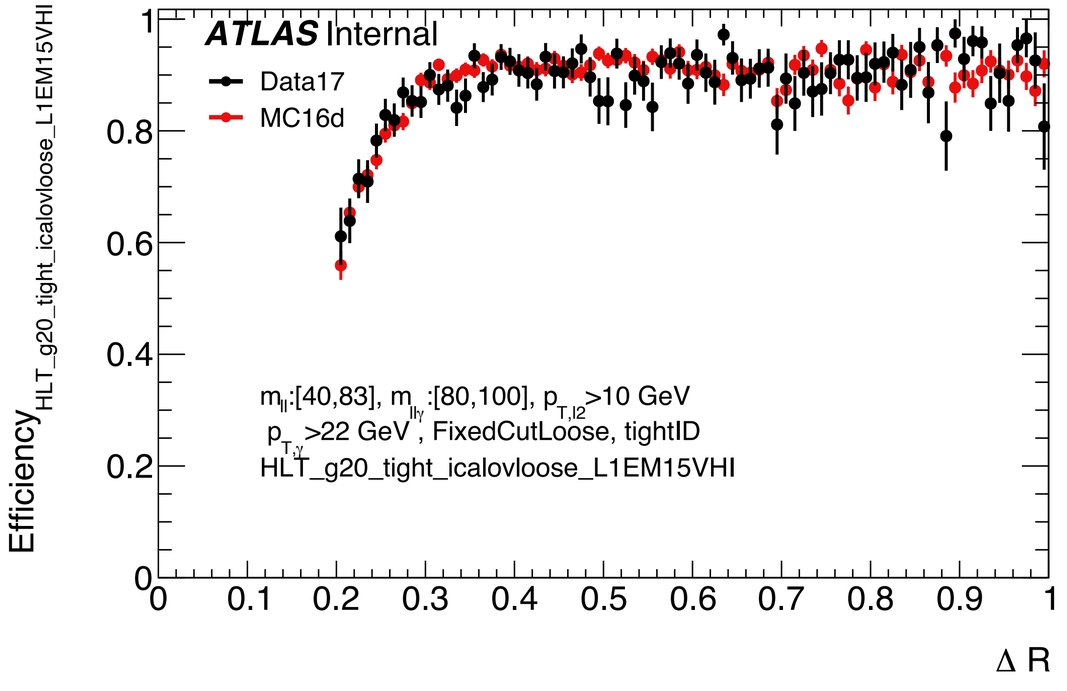

Background templates (I)

Methodology:

- Build irreducible template from sliced low-statistics fullsim Sherpa $\gamma\gamma$
- Build **corrected** reducible template from data CR (loose'4)
  - $\gamma\gamma$ contamination estimated from Sherpa $\gamma\gamma$ subtracted.
  - Differences coming from different triggers between signal and control regions corrected with simple function (per year)
    - Probably caused by different seeds at HLT level.

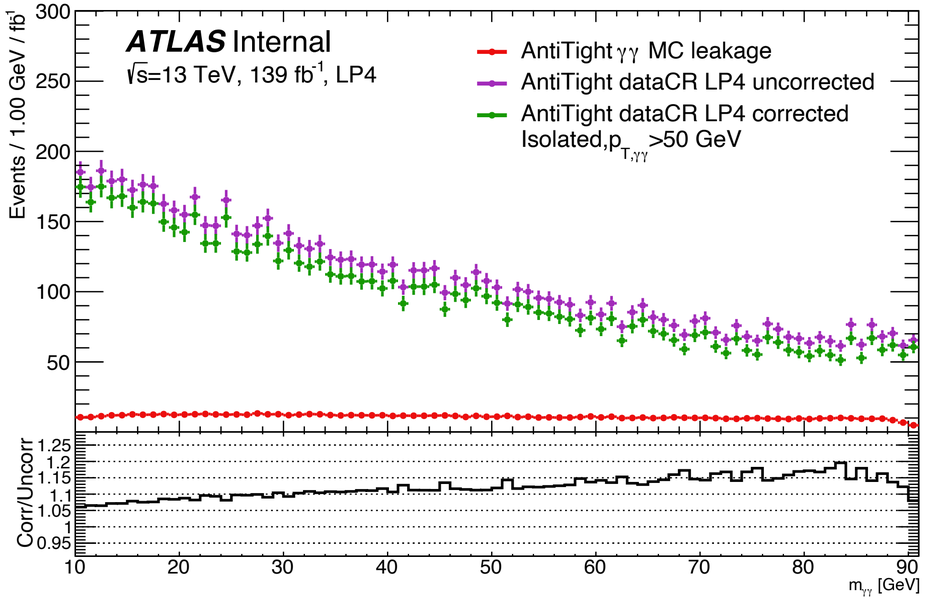

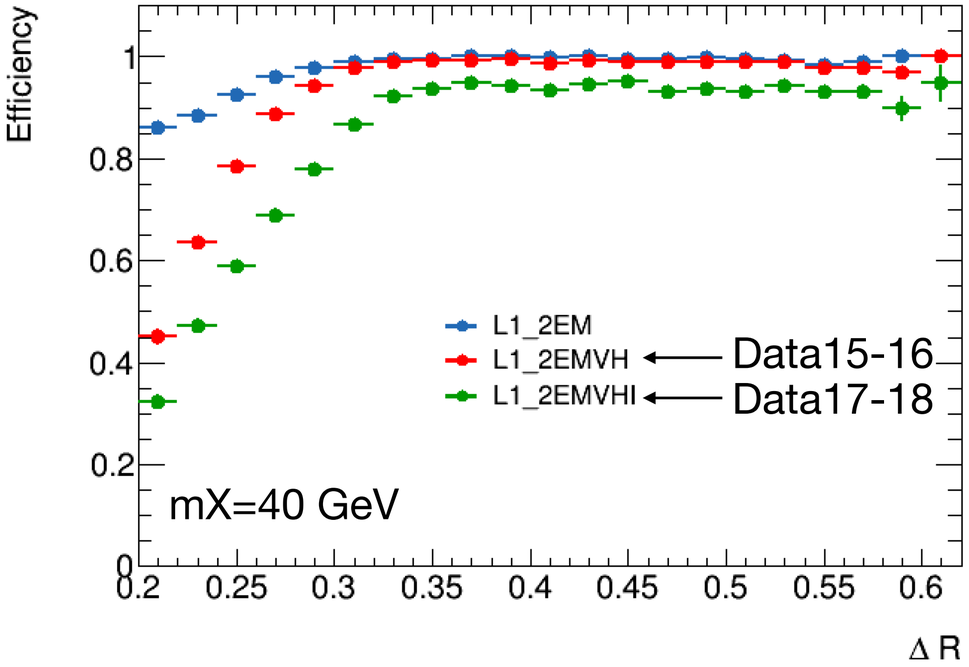

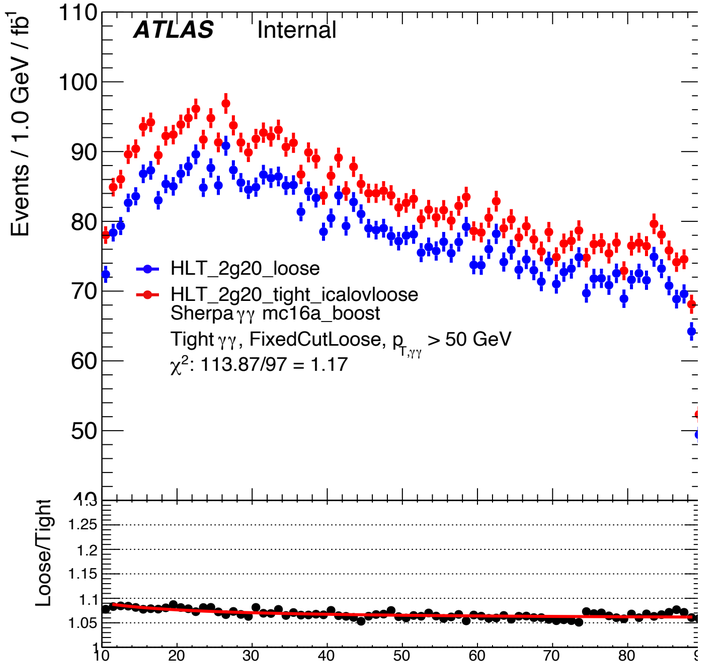

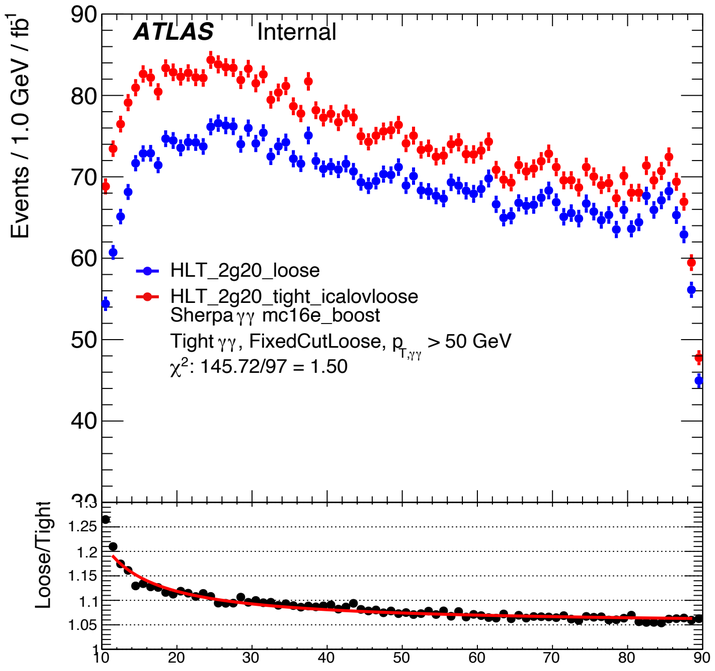

Future prospects for Run3

- Lower E_T triggers could help pushing the very low mass limit towards lower masses.
- To cope with the rate, new HLT and L1 items ($\Delta\phi$ and $m_{\gamma\gamma}$ cuts) are used.
- Selection 2.5 times more efficient and almost completely orthogonal to the existing triggers.

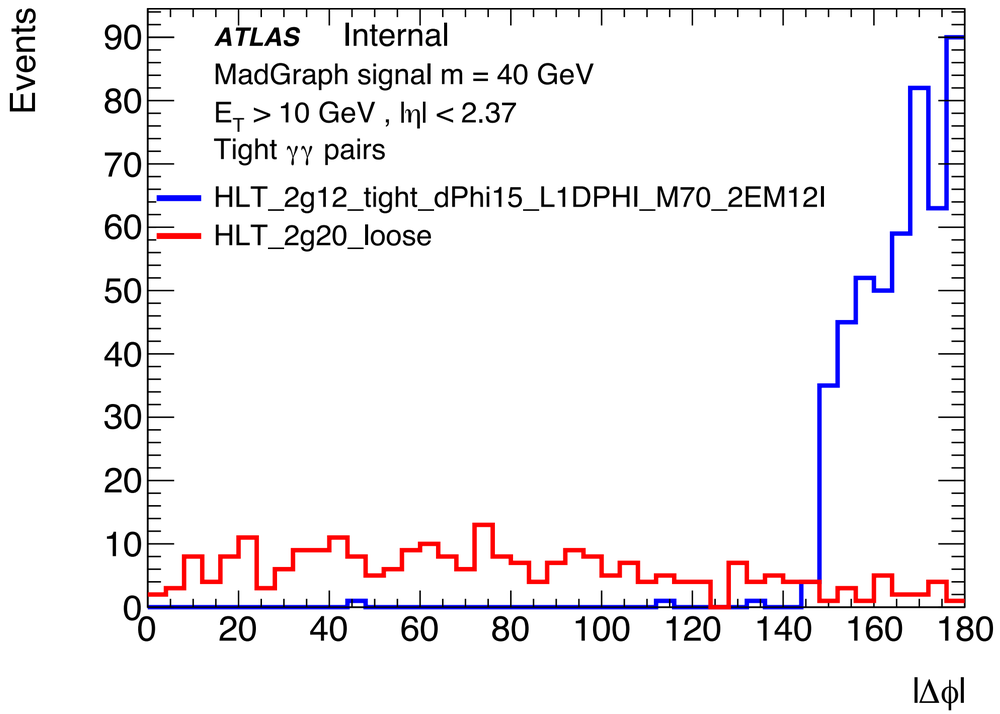

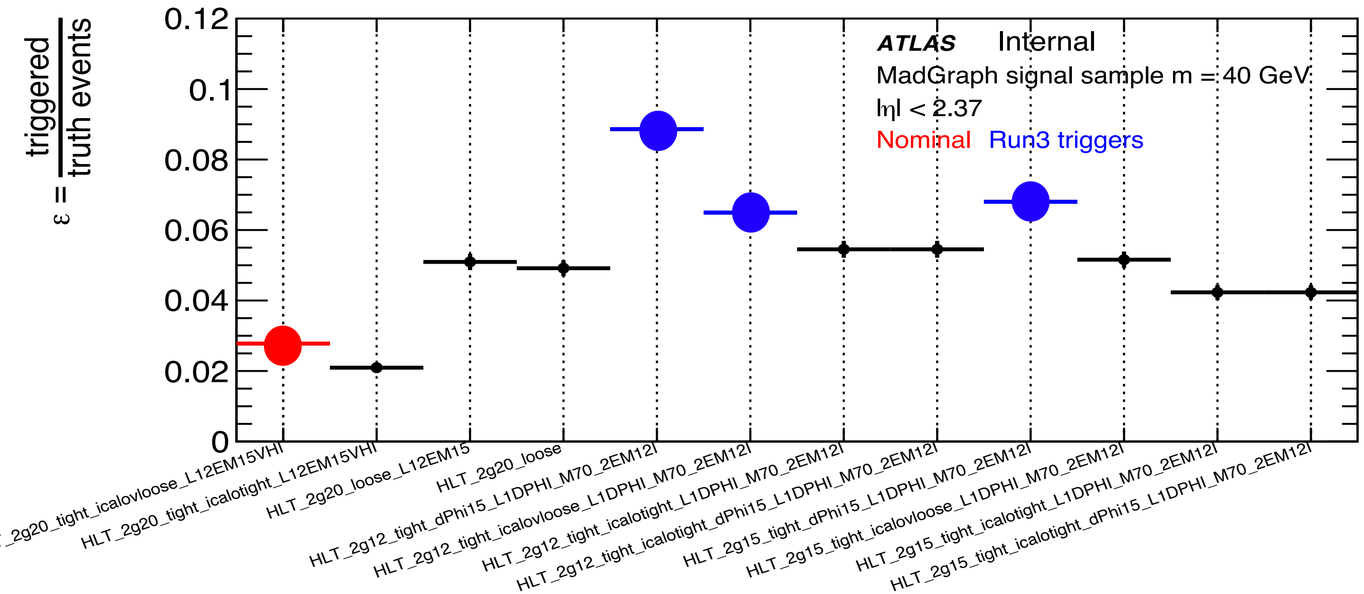

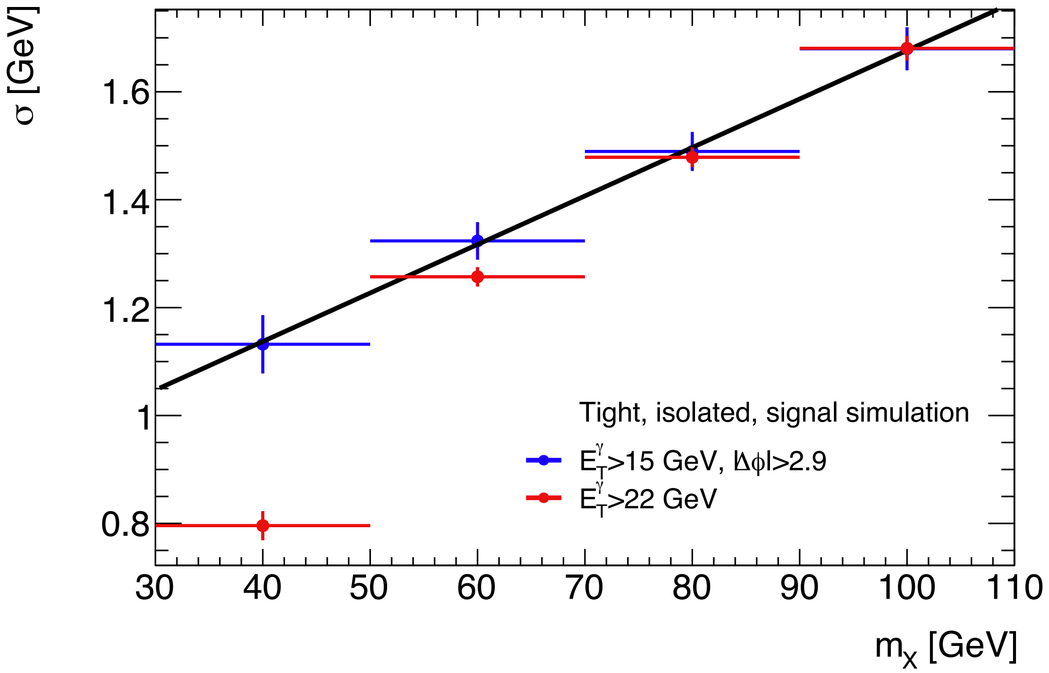
σ [GeV]
1.6
1.4
1.2
1
0.8
30
40
50
60
70
80
90
100
110
m_X [GeV]
Tight, isolated, signal simulation
E_T^γ>15 GeV, |Δφ|>2.9
E_T^γ>22 GeV

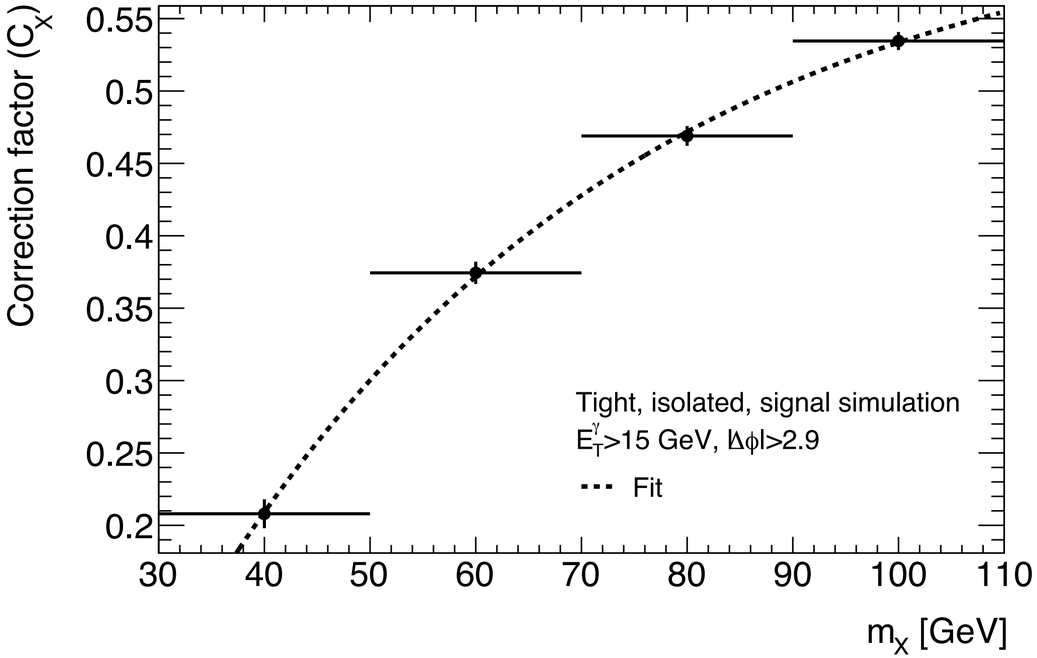
Correction factor (C_X)
0.55
0.5
0.45
0.4
0.35
0.3
0.25
0.2
30
40
50
60
70
80
90
100
110
m_X [GeV]
Tight, isolated, signal simulation
E_T^γ>15 GeV, |Δφ|>2.9
Fit

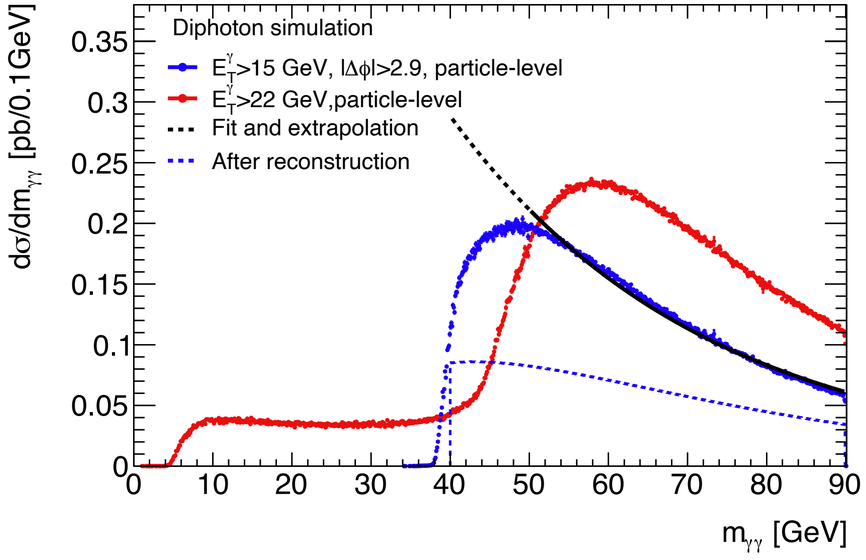
dσ/dm_γγ [pb/0.1GeV]
0.35
0.3
0.25
0.2
0.15
0.1
0.05
0
0
10
20
30
40
50
60
70
80
90
m_γγ [GeV]
Diphoton simulation
E_T^γ>15 GeV, |Δφ|>2.9, particle-level
E_T^γ>22 GeV,particle-level
Fit and extrapolation
After reconstruction

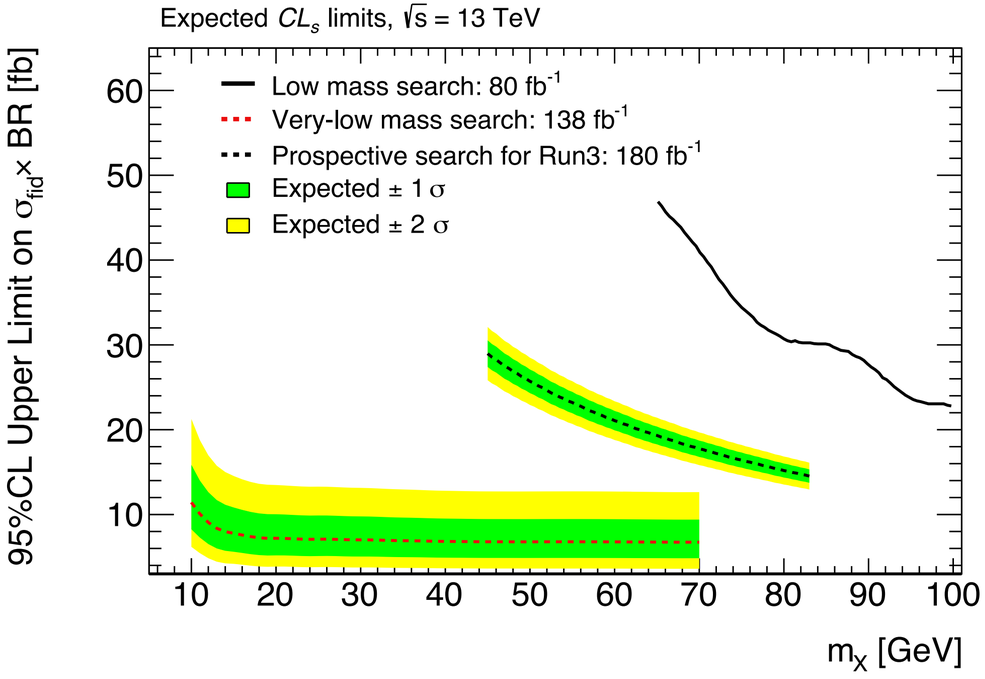
Expected CL_s limits, √s = 13 TeV
95%CL Upper Limit on σ_fid× BR [fb]
60
50
40
30
20
10
10
20
30
40
50
60
70
80
90
100
m_X [GeV]
Low mass search: 80 fb^-1
Very-low mass search: 138 fb^-1
Prospective search for Run3: 180 fb^-1
Expected ± 1 σ
Expected ± 2 σ

Why photons and not jets?

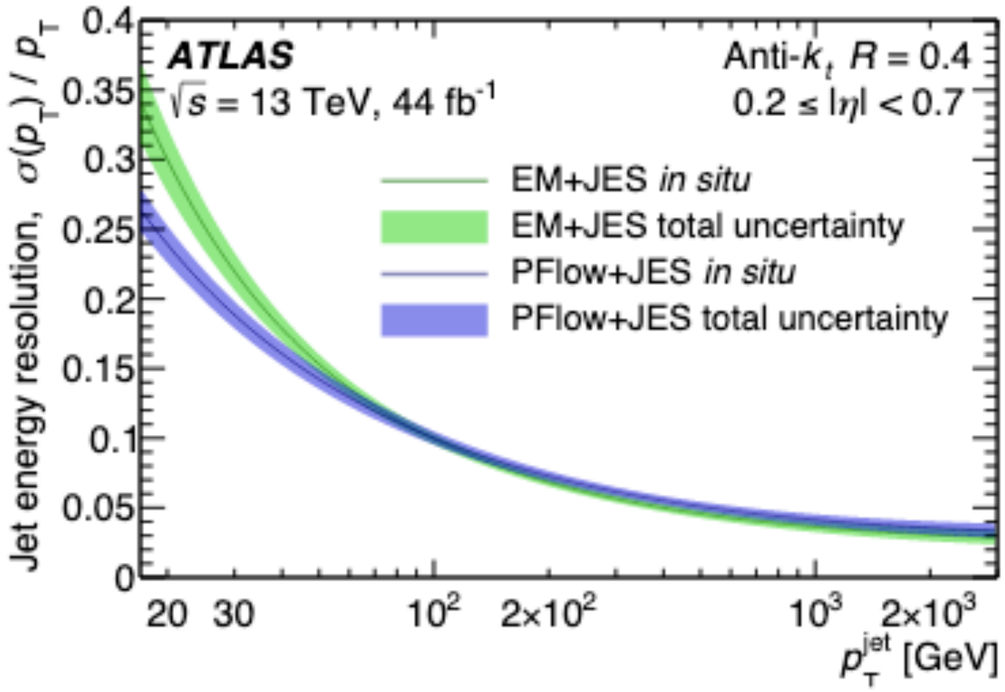

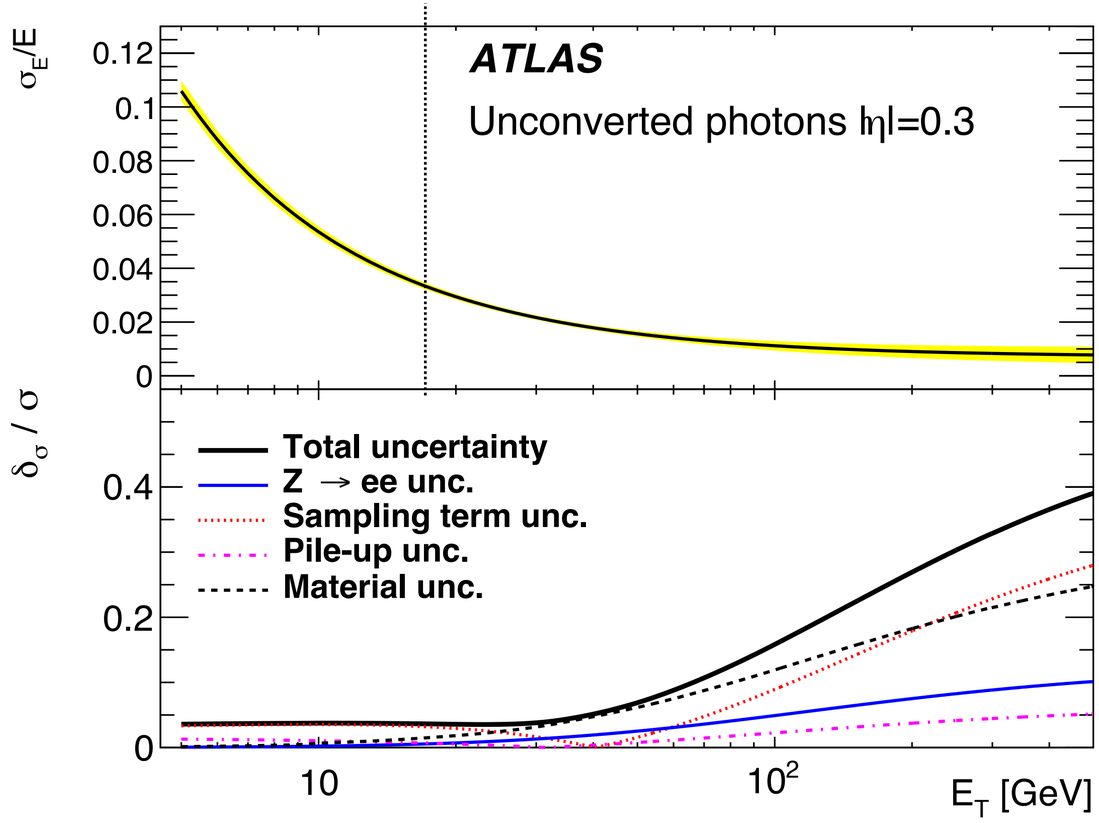

Width and long-lived particles

From 10-100 GeV, and given fa between 0.1-100 TeV, ALP exist that could live enough to decay inside the calorimeters

- Same EFT framework as a tool to probe different types of resonances.

$$\Gamma_{gg} \propto \alpha_s^2 \frac{m_a^3}{f_a^2}$$

$$\Gamma_{\gamma\gamma} \propto \alpha_{QED}^2 \frac{m_a^3}{f_a^2}$$

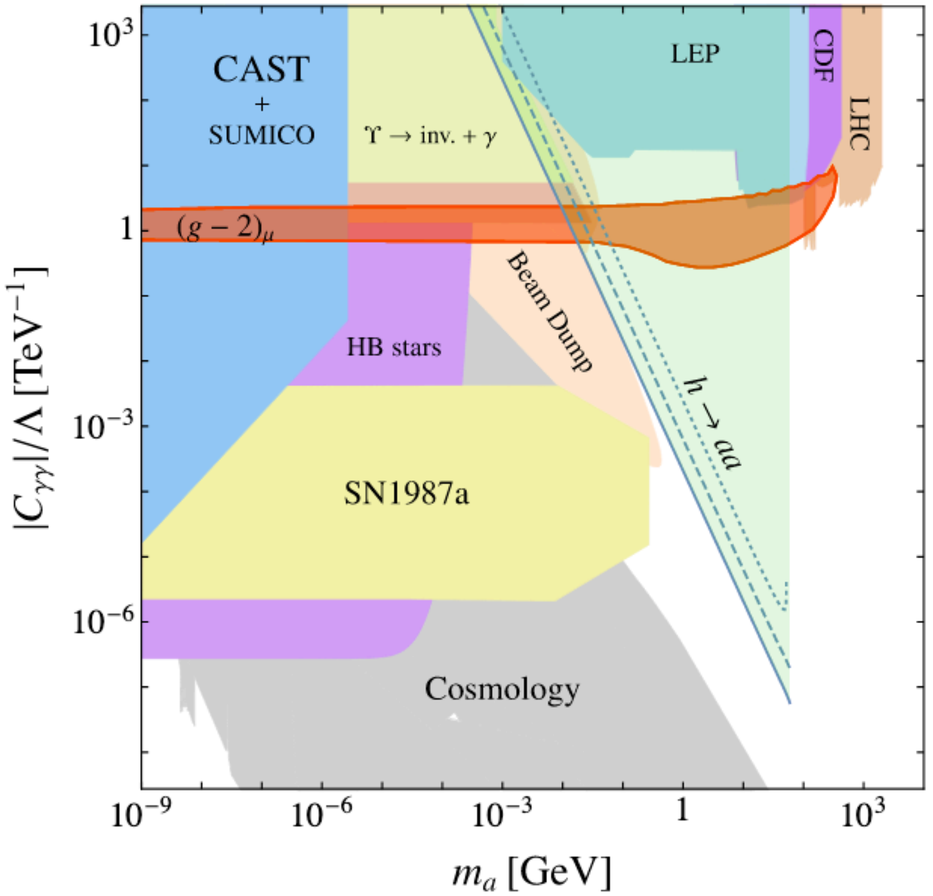

This plot assumes only couplings to photons

$$\frac{\Gamma_{tot}}{m_a} = \frac{\Gamma_{gg} + \Gamma_{\gamma\gamma}}{m_a} \sim \begin{cases} 10^{-6}\alpha_s^2 \\ 10^{-4}\alpha_s^2 \\ \alpha_s^2 \\ 10^{2}\alpha_s^2 \end{cases}$$